CRCLEME
Cooperative Research Centre for
Landscape Evolution & Mineral Exploration

AMIRA
Australian Mineral Industries Research Association Limited ACN 004 448 266

OPEN FILE
REPORT
SERIES

THE UNIVERSITY
OF QUEENSLAND

GEOCHRONOLOGY OF WEATHERING IN THE MT ISA AND CHARTERS TOWERS REGIONS, NORTHERN QUEENSLAND

P. Vasconcelos

CRC LEME OPEN FILE REPORT 139

April 2002

CRCLEME

(CSIRO Exploration and Mining Report 452R / CRC LEME Report 68R, 1998.
2nd Impression 2002.)

CRC LEME is an unincorporated joint venture between CSIRO-Exploration & Mining, and Land & Water, The Australian National University, Curtin University of Technology, University of Adelaide, University of Canberra, Geoscience Australia, Bureau of Rural Sciences, Primary Industries and Resources SA, NSW Department of Mineral Resources-Geological Survey and Minerals Council of Australia, established and supported under the Australian Government's Cooperative Research Centres Program.

CRC

AMIRA
Australian Mineral Industries Research Association Limited ACN 004 448 266

CRCLEME
Cooperative Research Centre for Landscape Evolution & Mineral Exploration

The University Of Queensland

GEOCHRONOLOGY OF WEATHERING IN THE MT ISA AND CHARTERS TOWERS REGIONS, NORTHERN QUEENSLAND

P. Vasconcelos

CRC LEME OPEN FILE REPORT 139

April 2002

(CSIRO Exploration and Mining Report 452R / CRC LEME Report 68R, 1998.
2nd Impression 2002.)

© CRC LEME 1998

CRC LEME is an unincorporated joint venture between CSIRO-Exploration & Mining, and Land & Water, The Australian National University, Curtin University of Technology, University of Adelaide, University of Canberra, Geoscience Australia, Bureau of Rural Sciences, Primary Industries and Resources SA, NSW Department of Mineral Resources-Geological Survey and Minerals Council of Australia.
Headquarters: CRC LEME c/o CSIRO Exploration and Mining, PO Box 1130, Bentley WA 6102, Australia

© CRC LEME

CSIRO/CRC LEME/AMIRA PROJECT P417
GEOCHEMICAL EXPLORATION IN REGOLITH-DOMINATED TERRAIN, NORTH QUEENSLAND 1994-1997

In 1994, CSIRO commenced a multi-client research project in regolith geology and geochemistry in North Queensland, supported by 11 mining companies, through the Australian Mineral Industries Research Association Limited (AMIRA). This research project, "Geochemical Exploration in Regolith-Dominated Terrain, North Queensland" had the aim of substantially improving geochemical methods of exploring for base metals and gold deposits under cover or obscured by deep weathering in selected areas within (a) the Mt Isa region and (b) the Charters Towers - North Drummond Basin region.

In July 1995, this project was incorporated into the research programs of CRC LEME, which provided an expanded staffing, not only from CSIRO but also from the Australian Geological Survey Organisation, University of Queensland and the Queensland Department of Minerals and Energy. The project, operated from nodes in Perth, Brisbane, Canberra and Sydney, was led by Dr R.R. Anand. It was commenced on 1st April 1994 and concluded in December 1997. The project involved regional mapping (three areas), district scale mapping (seven areas), local scale mapping (six areas), geochemical dispersion studies (fifteen sites) and geochronological studies (eleven sites). It carried the experience gained from the Yilgarn (see CRC LEME Open File Reports 1-75 and 86-112) across the continent and expanded upon it.

Although the confidentiality period of Project P417 expired in mid 2000, the reports have not been released previously. CRC LEME acknowledges the Australian Mineral Industries Research Association and CSIRO Division of Exploration and Mining for authority to publish these reports. It is intended that publication of the reports will be a substantial additional factor in transferring technology to aid the Australian mineral industry.

This report (CRC LEME Open File Report 139) is a second impression (second printing) of CSIRO, Division of Exploration and Mining Restricted Report 452R, first issued in 1998, which formed part of the CSIRO/AMIRA Project P417.

Copies of this publication can be obtained from:
The Publication Officer, c/- CRC LEME, CSIRO Exploration and Mining, P.O. Box 1130, Bentley, WA 6102, Australia.. Information on other publications in this series may be obtained from the above or from http://leme.anu.edu.au/

Cataloguing-in-Publication:
Vasconcelos, P.
Geochronology of weathering in the Mount Isa and Charters Towers Regions, Northern Queensland.
ISBN 0 643 06811 2
1. Regolith - Northern Queensland. 2. Landforms - Northern Queensland 3. Geochronology
I. Title
CRC LEME Open File Report 139.
ISSN 1329-4768

Geochronology of Weathering in the Mount Isa and Charters Towers Regions, Northern Queensland

Foreword

The K-Ar and $^{40}Ar/^{39}Ar$ geochronology results presented in this document were partly generated with support from AMIRA Project P417. Limited funds were available for the geochronology component of AMIRA P417; for this reason, a large component of the geochronology work presented here was undertaken under the umbrella of ARC Large Grants A39531815 and A39701507.

At the outset, the geochronology component of P417 was supposed to be carried out by a PhD student enrolled at the University of Queensland. The cancellation of the PhD scholarship delayed the execution of the investigation. Except where noted, all samples analysed in this project were collected by the author. All analytical work (optical microscopy, electron microscopy, electron microprobe analyses, and isotope analyses) were also performed by the author.

During the initial stages of this project, the $^{40}Ar/^{39}Ar$ geochronology was carried-out at the Berkeley Geochronology Center, in collaboration with T. Becker. During the late phase of this project, the $^{40}Ar/^{39}Ar$ isotope analyses were conducted at the UQ-AGES (Argon Geochronology in Earth Sciences) facility built at the Department of Earth Sciences at the University of Queensland. Inter-laboratory comparisons between BGC and AGES indicate that the results generated at AGES are indistinguishable, within error, from BGC results on the same samples.

Finally, this work would not have been accomplished without the field support and access to sampling sites made available by CRAE and Century Zinc (Century deposit); Mount Isa Mines (Mount Isa gossan and Mount Isa drill-cores, Lake Moondarra prospect, and Tick Hill deposit); ARIMCO (Selwyn Mine); and Normandy and Battle Mountain (Scott Lode deposit). This study also benefited greatly from field discussions with G. Broadbent, K. Hannan, D. Mump, J. Stone, W. Dietrich, M. Whitbread, E. Fleming, and G. Lilley. Many of the sites studied in this project were subject of further detailed investigation in Honours projects carried out in the region by T. Herlihy, M. Whitbread, E. Fleming, and G. Lilley.

Paulo Vasconcelos
Brisbane, March 31, 1998.

Executive Summary

The CRCLEME -AMIRA project "Geochemical exploration in regolith-dominated terrain of North Queensland" (P 417) has, as its overall aim, to substantially improve geochemical methods of exploring base metals and gold deposits under cover or obscured by deep weathering. The research includes geochemical dispersion studies, regolith mapping, regolith characterisation, geochronology of weathering profiles and investigation of regolith evolution. This report documents geochronology of weathering and provides a provisional quantitative chronological framework for landscape evolution and dispersion of trace elements in weathering profiles dominantly in the Mt Isa region and, to a lesser extent, in the Charters Towers region.

The weathering geochronology implies that the Mt Isa region has been subject to some very wet periods, when dissolution, redistribution and reprecipitation of elements within weathering profiles was facilitated by abundance of meteoric water. It appears that the late Cretaceous early Palaeocene, early to middle Oligocene, and early to middle Miocene were periods most conductive to dissolution and reprecipitation of Mn-oxides and, by implications, other trace elements. This report contains data produced by both P417 funding ($ 60,000) and partly ARC funding ($ 100,000) awarded to Paulo Vasconcelos. Details of sites investigated under the different funding regimes are outlined:

P417: Mount Isa
Lake Moondarra
Overhang
Tringadee
Cowie
Pegmont
Selwyn

ARC: Century
Mesa 1
Gunpowder Creek
Tick Hill
Scott Lode

R A Anand
Project Leader

I D M Robertson
Deputy Leader

Table of Contents:

List of Figures:

List of Tables:

1 Introduction

From a geochemical exploration viewpoint, weathering promotes the supergene enrichment of ore deposits and the dispersion of ore and tracer elements in the regolith surrounding an orebody. Often, this regolith records complex interactions between weathering and erosive processes. To understand the history and potential mechanisms and pathways of migration of ore and pathfinder elements in weathering profiles, it is necessary to unravel the complex superposition of events which may have occurred during regolith formation.

Recent advances in the study of regolith stratigraphy has helped to differentiate supergene minerals formed in situ from allochtonous regolith components. Regolith stratigraphy studies have also shown that complete weathering profiles, generally present in stable cratons, particularly in the southern hemisphere, are complex, chemically stratified, systems. Understanding this chemical stratigraphy has helped to select the most appropriate part of a stratified weathering profile as a sampling medium in mineral exploration. Understanding regolith stratigraphy has been instrumental in the recognition of truncated or buried weathering profiles.

Significant advances in regolith stratigraphy has also shown that weathering profiles host components formed during weathering-prone and erosion-prone conditions. The alternation between weathering- and erosion-prone conditions may have occurred for tens to hundreds of millions of years. To unravel this history, it is necessary to determine the evolution of each part of the regolith in space and in time.

In the present report, I will illustrate the application of $^{40}Ar/^{39}Ar$ geochronology of supergene minerals to the resolution of specific regolith stratigraphy problems in the Mount Isa and Charters Towers regions. The acquired knowledge about weathering chronology and the inferred knowledge about paleoclimatology and landscape evolution will provide the necessary database to:

- determine likely mechanisms of metal transport during supergene enrichment of ore deposits;
- identify geomorphic surfaces likely to host ore deposits with supergene enrichment blankets;
- identify the multiple stages of evolution of geomorphic surfaces;
- recognise the possible transfer of elements between these surfaces;
- interpret the complex surficial geochemical anomalies associated with ore deposits in weathered terrains in northern Queensland.

1.1 Methodology

The main emphasis in this project focussed on the application of K-Ar and $^{40}Ar/^{39}Ar$ dating of supergene Mn-oxides and jarosite to study the geochronological, geochemical, and paleoclimatological history of selected weathering profiles in Queensland (Fig. 1).

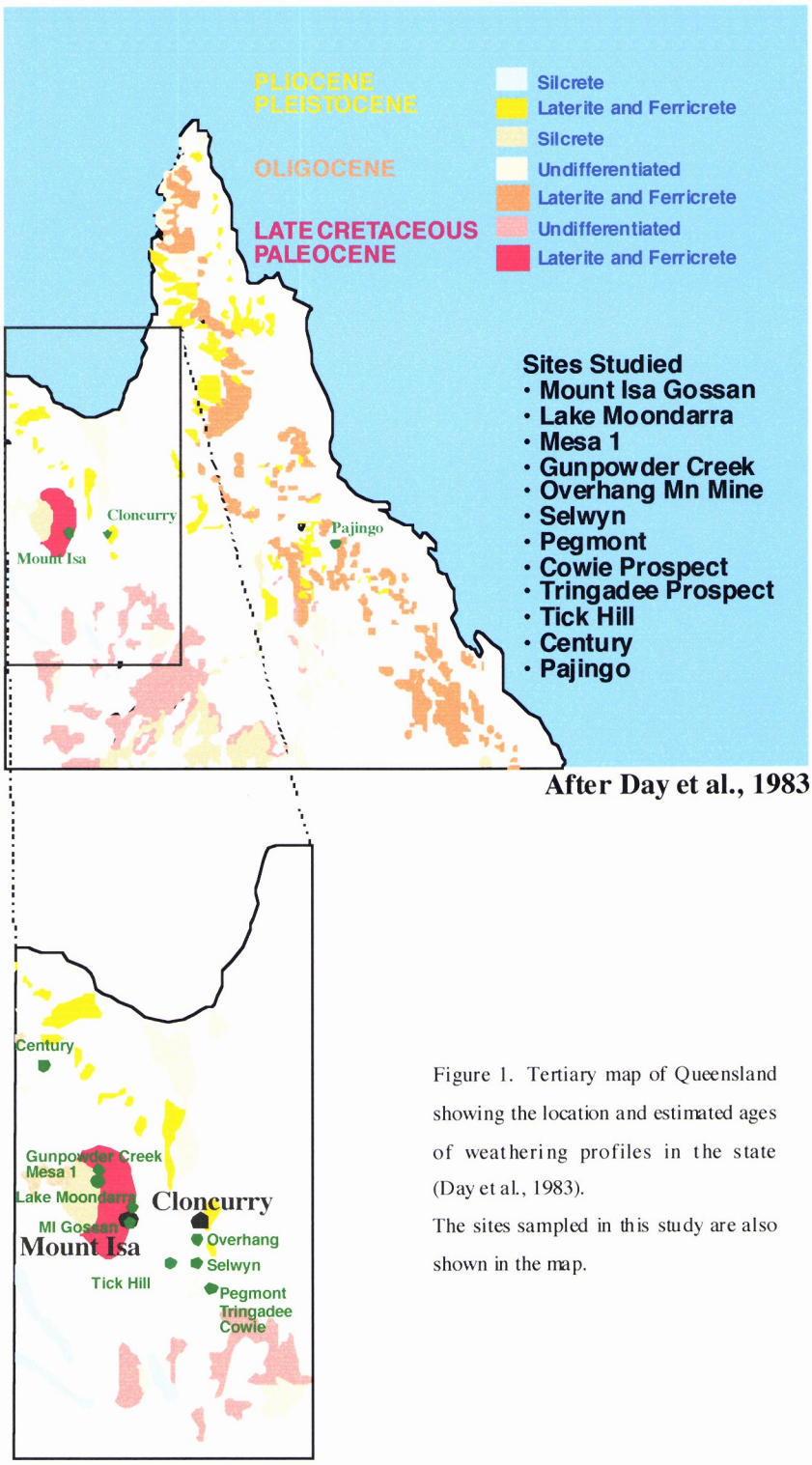

Figure 1. Tertiary map of Queensland showing the location and estimated ages of weathering profiles in the state (Day et al., 1983).
The sites sampled in this study are also shown in the map.

I applied geochronology of surficial minerals to test the following hypotheses:

- That weathering reactions lead to the precipitation of metastable minerals, such as K-bearing Mn-oxide and sulfates, which remained impervious to recrystallization and exchange reactions after precipitation, thus recording weathering ages.
- That deep weathering profiles and laterites common in the Queensland landscape have resulted from a protracted and episodic history of weathering which might have initiated in the Mesozoic.
- That the surficial Mesozoic and Cenozoic histories of Queensland have been shaped by the alternation between weathering- and erosion-prone conditions, leading to the development of the distinct weathering surfaces.
- That the migration and consequent dispersion or concentration of ore-forming elements depends on past climatic and hydrologic regimes, which might be drastically different from those at present.

Specific approaches to achieve the aims above included (Fig. 2):

- Field mapping of the distribution of weathered profiles and their geomorphologic setting, and detailed mineralogical description of selected profiles in the areas of interest.
- Petrographic, scanning electron microscope (SEM), electron microprobe (EMP), and X-ray diffraction (XRD) analysis of the datable phases to determine their size, precise composition, crystallinity, and the possible presence of intergrown minerals.
- K-Ar analysis of bulk mineral separates, if the supergene minerals were present in abundant quantities.
- Dating of single grains or monomineralic clusters of K-rich supergene minerals by laser-heating $^{40}Ar/^{39}Ar$ analysis.
- Incorporation of geochronological and geochemical information into the regolith stratigraphy to investigate the temporal and spatial migration of elements within each profile.
- Incorporation of the geochronological results in local-scale aerial photos and topographic maps to test the correlation between weathering ages and the elevation and distribution of weathering surfaces.

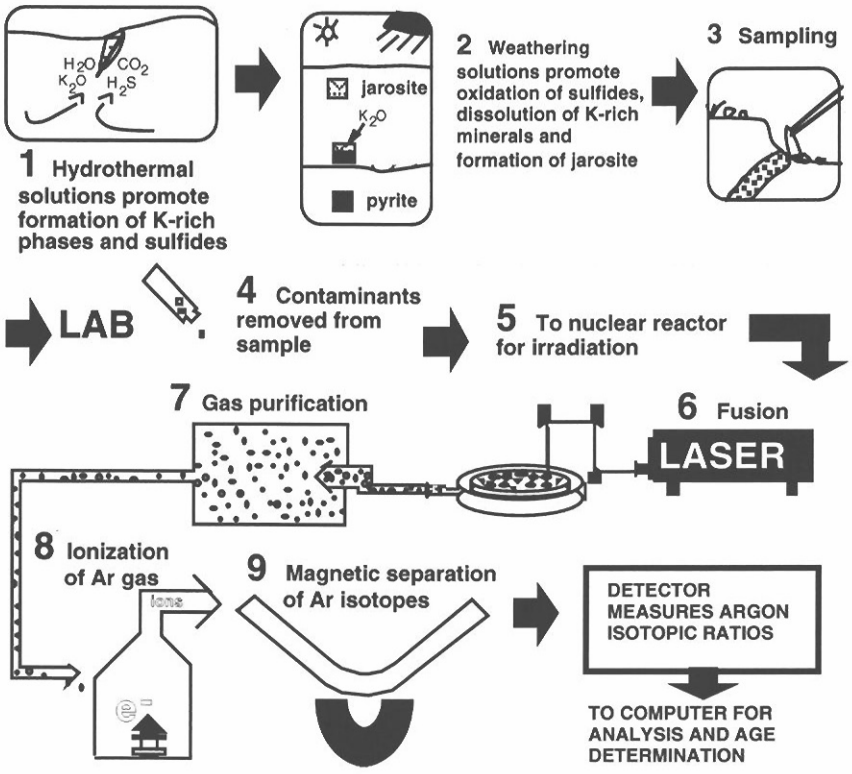

Figure 2. Diagrammatic illustration showing the steps necessary for the application of $^{40}Ar/^{39}Ar$ dating of supergene minerals in the study of weathering and landscape evolution.

1.2 Sample Characterisation

1.2.1 Site Selection Criteria

The selection of appropriate sites for regolith geochronology was primarily driven by the availability of access (exposure or drill holes) to complete or near complete weathering profiles, the presence of supergene minerals suitable for dating, the significance of the ore deposit associated with the site, and the location of the site in relation to geomorphological setting. Other sites were date at CSIRO researchers' request.

1.2.2 Sample in Relation to Landscape Position

For each sample analysed, its geographic coordinates and elevation are given. Each sample is also assigned a landscape position according to whether the sample was collected in a relict, erosional, or depositional part of the landscape.

1.2.3 Sample in Relation to Regolith

Each sample analysed in this study is placed in its position within the regolith stratigraphy. For this purpose, the sample will be characterised as derived from one of the six stratigraphic horizons illustrated in Fig. 3a.

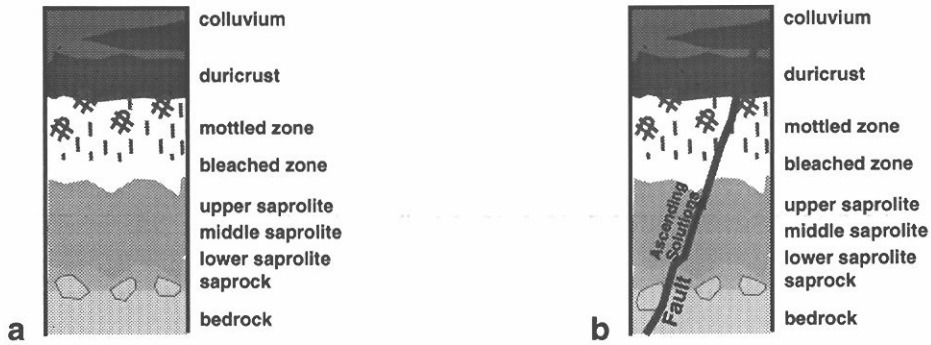

Figure 3. Diagrammatic illustration of hypothetical complete weathering profiles showing the stratigraphy of weathering in the system.

1.2.4 Datable Minerals/Host Rock Relationship

To derive pertinent geochemical information from the samples analysed, the textural relationships between the datable phases and the host lithologies will be defined. Given the host rock composition and the position of the sample in the regolith stratigraphy, the datable minerals will be classified as having been derived from: 1) in situ weathering of local minerals, with minor textural disruption; 2) local recrystallisation of minerals, with major textural disruption; 3) influx of elements, in solution, from outside sources located at positions stratigraphically equivalent to or higher than the deposition site; 4) influx of elements, in solution, from outside sources located at stratigraphic positions below the precipitation site (Fig. 3b).

1.2.5 Sample Composition/SEM-Probe

The composition of each sample, when possible, will be characterised qualitatively by energy dispersive X-ray analyses (EDS) in the SEM and quantitatively by EMP analyses. This characterisation is essential to determine if the sample mineralogy is suitable to $^{40}Ar/^{39}Ar$ geochronology and to determine if the samples are devoid of potential contaminants inherited from the host lithologies. When possible, electron microprobe analyses are programmed as traverses across growth bands in the samples. These traverses reveal the complex variation in the composition of supergene phases, indirectly revealing the change in compositions of the weathering solutions during mineral precipitation.

The detailed electron microprobe traverses presented in this report are vital for the proper interpretation of the geochronology results. In addition, the electron microprobe analyses are a very useful database to exploration geochemists/geologists interested in relating geochemical anomalies in weathering profiles to the presence of specific mineral phases. Since partial digestions and leaching techniques are increasingly used in geochemical exploration programs, it is crucial that we know the host minerals to the elements analysed. Crystal chemistry,

obtained from electron microprobe analyses, allows the explorationist to determine which extraction procedure is the most effective in liberating the element(s) of interest from their host phases.

1.2.6 Sources of Elements

For each sample analysed, the possible sources of the elements which constitute the datable phase will be tentatively identified. In some instances, the sources are quite clear, since the host rock primary mineralogy is rich in the elements which constitute the datable supergene phases (i.e., Overhang deposit). In other instances, the sources are much more difficult to identify, since the host rocks are completed depleted in the elements contained in the datable supergene mineral (i.e., Tick Hill occurrences).

1.3 Analytical Techniques

1.3.1 K-Ar Analyses

The K-Ar isotopic method is a bulk analytical method which requires 0.1-1 gram of pure and homogeneous sample of the supergene phases. The large and homogeneous samples required make this method of limited application in weathering studies, unless unusual concentrations of supergene K-Mn-oxides or K-bearing sulphates are present. The impossibility of distinguishing between multiple generations of supergene phases or intergrown generations of supergene and hypogene phases also limits the reliability of this method. In this study, the K-Ar method was used only as a screening method to determine the suitability of some minerals to further geochronological investigation.

1.3.1.1 Analytical Method

Visually pure Mn-oxide samples were crushed, sieved, and the 250-300 μm and 150-250 μm grain size aliquots were washed in distilled water in an ultrasonic cleaner for 30 minutes. The sample was split into two subsamples; one aliquot was used for isotope analysis while another was used in K analysis by atomic absorption spectroscopy (AAS). Analytical procedures were the same used by Vasconcelos *et al.* (1994a). All samples were analysed by the K-Ar at the isotope laboratory at UQ. The samples were loaded into a molybdenum crucible and baked-out overnight at 130 °C. After fusing the K-Mn oxides by an external radio frequency induction coil, the gases released were subjected to a two stage purification procedure: in the first stage a CuCuO getter and zeolite trap was used to adsorb and remove active gases and to oxidise hydrogen gas to water; in the second stage a Ti getter was used to further remove any remaining active gas. The isotope analyses were performed in a MM880 mass spectrometer operated in the static mode. Data acquisition, calibration, isotope measurements, and blank and atmospheric corrections followed the procedure described in www.uq.edu.au-geochem.

1.3.2 $^{40}Ar/^{39}Ar$ Analyses

1.3.2.1 Principle

The $^{40}Ar/^{39}Ar$ technique is a variant of the K-Ar technique. The major differences between the K-Ar and the $^{40}Ar/^{39}Ar$ methods are listed in the table below:

Table 1. Tabulated comparison between the K-Ar and $^{40}Ar/^{39}Ar$ methods.

K-Ar	Parameter	$^{40}Ar/^{39}Ar$
0.1-1.0 grams	Sample Size	0.5 μm-1.0 grams
AAS or flame photometry, on separate aliquot	K Determination by	Mass Spectrometric Analyses of ^{39}Ar generated by neutron irradiation of ^{39}K
0.1-3%	Analytical Precision	0.1%
Isotope Dilution Mass Spectrometry	Ar Determination by	Mass Spectrometry
~ 1-10 x 10^{-11} moles	Ar Detection Limit	~ 1 x 10^{-16} moles
0.5-5%	Analytical Precision	0.05-1%
NO	Able to Identify Excess Ar	YES
NO	Able to Identify Ar Loss	YES
NO	Able to Identify Mixed Phases	YES
NO	Able to Determine Thermal History	YES
0.5-1 Day	Duration of One Analyses	15-30 minutes
Partial, data reduction only	Automation	Full Automation
NO	Crystallographic Information	YES
~ 1 week	Minimum Time Between Sampling and Analyses	2-4 months

Contrary to the K-Ar technique, where K and Ar are determined in different aliquots of the sample, in the $^{40}Ar/^{39}Ar$ method K and Ar contents are determined from the same aliquot, mineral grain, or crystallographic site in a sample. This is possible because in the $^{40}Ar/^{39}Ar$ method K is indirectly determined through the measurement of the nucleogenic $^{39}Ar^{\ddagger}$ generated by neutron irradiation of the sample. Since K and radiogenic $^{40}Ar^{*}$ occupy the same crystallographic site, the nucleogenic $^{39}Ar^{\ddagger}$ also occupies the same site (in the absence of recoil) (Vasconcelos, 1994a).

The advantages of the application of the $^{40}Ar/^{39}Ar$ method in weathering studies are:

- The large time-span datable by this method, which can be used to determine the age of supergene minerals as young as ~250,000 years and as old as the solar system.

- The fine-scale resolution of the method, which allows the age determination of very fine-grained phases (50-100 μm grains can be dated).
- The multiple-step analysis of single grains, which enables the determination of the Ar retention history for a mineral, the presence of excess/inherited Ar, and the possibility of K and/or Ar loss.
- The ease of automated analysis, which allows multiple age determinations for each profile, thus providing improved statistics and a comprehensive weathering history database.

1.3.2.2 Irradiation

All samples were irradiated together with Fish Canyon sanidine neutron flux standards in the Triga Reactor at the Oregon State University. Irradiation times ranged from 10-14 hours. The J-factors yielded during each irradiation are shown together with the sample results for each sample.

1.3.2.3 Mass Spectrometry

After at least a one-month cooling period, each sample was step-heated under a continuous Ar-ion laser with defocussed beam. The fraction of gas released was cleaned through a cryocooled cold-trap (T=-130 °C) and two C-50 SAES™ Zr-V-Fe getters and analysed for Ar isotopes in a MAP-215C mass spectrometer. During the initial stages of this project, the samples were analysed at the Berkeley Geochronology Center (BGC), Berkeley, CA. Automation and analytical procedures followed are described in Deino and Potts (1990) and Deino *et al.* (1990). Data corrected for mass discrimination, nucleogenic interferences, and atmospheric contamination were used to calculate apparent ages for each degassing step.

During the late phase of the project, the $^{40}Ar/^{39}Ar$ analyses were carried-out in the newly built UQ-AGES (Argon Geochronology in Earth Sciences) laboratory at the University of Queensland. The system uses a 10W continuous Ar-ion laser as the heating device. The fraction of gas released was cleaned through a Polycold™ cryocooled cold-trap (T=-130 °C) and two C-50 SAES™ Zr-V-Fe getters. The clean gas fraction was analysed for ^{36}Ar, ^{37}Ar, ^{38}Ar, ^{39}Ar and ^{40}Ar isotopes in a MAP-215-50 mass spectrometer. Automation and analytical procedures followed are the same as described in Deino and Potts (1990) and Deino *et al.* (1990). Data corrected for mass discrimination, nucleogenic interferences, and atmospheric contamination were used to calculate apparent ages for each degassing step.

1.3.2.4 Mineralogy

The minerals selected for analyses in this study were hollandite-group Mn-oxides (hollandite, cryptomelane, and coronadite) (Fig. 4) and jarosite (Fig. 6). Minerals were identified by visual inspection, reflected light and electron microscopy, electron microprobe analyses, and x-ray diffractometry.

1.3.2.5 Date

In the context of this report, a date is simply a numerical result from the application of a geochronological technique. No quality filter is applied to that result, and the date may represent an accurate geological time (an age) or may be an artefact resulting from the study of an unsuitable sample, from poor analysis, from undetected analytical error, etc. By definition, a date may or may not have an age significance.

1.3.2.6 Apparent Age

The term **apparent age** shares the same definition as the word **date**.

1.3.2.7 Age

In the context of this report, an age is a numerical result from the application of a geochronological technique, which, given the uncertainties about decay constants for radioactive elements and the analytical uncertainties inherent to the method used, is as good as result as can be obtained. In addition, the sample analysed is representative of its geological environment, it is suitable to geochronology by the method applied, and the sample is devoid of contaminants. An age, therefore, represents a time in the geological past when a geological phenomena took place.

1.3.2.8 Plateaus

Age plateaus are arbitrarily defined. In this study, I define an age plateau as a sequence of two or more steps corresponding to at least 40% of the total ^{39}Ar released and whose age values are within two sigma from the mean value. If a sample reaches a well defined plateau, it implies that the sample hosts its radiogenic and nucleogenic gas fractions in a tight crystallographic reservoir, that the reservoir has been closed during the history of the sample, and that contaminating hypogene phases are unlikely to be present. However, some geological and analytical factors may make a sample deviate from a well defined plateau without any implication that the plateau-like spectra obtained is not a valid age for the sample.

Supergene Mn-oxides often occur in micrometric growth bands spanning a prolonged period of precipitation (e.g., Figs. 10 and 13). When these banded samples are analysed by the step-heating method, incremental laser-heating releases gases from different growth bands simultaneously. Given the high analytical precision of the $^{40}Ar/^{39}Ar$ method, samples of gas containing varying gas fractions from distinct bands may yield slightly different ages. The age variation reflects the length of time during which the precipitation of the various growth bands occurred.

In addition, analytical uncertainties associated with memory effects in the mass spectrometer, particularly following steps yielding large gas fractions, will introduce errors which may force a step to deviate from the mean.

Because of the geological and analytical reasons explained above, a sequence of steps whose ages cluster about the mean are defined as "plateaus" or plateau-like sequences.

1.3.2.9 Isochron (isotope correlation diagrams)

When a sample hosts argon in different crystallographic sites, with varying ratios of atmospheric, nucleogenic, and radiogenic components, the results may be plotted as a $^{40}Ar/^{39}Ar$ versus $^{40}Ar/^{39}Ar$ isotope correlation diagram. For supergene minerals, the $^{40}Ar/^{39}Ar$ intercept should fall close to the atmospheric ratio of 295.5. Isochrons are useful to test the reliability of the age obtained for a sample. Under ideal circumstances, rarely achieved, plateau ages and isochron ages should yield exactly the same results.

1.3.2.10 Integrated Age

In the $^{40}Ar/^{39}Ar$ method, an integrated age is the apparent age calculated from the total gas yielded by a sample during the step-heating analyses. If recoil is not an issue, the integrated age in the $^{40}Ar/^{39}Ar$ method should correspond to the K-Ar age for the sample.

1.3.2.11 Ideogram

An ideogram is an age-probability diagram. It is based on the assumption that the errors for an age determination have a gaussian distribution. To construct an age probability plot, the values for the individual gaussian curves for each age increment are plotted for the age range of interest (Deino, 1997).

One of the main disadvantages of using ideograms to illustrate the probability of age distributions is the fact that ideograms do not take into consideration the amount of gas released during each step. As a result, an age-step or a sequence of age-steps which yield(s) insignificantly small amounts of gas, but whose age(s) is(are) determined very precisely in the mass spectrometer, may misleadingly plot as a very high probability age estimate for the sample. An useful criterion for differentiating between true high probability peaks and artefacts of the ideogram method is to compare the ideogram peaks with the plateau ages. If the most probable peaks correspond to well defined plateau ages, the ideogram method is reliably indicting the most probable age intervals for the sample. If the most probable peaks have no plateau ages counterparts, these peaks are analytical artefacts and should be disregarded.

1.3.2.12 Interpretation of Results

Geochronology is not an end in itself. Once geochronological results are obtained, they must be interpreted. The usefulness of any geochronological technique rests on the quality and soundness of the interpretation. Therefore, in order to answer the question *"O.K., you can date supergene Mn-oxides and K-bearing sulphates; but what do the results mean?"*, we must understand the relationship between the minerals being dated and the host lithology, we must know the position of the datable phase in relation to regolith stratigraphy, and we must know something about the solution chemistry of the elements present in the datable mineral. Last, we must also know the environmental factors controlling the precipitation of the datable phase. In order to interpret the results in this report, we need to understand manganese mineralogy and geochemistry. We also need to know basic principles about the geochemistry of sulphur in weathering systems and the environmental factors controlling the precipitation of sulphates, particularly jarosite.

1.4 Manganese Mineralogy

The common K-bearing Mn-oxides are illustrated in the table below:

Table 2. Manganese oxides found in the weathering profiles in the Mount Isa region:

Mineral	Formula	Group	Structure
PYROLUSITE	MnO_2	Pyrolusite	1x1 tunnel
RAMSDELLITE	MnO_2	Pyrolusite	1x1 tunnel
HOLLANDITE	$(Ba,K)_{1-2}Mn_8O_{16}.xH_2O$	Hollandite	2x2 tunnel
CRYPTOMELANE	$(K,Ba)_{1-2}Mn_8O_{16}.xH_2O$	Hollandite	2x2 tunnel
CORONADITE	$(Pb,Ba,K)_{1-2}Mn_8O_{16}.xH_2O$	Hollandite	2x2 tunnel
ROMANECHITE	$(Ba,K,Mn^{2+},Co)_2Mn_5O_{10}.XH_2O$	Romanèchite	2x3 tunnel
TODOROKITE	$(Ca,Na,K)(Mg,Mn^{2+})Mn_5O_{12}.xH_2O$	Todorokite	3x3 tunnel
BIRNESSITE	$(Na,Ca,K)(Mg,Mn)Mn_6O_{14}.5H_2O$	Birnessite	Layered
CHALCOPHANITE	$ZnMn_3O_7.3H_2O$		Layered
LITHIOPHORITE	$(Al,Li)MnO_2.(OH)_2$		Layered

Except for birnessite, chalcophanite, and lithiophorite, which display layered structures (Fig. 4), all other K-bearing Mn-oxide minerals listed above display tunnel structures (Fig. 4). The tunnel structure minerals vary considerably in physical properties, depending on the size of the tunnels. Hollandite-group minerals (hollandite, cryptomelane, and coronadite) all display a 2x2 structure (Fig. 4). Romanèchite and todorokite display 2x3 and 3x3 tunnel structures, respectively. The suitability of hollandite-group minerals to geochronology has been

substantially tested in the past few years (Vasconcelos *et al.*, 1992, 1994a, 1994b, 1995). The suitability of 2x3 and 3x3 structures to geochronology is still under investigation (Vasconcelos, 1996). Therefore, only results obtained from hollandite-type structures are discussed in the present study.

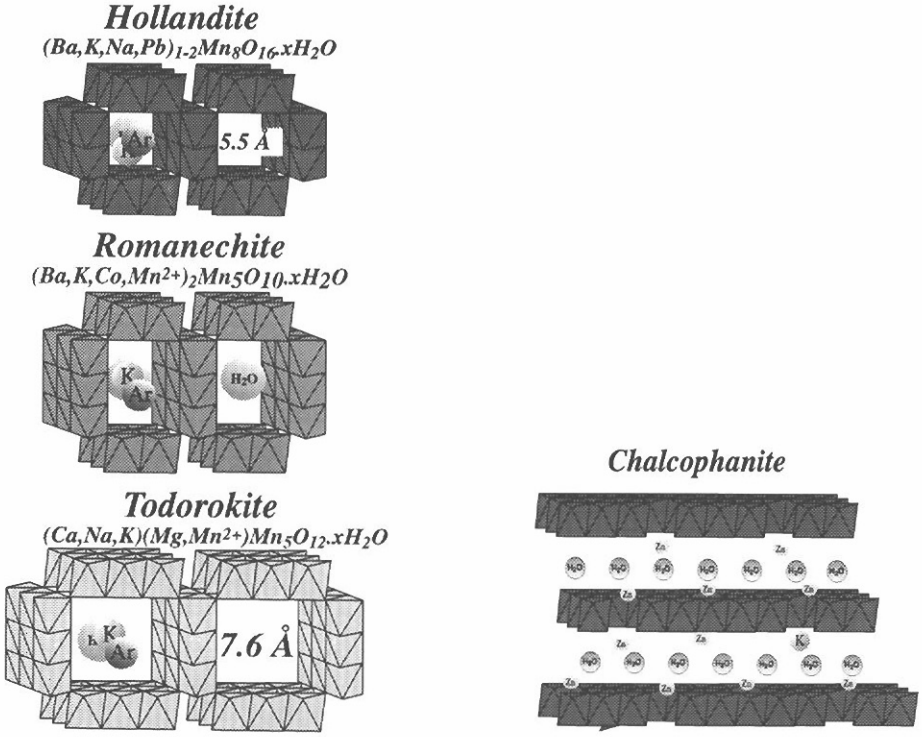

Figure 4. Diagrammatic illustration showing the structures of the various groups of manganese oxides analysed in this study.

1.4.1 Manganese Geochemistry

Manganese is the most common transition element in the Earth, after iron. It often occurs as a minor element in most igneous, sedimentary and metamorphic rocks; it is also found sporadically as a major element in these rocks. Manganese occurs in five different oxidation states: Mn^{2+}, Mn^{3+}, Mn^{4+}, Mn^{6+}, and Mn^{7+} but only Mn^{2+}, Mn^{3+}, and Mn^{4+} are common in natural environments (Crerar *et al.*, 1980). Mn^{2+} and less often Mn^{3+} are the most common component of rocks formed at depth in the earth, while Mn^{3+} and Mn^{4+} prevail in minerals formed in the surficial environment (Crerar *et al.*, 1980).

In igneous and metamorphic rocks, Mn^{2+} and Mn^{3+} are present (generally $\leq$ 1 wt%) substituting for Fe^{2+} in the ferromagnesian minerals olivine, pyroxenes, biotite, chlorite, and hornblende. Manganese is also present in the oxides magnetite, hematite, and ilmenite (up to 8 wt% Mn) (Crerar *et al.*, 1980). It can substitute for Ca^{2+} in apatite, garnet, wollastonite, sphene, and pectolite; or it may occur in complex minerals such as tourmaline and vesuvianite

(Crerar *et al.*, 1980). Mn^{3+} substitutes for Al^{3+} in andalusite (manganandalusite and viridine), or for Al^{3+} and Fe^{3+} in epidotes (allanite and piedmontite). In pegmatites, Mn commonly occurs in spessartine garnet, mangano-columbite, mangano-tantalite, manganaxinite, and in a large variety of manganese phosphates (apatite, lithiophilite, rockbridgeite, mangano-variscite, frondelite, strunzite, jahnsite) and carbonates (ankerite, rhodochrosite, manganocalcite) (Crerar *et al.*, 1980).

In the Mount Isa region, manganese is an extremely common element in the alteration haloes of hydrothermal ore deposits. Hydrothermal carbonates associated with the alteration haloes in sediment-hosted Pb-Zn-Ag sulphide deposits are often Mn-bearing ankerites, dolomites, and rhodochrosite (Andrews, 1998). Manganese is also common in the structure of silicates (chlorites, amphiboles, micas) and carbonates (ankerite and dolomite) associated with hydrothermal alteration in Cu-Au deposits (Vasconcelos, 1992). Manganese occurs as trace impurities in magnetite or as manganese silicates (rhodonite, pyroxmangite) and carbonates (rhodochrosite) in metamorphosed banded iron-, banded manganese-formations in the high-grade metamorphic terrains of the Eastern succession. Weathering of these mineralised assemblages leads to the precipitation of Mn-oxides in the vicinity of the weathering ore deposits.

During weathering processes, manganese is mobile as Mn^{2+} (Hem, 1963) (Fig. 5). The cation Mn^{2+} predominates for most of the range of conditions characteristic of natural-water systems (Hem, 1963). At pH > 10.5, the complex $MnOH^{+}$ becomes the predominant form, and in solutions with high concentrations of HCO_3^{-} or $SO_4^{=}$ the complexes $MnHCO_3^{+}$ and $MnSO_4$ (aq) may be important (Hem, 1989). In addition, organic acids have been shown to control manganese solubility in the surficial environment (Crerar *et al.*, 1972; Stone and Morgan, 1984a,b; Stone, 1987). Mn^{3+} species may occur in strongly acid or organic-rich solutions. Nevertheless, the tendency of the Mn^{3+} species to disproportionate by the reaction

$$2\ Mn^{3+}\ (aq) + 2\ H_2O\ (l) \ <=>\ Mn^{2+}\ (aq) + Mn^{4+}O_2(s)\ + 4\ H^{+}\ (aq)$$

indicates that the Mn^{3+} species does not play a major role in the solution chemistry of manganese under surface conditions.

The chemical oxidation of Mn^{2+} and Mn^{3+} and the disproportionation of Mn^{3+} in aerated surface water leads to the precipitation of Mn^{4+} oxides. These oxides further catalyse the oxidation process. Thus, Mn-oxide precipitation tends to occur on previously precipitated oxides, forming accretionary bands typical of botryoidal manganese minerals. In addition to the simple oxides shown in Fig. 5, supergene oxides tend to catalyse the precipitation of other cations in

solution (Ba, Ni, Co, Cu, K, Pb, etc.), leading to the formation of complex supergene phases (Burns and Burns, 1979). Hollandite, coronadite, cryptomelane, birnessite, psilomelane, todorokite and chalcophanite are some of the complex Mn-oxides commonly found in soils and weathering profiles (Fig. 4) (Burns and Burns, 1979).

In addition to oxidation, an increase in pH also leads to the precipitation of manganese from solution. When soluble Mn^{2+} encounters high pH conditions, it precipitates as $Mn(OH)_2$ (pyrochroite) or as Mn_3O_4 (bixbyite) (Fig. 5)

Because of the large number of oxidation states, the wide variety of manganese minerals in nature, the common occurrence of mixed valance manganese in minerals, and the temperature dependence of manganese phases, manganese minerals are excellent indicators of pH, Eh, oxygen fugacity, temperature, biological processes, and other geochemical conditions prevailing during precipitation (Hem, 1963; Bricker, 1965; Crerar *et al.*, 1980). The study and quantification of the responses of Mn-oxide minerals to changing environmental conditions may be vital to understanding past surficial processes.

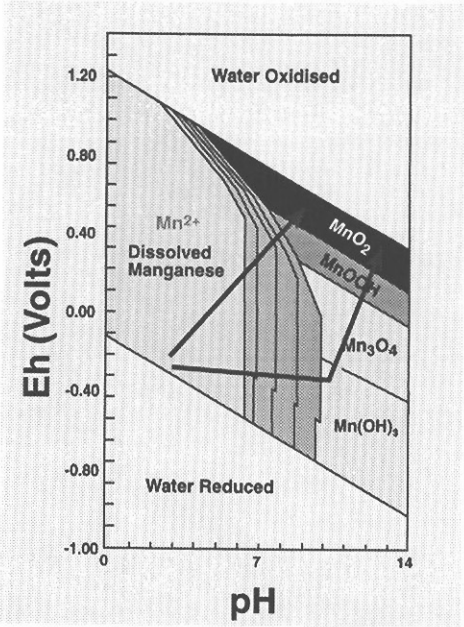

Figure 5. Eh-pH diagram illustrating the stability field aqueous manganese ions and the various manganese minerals commonly found in weathering profiles. Unfortunately, due to the lack of reliable thermodynamic data, the stability fields of complex manganese solid-solutions cannot be shown. However, these Mn^{4+} oxides would likely occupy the field covered by MnO_2. Solid solution would promote their stability under a wide range of conditions, extending their stability fields beyond the MnO_2 boundaries.

1.5 Jarosite-Alunite Mineralogy

Among the K-bearing supergene minerals commonly present in weathering profiles, two mineral groups have widespread distribution: the hollandite-group Mn-oxides and the alunite-group sulfates (Fig. 6). Jarosite and alunite, although not as abundant as K-Mn oxides, are often found in diverse environments. They are present in the oxidation zones of ore deposits, acid mine drainages, hydrothermal ore deposits, hot springs, soils, coal deposits, paleosols, silcretes, and salt-lake sediments (Blanchard, 1968; Michel and van Everdingen, 1987; Anderson, 1981; Bladh, 1982; Nordstrom, 1982; Scott, 1987; Scott, 1990; van Breeman, 1988; Alpers and Brimhall, 1988; Alpers *et al.*, 1989; Chivas *et al.*, 1991).

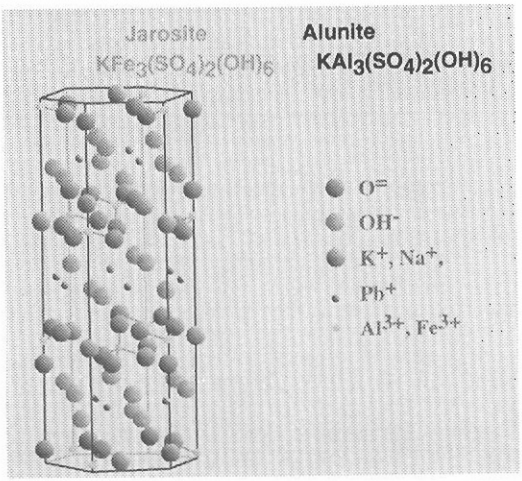

Figure 6. Diagrammatic illustration of the alunite-group (alunite and jarosite) structures.

The minerals alunite and jarosite (general formula $AB_3(SO_4)_2(OH)_6$) crystallise in the hexagonal system (Brophy *et al.*, 1962; Brophy and Sheridan, 1965) (Fig. 6). The B-site, occupied by Al^{3+} (in alunite) and Fe^{3+} (in jarosite), occurs in 6-fold coordination with two $O^=$ ions from the $SO_4^=$ tetrahedra and 4 OH^- groups (Fig. 6)(Brophy *et al.*, 1962). K^+ occurs in the large 12-fold coordination A-site surrounded by six $O^=$ ions from the $SO_4^=$ tetrahedra and six OH^- ions (Fig. 6)(Brophy *et al.*, 1962). A variety of monovalent cations, such as Na^+, H_3O^+, NH_4^+, and Ag^+ may substitute for K^+ in the A-site; in addition, divalent and trivalent cations such as Pb^{2+}, Ca^{2+}, Ba^{2+}, Sr^{2+} and Ce^{3+} may also substitute for K^+ in the A-site if charge compensation occurs by the presence of vacancies, by the substitution of divalent cations (Cu^{2+}, Zn^{2+}, etc.) in the B-site, or by the substitution of PO_4^{3-}, AsO_4^{3-}, or SbO_4^{3-} in the $SO_4^=$ site (Fig. 6) (Scott, 1987; Alpers *et al.*, 1989).

1.5.1 Sulphate Geochemistry

Jarosite and alunite precipitation is generally associated with acid conditions. The stability fields of these minerals (Fig. 7) indicates that oxidising conditions and pH below 4 are required conditions for jarosite-alunite precipitation. In weathering orebodies, such low pHs are

associated with weathering pyrite. Other sulphides may release H^+ during weathering, but the amount of H^+ released by the oxidation of one mole of pyrite or pyrrhotite is four times greater than the amount of acid produced during the oxidation of one mole of chalcopyrite. For these reasons, supergene jarosite and alunite are associated with nearby oxidising pyrite-rich orebodies.

Alunite-group minerals may also be associated with acid sulphate alteration in epithermal systems or with acidic, sulphate-bearing groundwaters.

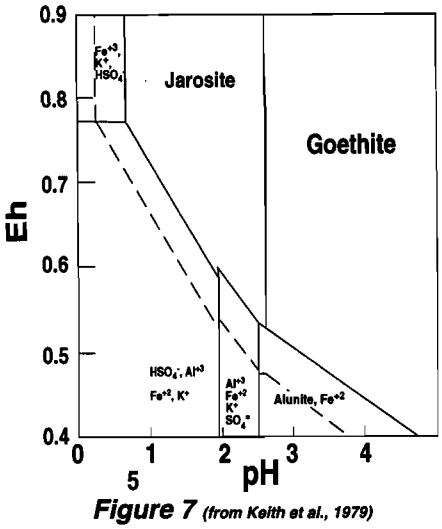

Figure 7. Eh-pH diagram illustrating the stability field for the system Al-Fe-S-K-H_2O at 25°C after Keith *et al.*, 1979).

1.6 Terminology/Glossary/Concepts

1.6.1 Weathering Surface

In this report, the word surface or the term weathering surface has a very specific meaning. A surface is defined as a set of points in space that characterises the interface between the regolith and the atmosphere at a specific time. In this definition, a surface may have any geometric shape. The important aspect of this definition of surface is that all points in a given surface were exposed to the same climatic elements at a point in time. Weathering conditions may have varied at different points of the surface depending on the point's topographic position and aspect within the surface. The term surface does not imply a flat, even, featureless regolith-atmosphere interface.

1.7 Areas Studied and Results

In the following sections, I will describe each site sampled, describe and illustrate each sample collected, and present the results of petrographic investigations, SEM/EMP analyses, and isotope studies. I will discuss the quality and significance of the results obtained for each

sampled site. A brief interpretation of the results and their implication for the evolution of surficial deposits in the site area will be presented.

To facilitate the interpretation of results and to permit interpretations in terms of geomorphologic regimes, I have divided the studied areas into the following groups:

Table 3. Localities sampled for weathering geochronology in this study.

Region	Area	Study Site
Mount Isa Region	Mount Isa City and vicinity	Mount Isa gossan Drill cores through Mount Isa weathering profiles Lake Moondarra gossans
	Western Succession	Mesa 1 outcrop Gunpowder Creek outcrop Drifter prospect
	Lawn Hill	Century deposit
	Eastern Succession	Dugald River deposit Overhang manganese mine Selwyn mine
	Tick Hill	Tick Hill mine and vicinity
	Cannington Area	Tringadee prospect Pegmont prospect Cowie prospect
Charters Towers Region	Pajingo Area	Scott Lode deposit

At the end of the report, I will interpret the implications of the geochronological and mineralogical studies to the formation of weathering profiles and evolution of landscapes in the Mount Isa and Charters Towers regions, separately. Finally, I will summarise the information for the whole of northern Queensland, will suggest future studies to complement the results presented here, and will speculate on the implications of the results in this report to geochemical exploration strategies in the areas studied.

2 Mount Isa Region

The Mount Isa region of northwest Queensland is blanketed by silcretes, laterites, gossans, and other undifferentiated weathering profiles (Day *et al.*, 1983; Scott, 1987; Anand *et al.*, 1997). Abundant jarosite, alunite, K-phosphates, and Mn-oxides occur in the gossans overlying Pb-

Zn-Cu deposits (Taylor and Scott, 1982; Scott, 1987). Cenozoic duricrusts and deeply weathered profiles found in the area supposedly developed during three main periods: late Cretaceous-Paleocene, Oligocene, and Pliocene-Pleistocene (Day *et al.*, 1983) (Fig. 1).

The area immediately surrounding Mount Isa is characterised by a series of roughly N-S oriented flat-top hills and ridges surrounded by deeply dissected plains (Figs. 8 and 9). The hill summits range from 440 to 520m (Fig. 8). Base level in the surrounding valleys and plains, as determined by the level of water in the perennial springs in the area, ranges from 300-320 m (Figs. 8 and 9). The highest summits in the area are generally lithologically controlled. Quartzites are often the least weathereable, least erodable material, forming the majority of the hill tops. Volcanic rocks, calcareous or carbonaceous shales, and siltstones generally underlie the more deeply dissected parts of the landscape (Fig. 9).

Flat summits are devoid of complex, stratified weathering profiles. The absence of these profiles may be a function of lithology. However, careful examination of thin soil layers and soil material associated with rock ledges and crevasses in these summits reveals the presence of pisoliths and other ferruginous lag materials, suggesting that even these summits may have been blanketed by a more complex and well developed weathering profile, now eroded. Exposed bedrock on summit tops often display weathering related silicification.

The valleys and small ridges on valley floors are more deeply weathered than summit tops. However, depth of weathering varies depending on lithology and position on the landscape. In the Mount Isa Mines and Hilton Mines, depth of weathering in the Urquart Shale is consistently greater than on adjacent unmineralised siltstones. In the Mount Isa and Hilton Mines, depth of complete oxidation lies at 50-60 m below the current surface, although oxidation can be deeper along faults zones. Below the zone of complete oxidation, there is a transition zone, where moderate leaching of the bedrocks is identified by the changes in colour and loss of certain elements. This zone of moderate leaching extends in places to 400m below the present surface; again, this depth is often dependent on structural features.

Despite an extensive search between 1994-1996, no minerals suitable for weathering geochronology were found on the 440-520 m summits. However, datable supergene minerals were abundantly present on the dissected valleys and plains surrounding these hills. The following sites were sampled for the study of weathering geochronology:

2.1 Mount Isa City and Vicinity

2.1.1 Mount Isa Gossan (Figs. 9-15)

2.1.1.1 Site Selection Criteria: good exposures of weathering assemblages on mining and road cuts; presence of a significant ore deposit and availability of drill-cores for the weathering profile.

2.1.1.2 Location: 342560E-7707000N

2.1.1.3 Elevation: 320-360 m

2.1.1.4 Geomorphologic Setting: dissected terrain proximal to 400-520 m mesas.

2.1.1.5 Geomorphologic Regime: erosional.

2.1.1.6 Sample in Relation to Landscape Position: Mn-oxide overgrowths on silicified ridges. These ridges occur as north-south oriented features, reaching 360 m in elevation. The ridges are strongly silicified and are considered to be the product of weathering of the sulphide-rich parts of the Urquart shale (Figs. 8 and 9).

2.1.1.7 Sample in Relation to Regolith: the silicified ridge tops hosting the samples analysed in this study immediately overlie the saprolite developed on the Urqhart Shale. These ridges are probably the product of silicification of middle to upper saprolite.

2.1.1.8 Datable Minerals/Host Rock Relationship: influx of elements, in solution, from outside sources located at stratigraphic positions equivalent to or higher than the deposition site.

2.1.1.9 Sources of Elements: Manganese is probably derived from weathering carbonates, Pb and Zn are derived from weathering sulphides, K is derived from feldspars and micas, while Ba may be derived from feldspars, micas, or sulphates in the system.

2.1.1.10 Overview

Mn-oxides are common in the ferruginous silicified ridge (Mt Isa gossan) which overlies the Mount Isa Pb-Zn orebody. These Mn-oxide samples occur as 1-5 cm thick crusts precipitated along bedding and fracture planes (Figs. 9 and 10). These Mn-oxide coatings were sampled in detail for weathering geochronology. These samples were studied by optical microscopy and SEM/EMP investigation before $^{40}Ar/^{39}Ar$ dating (Figs. 10 to 15). In addition to the surface samples, several drill cores were also investigated as possible sources of Mn-oxides at depth. Unfortunately, the drill-cores examined did not contain Mn-oxide samples suitable to geochronology.

2.1.1.11 Results

2.1.1.11.1 Electron Microprobe and SEM Analysis

Petrographic and SEM analyses of these Mn-oxide coatings reveal a complex, banded Mn-oxide assemblage partially replacing and filling fractures in the silicified ferruginous metasediments (Figs. 9 and 10). The banded textures indicate several generations of Mn-oxide

Figure 9. (a) North-South oriented silicified ridges (Mount Isa gossan) overlie the Mount Isa Pb-Zn orebodies. (b) Crevasses and bedding planes in the Mount Isa gossan are often enriched in botryoidal Mn-oxides, particularly coronadite, cryptomelane, hollandite, and chalcophanite. (c-d) Botryoidal Mn-oxides in the Mount Isa gossan are often covered by a thin layer of sulphate (gypsum and barite). (e) 1-3 cm thick Mn-oxide crusts suggest open space precipitation; these samples can be micro-drilled and dated by the $^{40}Ar/^{39}Ar$ method.

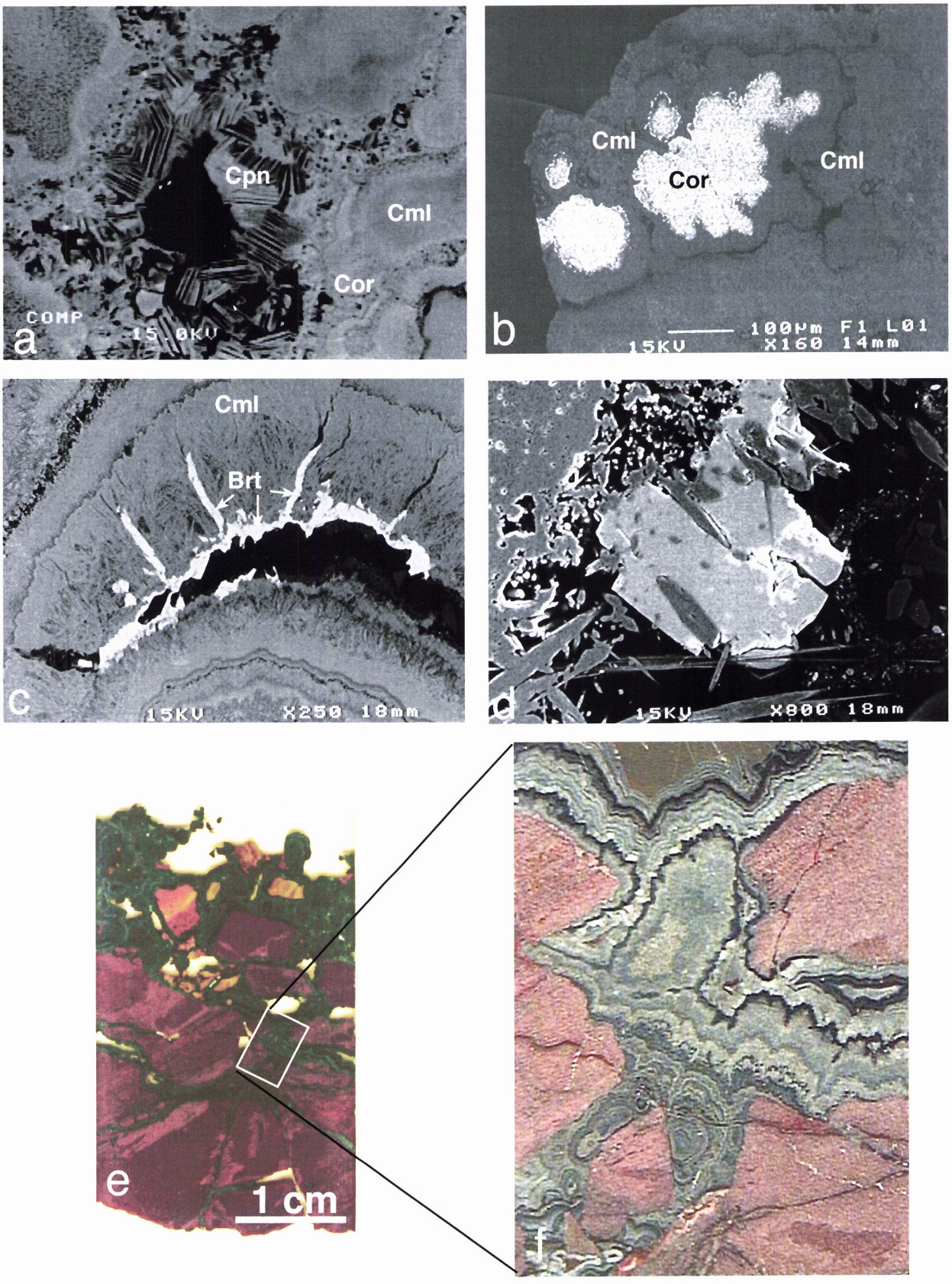

Figure 10. (a) Backscattered SEM photomicrograph illustrates the alternating bands of cryptomelane (Cml), coronadite (Cor), and cavity filling chalcophanite (Cpn), suggesting changes in the composition of the weathering solutions. The alternating shades of grey in backscattered mode reflect the average atomic weight of the sample. High atomic weight Mn-oxides (Pb-rich coronadite) show as white to light grey bands while low average atomic weight Mn-oxides (K-rich cryptomelane or Al-rich lithiophorite) show as darker bands. (b) Coronadite (Cor) cores are often surrounded by cryptomelane, indicating deposition of Pb early in the history of precipitation of the Mn-oxide crusts. (c) Desiccation cracks in botryoidal Mn-oxides often host late-stage barite (Brt), suggesting a transition towards less humid conditions. (d) Euhedral barite (Brt) crystals often encase bladed and acicular hollandite crystals. (e) Fractures in the ferruginised and silicified Urquart shale often contain banded Mn-oxide fillings. (f) Petrographic relationships are not conclusive in demonstrating whether Mn-oxide precipitation precedes or postdates ferruginisation and silicification of the Urquart shale.

precipitation. The botryoidal textures also indicate that much of the Mn-oxide precipitation occurred in open cavities. This mode of precipitation ensures that the minerals are pure, devoid of hypogene contaminants, and suitable for $^{40}Ar/^{39}Ar$ geochronology.

Scanning electron microscopy reveals the presence of several distinct types of Mn-oxides. Cryptomelane, hollandite, coronatite, and chalcophanite are common in the samples, and they may occur as alternating bands (Fig. 10). Minor lithiophorite is also present. The SEM images also reveal the presence of what can be interpreted as desiccation cracks in the samples (Fig. 10c). These desiccation cracks are often filled with barite (Fig. 10c). In some instances, barite occurs as euhedral crystalline overgrowths on these samples, partially encasing previously precipitated Mn-oxides (Fig. 10d).

Electron microprobe analyses (EMPA) of the Mn-oxide samples (Figs. 11 to 15) clearly identify the presence of chalcophanite, coronadite, cryptomelane, and hollandite in the samples. The EMPA traverses also identify several generations of goethite in the samples (Figs. 11, 14 and 15). Although not the objective of this study, the EMPA results permit a comparison between the relative incorporation of trace elements by iron and Mn-oxides during mineral precipitation (Figs. 11, 14 and 15).

2.1.1.11.2 Geochronology

Four Mn-oxide samples collected at the Mount Isa gossan outcrops were dated by the K-Ar method at UQ, yielding the following results:

Table 4. K-Ar results for samples from the Mount Isa gossan outcrops.

Sample No.	Weight (g)	Wt% K_2O	$^{40}Ar^*$ (cc/g)	*Age (Ma)*	*± 1σ (Ma)*	% Rad
Mn8	0.5791	3.020	1.508×10^{-6}	***15.8***	***3***	16.6
Mn9	0.4475	4.080	2.247×10^{-6}	***17.4***	***4***	12.9
Mn11	0.4451	4.150	2.694×10^{-6}	***20.5***	***2***	28.9
MnPV	0.4665	4.315	2.335×10^{-6}	***17.1***	***1***	28.2

In addition, 15 Mn-oxide grains from six distinct hand specimens were analysed by the laser-heating $^{40}Ar/^{39}Ar$ dating method at the BGC. The results are illustrated in Figs. 17-19. The Mn-oxides $^{40}Ar/^{39}Ar$ results yielded well defined plateau ages ranging from 14.6 ± 0.1 to 21.5 ± 0.3 Ma, consistent with the K-Ar results. Samples analysed in duplicate (Fig. 17, Runs 10006-01 and 10006-02; 10007-01 and 10007-02; 10018-01 and 10018-02) yielded statistically indistinguishable results, attesting to the high quality of the ages obtained. In addition, samples 10006 and 10007 represent the overgrowth and the inner bands of a

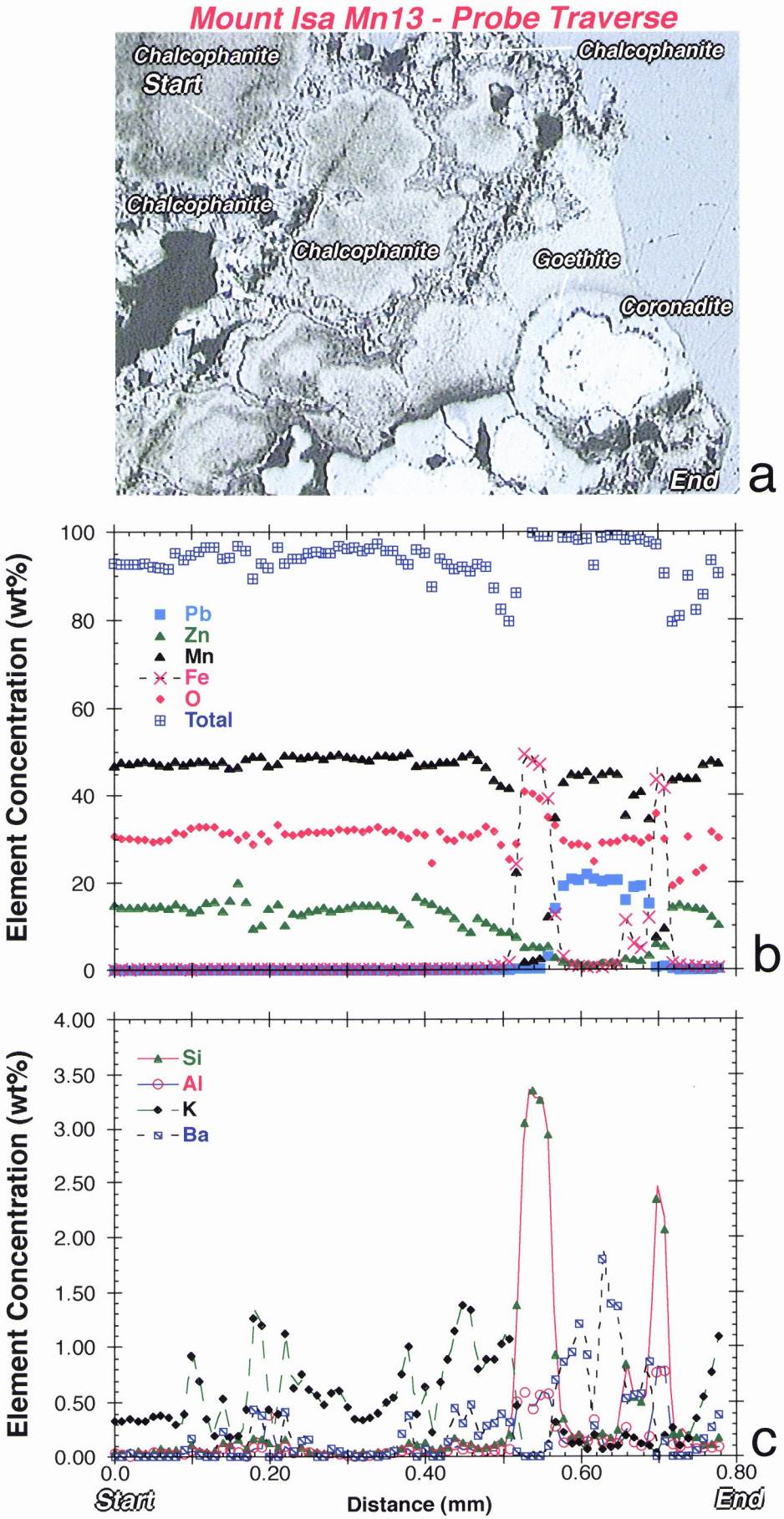

Figure 11. (a) Reflected-light photomicrograph illustrates the distribution of Fe- and Mn-oxides in this sample. Also shown is the location of the EMP (electron microprobe) traverse plotted in (b) and (c). Note the relatively high Si and Al contents of the goethite and the preferential uptake of Pb and Zn by the Mn-oxide phases.

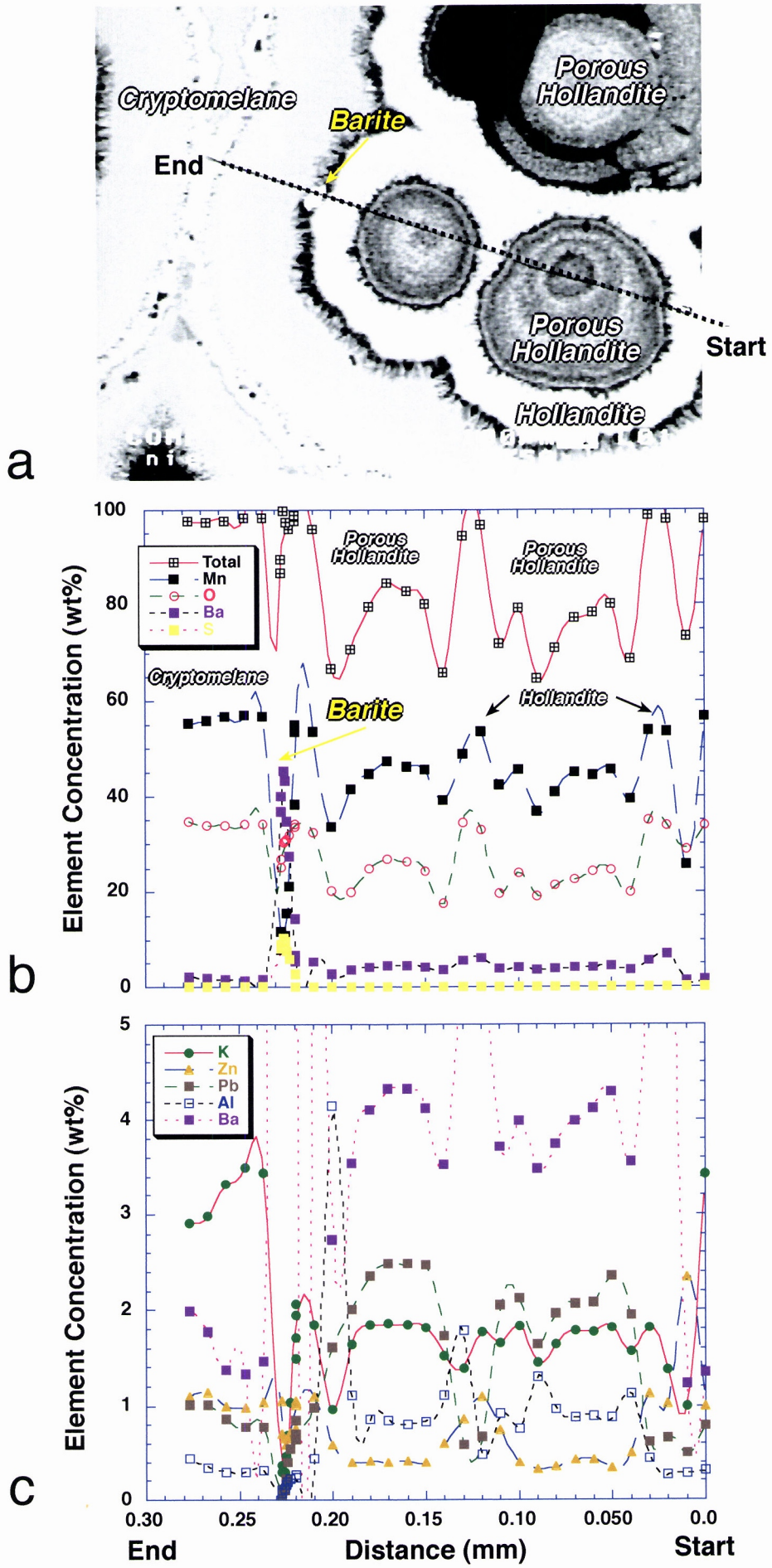

Figure 12. (a) SEM photomicrograph illustrating the botryoidal textures of the supergene Mn-oxides and also illustrating the location of the EMP traverse plotted in (b) and (c). Notice again the early precipitation of the Pb-rich Mn-oxide.

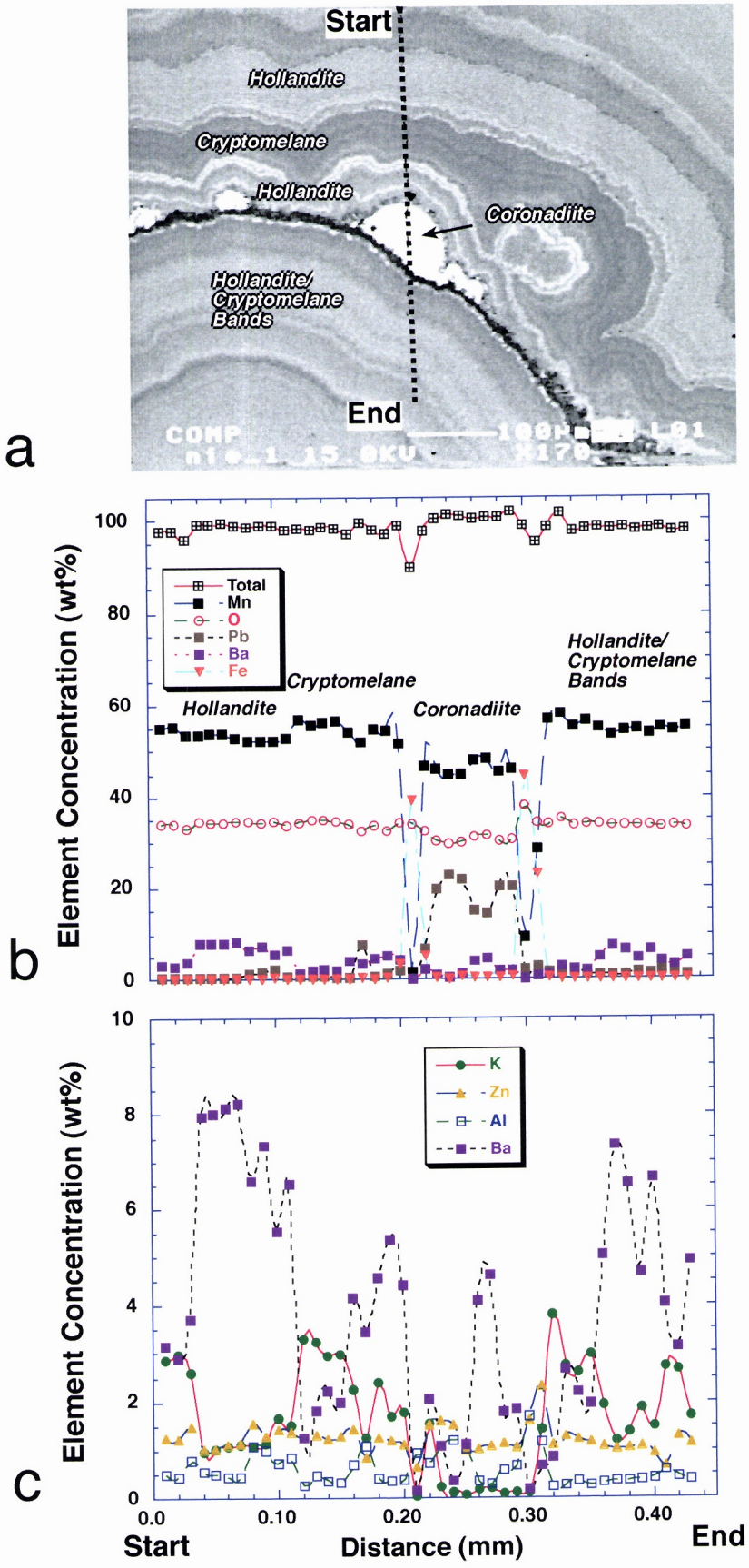

Figure 13. (a) SEM photomicrograph illustrating the botryoidal textures of the supergene Mn-oxides and also illustrating the location of the EMP traverse plotted in (b) and (c).

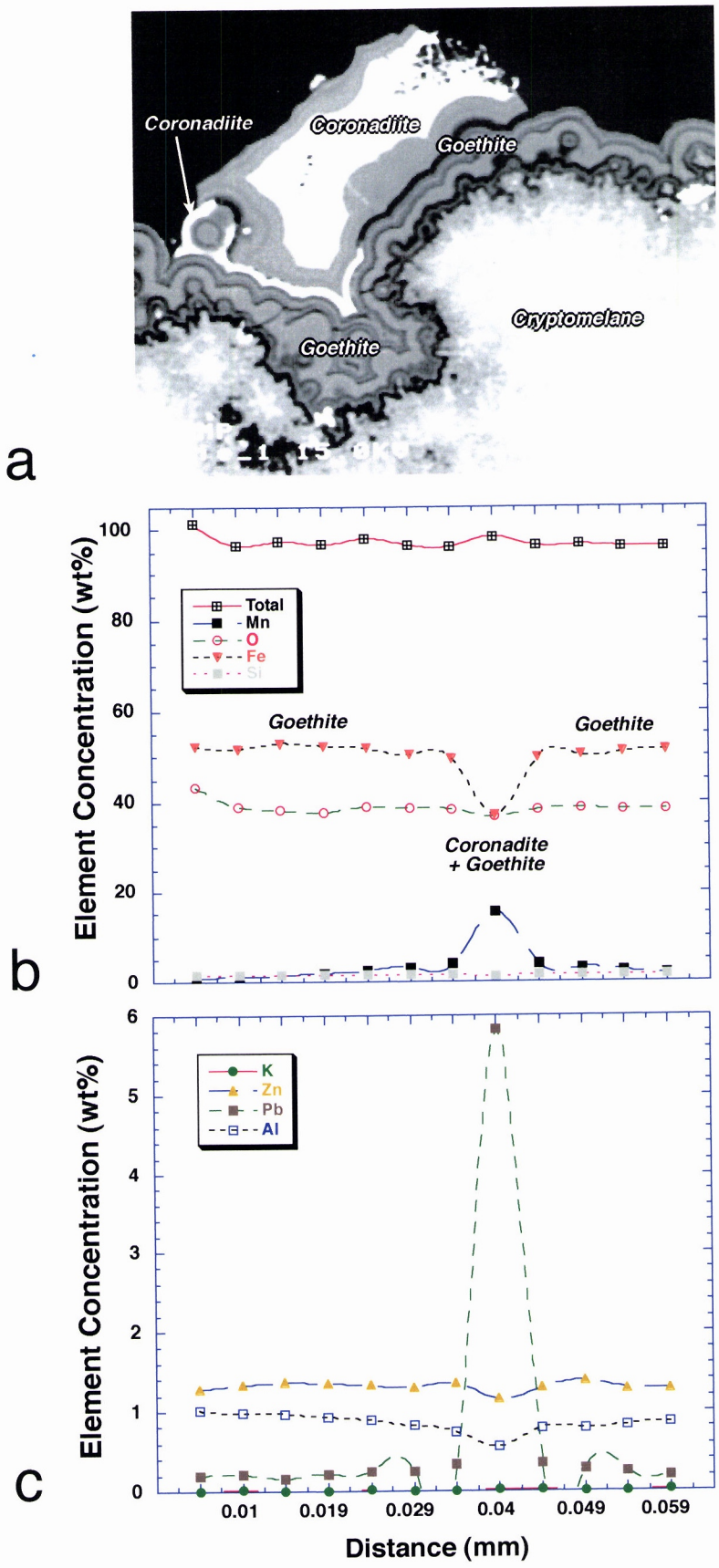

Figure 14. (a) SEM photomicrograph illustrating the botryoidal textures of the supergene Fe- and Mn-oxides; (b) and (c) illustrate the composition of the goethite in this sample. Notice the dramatic increase in Pb content with an increase in the Mn-content of the analysis.

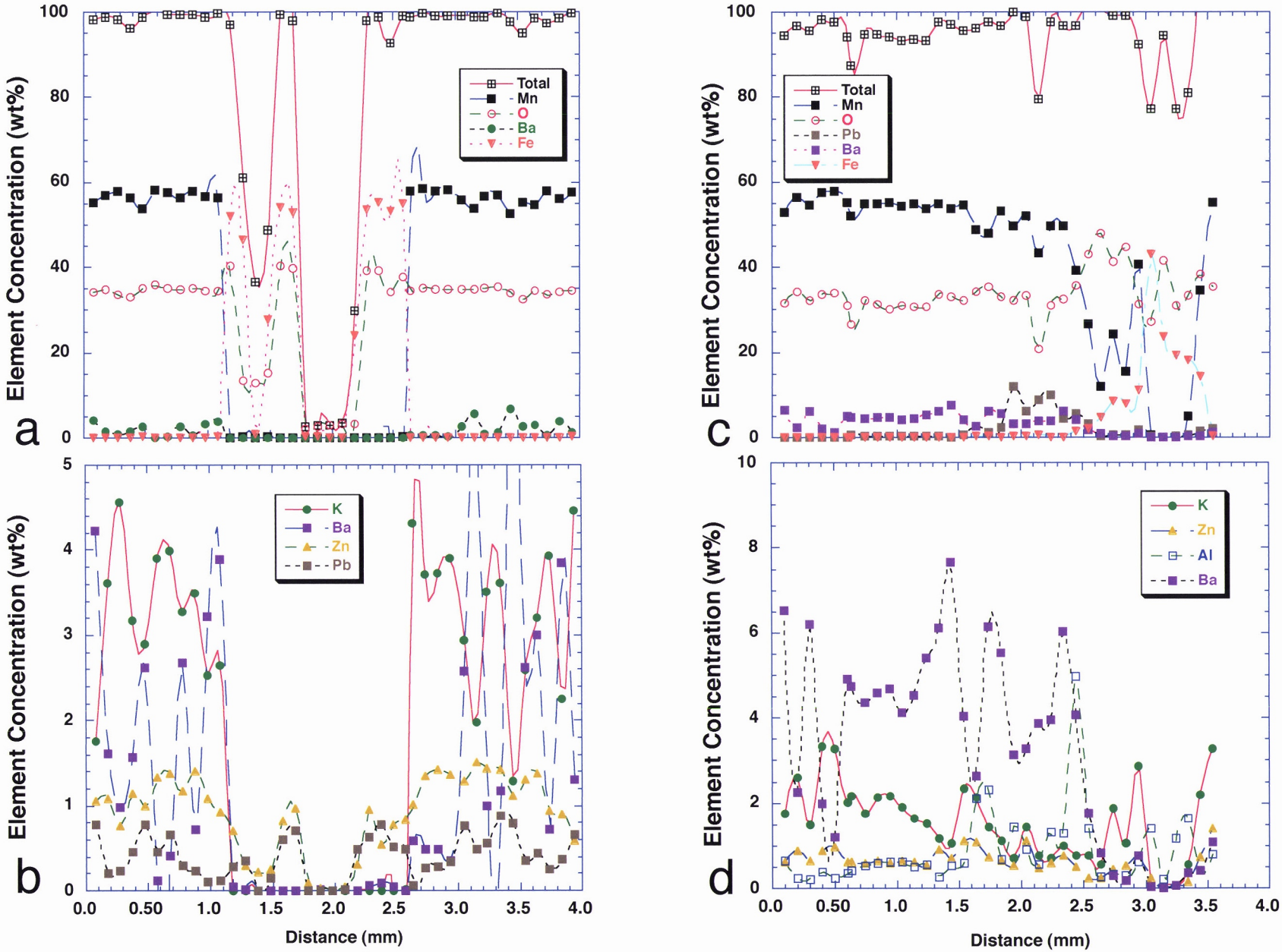

Figure 15. (a) Major and (b) minor element distribution as measured by the EMP analyses of Mount Isa Gossan Mn-oxide. The large drop in totals in the center is attributed to the presence of an open cavity in the sample. This traverse also illustrates the preferential uptake of Zn and Pb by Mn-oxides when compared to Fe-oxides, although this preferential uptake is less dramatic than observed in previous samples. (c) Major and (c) minor element distribution as measured by the EMP analyses of Mount Isa Gossan Mn-oxide.

botryoidal Mn-oxide crust. The older inner growth (Runs 10007) and the younger overgrowth (Runs 10006) further confirm that the results obtained can be interpret as true precipitation ages for the Mn-oxide samples. One sample (runs 10056-01 and 10056-02) yielded two very different ages for two grains analysed. Since these grains were separated from a large crushed piece of the Mount Isa gossan, they likely represent different generations of Mn-oxide present in these outcrops. The results obtained by the K-Ar and $^{40}Ar/^{39}Ar$ analyses indicate that the most significance timing of Mn-oxide precipitation in the Mount Isa gossans was early to middle Miocene.

However, two samples yielded disparaging results. Two grains from sample Mn-13, (runs 10038-01 and 10038-02), collected at a high elevation (~380m) point of the Mount Isa gossan outcrop next to the copper smelter, do not yield plateaus. Both age spectra obtained climb from ca. 40 Ma to ca. 65 Ma. These results were not obtained from any other sample in the area, and must be independently confirmed before further interpretation. However, if these older ages are confirmed in further studies, they have important implications to the genesis of the weathering profiles in the area, as will be discussed at the end of this report.

One other disparaging result obtained was a "zero-age" plateau (-1.1 ± 6.2 Ma) obtained for a Mn-oxide sample collected by a student (Tara Herlihy) on the grounds next to the sidewalk on the MIM barracks. This sample comes from the lowest elevation site sampled in the area. Zero-age plateaus may indicate either that the mineral precipitated in the last ~ 200,000 years (the lowermost resolution of the dating method for Mn-oxide samples) or that the mineral contains virtually no K. Since this sample was not studied in detail by electron microprobe analyses, the result must be interpreted with care.

2.1.2 Mount Isa Mines Drill Core (Z625 ED1)

2.1.2.1 Site Selection Criteria: availability of drill-cores intercepting weathering profile overlying significant Pb-Zn orebodies.

2.1.2.2 Location: 341823E-7707558N

2.1.2.3 Elevation: 280-300 m

2.1.2.4 Geomorphologic setting: Dissected terrain proximal to 400-520 m mesas.

2.1.2.5 Geomorphologic Regime: Erosional.

2.1.2.6 Sample in Relation to Landscape Position: Jarosite precipitated in saprolite present in dissected terrain.

2.1.2.7 Sample in Relation to Regolith: Jarosite crystals filling fractures in weathered shales (lower saprolite).

2.1.2.8 Datable Minerals/Host Rock Relationship: Influx of elements, in solution, from outside sources located at stratigraphic positions equivalent to or higher than the deposition site.

2.1.2.9 Sources of Elements (jarosites): Sulphur and Fe are derived from weathering pyrite; Pb and Zn are derived from weathering galena and sphalerite, respectively; Al and K are derived from feldspars and micas.

2.1.2.10 Overview

In addition to Mn-oxides, the weathering profiles overlying the Mount Isa deposit host jarosite suitable for $^{40}Ar/^{39}Ar$ geochronology. These jarosite occurrences were studied by optical microscopy and by SEM/EMPA. Six distinct jarosite samples were dated by the laser-heating $^{40}Ar/^{39}Ar$ method at the BGC and the results are discussed below.

2.1.2.11 Results

2.1.2.11.1 Electron Microprobe and SEM Analysis

SEM investigation of jarosite samples shows that most of the jarosite occurs as free crystals and crystalline aggregates filling cavities (Fig. 16). The euhedral jarosite crystals range from 10 to 1000 μm diameter crystals (Fig. 16). The larger jarosite single crystals are ideal for $^{40}Ar/^{39}Ar$ geochronology. Several of these grains were separated and irradiated for $^{40}Ar/^{39}Ar$ dating.

EMPA of several jarosite samples are provided in the electron microprobe table at the end of this report. One traverse is plotted in Fig. 16. The traverse illustrates a fairly homogeneous distribution of the main elements in the jarosite, which also displays a relatively high K content (~ 7wt%). The only significant variations in composition are associated with varying Pb contents, which partially replaces K in the A-site, and Al, which partially replaces iron in the B-site (Fig. 16c). There is a positive correlation between Pb and Al in the samples, indicating that they show a coupled substitution in the jarosite structure. Phosphorous replacing S may also be coupled to the Pb and Al substitutions, although the electron microprobe results are less conclusive (Fig. 16c).

2.1.2.11.2 Geochronology

Jarosite results are plotted, together with the Mn-oxide results, on the ideogram below (Fig. 24). $^{40}Ar/^{39}Ar$ dating of six jarosite grains from two drill-core samples yielded dates ranging from 0.5 to 3 Ma, with the exception of one sample which yielded a 13 Ma date. The jarosite results indicate that sulphates precipitated at the lower parts of the weathering profiles are much younger than the Mn-oxide samples found in outcrops. This is consistent with the downward propagation of weathering fronts. The results are also consistent with current understanding of the chemistry of these supergene minerals. Supergene sulphates are much more soluble and prone to dissolution-reprecipitation reactions with weathering solutions than supergene Mn-oxides. Therefore, when present in the same system, supergene sulphates will in general record younger ages than supergene Mn-oxides found in the same profiles. In some areas, the

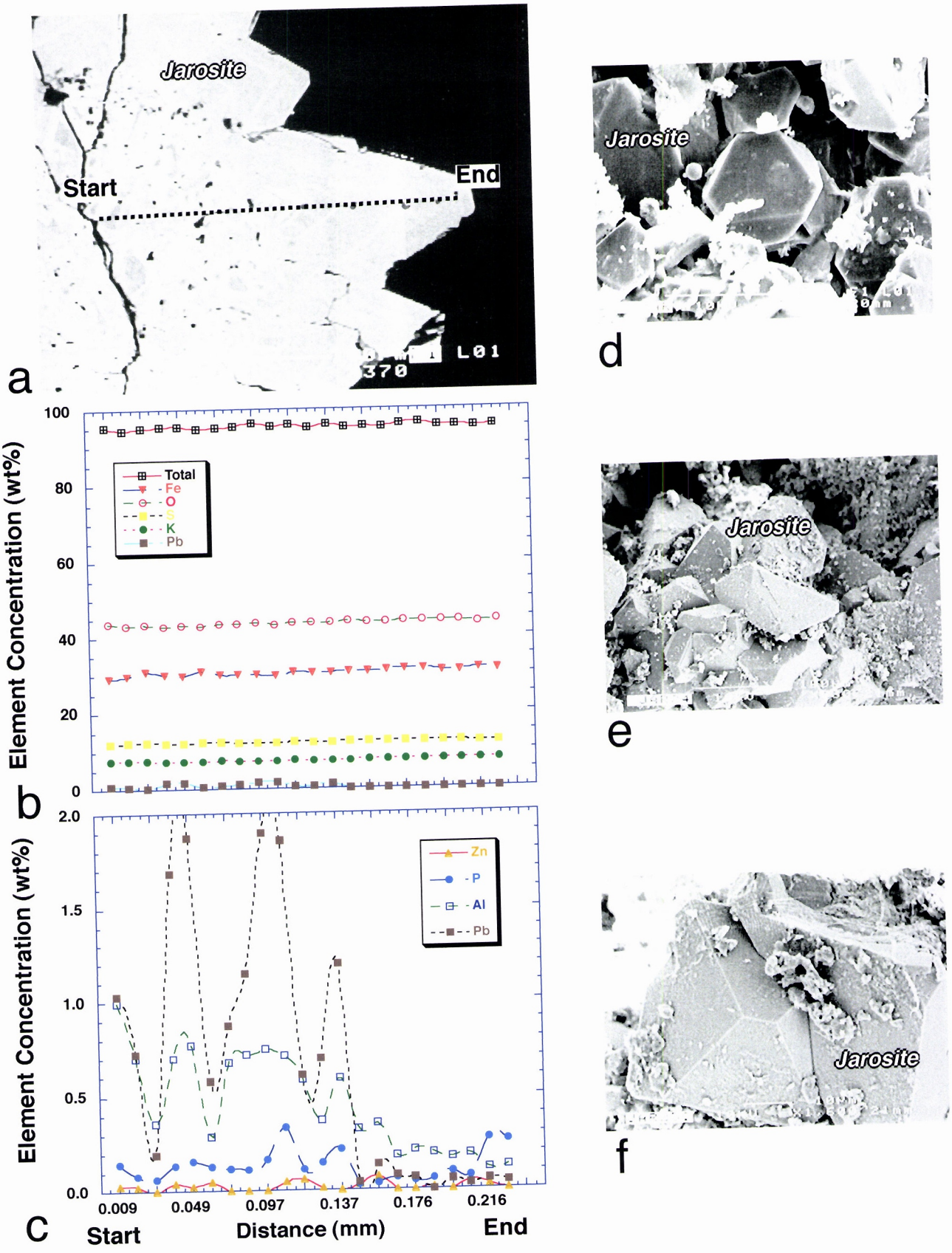

Figure 16. (a) SEM photomicrograph of jarosite crystal illustrating the location of the EMP traverse shown in (b) major elements and (c) minor elements; (d), (e), and (f) illustrate the size and the morphology of the jarosite crystals analysed by the $^{40}Ar/^{39}Ar$ method in this study.

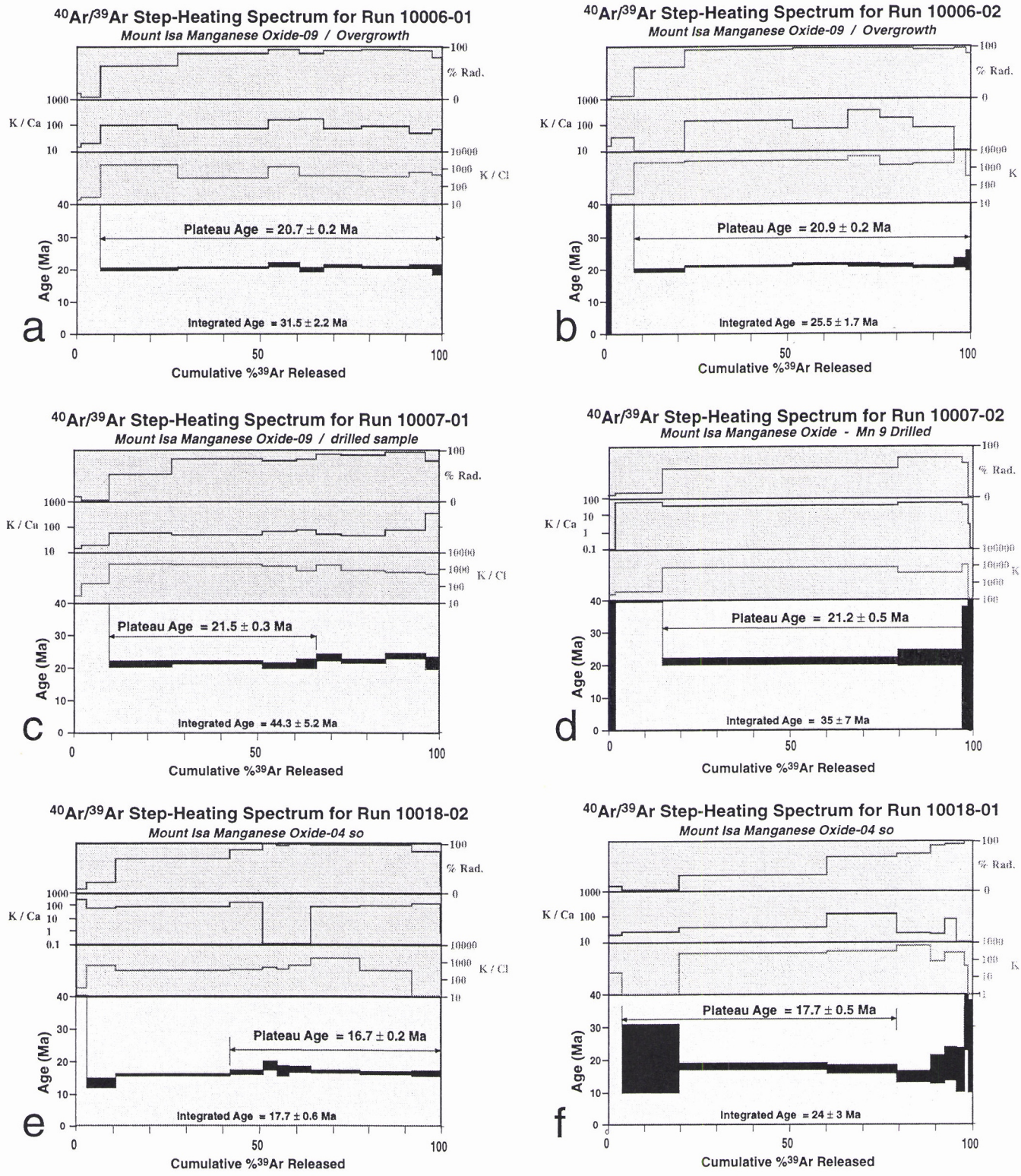

Figure 17. (a) and (b) Ar/Ar step-heating spectra for Mount Isa Gossan Mn-oxide samples. Notice the reproducible results obtained for the analyses of two grains from the same sample. The same is also true for the samples analysed in duplicate and illustrated in (c)-(d) and (e)-(f). The step-heating spectra also show that the inner bands (c)-(d) of the botryoidal Mn-oxide sample is older than the outer bands (a)-(b), consistent with the paragenesis observed.

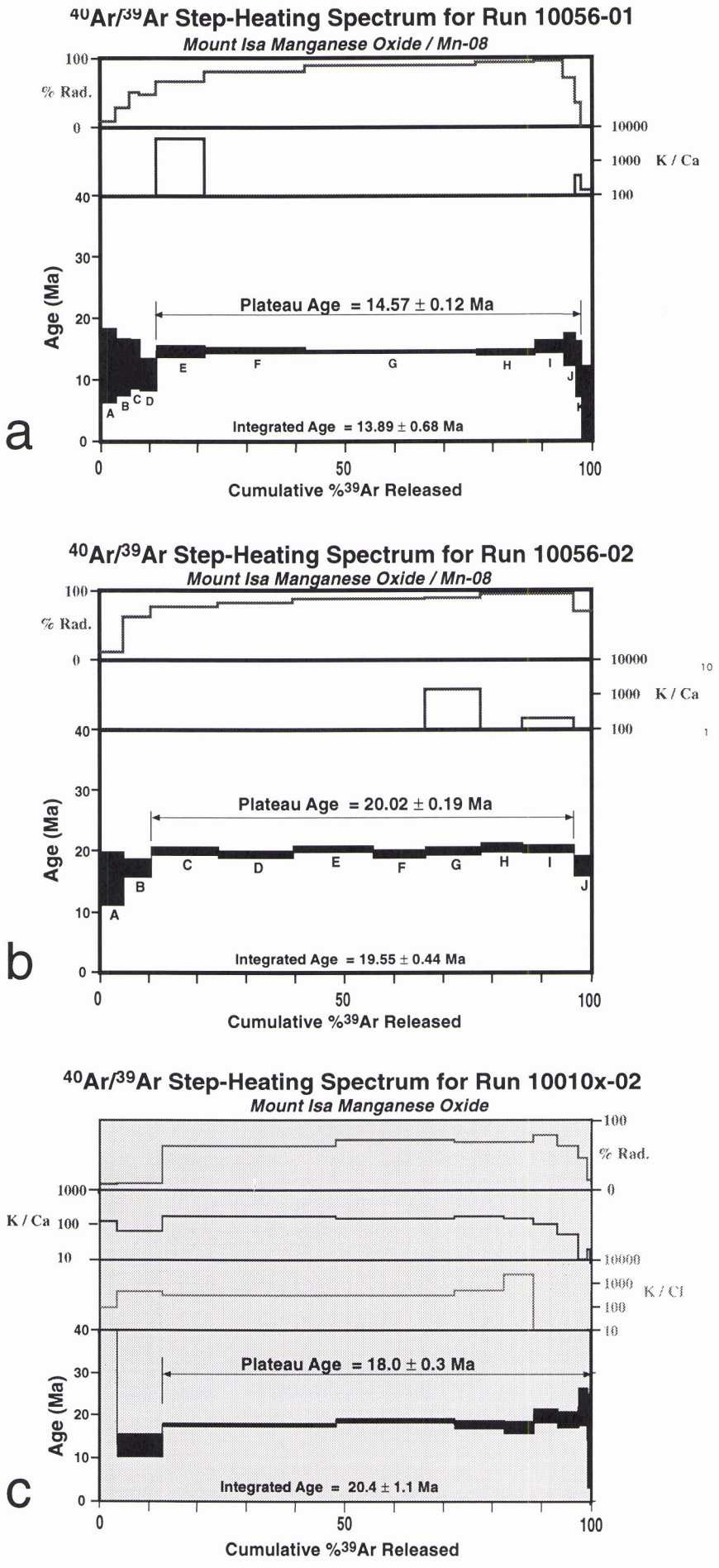

Figure 18. Well defined plateaus for Mn-oxide samples from the Mount Isa gossan show that the ages of precipitation of botryoidal samples may span several million years, consistent with results obtained from supergene Mn-oxide samples elsewhere (Vasconcelos *et al.*, 1992 and 1994; Dammer *et al.*, 1996).

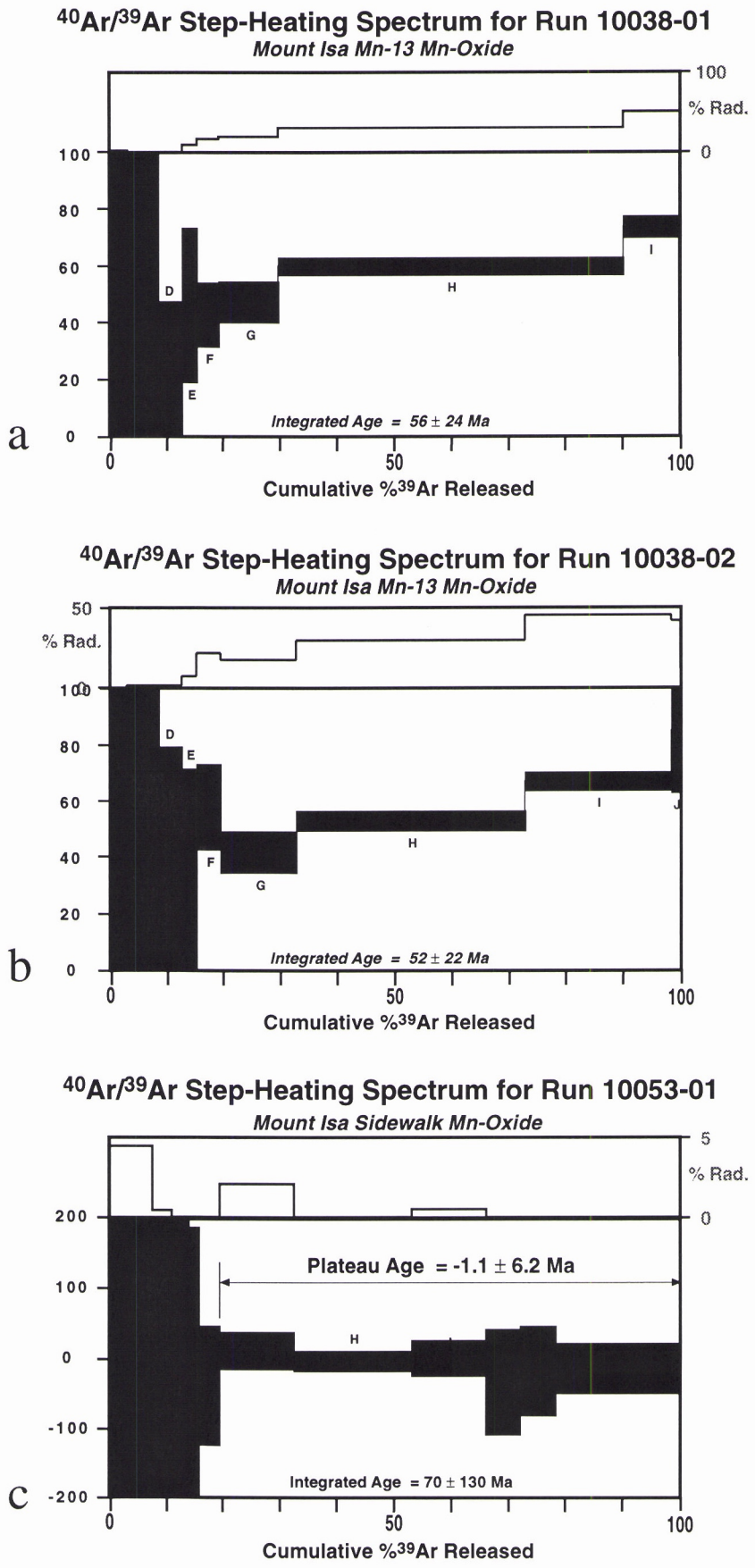

Figure 19. (a) and (b) Reproducible, but poorly defined climbing spectra obtained from two grains from a Mn-oxide sample collected at the highest elevation outcrop of the Mount Isa gossan, next to the Cu-smelter. The older ages implicit in these two climbing spectra need further validation. (c) The "zero-age" obtained for the Mn-oxide sample collected next the Mount Isa Mines Exploration barrack could reflect very recent (ca. 250,000 years) precipitation of Mn-oxides in the area. Alternatively, the zero-age could reflect lack of K in the sample. Since no EMP analyses were obtained for this sample, it is presently impossible to decide between the two alternatives.

Mn-oxides may indicate the timing of most moisture availability, while supergene sulphates may indicate timing of transition towards more arid conditions.

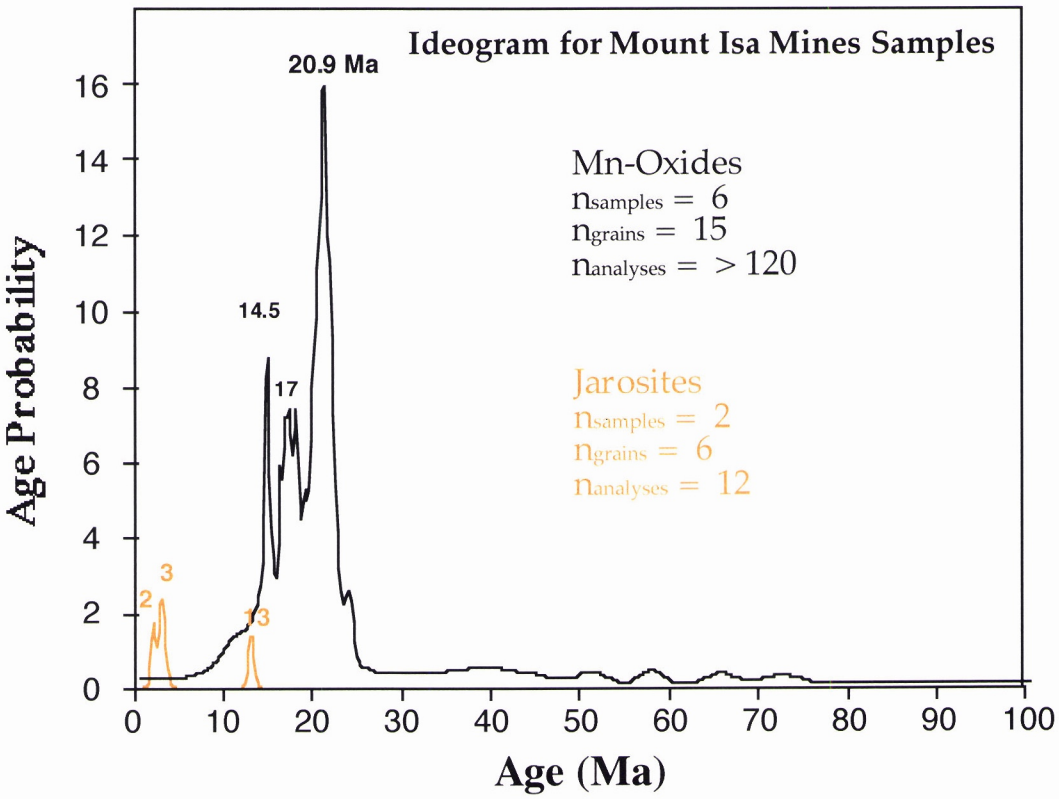

Figure 20. Ideogram illustrating the distribution of ages for the Mount Isa weathering profiles samples (Mn-oxide analyses in balck, jarosite analyses in grey), indicating an early Miocene "most probable" age for the precipitation of Mn-oxides in this area.

2.1.3 Lake Moondarra Prospect (Figs. 8 and 20)

2.1.3.1 Site Selection Criteria: significant gossan in area of active exploration for Mount Isa-type copper orebody.

2.1.3.2 Location: 354500E-7723600N

2.1.3.3 Elevation: 320 m

2.1.3.4 Geomorphologic Setting: dissected terrain proximal to 400-520m mesas.

2.1.3.5 Geomorphologic Regime: erosional.

2.1.3.6 Sample in Relation to Landscape Position: Mn-oxide filling void spaces in hydrothermal fault breccia in a dissected valley surrounded by 400m high ridges.

2.1.3.7 Sample in Relation to Regolith: the samples are present in the lower saprolite to saprock transition zone.

2.1.3.8 Datable Minerals/Host Rock Relationship: local recrystallisation of minerals with major textural disruption.

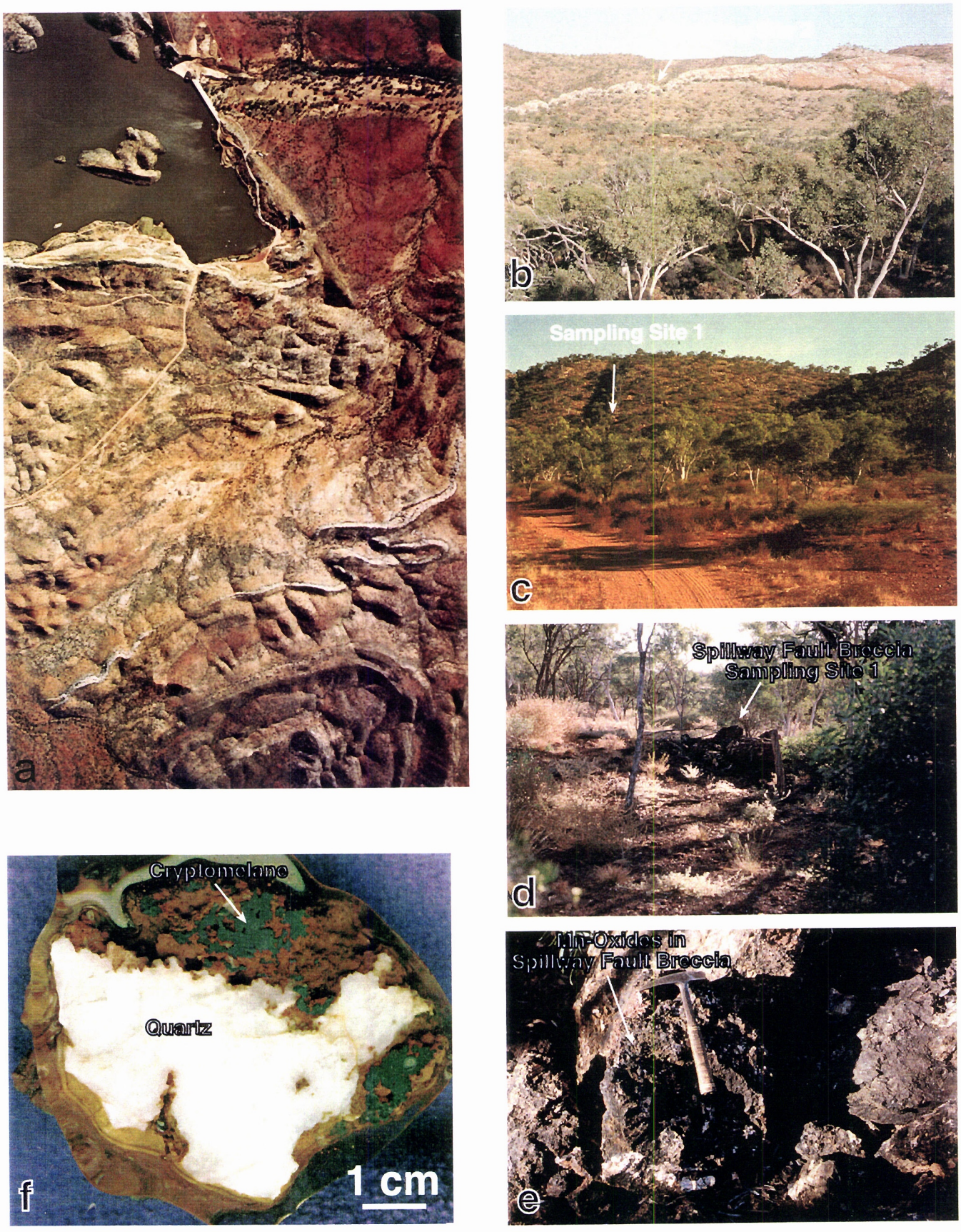

Figure 21. (a) Airphoto illustrating the terrain in the Lake Moondarra prospect and the location of the weathering profiles sampled in the area. (b) Photograph facing SE, as shown in (a), illustrates sampling site 2. (c) Photograph facing WSW, as shown in (a), illustrates sampling site 1. (d) Spillway Fault breccias are enriched in the Fe- and Mn-oxides sampled for this study. (e) Close-up showing the strongly deformed, sheared, and silicified conglomerate which constitutes the Spillway Fault breccias. (f) This hand-specimen illustrates the distribution of botryoidal cryptomelane on silicified vein from the Spillway Fault.

2.1.3.9 Sources of Elements: void spaces are the result of dissolution of sulphides and/or carbonates during weathering. The Mn-oxides are precipitated on quartz and are associated with iron oxides. Manganese is probably derived from weathering carbonates hosted by the fault breccias and hydrothermal veins, K is derived from feldspars and micas in the host rock.

2.1.3.10 Overview

In the Lake Moondarra area, oxidised fault breccias associated with the Spillway Fault host Mn-oxide samples in a similar topographic/geomorphologic setting as those found in the Mount Isa gossan (Figs. 8 and 20). The outcrops occur in the low lying areas in the landscape, where deformation associated with the Spillway Fault has made the local lithologies more erodable. Mn-oxides precipitated in cavities in these gossans (Fig. 20) were irradiated and analysed by the $^{40}Ar/^{39}Ar$ method. Samples from this area should provide good constraints on the results obtained for the Mn-oxide samples from the Mount Isa gossan. Given the geographical proximity and similar geomorphologic setting, similar results should be expected from both areas.

2.1.3.11 Results

2.1.3.11.1 Electron Microprobe and SEM Analysis

Samples from this outcrop were only described petrographically and by SEM investigation. No electron microprobe analyses were performed.

2.1.3.11.2 Geochronology

Three Mn-oxide grains from one hand specimen were analysed by the laser-heating $^{40}Ar/^{39}Ar$ method at the BGC. The results are illustrated in Fig. 21. The three grains analysed yielded reasonably well defined plateau ages of 19.0 ± 0.4, 19.7 ± 0.1, and 20.7 ± 0.3 Ma. The plateau and integrated ages for the three grains are also concordant. In addition, the isochron age obtained for the three grains, 19.76 ± 0.05 Ma, is also concordant with the plateau and integrated ages. Finally, as illustrated by the ideogram below, the samples analysed at the BGC yield two "most probable" age peaks, one at 19.5 Ma and the other at 20.7 Ma.

To add to these results, 7 grains from two distinct hand specimens were dated at the UQ-AGES Laboratory. The samples yielded well defined plateaus ranging from 17.2 ± 0.2 to 24.0 ± 0.7 Ma (Figs. 22 and 23). The ideogram above indicates that the most probable age for the samples is also 20.7 Ma.

In addition to the results presented here, Mn-oxide samples from a second outcrop from the Lake Moondarra prospect were subsequently analysed at the UG-AGES laboratory. The

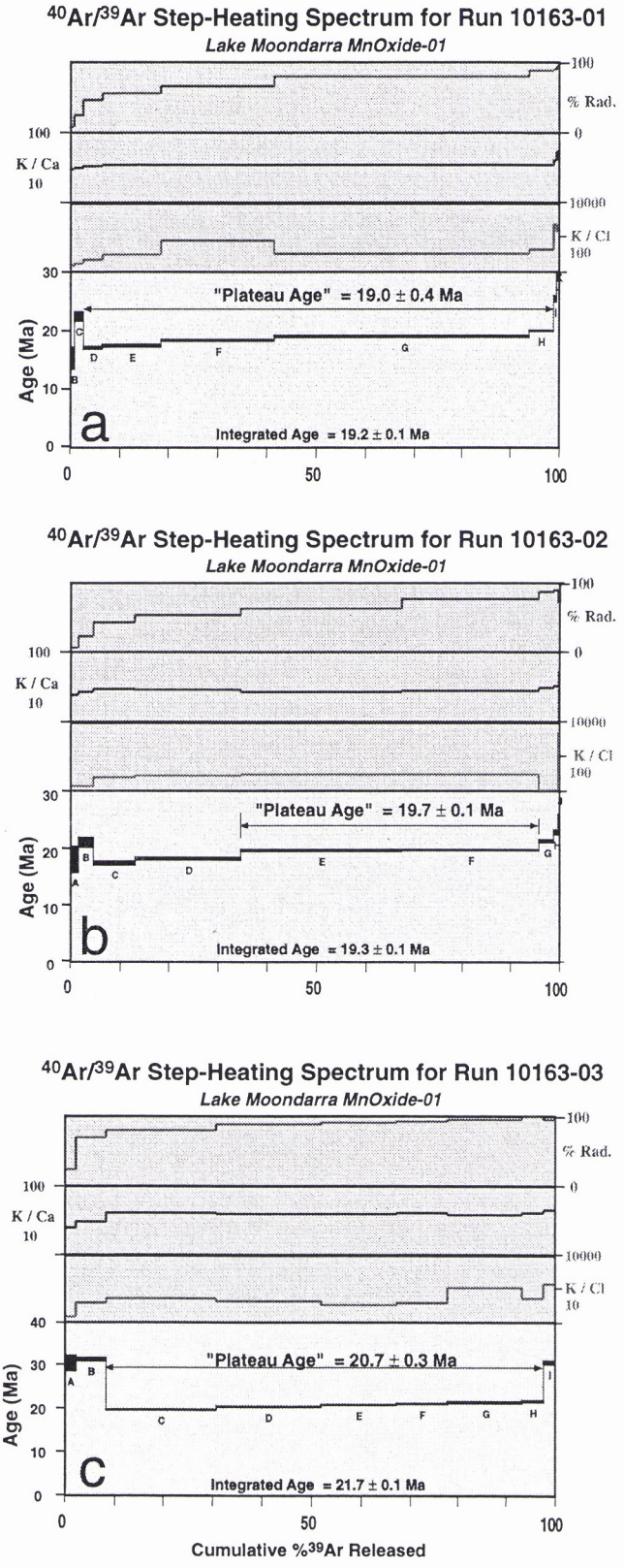

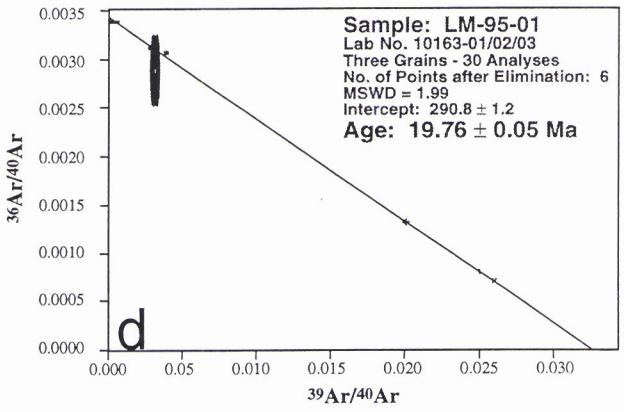

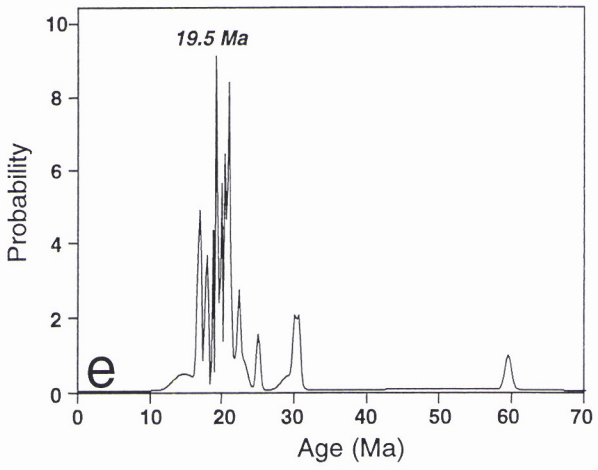

Figure 22. Laser-probe Ar/Ar step-heating spectra (a-c) for three grains of botryoidal Mn-oxides collected from the Spillway Fault breccias (analyses performed at the BGC). The plateaus are very consistent, suggesting a Miocene precipitation age for the Mn-oxide samples. The ages obtained for these samples is consistent with the ages obtained from the Mount Isa Mines gossan samples. (d) The isochron age and the intercept obtained for the samples is consistent with the plateau ages and with an atmospheric intercept, further confirming the suitability of these samples for weathering geochronology. (e) Ideogram illustrating the "most probable" age for the sample studied.

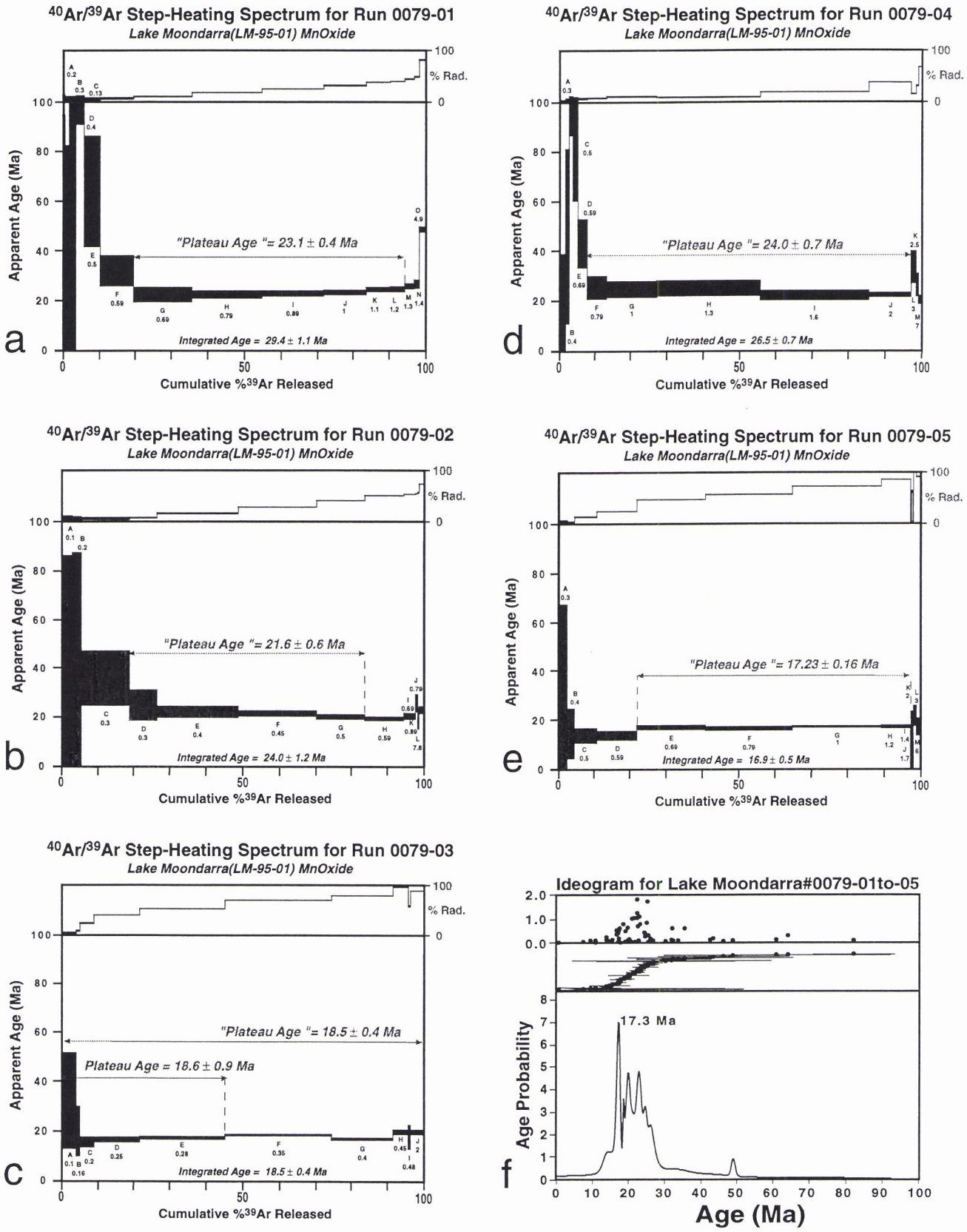

Figure 23. Laser-probe $^{40}Ar/^{39}Ar$ step-heating spectra ((a), (b), (c), (d) and (e)) for five grains of botryoidal Mn-oxides collected from the Spillway Fault breccias (analyses performed at UQ-AGES). The results show a larger spread than results of samples analysed at the BGC; however, the ages are still consistent with the BGC ages and with the range in ages obtained for Mount Isa Mines Gossan samples, indicating a Miocene age for the precipitation of Mn-oxides in this system. The probability plot (f) for all the analyses (a-e) yields a similar ideogram as obtained for the samples in Figure 21, although the most probable peak is shifted toward a slightly younger age due to the very precise steps obtained in Run 0079-05.

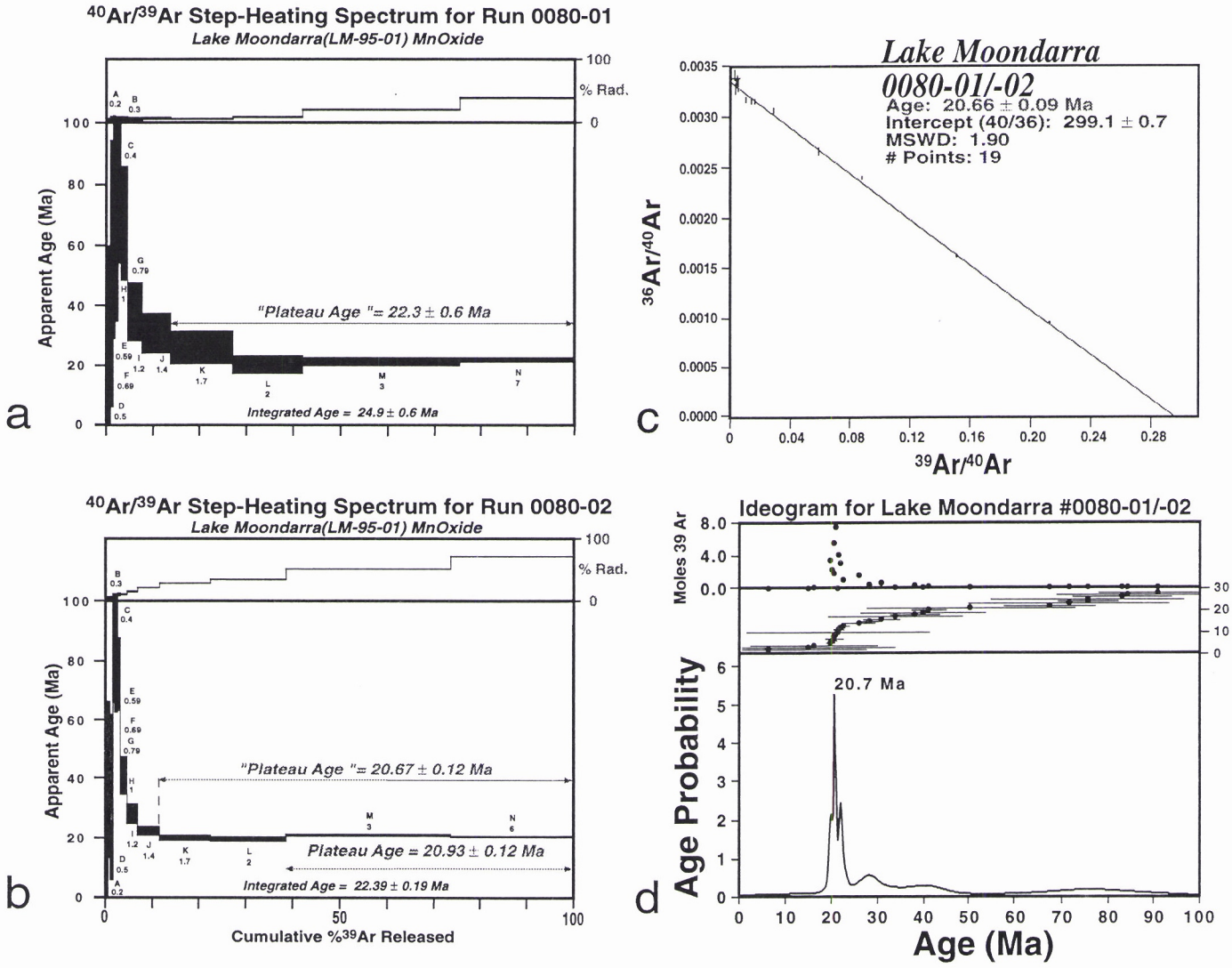

Figure 24. Laser-probe $^{40}Ar/^{39}Ar$ step-heating spectra (a-b), isochron (c) and ideogram (d) for two additional grains from a different outcrop at the Spillway Fault breccias. The ages obtained are also consistent with previous results.

plateau ages obtained for two grains from one hand specimen, 15.2 ± 1.2 and 16.0 ± 1.7 Ma, are also consistent with the youngest ages obtained for the Mount Isa gossan outcrops.

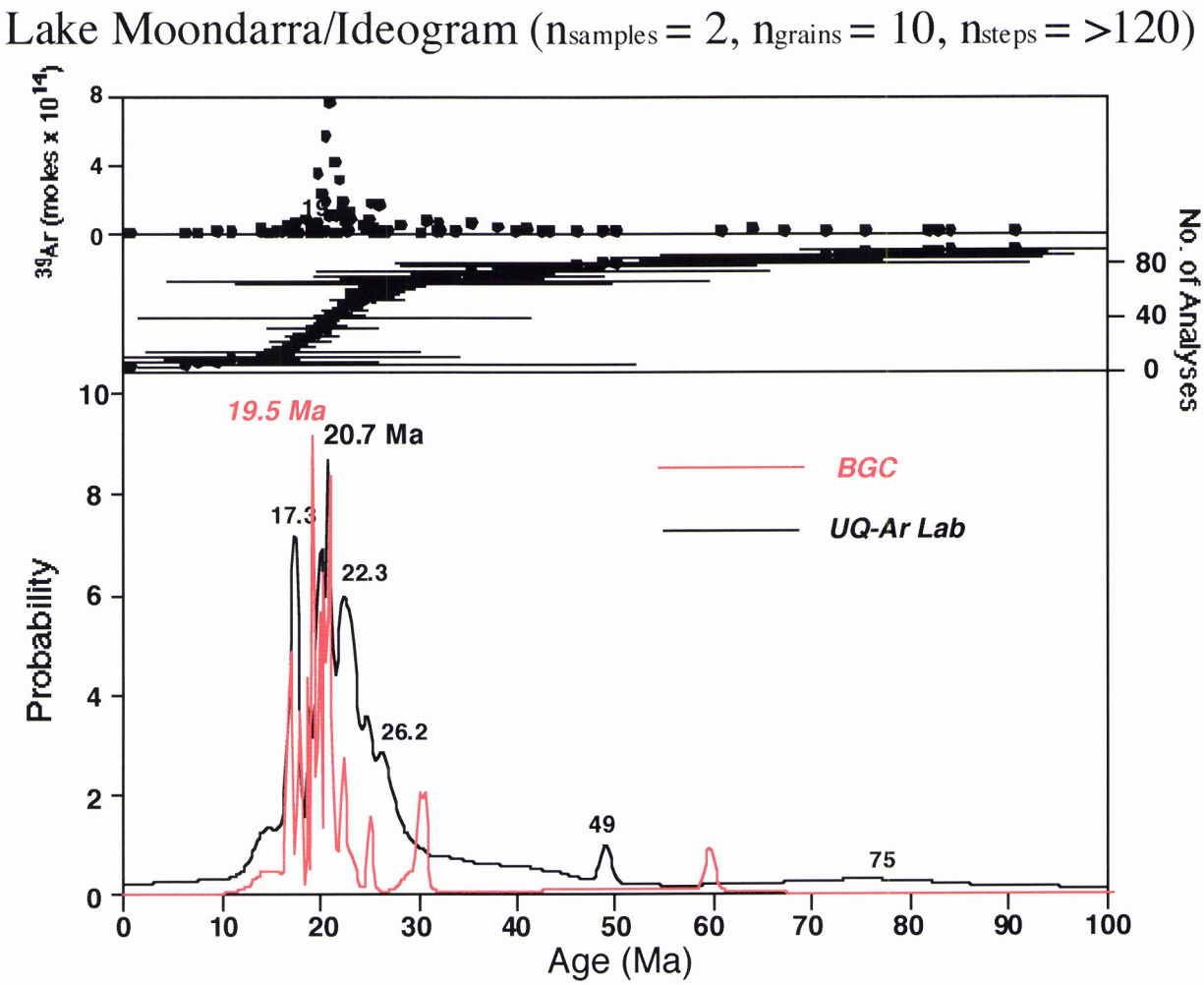

Figure 25. Ideogram illustrating the distribution of ages for the Spillway Fault breccias Mn-oxide samples (BGC analyses in red, UQ-AGES analyses in black), indicating an early Miocene "most probable" age for the precipitation of Mn-oxides in this area.

2.1.4 Discussion - Mount Isa City and Vicinity

The predominance of Miocene weathering ages for all the samples from the Mount Isa area and vicinity imposes some constraints on landscape evolution models applicable to the region. Since only the dissected part of the landscape yielded samples suitable for geochronology, and since both sites studied are located in areas characterised by erosional regimes, the ages obtained must be interpreted as the minimum age of formation of the weathering profiles in the region. There are several possible scenarios to explain the predominance of Mn-oxides preserving Miocene ages in the present surface. These will be discussed at the end of the Mount Isa Region section.

The absence of complete weathering profiles in the Mount Isa area and vicinity either suggests that these profiles never existed in the region or that the profiles once present have now been eroded. The local occurrence of fragments of ferruginous duricrusts and loose pisoliths suggests that the second hypothesis is more likely. If lateritic duricrusts were once present in this area, the second important question is whether these duricrusts blanketed the whole region or whether they were preferentially developed on more suitable lithologies. These questions will also be at the end of the Mount Isa Block section.

The presence of Pb- and Zn-bearing Mn-oxides of Miocene ages may indicate that Miocene weathering conditions were conducive to the large scale dissolution, transport and reprecipitation of base metals in the weathering profiles. An alternative hypothesis is that dissolution, transport, and reprecipitation of metals in the weathering profiles occurs at a constant rate throughout the weathering history of a region. The presence of Miocene ages Pb- and Zn-bearing Mn-oxides at the surface today simply indicate that erosion has exposed at the present surface the groundwater levels where those reactions were occurring during the Miocene. I will discuss the likelihood of either scenario later in this report.

Irrespective of the modes of evolution of the weathering profiles in the Mount Isa area and vicinity, the electron microprobe analyses of Mn-oxides from outcrops in these areas clearly suggest that these minerals strongly fractionate base metals. The enrichment of Mn-oxides in base metals, as compared to the bulk samples, co-existing iron oxides, clay minerals, and other supergene phases, suggests that the crystal chemistry of the Mn-oxides may be an useful indicator of underlying mineralisation, as previously suggested by Taylor and Scott (1982).

2.2 Western Succession

The region NNW of the Mount Isa city, particularly around the Buckley River valley, was subject to intensive studies by CRCLEME participants to AMIRA P417 (Anand et al., 1996). To complement their geochemical and regolith mapping studies, two areas in the Kennedy Gap sheet were chosen for weathering geochronology.

The main characteristic of the weathering profiles in the Kennedy Gap area is the more noticeable distribution of ferruginous duricrusts and silcretes and the widespread presence of lateritic gravels in colluvial deposits and stream channels. Similarly to the Mount Isa area, this region is also characterised by 450-500 m elevation ridges, oriented NS. These ridges are also formed on the more resistant lithologies, such as quartzites, while metamorphosed shales and basalts underlie the more dissected parts of the landscape. While the dissected parts of the landscape are undergoing active erosion in the present regime, two features distinguish the Buckley River valley from the Mount Isa area: the valley bottoms in the Kennedy Gap area sit at 400 m elevation, as opposed to the 300 m elevation prevalent in the Mount Isa area; and, in some areas, the dissected valleys still host remnants of lateritised duricrust, as exemplified by the Mesa 1 outcrop investigated in this study (Anand et al., 1996).

2.2.1 Mesa 1 Outcrop (Kennedy Gap)

2.2.1.1 Site Selection Criteria: Mn-oxides present in a relict, deeply weathered, mesa. The relict regime suggests that weathering in this area may have predated weathering in the dissected valleys sampled at Mount Isa. This site was also studied in detail by CRCLEME (Anand et al., 1996) researchers and the mining of road metal provided access to the lower parts of the weathering profile.

2.2.1.2 Location: 324605E-7755409N

2.2.1.3 Elevation: 410-430 m

2.2.1.4 Geomorphologic Setting: plateau remnant in dissected valley.

2.2.1.5 Geomorphologic Regime: relict.

2.2.1.6 Sample in Relation to Landscape Position: Mn-oxide coating quartz and filling void spaces in a hydrothermal vein which cross cuts the mesa. The vein extends from the exposed saprolite to the mega-mottled zone and ferruginous duricrust (Figs. 26e and g). The samples analysed were derived from a relic part of the landscape.

2.2.1.7 Sample in Relation to Regolith: the samples occur in the upper saprolite to mottled-zone transition.

2.2.1.8 Datable Minerals/Host Rock Relationship: Mn-oxide filling void spaces and fractures in hydrothermal quartz, suggesting local recrystallisation of minerals with major textural disruption (Figs. 26f-i).

2.2.1.9 Sources of Elements: Mn is probably derived from weathering carbonates and/or silicates hosted by the fault breccias/hydrothermal veins, K and Ba are derived from feldspars and mica in the host rock.

2.2.1.10 Overview

A small isolated mesa capped by ferruginous duricrust and a mottled zone was studied in detail by CRCLEME (Anand et al., 1996) (Fig. 26). Additional geochemical results were presented in the Mount Isa field trip guide for AMIRA P417.

At the southern end of the mesa, mining for road metal exposed a section of the underlying saprolite, where small quartz veins can be traced all the way to the mesa surface (Fig. 26). These quartz veins were coated by small encrustations of Mn-oxides. Mn-oxides in the samples are not very abundant and are intimately intergrown with the host quartz and silicate minerals (Fig. 26f-i). However, some samples display clean, visually pure, botryoidal Mn-oxides. Given the wealth of geochemical information for the outcrop and the unique geomorphologic setting for the mesa, I considered it worthwhile to attempt to date these marginally suitable Mn-oxide samples.

2.2.1.11 Results

2.2.1.11.1 Electron Microprobe and SEM Analysis

Petrographic investigations and SEM/EMP analyses (Figs. 26, 27 and 28) indicate that the Mn-oxides in these samples are composed essentially of hollandite and cryptomelane. The EMP analyses indicate that the Zn and Pb content is low, as compared to other Mn-oxides in the Mount Isa region. However, the Co contents of the Mn-oxides may reach up to 2.5wt%. The significance of this high Co content will be discussed later.

The petrographic and SEM/EMP work also shows that the areas of pure Mn-oxides are small (generally less than 0.5mm), which requires great care in sampling to avoid the contamination of the Mn-oxides by fragments of unweathered primary quartz and possibly micas.

2.2.1.11.2 Geochronology

Twenty-five Mn-oxide grains extracted from 8 distinct samples of MnOx-bearing quartz veins were dated by the laser-heating $^{40}Ar/^{39}Ar$ method at the UQ-Ar Lab (Figs. 29-36). Among the 25 grains analysed, only 15 yielded well defined plateaus. In addition, the plateau ages obtained varied from 13.2 ± 0.9 to 38.7 ± 0.6 Ma. Plateau, isochron, and ideograms for each sample are illustrated in Figures 28 to 35. Despite the scatter in this data set, the ages obtained are not random.

The youngest plateau age obtained (a very well defined plateau at 13.2 ± 0.9 Ma, Fig. 35c) is consistent with the youngest Mn-oxide ages obtained for samples from the Mount Isa gossan and from the Lake Moondarra prospects. The oldest ages obtained, plateau-like steps at 60-70 Ma ("plateau-ages" at 63.5 ± 0.2 Ma, Fig. 29a and 66.9 ± 0.14 Ma, Fig. 31b) are remarkably consistent with the old ages obtained from the Overhang and Selwyn deposits, as discussed below.

The middle range ages obtained, very well defined plateau ages ranging from 24.3 ± 0.8 Ma (Fig. 34a) to 38.7 ± 0.6 Ma (Fig. 35b), with well defined plateau ages in between, present a much larger variation. However, when all the steps (> 350 individual gas analyses) are plotted on the ideogram shown below (Fig. 37), the results suggest that despite the scatter in the data set, which is expectable given the nature of the samples, two well defined "most likely age peaks" occur at approximately 32 and 37 Ma. These results are very significant when compared to the results obtained from another weathering profile in the same region (Gunpowder Creek road outcrop).

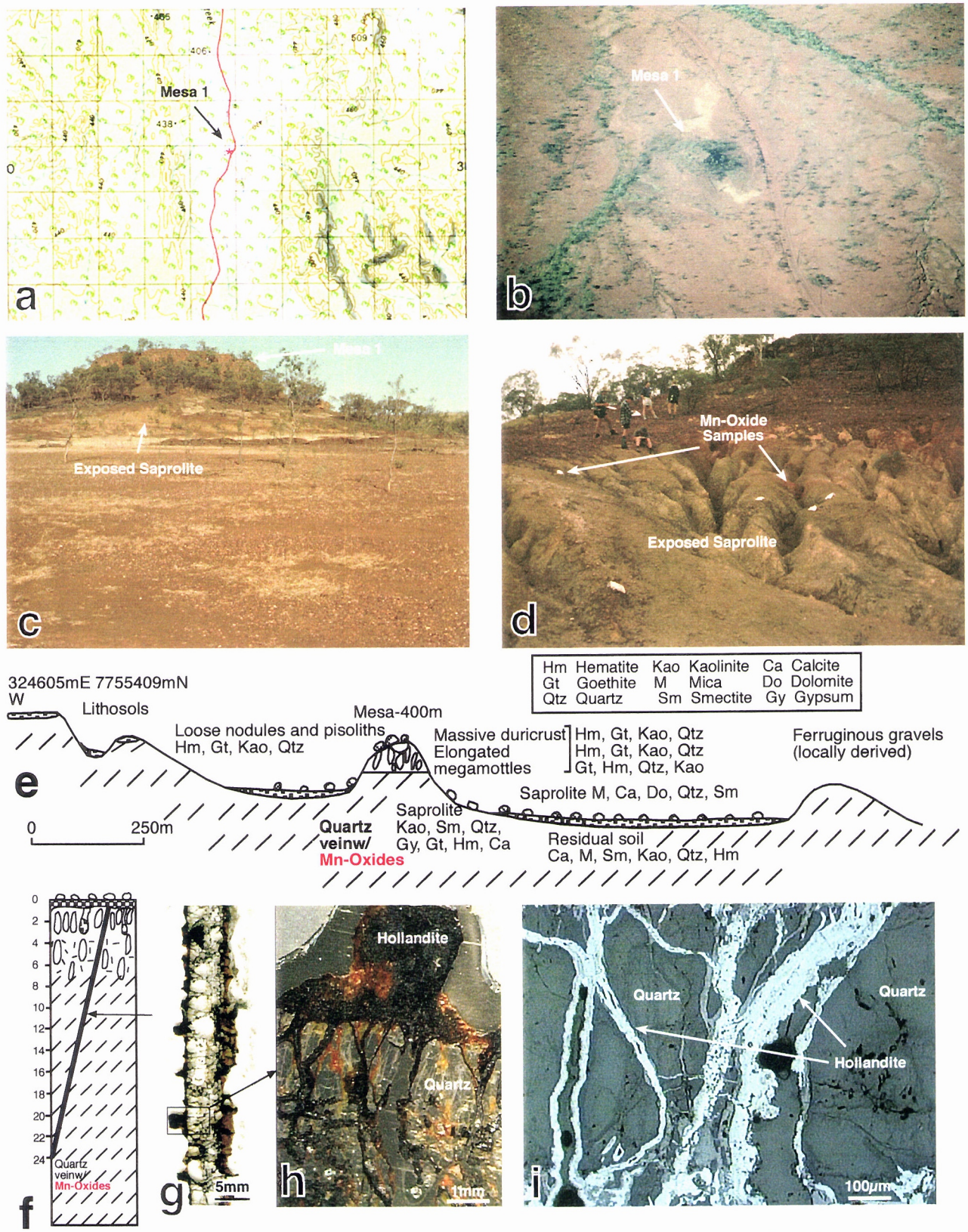

Figure 26. (a) Topographic map illustrating the geomorphologic setting in the Mesa 1 outcrop area. The Mesa 1 outcrop occurs as a remnant mesa in a dissected valley. (b) Airphoto showing the landscape around the Mesa 1 outcrop. North flowing creeks in the area are covered by a thin alluvial veneer. The plains surrounding the mesa are covered by a thin layer of colluvium overlying a smectitic soil rich in carbonates and sulphates. Gilgais are locally present. (c) North facing view of the Mesa 1 outcrop, illustrating the distinct residual duricrust which overlies the mesa. (d) Mining of ferruginous duricrust eluvium for road metal has exposed a smectite-rich saprolite. Manganese-oxides are present in quartz veins which cross-cut the saprolite and which are continuous to the mesa's top. (e) Diagrammatic illustration of the Mesa 1 outcrop, with main minerals and regolith units noted (after Anand *et al.*, 1996). (f) Vertical section through the Mesa 1 outcrop illustrating the continuity of quartz veins through the profile, which suggests that the duricrust overlying the mesa is the result of in situ weathering of the underlying lithologies. (g) Cross-section through one of the quartz veins illustrating the distribution of Mn-oxides as fracture fills and overgrowths on the veins. (h) Expanded view of the area indicated illustrating in further detail the relationship between the Mn-oxides and the quartz vein. The small size of the manganese oxide bands and the intimate overgrowth between the Mn-oxides and the quartz veins make these samples marginally suitable to geochronology and a challenge to the resolution of the technique. (I) Reflected-light photomicrograph illustrating the size and the purity of the hollandite hosted by the quartz vein.

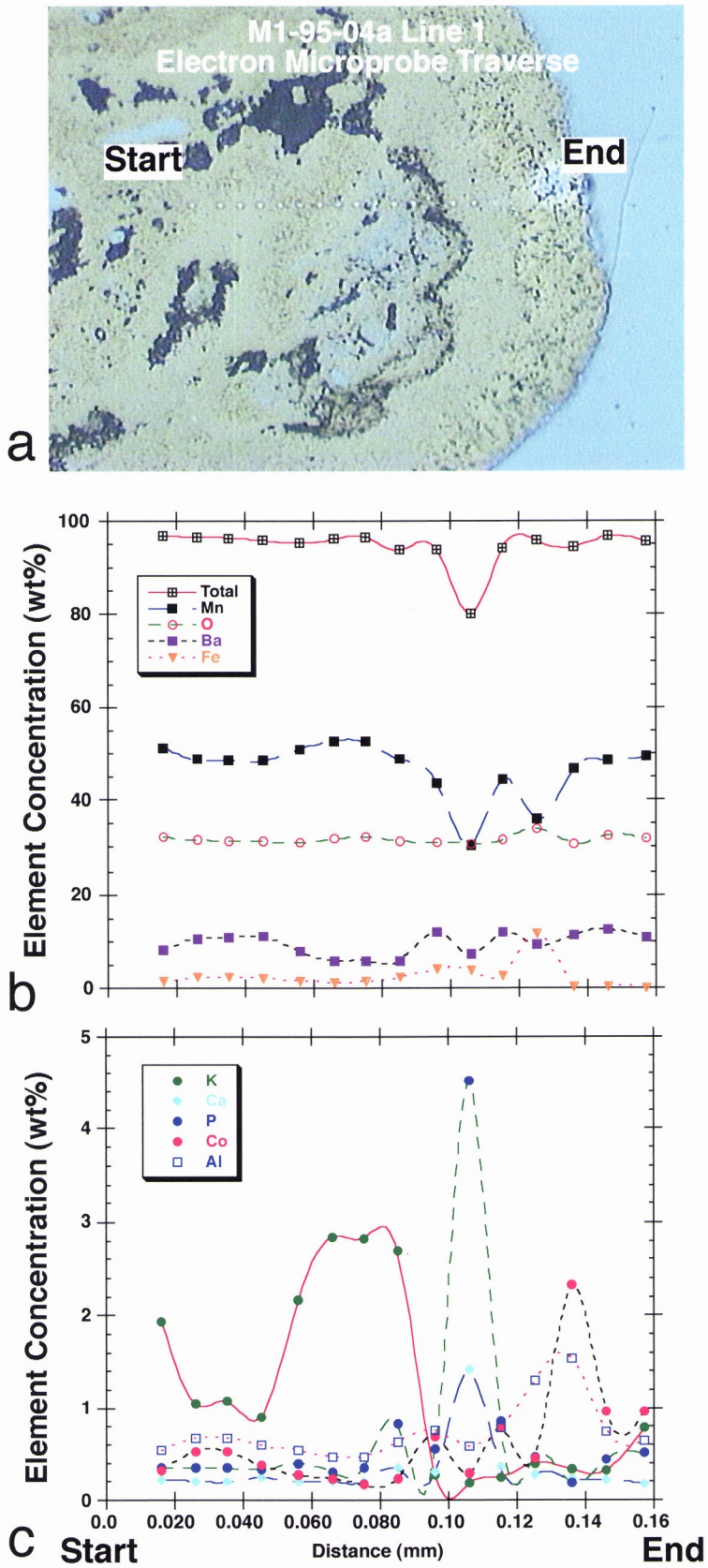

Figure 27. (a) Reflected-light photomicrograph illustrating a botryoidal Mn-oxide and the spots where EMP analyses were performed. (b) major and (c) minor elements distribution along the traverse shown in (a). Notice the relatively high Ba and Co contents in the sample. Notice also the positive correlation between P and Ca, which suggests the present of some phosphate in the sample.

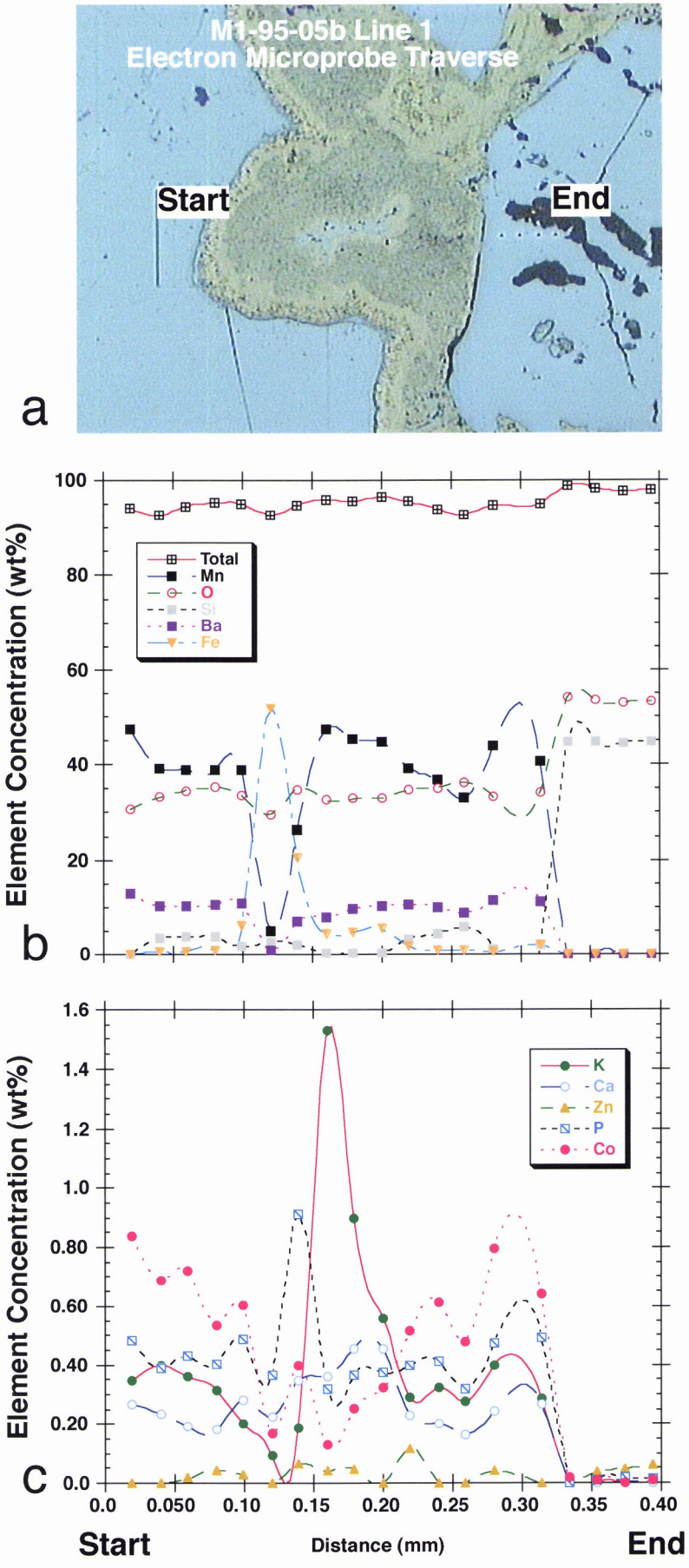

Figure 28. (a) Reflected-light photomicrograph illustrating a botryoidal Mn-oxide and the spots where EMP analyses were performed. (b) major and (c) minor elements distribution along the traverse shown in (a). This sample is also relatively enriched in Ba and Co, but depleted in Zn when compared to Mount Isa Gossan Mn-oxides.

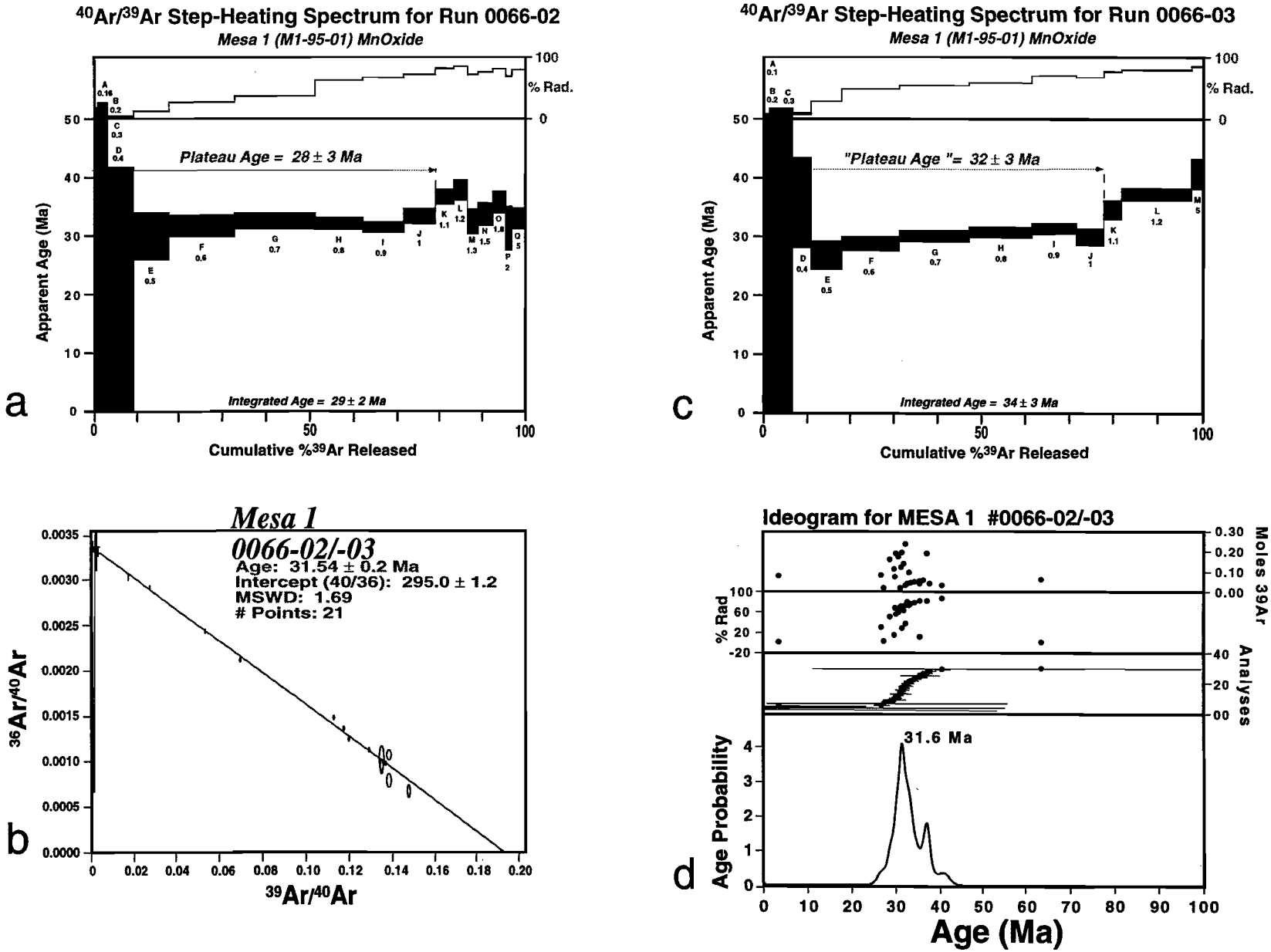

Figure 29. (a) and (b) illustrate two step-heating spectra for sample M1-95-01. One sample (a) yielded a well defined plateau age while the other sample yielded a series of plateau-like steps. The plateau ages obtained are indistinguishable within two sigma confidence interval. The plateau ages obtained are also consistent with the isochron (c) and ideogram (d) ages for the same grains.

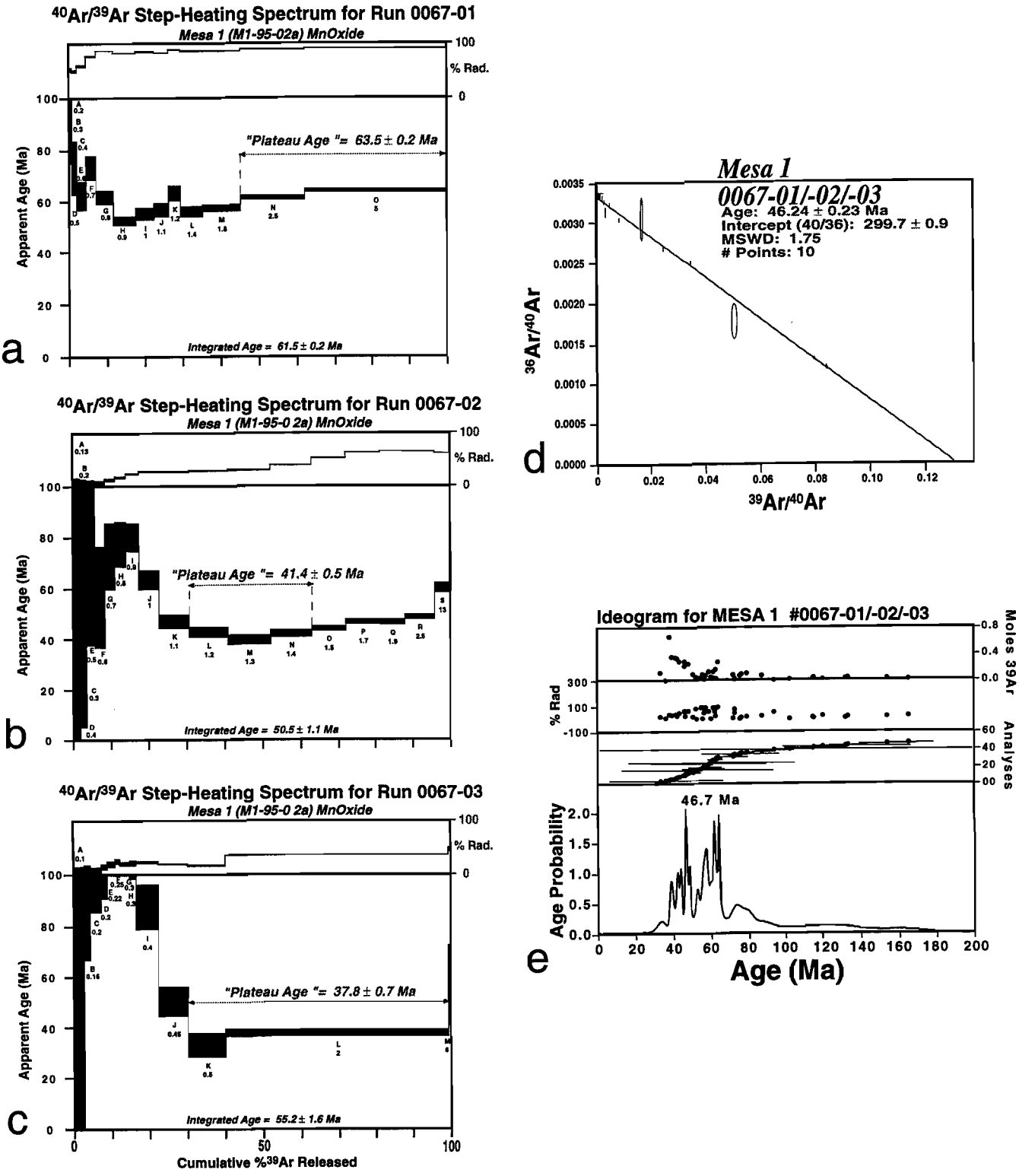

Figure 30. Three distinct grains from the same sample yielded "plateau" and plateau ages ranging from (a) 63.5 ± 0.2 Ma, (b) 41.4 ± 0.5 Ma, and (c) 37.8 ± 0.7 Ma. Isochron (d) and ideogram (e) plots for the sample yielded results consistent with the plateau ages obtained. The significance of these results is discussed in the text.

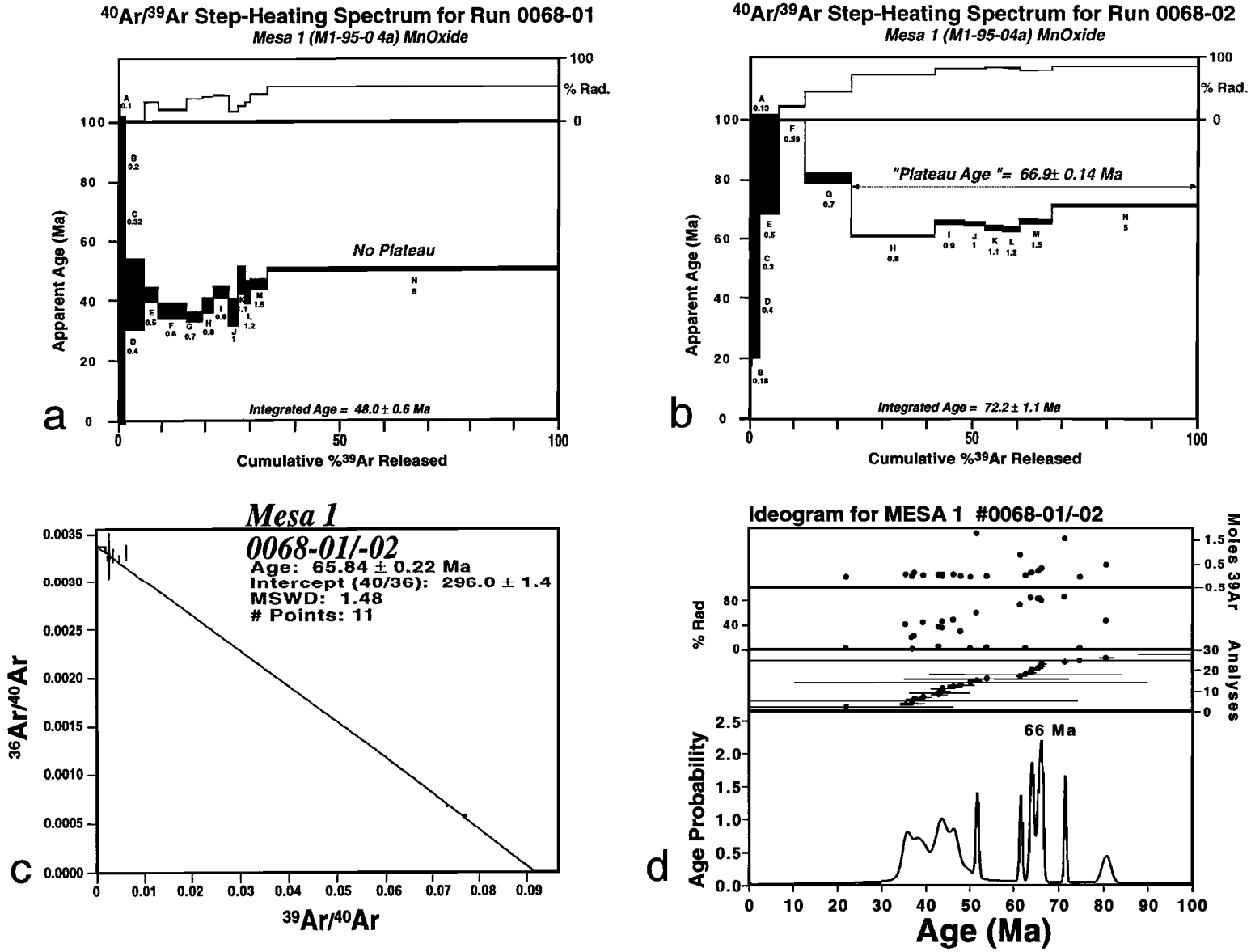

Figure 31. The two grains analysed from this sample also do not yield well defined plateaus. However the plateau-like spectra obtained in (a) and (b) yield results which fall within the range of ages obtained for other samples in the same profile. The older ages obtained from the "plateau-ages" in this sample and also from the isochron (c) and ideogram (d) for the two grains is also consistent with older ages obtained from weathering profiles in the Eastern Succession.

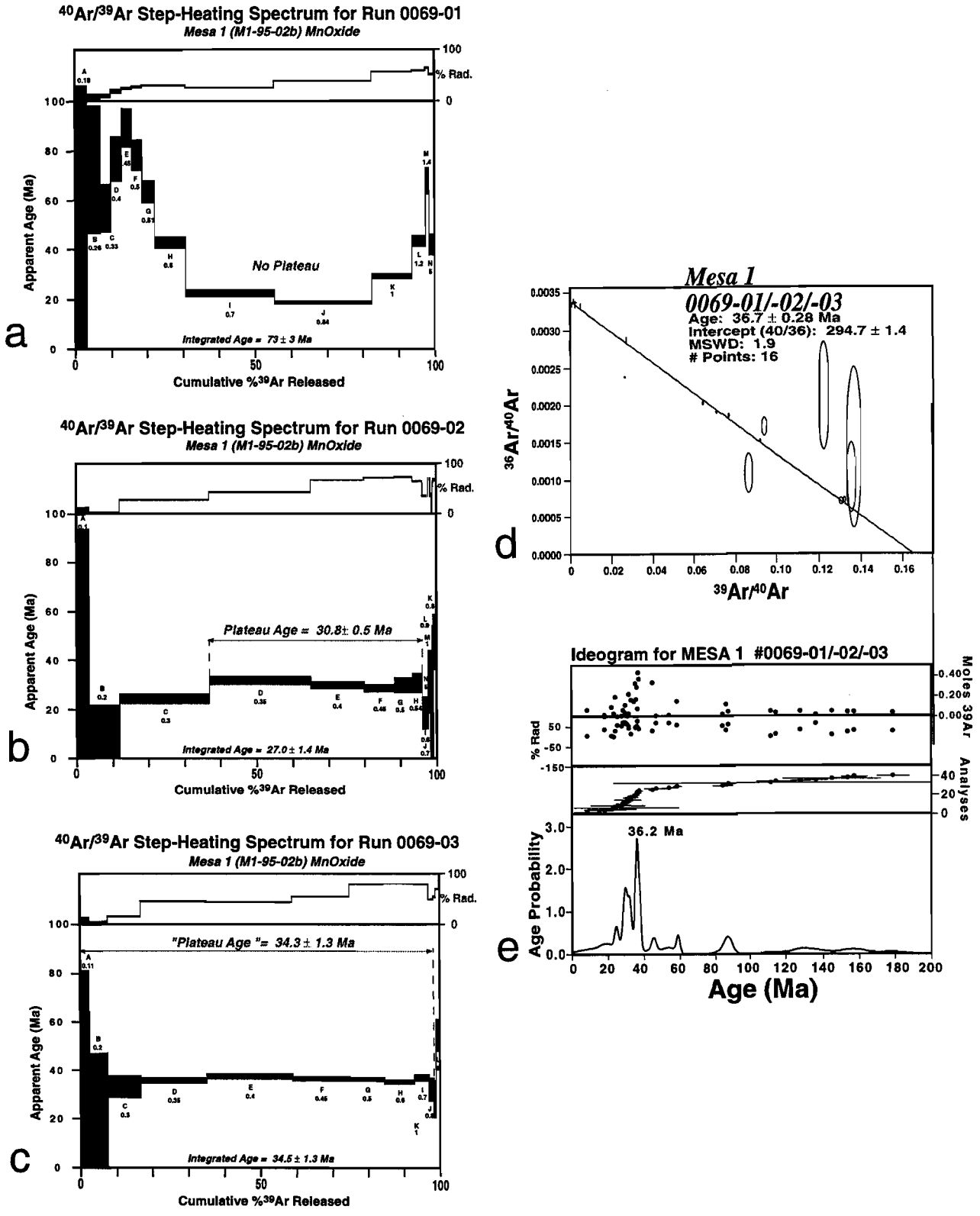

Figure 32. Two ((b) and (c)) of the three grains analysed for this sample yielded well defined plateau ages. The other grain yielded a complex, saddle-shaped spectrum, suggesting that major amounts of Ar recoil may have taken place in this sample. The isochron (d) and ideogram (e) ages obtained for this sample are strongly influenced by the very well defined plateau obtained in Run 0069-03 (c).

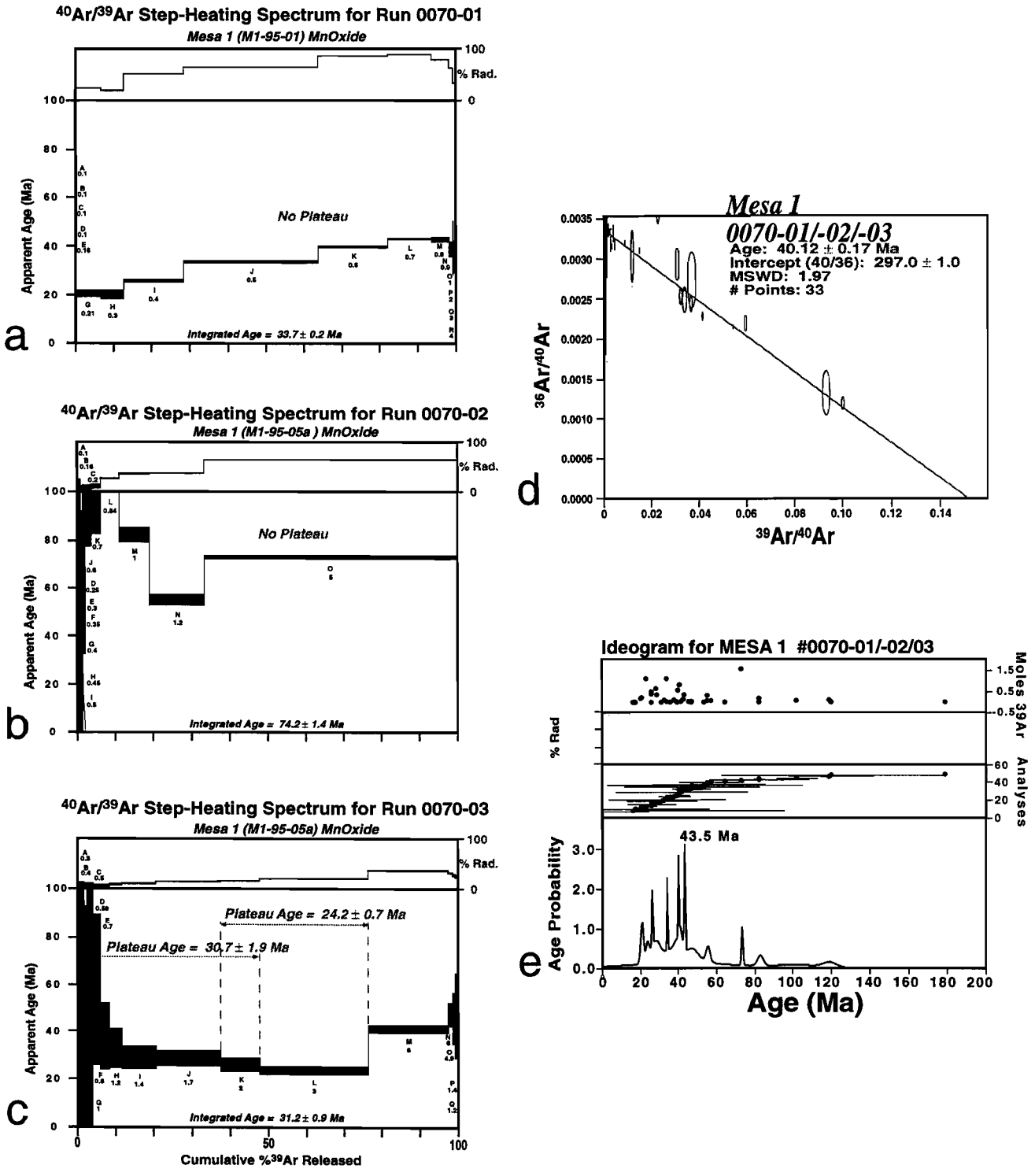

Figure 33. Only one (c) of the three grains analysed from this sample yielded a plateau. The irregular spectra obtained for the two other samples (a-b) yielded steps ranging from 20 to 70 Ma. The isochron (d) and ideogram (e) ages for these samples are consistent with ages obtained from other samples in this profile.

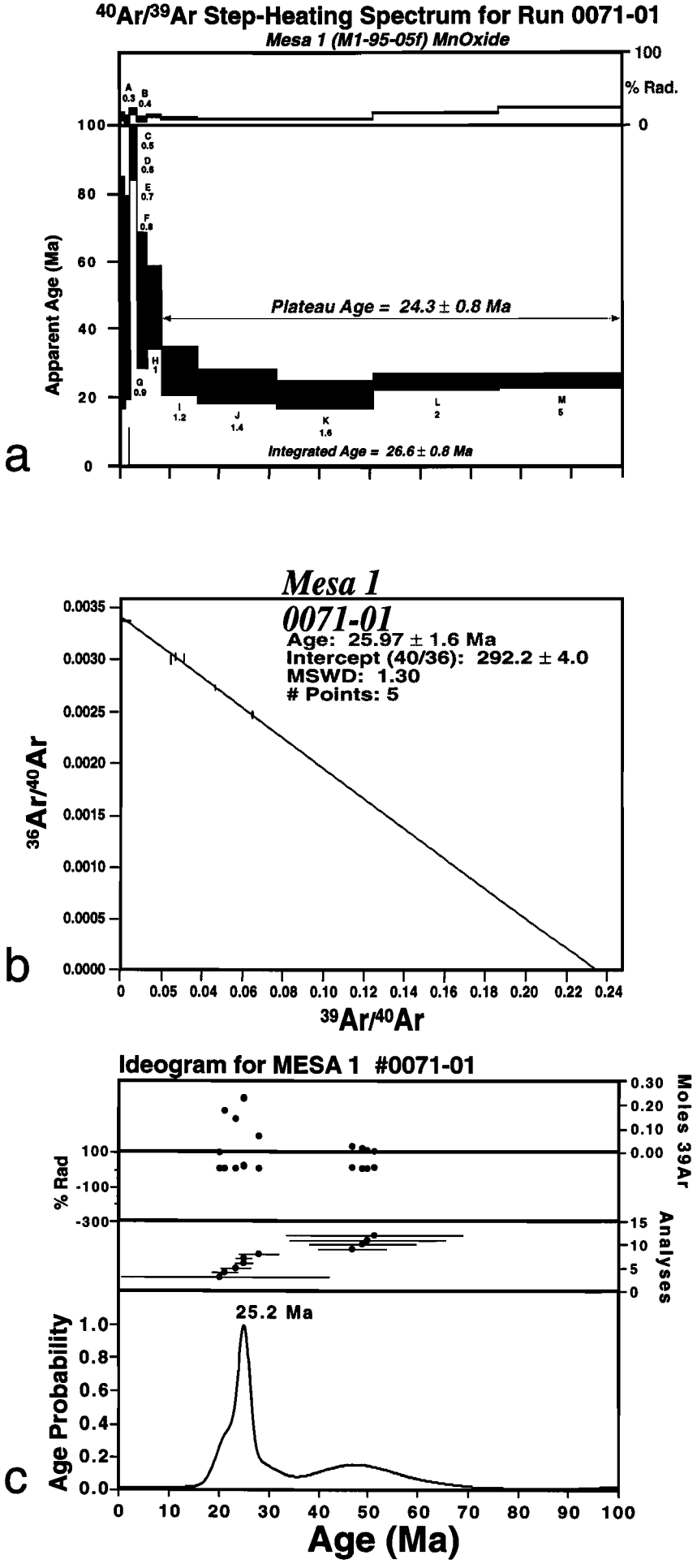

Figure 34. The only one grain analysed for this sample yields internally consistent plateau (a), isochron (b) and ideogram (c) ages.

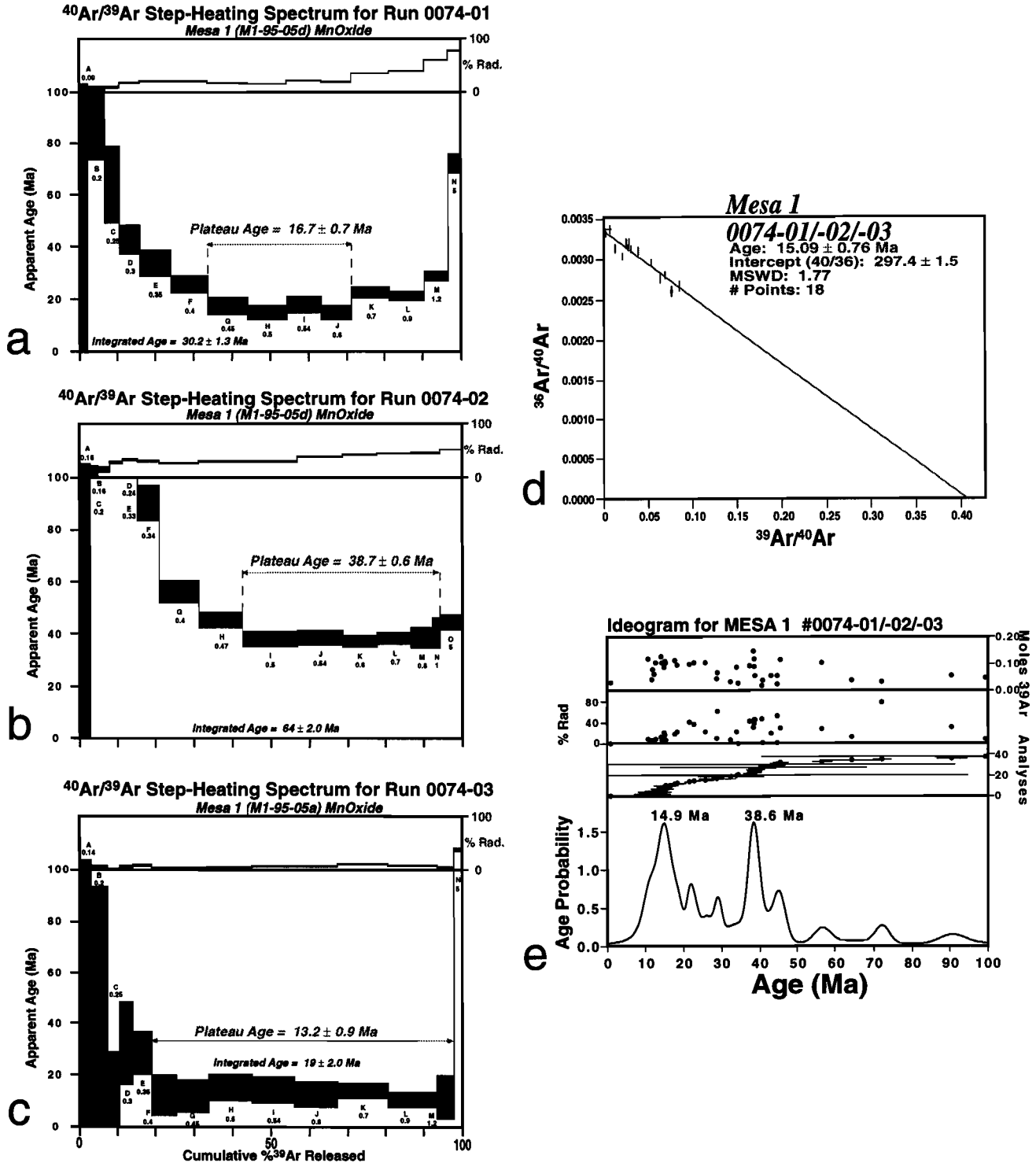

Figure 35. Three grains analysed for sample M1-95-05a yielded plateau ages. However, the plateau ages obtained ((a) 16.7 ± 0.7 Ma; (b) 38.7 ± 0.6 Ma; and (c) 13.2 ± 0.9 Ma)) are not internally consistent, suggesting several generations of Mn-oxides in the sample. The isochron age (d) obtained for this sample shows a strong influence of the well defined younger plateau ages, while the ideogram plotted for this sample shows two equally probable age groups, reflecting the distinct plateau ages obtained for the step-heating spectra.

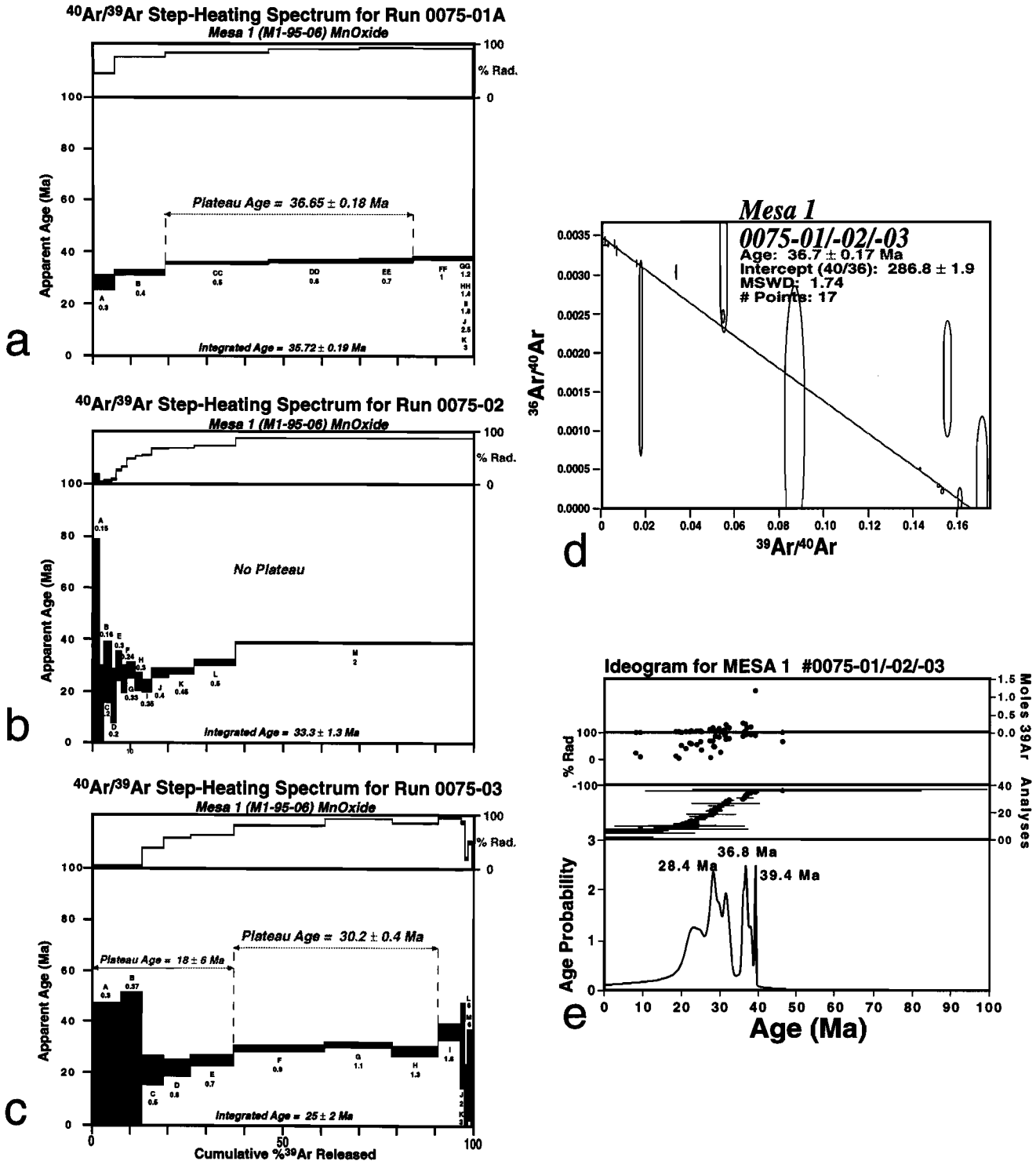

Figure 36. Two of the three grains analysed for sample M1-95-06 yielded plateau ages which correspond to plateau ages obtained for other samples in this profile.

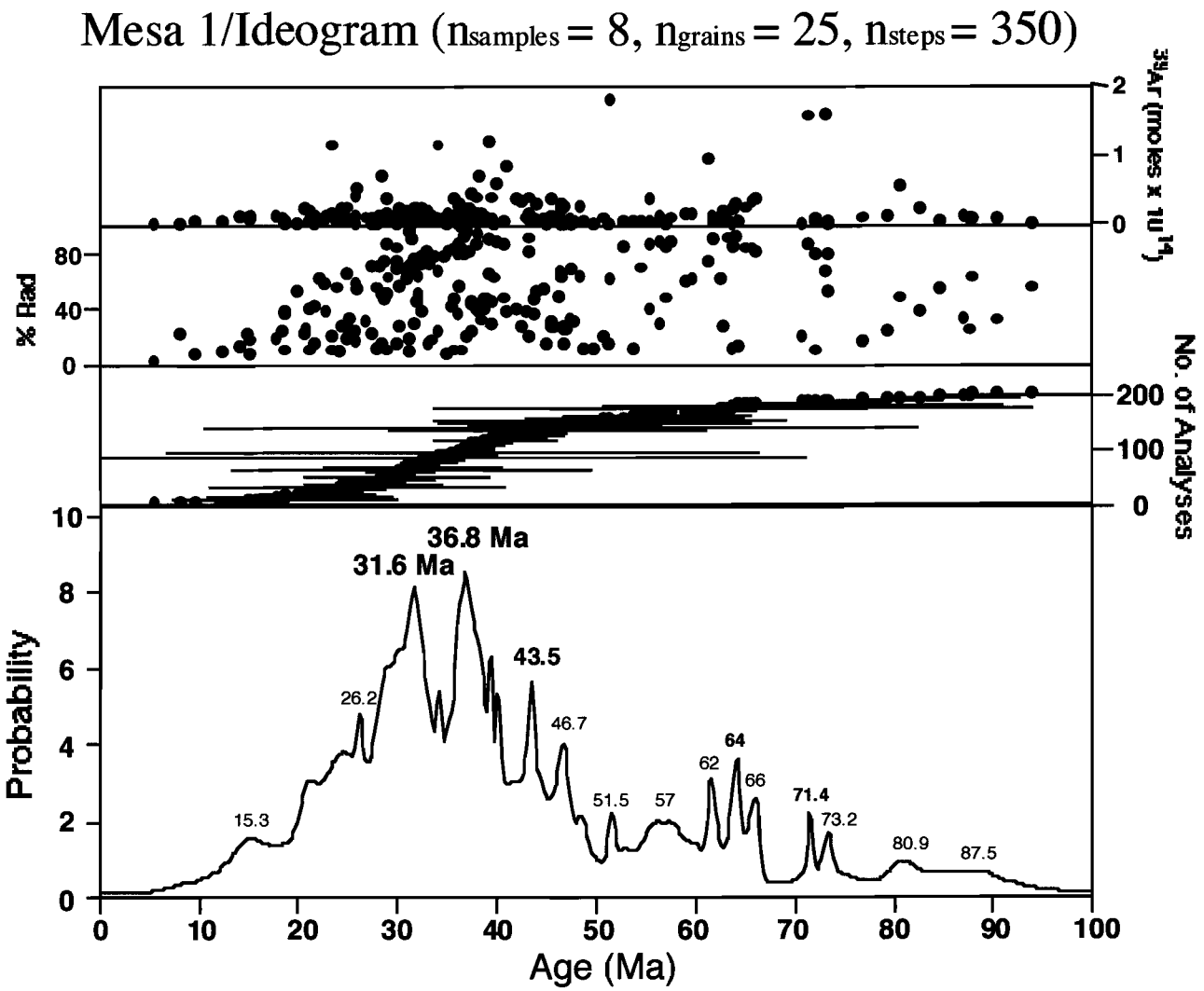

Figure 37. An ideogram for all the samples analysed from the Mesa 1 outcrop illustrates the large spread in ages obtained for this site, which hosts Mn-oxides with precipitation ages ranging from the late Cretaceous (ca. 70 Ma) to the Miocene (ca. 15 Ma). The most represented age group, however, is concentrated in the late Eocene (36.8 Ma) to the early Oligocene (31.6 Ma) time interval.

2.2.2 Gunpowder Creek Road Outcrop (Kennedy Gap)

2.2.2.1 Site Selection Criteria: exposed Mn-oxide crusts on massive quartz vein in an area of the Western Succession for which no other sampling sites were available (Fig. 38).

2.2.2.2 Location: approximately 301550E-7783000N (exact location not well defined).

2.2.2.3 Elevation: 380-420 m

2.2.2.4 Geomorphologic Setting: dissected plateau on weathered Proterozoic bedrock. Erosional landscape surrounded by mesas and ridges.

2.2.2.5 Geomorphologic Regime: erosional.

2.2.2.6 Sample in Relation to Landscape Position: exposed quartz veins at the lowermost part of a now mostly eroded weathering profile capping the mesas in the area.

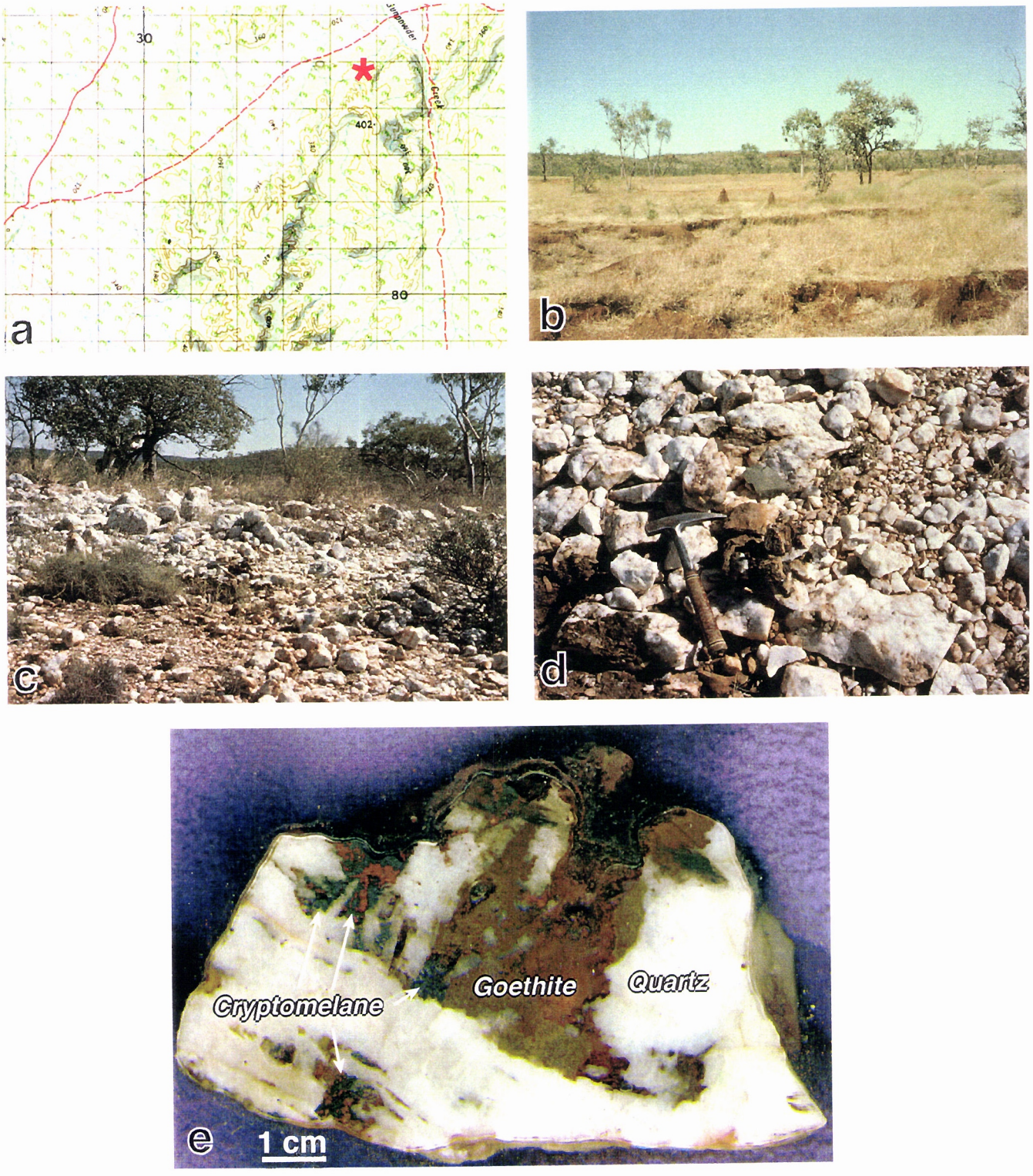

Figure 38. (a) A topographic map illustrates the geomorphologic setting in the Gunpowder Creek outcrop area. (b) ESE facing view of the sampled outcrop depicts its relatively high landscape position. (c) Scattered massive quartz veins in the area host Fe- and Mn-oxides in vugs and fractures. (d) Close-up showing the samples collected for geochronology in this outcrop. (e) This cross-section through the quartz vein shows cavities filled by Fe- and Mn-oxides.

2.2.2.7 Sample in Relation to Regolith: the exposed quartz veins and host rock are at the lower saprolite/saprock weathering stages.

2.2.2.8 Datable Minerals/Host Rock Relationship: local recrystallisation of minerals with major textural disruption.

2.2.2.9 Sources of Elements: Mn-oxide fill void spaces in hydrothermal vein quartz in exposed, slightly weathered, basalt. Mn-oxide filling void spaces in hydrothermal quartz. Void spaces are the result of dissolution of sulphides and carbonates during weathering. The Mn-oxides are precipitated on quartz and are associated with iron oxides. Manganese is probably derived from weathering carbonates and/or silicates hosted by the fault breccias/hydrothermal veins, K and Ba are derived from feldspars and mica in the host rock and in the quartz veins.

2.2.2.10 Overview

A large quartz vein outcropping at this location hosts abundant samples of well crystallised Mn-oxides (Fig. 38). These samples are derived from an erosional part of the landscape, but in an area whose elevation is only slightly lower than the mesa summits in the area. Petrographic investigation and electron microscope studies indicated that these samples were suitable for $^{40}Ar/^{39}Ar$ geochronology.

2.2.2.11 Results

2.2.2.11.1 Electron Microprobe and SEM Analysis

The results of petrographic investigation and SEM/EMP analyses show that large, botryoidal Mn-oxide masses occur filling void spaces in the vein quartz (Fig. 38e). The Mn-oxides are very pure and well crystallised, and they are composed of alternating bands of hollandite, cryptomelane, and lithiophorite (Figs. 39 and 40). The Pb and Zn contents of these Mn-oxides is low; however, the lithiophorite bands show up to 10.5 wt% cobalt.

2.2.2.11.2 Geochronology

Three grains from two hand specimens were analysed by the laser-heating method at the BGC. The samples yielded well defined plateau ages (35.9 ± 0.2 Ma, 37.1 ± 0.2 Ma, and 38.9 ± 0.8 Ma) (Fig. 41). In addition, the plateau and isochron ages are internally consistent. A best estimate for the ages of three grains analysed at the BGC is 36.6 Ma, as illustrated by the ideogram in Fig. 41f.

Thirteen additional grains from two hand specimens were subsequently analysed at the UQ-AGES laboratory. These grains also yielded well defined plateau ages (Figs. 42 to 44); however, the samples showed a greater age spread (29.8 ± 0.3 Ma to 41.6 ± 0.6 Ma). Only three of the thirteen grains analysed did not yield a well defined plateau (Figs. 43c and f, Fig. 44a). The samples analysed also yielded well defined isochrons (Figs. 42g and 44b).

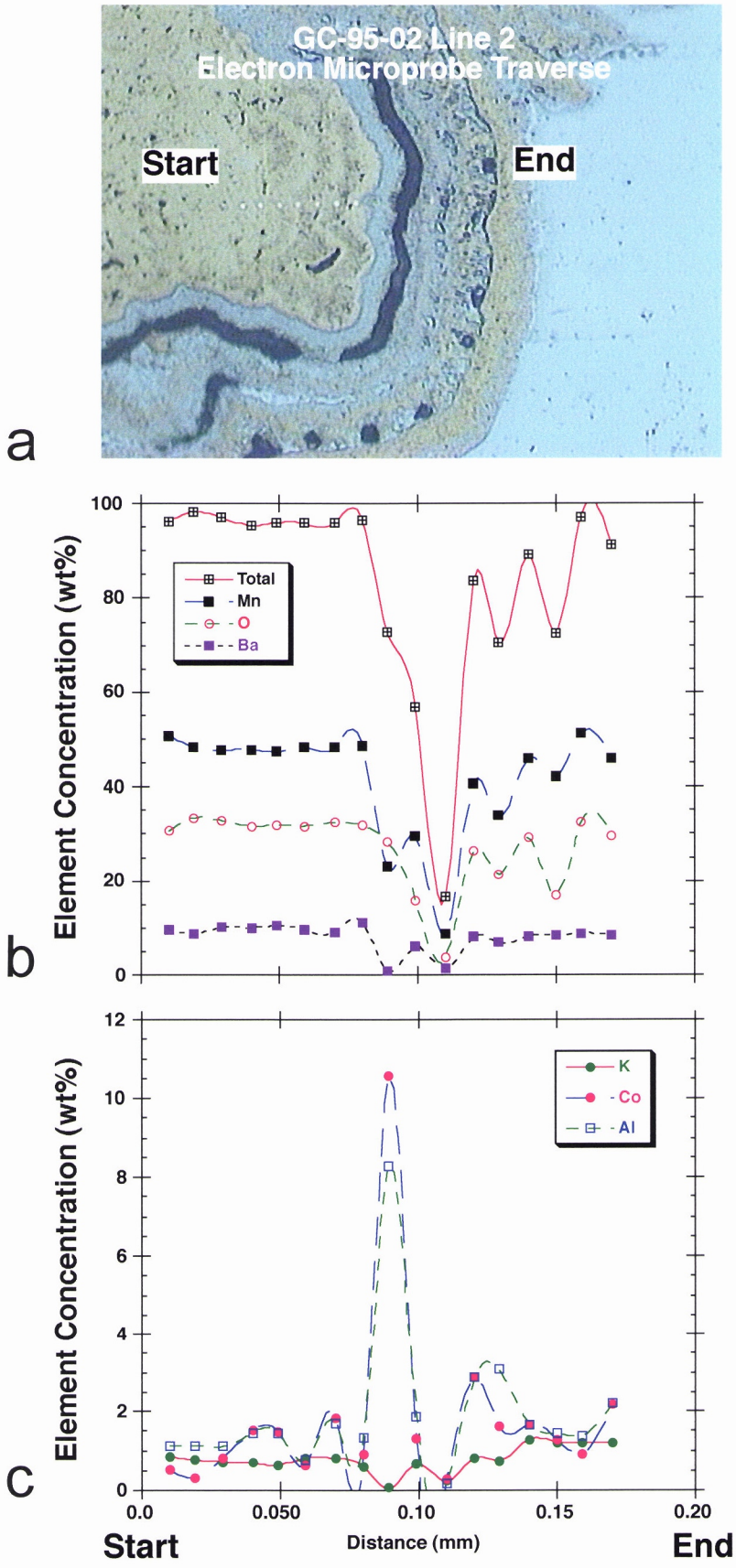

Figure 39. (a) Reflected-light photomicrograph illustrating a botryoidal Mn-oxide and the spots where EMP analyses were performed. Major (b) and minor (c) element distribution along the traverse shown in (a). Notice the relatively high Ba and Co contents in the sample. The drop in the Total in the middle of the traverse is due to the cavity, shown in black in (a), in the sample. The high Co (>10 wt%) and Al (>8 wt%) contents of the light grey vein adjacent to the cavity (a) suggests that that band consists of lithiophorite.

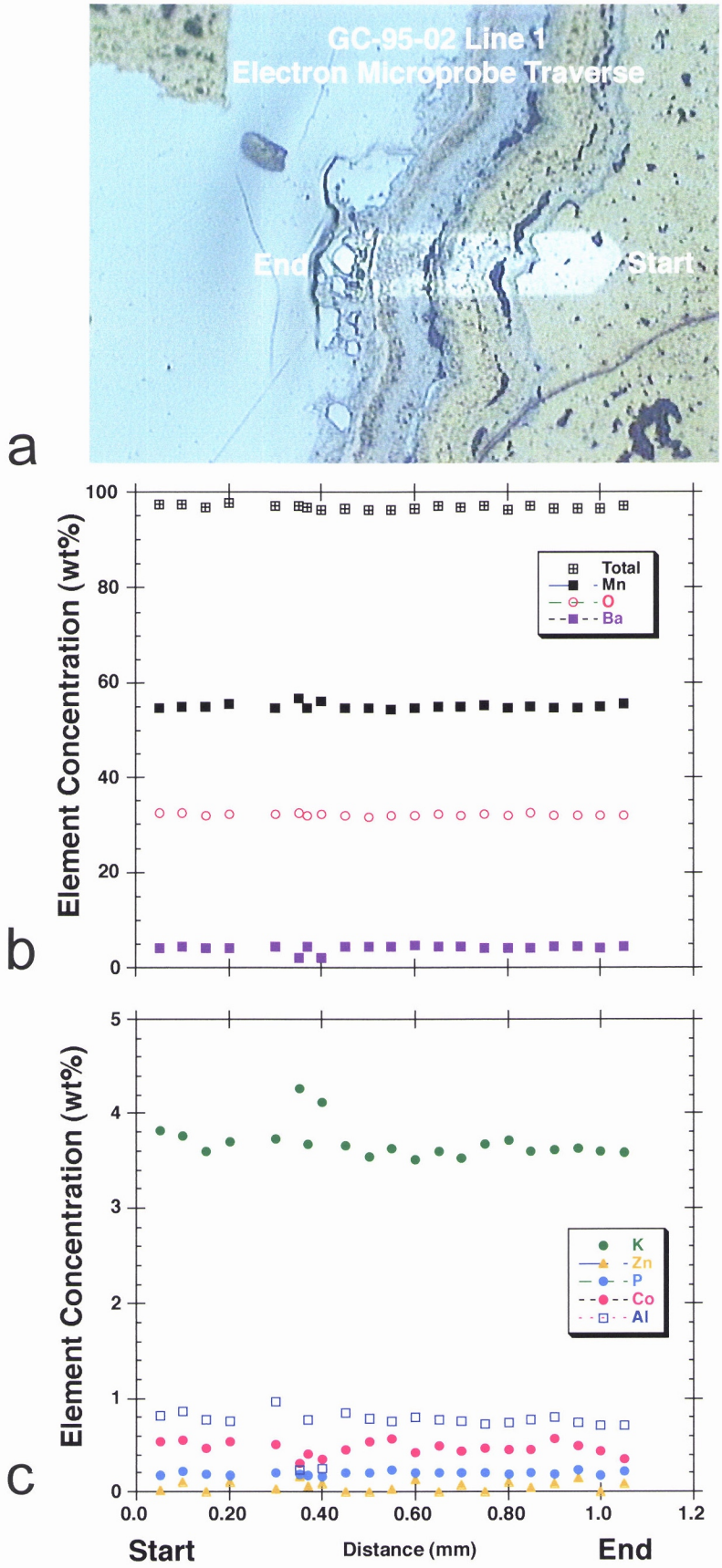

Figure 40. (a) Reflected-light photomicrograph illustrating a botryoidal Mn-oxide and the area (discoloured by the scanning electron beam) where EMP analyses were performed. Major (b) and minor (c) element distribution along the traverse shown in (a). Notice the relatively high K content of this sample, indicating that this Mn-oxide is ideal for geochronology.

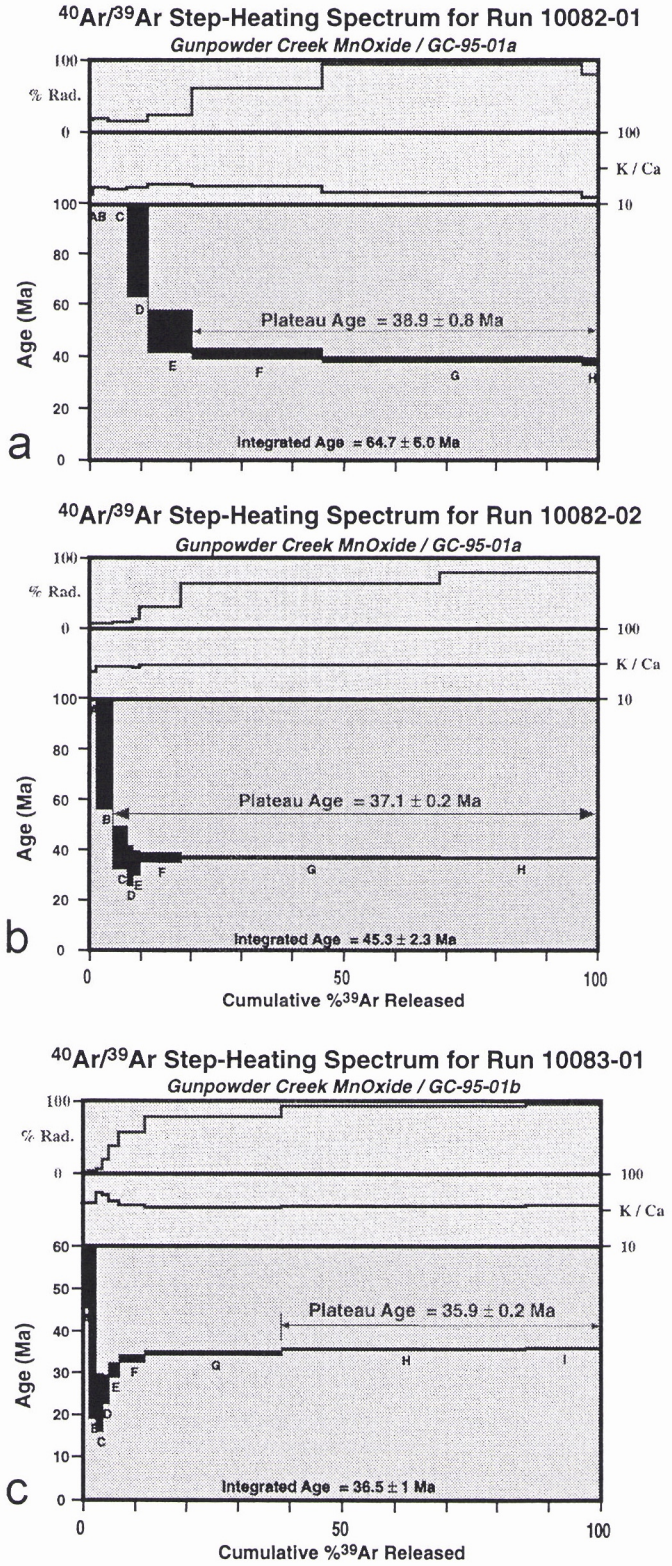

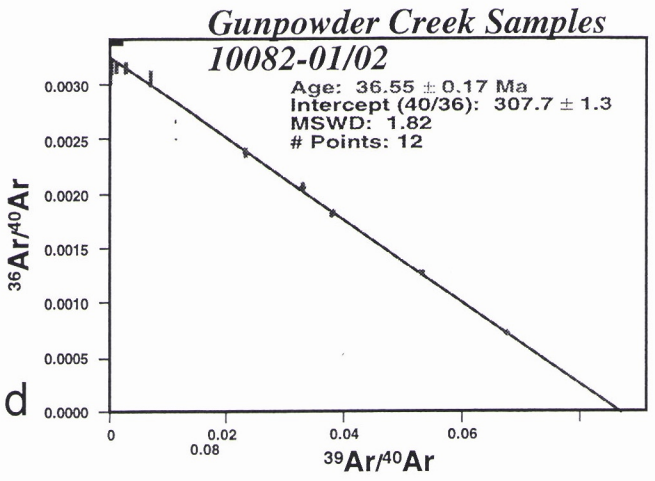

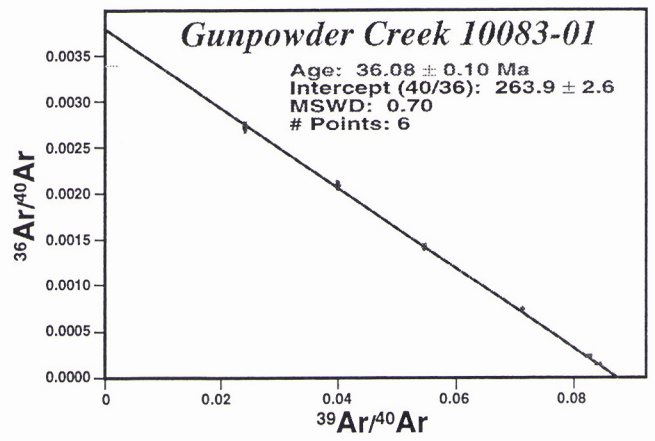

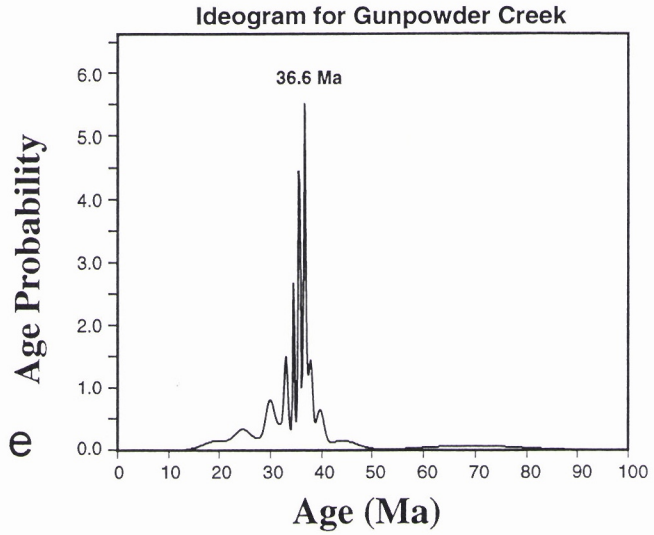

Figure 41. (a), (b) and (c) illustrate three step-heating spectra obtained for three grains extracted from two distinct hand specimens. The plateau ages are well defined at 38.9 ± 0.8 (a), 37.1 ± 0.2 (b), and 35.9 ± 0.2 Ma (c). The two plateau ages for grain GC-95-01a are reproducible within two sigma. The isochron ages obtained for each distinct hand specimen, GC-95-01a (d) and GC-95-01b (e), agree reasonably well with the plateau ages obtained. However, the intercepts are distinct from the 295.5 atmospheric value expected. The reason for this discrepancy is not clear from the analyses. The ideogram age (best age estimate) for the samples is 36.6 Ma (f).

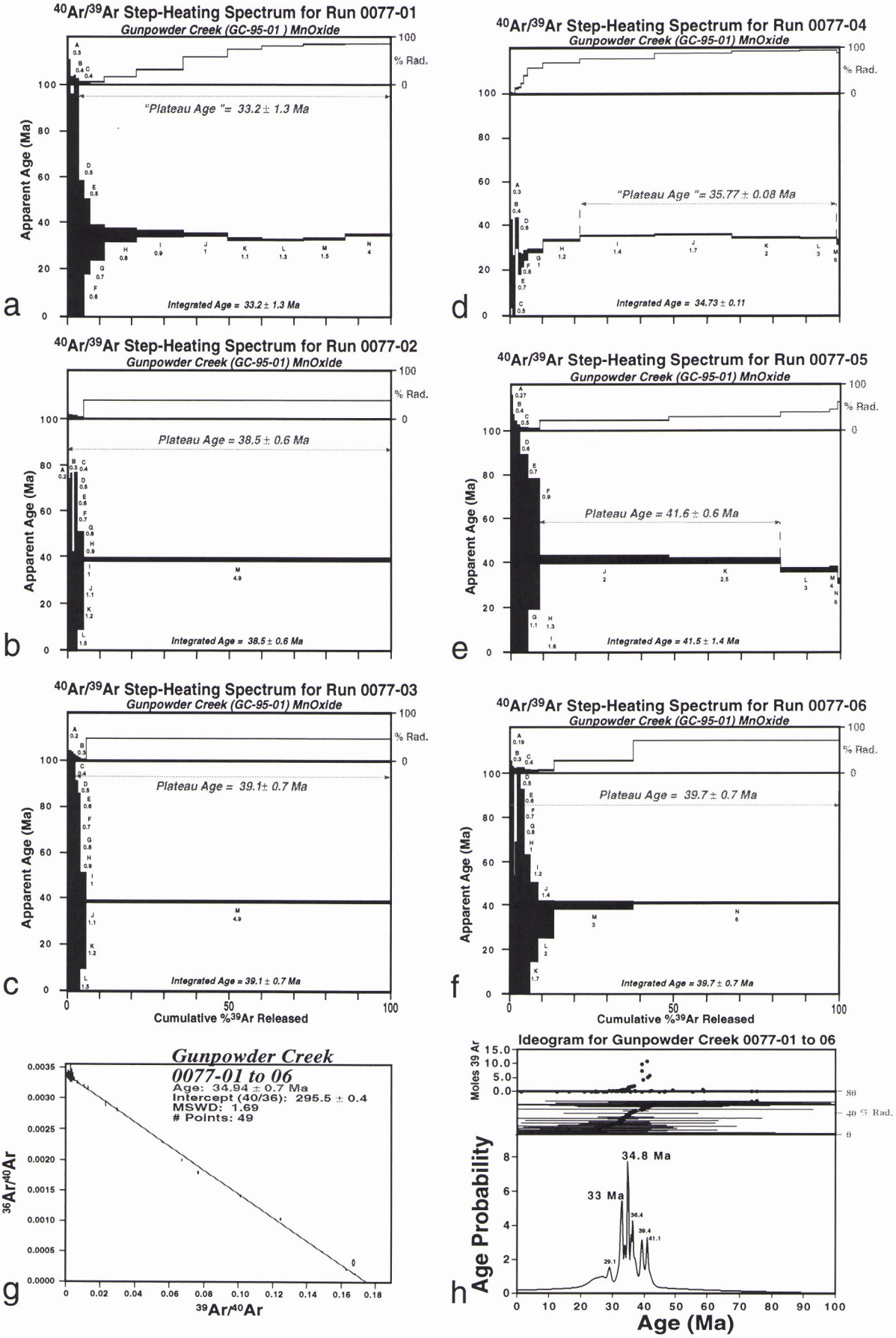

Figure 42. (a)-(f) illustrate the step-heating spectra obtained for six grains extracted from one hand specimen. The plateau ages are well defined and they range from 33.2 ± 1.3 to 41.6 ± 0.6 Ma. The isochron (g) and ideogram (h) ages for this sample suggested a best age estimate ca. 35 Ma.

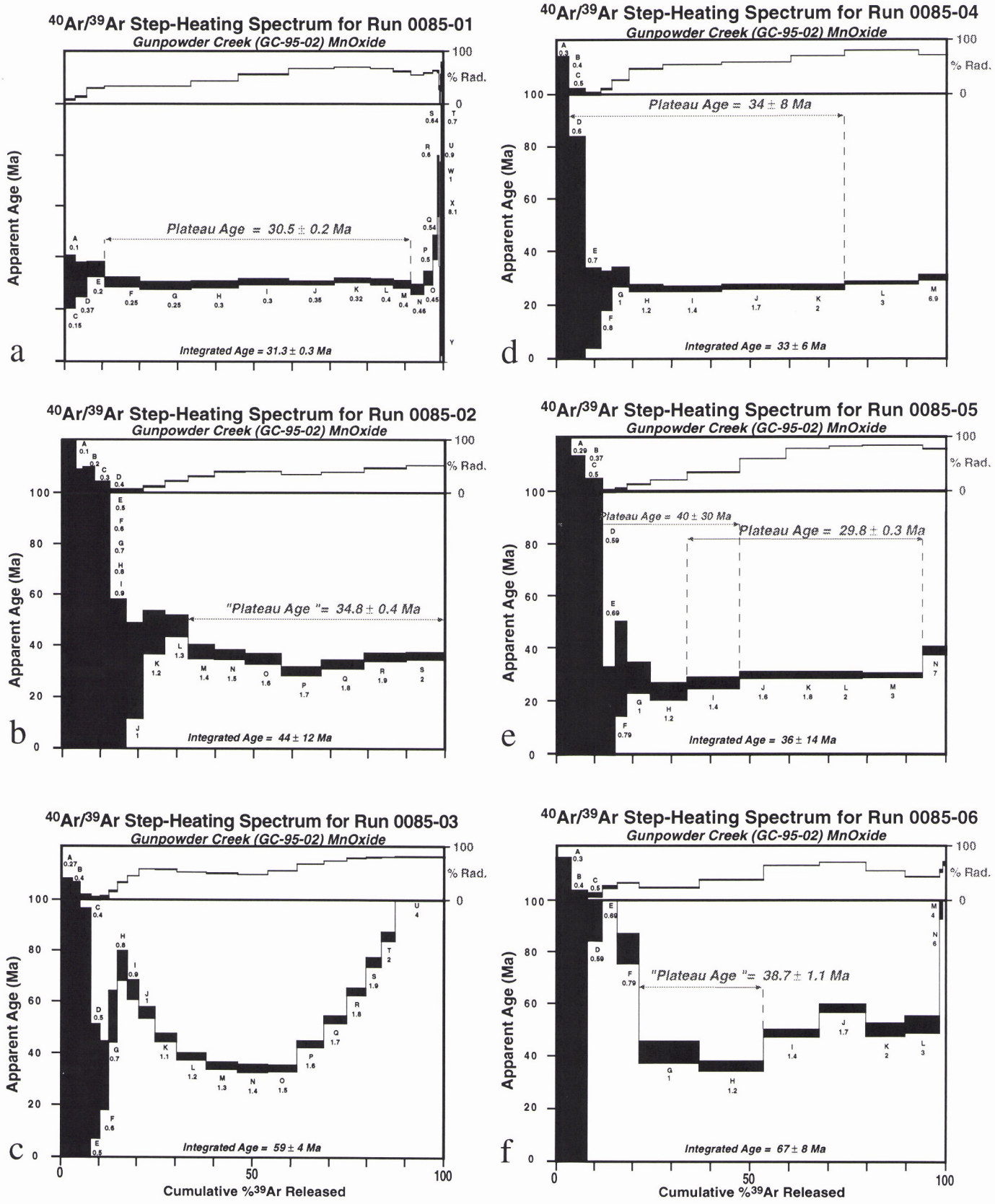

Figure 43. (a)-(f) illustrate the step-heating spectra obtained for seven grains extracted from one hand specimen. Some grains yielded well defined plateaus (a, b, d, and e) while two grains did not yield plateaus (c and f).

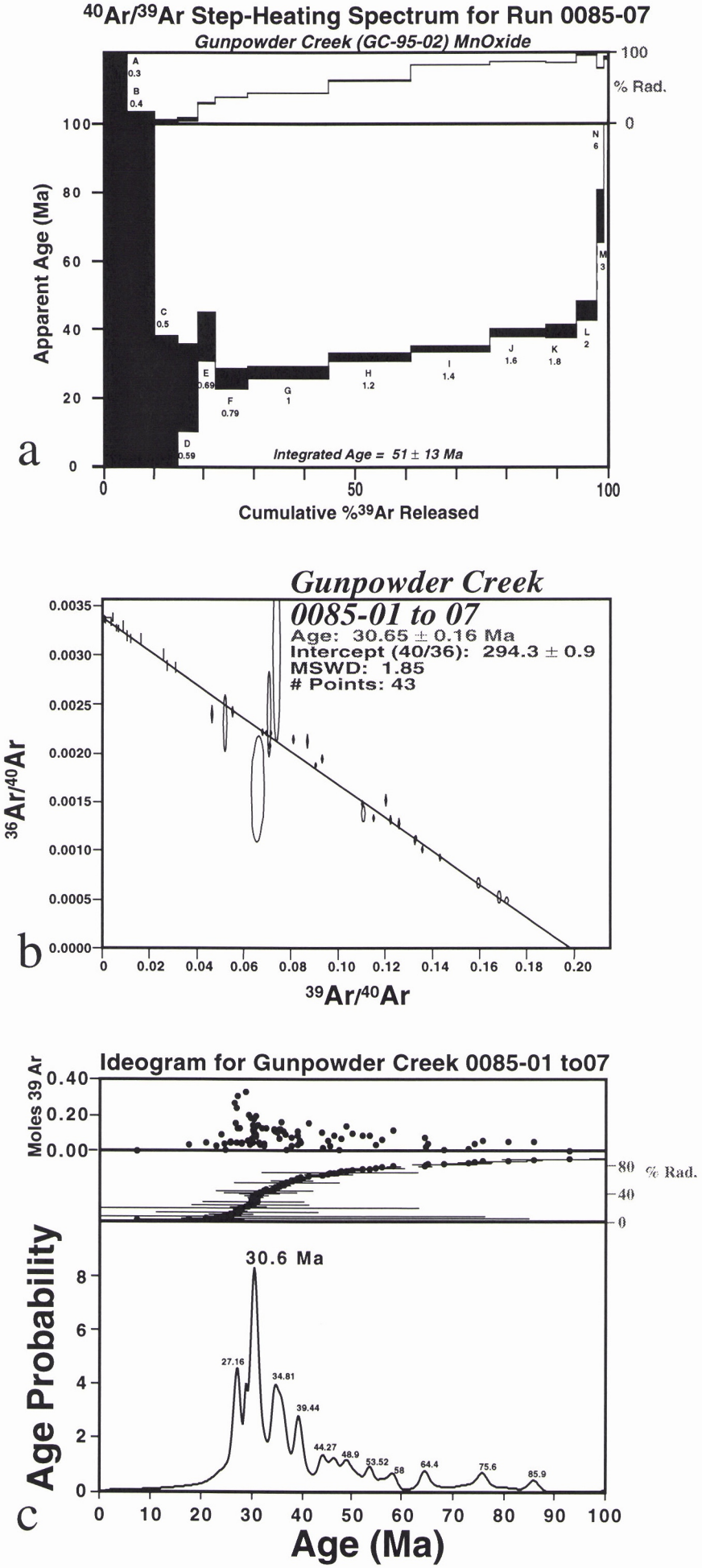

Figure 44. (a) illustrates the step-heating spectra obtained for a seventh grain extracted sample GC-95-02. This grain did not yield a plateau age either. The plateau ages obtained for seven grains from sample GC-95-02 range from 29.8 ± 0.3 to 34.8 ± 0.4 Ma. The isochron (b) and ideogram (c) ages for this sample suggest a best age estimate ca. 31 Ma.

When all the results are plotted on an ideogram (Fig. 45), the best age estimate for the samples analysed at UQ-AGES is 34.8 Ma, close to the 36.6 Ma obtained for the samples analysed at the BGC (Fig. 45).

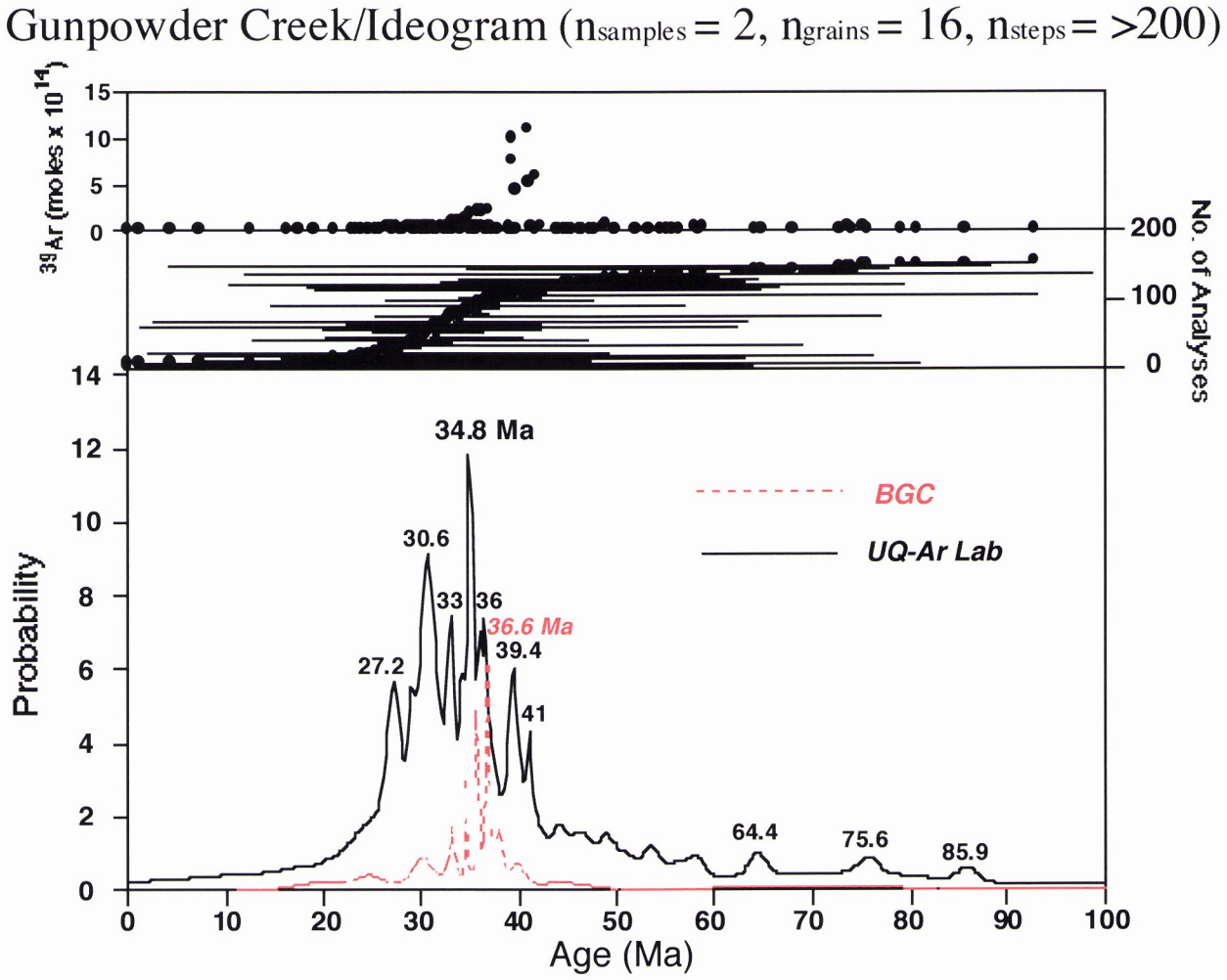

Figure 45. The ideogram for all the samples collected at the Gunpowder Creek outcrops indicate a broad range of weathering ages spanning the late Eocene and early Oligocene, very similar to the ideogram obtained for the samples collected at the Mesa 1 outcrop (Fig. 37).

2.2.3 Drifter Prospect

2.2.3.1 Site Selection Criteria: sample supplied by CSIRO researchers.

2.2.3.2 Location: approximately 298500mE-7829400mN.

2.2.3.3 Elevation: undetermined.

2.2.3.4 Geomorphologic Setting: broad valley on weathered Mesozoic sediments overlying Proterozoic bedrock (Fig. 46). Erosional landscape surrounded by mesas.

2.2.3.5 Geomorphologic Regime: erosional.

2.2.3.6 Sample in Relation to Landscape Position: samples located on local depositional valley.

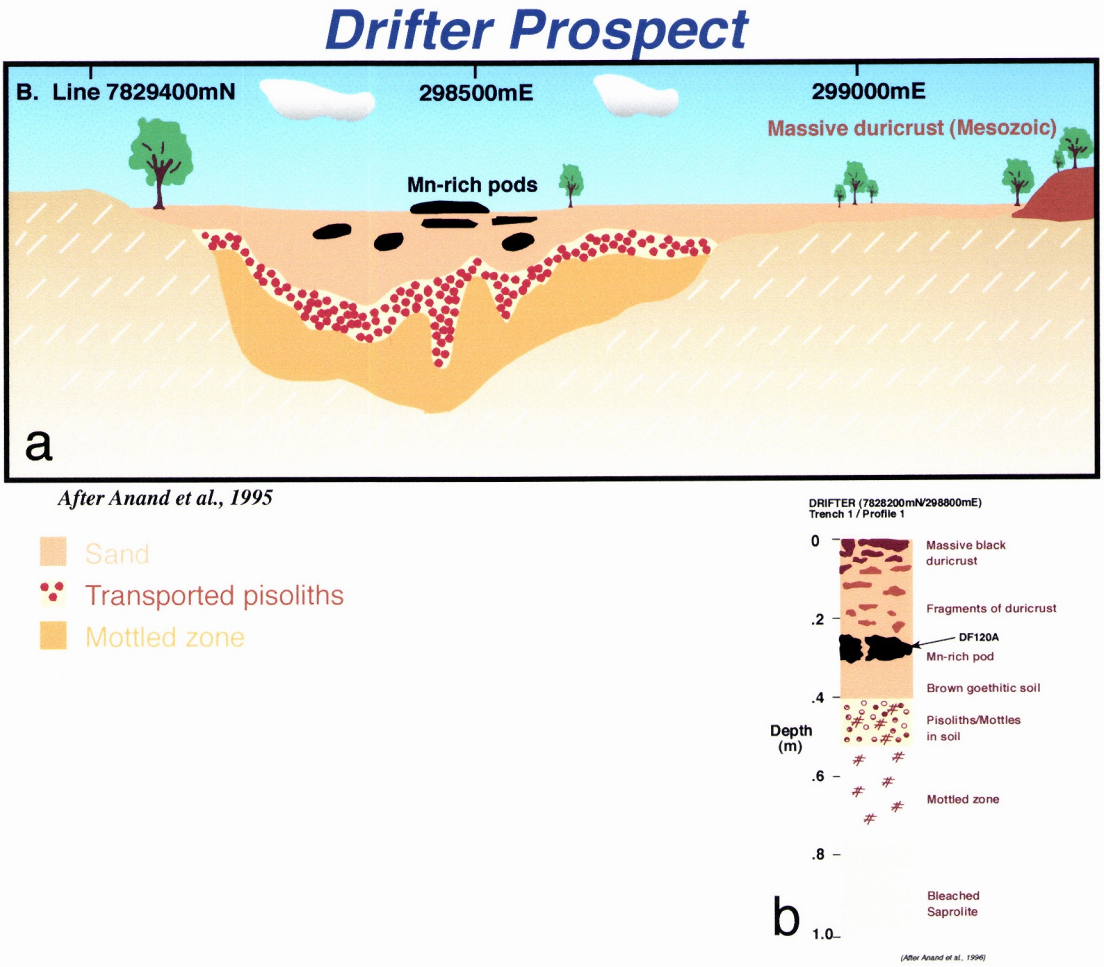

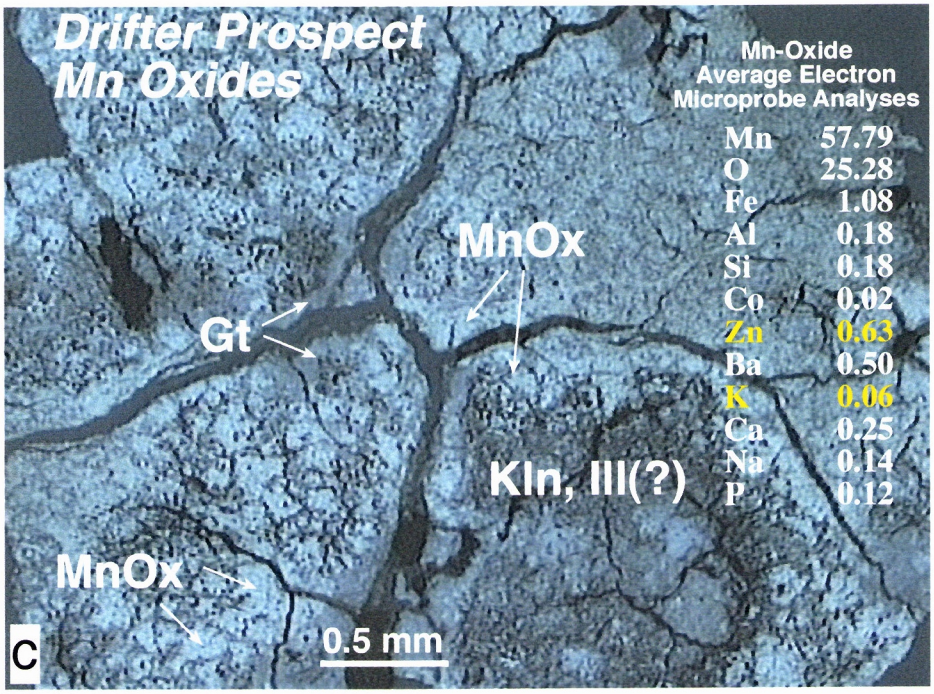

Figure 46. (a) Diagrammatic illustration of Mn-oxide rich zones in the weathering profile in the vicinity of the Drifter prospect. (b) Schematic cross-section illustrating the location of Mn-oxide samples in the regolith profile at the Drifter Prospect. (c) SEM photomicrograph of Drifter Mn-oxide samples illustrating the presence of abundant desiccation cracks and intergrown clay minerals and iron oxides. Average EMP analyses for this sample indicate that the Mn-oxides are devoid of K, making them unsuitable for geochronology. The low totals obtained and the lack of tunnel cations (Ba, K, or Pb) suggest that this sample is not composed of hollandite.

2.2.3.7 Sample in Relation to Regolith: Manganese and iron oxide pods cementing transported sands. Mn-oxides occur below a massive duricrust horizon.

2.2.3.8 Datable Minerals/Host Rock Relationship: influx of elements, in solution, from outside sources located at stratigraphic positions equivalent to or higher than the deposition site?

2.2.3.9 Sources of Elements: "Iron and Mn rich bodies occurs as pods and slabs up to 3 m across and are dominated by hollandite and goethite. Enrichment of Fe and Mn on the broad valley floors is a modern process." (Anand *et al.*, 1996).

2.2.3.10 Overview

2.2.3.11 Results

2.2.3.11.1 Electron Microprobe and SEM Analysis

The Mn-oxide sample obtained CRCLEME researchers occur as friable Mn-oxide coatings on iron oxides. These coatings were easily scrapped from the sample with a steel pointer and were extremely easy to press into powder with bare fingers. These physical properties suggest that the oxides are poorly crystalline and are not hollandite-group minerals, which are generally very hard (up to 7 in the Mohs' scale). SEM and EMP investigations of the samples confirmed the poorly crystalline nature of the samples, the intimate intergrowth of Mn-oxides with iron oxides and clay minerals, and the lack of significant Ba or K (or Pb) in the sample, which precludes them from being hollandite-group minerals (Fig. 46b). Attempts to crush the samples and separate pure Mn-oxides by desegregating the sample in an ultrasonic bath did not yield any results either. The results of the tests above indicate that the sample is not suitable for geochronology. Thus, samples from this area were not dated.

2.2.3.11.2 Geochronology

The Mn-oxide from the Drifter prospect were not suitable for geochronology and were not analysed.

2.2.4 Discussion - Western Succession

The ideograms for the results obtained from the Mesa 1 and Gunpowder Creek outcrops are remarkably consistent (Fis. 37 and 45). The geochronology results show a predominance of ages in the range 30-40 Ma, with the strongest component at approximately 35 Ma. In addition, both areas show the possible existence of older ages (low 40's and approximately 65 Ma), although these dates need confirmation with more well defined analyses. However, these older dates are the same identified in the weathering profiles in the Overhang and Selwyn deposits, suggesting that these results are not analytical artefacts and may indeed have age significance. The implications to landscape evolution in the area will be discussed at the end of the Mount Isa Block section.

The possibility of younger Mn-oxide precipitation in the duricrusts at the Drifter prospect area needs to be further investigated. If suitable samples for geochronology were found in that site, they could provide important information on the nature and timing of duricrust formation in the valleys and on whether the manganese oxides found in these duricrusts are associated with modern processes as suggested.

The chemistry of the Mn-oxide samples analysed from the Mesa 1 and Gunpowder Creek sites at the Western Succession differ markedly from the chemistry of Mn-oxide samples from the Mount Isa area. Of particular interest are the relative low Zn content, the absence of Pb, and the relatively high Ba and Co values (Figs. 27, 28, 39, and 40). Unfortunately, Cu was not analysed routinely by the electron microprobe methodology during this project. This missing information could be crucial for identifying the style of mineralisation possibly associated with the sites sampled. However, the chemistry of the Mn-oxides in this area suggest an affinity toward Cu-mineralisation, based on comparison between the chemistry of the Mn-oxides in this area and the Mn-oxides analysed from other areas (this report and Vasconcelos, 1992). However, the Zn contents of the Mn-oxide sample from the Drifter prospect (Fig. 46) suggest a base metal affinity.

2.3 Lawn Hill Region

Contrary to the weathering profiles developed in the Mount Isa and Buckley River areas, weathering profiles in the Lawn Hill region are poorly developed. Even profiles overlying the Century sulphide orebody (Figs. 47 and 48), a fairly reactive mineral assemblage, do not show the same extent of weathering displayed by the Mount Isa or Hilton orebodies. No supergene enrichment blankets are present, and the exposed mineralised lithology is in the saprock/lower saprolite stages of weathering. Despite the absence of deep weathering profiles, the area is characterised by several iron/Mn-oxide-rich outcrops (Figs. 47 and 48), locally denominated "false gossans".

2.3.1 Century Deposit

2.3.1.1 Site Selection Criteria: massive, conspicuous Mn-oxide crusts in the vicinity of an outcropping world-class Zn-Pb-Ag orebody, access to several exposures, an open pit, and many drill-cores made this site ideal for investigation.

2.3.1.2 Location: 46600mE-27400mN

2.3.1.3 Elevation (sampled outcrops): ~ 150-180 m

2.3.1.4 Geomorphologic Setting: dissected, low elevation hills on shallowly weathered Proterozoic bedrock. Minor Cambrian limestone caps occur in these hills.

2.3.1.5 Geomorphologic Regime: erosional.

2.3.1.6 Sample in Relation to Landscape Position: Mn-oxides in lower saprolite, saprock, and in silicified hardcaps.

2.3.1.7 Sample in Relation to Regolith: Mn-oxides in lower saprolite, saprock, and in silicified hardcaps.

2.3.1.8 Datable Minerals/Host Rock Relationship: influx of elements, in solution, from outside sources located at stratigraphic positions equivalent to or higher than the deposition site.

2.3.1.9 Sources of Elements: Mn is probably derived from weathering carbonates associated with the alteration halo in the Century deposit. K and Ba are derived from feldspars and micas in the host Proterozoic metasediments. Pb and Zn are derived from the sulphides in the nearby Century orebody.

2.3.1.10 Overview

Massive Mn-oxide outcrops occur on several hilltops (Discovery Hill, No Name Hill, Magazine Hill) in the Century area (Fig. 47). The most massive Mn-oxide concentration occur at the contact between the underlying Proterozoic mineralised sequence and the overlying Cambrian limestone (Figs. 47 and 48). This Mn-oxide concentration was locally called "false gossan" because the oxides were hosted preferentially by Cambrian limestones stratigraphically overlying the Proterozoic sequence which hosts the Century deposit. Mn-oxides occur as massive and botryoidal concentrations (Fig. 49). These oxides often contain remnants of chert

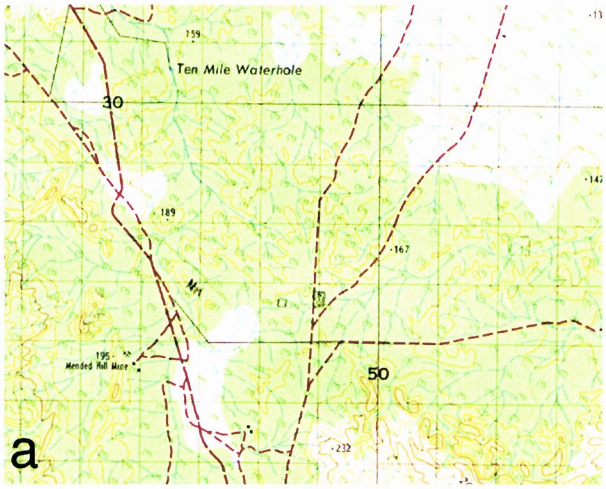

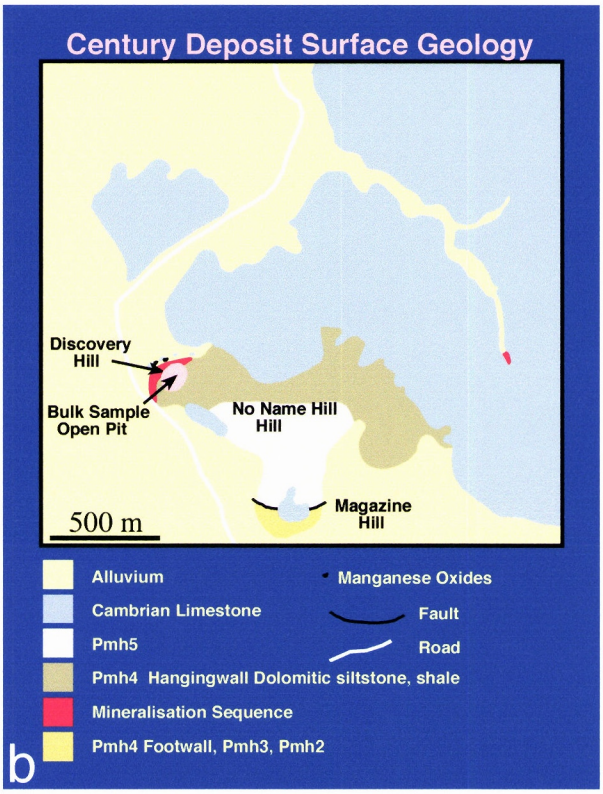

Figure 47. (a) The topographic map illustrates the geomorphologic setting of the Century deposit. (b) A simplified geological map illustrates the local geology, the location of the three outcrops sampled for Mn-oxide geochronology (Discovery Hill, No Name Hill, and Magazine Hill) and the location of the outcropping mineralisation and the experimental pit illustrate in (g). (c) West-facing view shows the dissected landscape surrounding the Century Discovery Hill. (d) West-facing view of Magazine Hill shows the distribution of silicified outcrops of Cambrian Limestone overlying the Proterozoic mineralised sequence. (e) Close-up view depicts the Mn-oxide rich outcrops on Magazine Hill. (f) No Name hill outcrop is shown here. (g) NNE view shows exposed mineralised sequence in experimental pit.

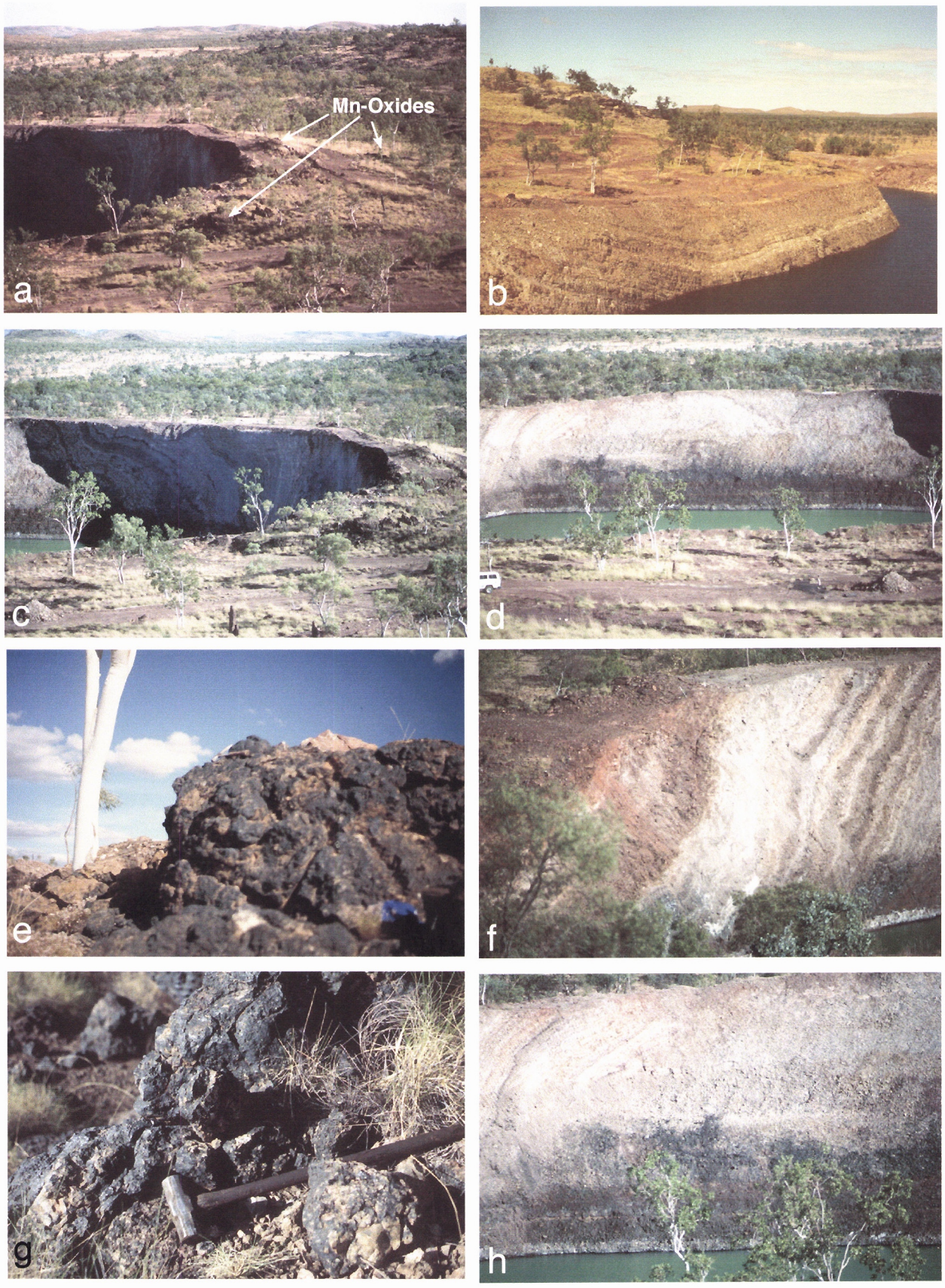

Figure 48. (a) West-facing view of the Century experimental pit illustrates the geomorphologic setting of the Discovery Hill and the location of Mn-oxide rich outcrops surrounding the exposed mineralised Proterozoic sequence. (b) NNE view shows exposed mineralised sequence in experimental pit. (c) Close-up of area shown in (c). (d) West-facing view of Century experimental pit illustrates the concentration of Mn-oxides at the contact between the aerated zone and the partially saturated (capillary fringes) zone of the weathering profile overlying the Century deposit. The distribution of Mn-oxides in this zone suggest significant migration of Mn in solution in the present water table. (e) Close-up view illustrating the massive Mn-oxide outcrops at the boundary between the Cambrian limestone overlying the Discovery Hill outcrop and the underlying mineralised Proterozoic sediments. (f) A view of the experimental pit wall illustrating the contact between Proterozoic sediments and overlying Cambrian limestone. (g) Close-up view of massive Mn-oxide cements hosted by chert-rich lowermost Cambrian limestone. (h) Close-up view of (d).

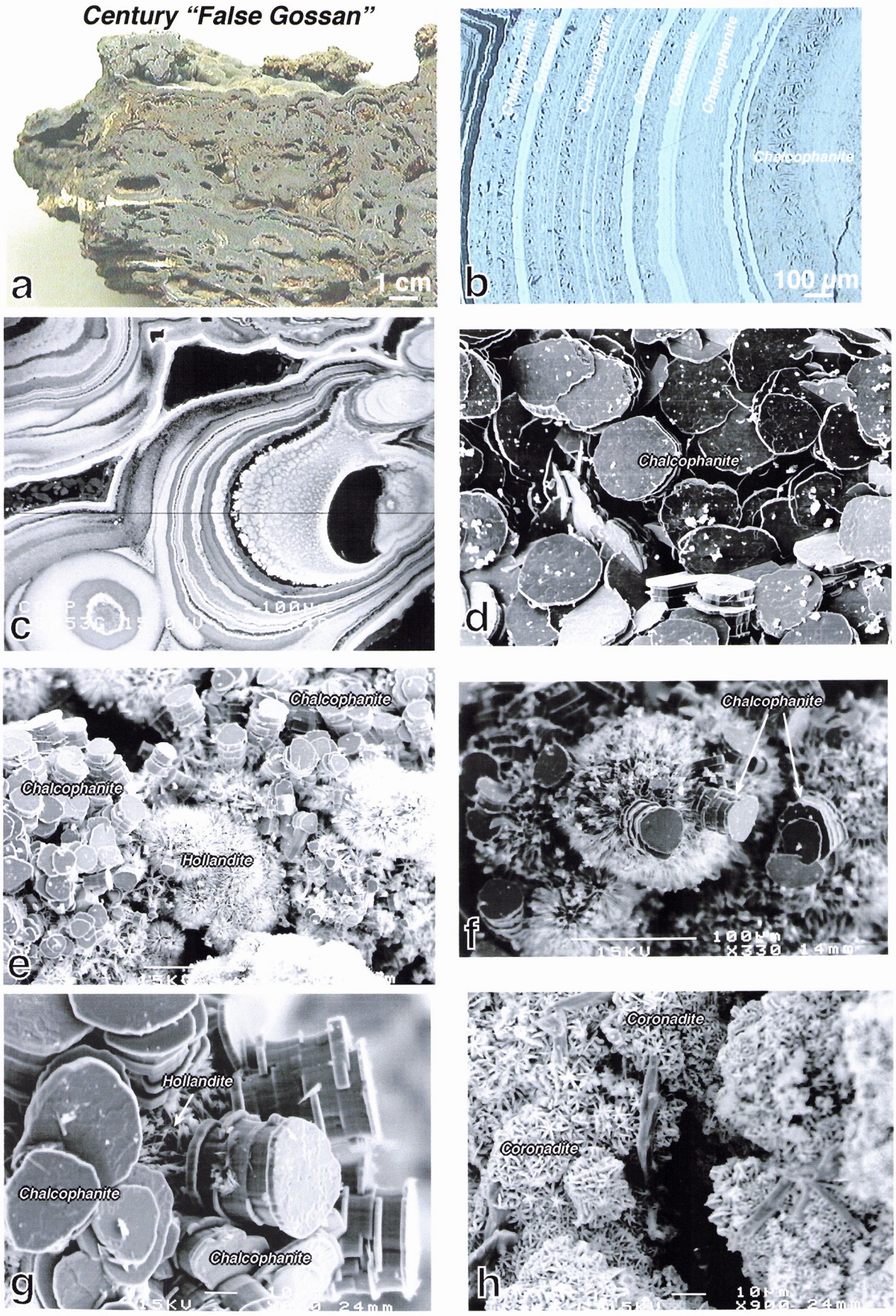

Figure 49. (a) Cross-section through Century "False Gossan" illustrating the botryoidal character of the Mn-oxides present in this outcrop. (b) Reflected-light photomicrograph of botryoidal Mn-oxides illustrated in (a) showing the alternating bands of Zn-rich (chalcophanite) and Pb-rich (coronadite) Mn-oxides. (c) Backscattered SEM photomicrograph of the Mn-oxides shown in (a) illustrating the complex alternation between Pb-rich (light colour bands) and K-rich (dark colour bands) hollandite and a central (light colour) band of plumbogummite in the samples. (d) SEM photomicrograph of chalcophanite crystals in the Century "False Gossan" samples. (e) SEM photomicrograph illustrating stacks of chalcophanite crystals and associated bundles of hollandite (possibly coronadite) needles. (f) SEM photomicrograph illustrating close relationship between chalcophanite and the acicular hollandite phase. (g) Same as (f). (h) SEM photomicrograph of star-shape coronadite crystals. The presence of coronadite, chalcophanite, and plumbogummite in these samples suggests a close proximity of the Pb and Zn sources.

fragments common in the lower Cambrian rocks in the area (Figs. 48 and 49). The oxides are also intimately intergrown with Al- and Pb-phosphates and are partially replaced by iron oxides (Fig. 50).

Several Mn-oxide samples from the Discovery Hill outcrops were collected for mineralogical and geochronological investigation. In addition, samples from several other outcrops in the region (No Name Hill, Magazine Hill, Tunnel Hill, Silver King old workings, and Termite Range outcrops) were collected. Unfortunately, in this study only a limited number of samples could be analysed. The Discovery Hill outcrop was deemed the most important site and most samples analysed were collected at this location. Only one additional grain, from the Termite Range outcrop, was analysed. A sample from the Magazine Hill was also dated by the K-Ar method.

2.3.1.11 Results

2.3.1.11.1 Electron Microprobe and SEM Analysis

Century Mn-oxides were subject to intensive studies during this project and during a CRA funded Honours project in the area (Whitbread, 1995). The abundance and complexity of the Mn-oxide mineralogy in the area is the subject of continuing studies by the author. Figures 47 and 48 illustrate the Mn-oxide outcrops. Figures 49 to 52 provide more detailed hand-specimen, petrographic, and electron microscopic information about the Century samples. The photomicrographs illustrate the presence of abundant botryoidal Mn-oxides (Figs. 49a-c). Cavity fillings in these samples reveal the presence of superb chalcophanite (Figs. 49d-g), acicular hollandite (Figs. 49e-g), and star-shaped coronadite (Fig. 49h) crystals. Petrographic and SEM/EMP investigations also reveal the presence of euhedral, cavity-filling plumbogummite (Fig. 52).

Several EMP traverses were analysed in the samples. Figures 50 and 51 illustrate three such traverses. The EMP results show the alternation between cryptomelane, plumbogummite, chalcophanite, and coronadite bands, suggesting large shifts in the compositions of the weathering solutions during the precipitation of the Mn-oxide crusts. In addition, the EMP analyses and SEM results identify the presence of a late stage Si-Al-Fe phase (Fe is not plotted in the traverses illustrated). Lastly, the electron microprobe results clearly indicate that the samples investigated are rich in K and suitable for $^{40}Ar/^{39}Ar$ geochronology.

2.3.1.11.2 Geochronology

To determine the timing of Mn-oxide precipitation, several samples were analysed by the K-Ar and $^{40}Ar/^{39}Ar$ methods. Four Mn-oxide samples were dated by the K-Ar method at UQ (Whitbread, 1995). The results are listed below:

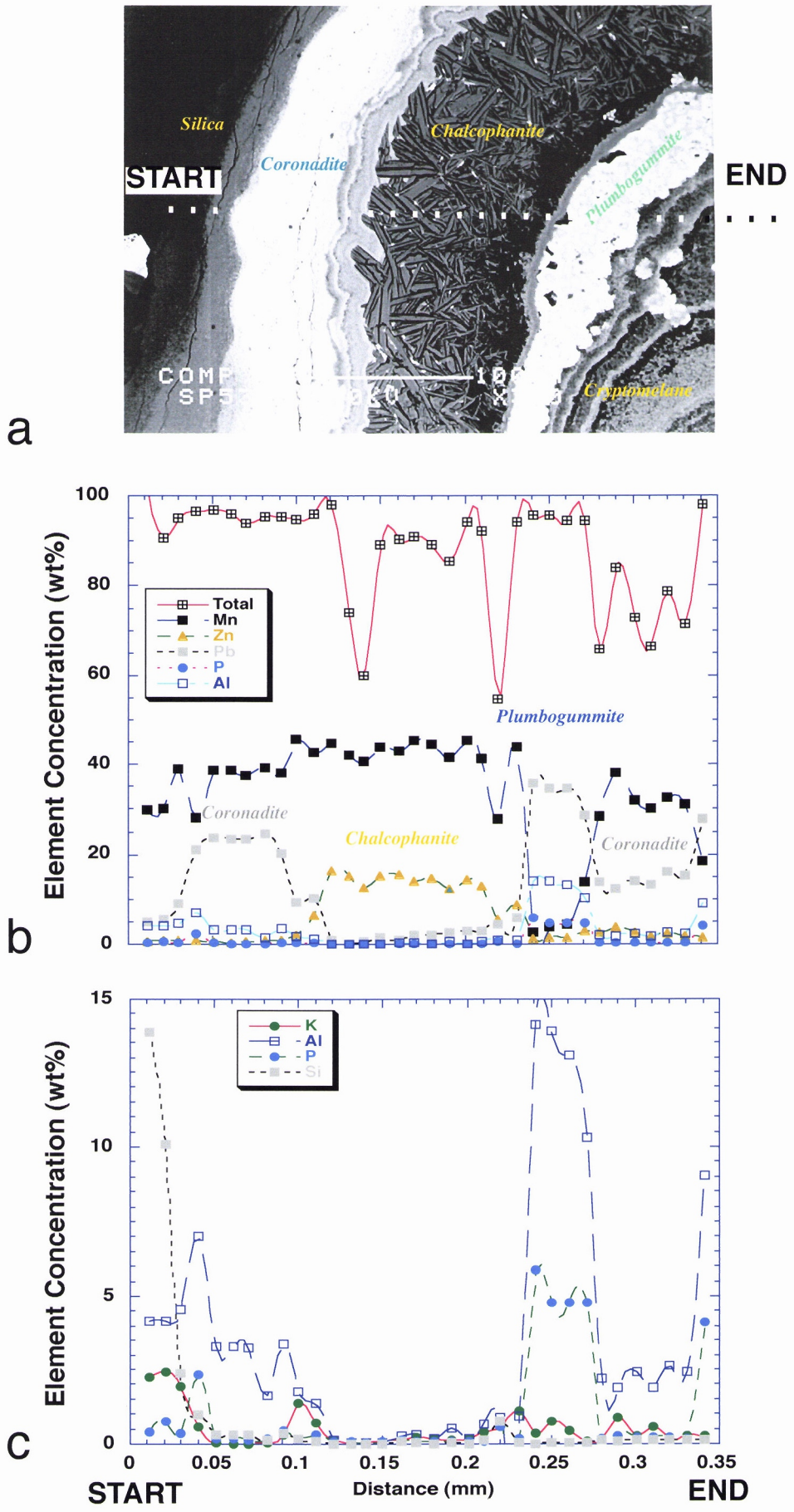

Figure 50. (a) Backscattered SEM photomicrograph illustrating alternating bands of cryptomelane, plumbogummite, chalcophanite, coronadite, and supergene silica (opal) in the Discovery Hill Mn-oxide samples. The location of the EMP traverse analysed in this sample is also shown. Major (b) and minor (c) elements analysed in the EMP traverse are illustrated.

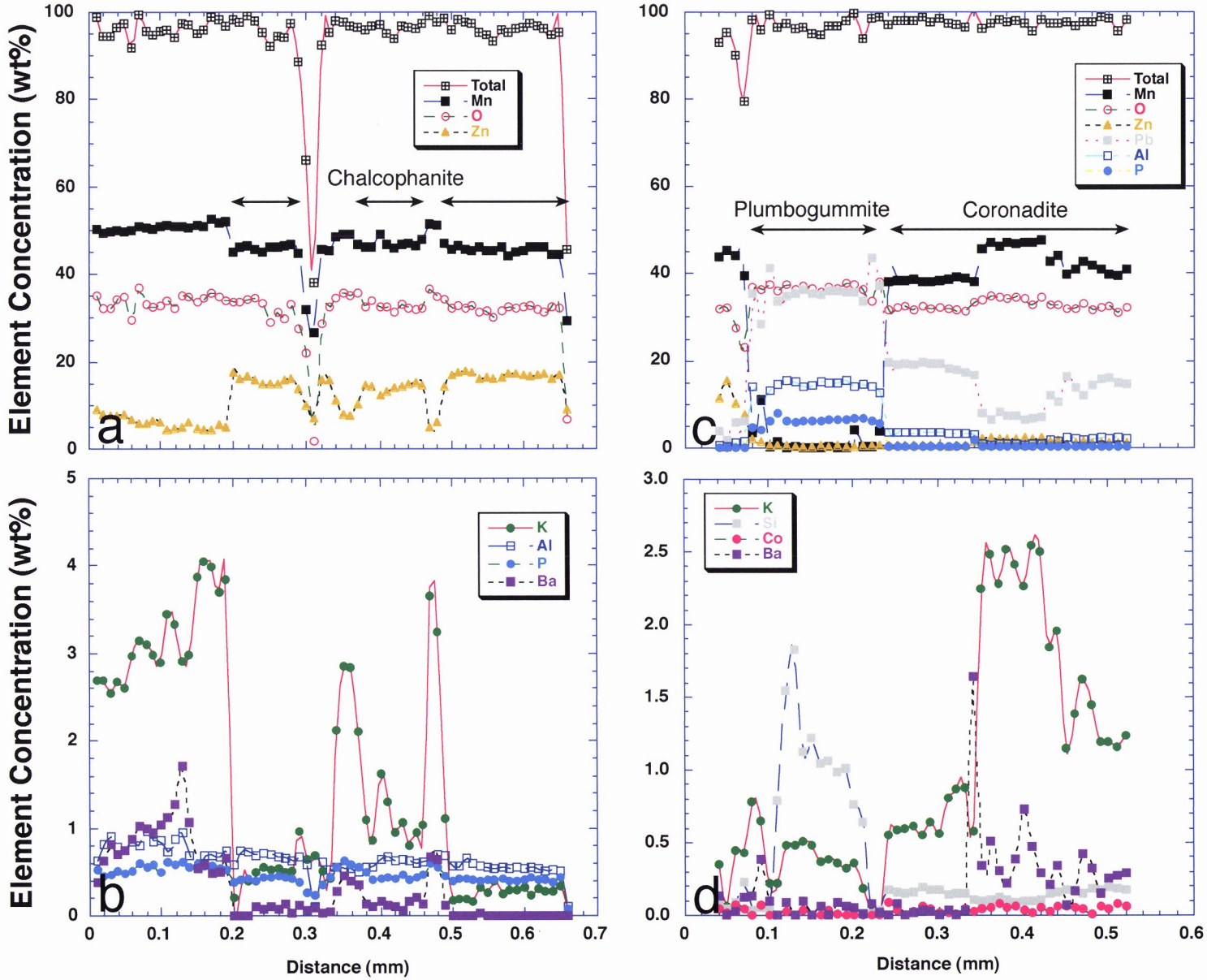

Figure 51. Major (a) and minor (b) elements analysed in an EMP traverse through botryoidal Mn-oxide samples show the variations of Zn and K-Ba in the sample corresponding to alternating chalcophanite and hollandite bands. Notice also that some of the chalcophanite bands may contain up to 0.6 wt% K, suggesting that chalcophanite could be potentially datable by the Ar/Ar method. Major (c) and minor (d) elements analysed in another traverse, this time illustrating alternation between plumbogummite, chalcophanite, coronadite, and cryptomelane samples.

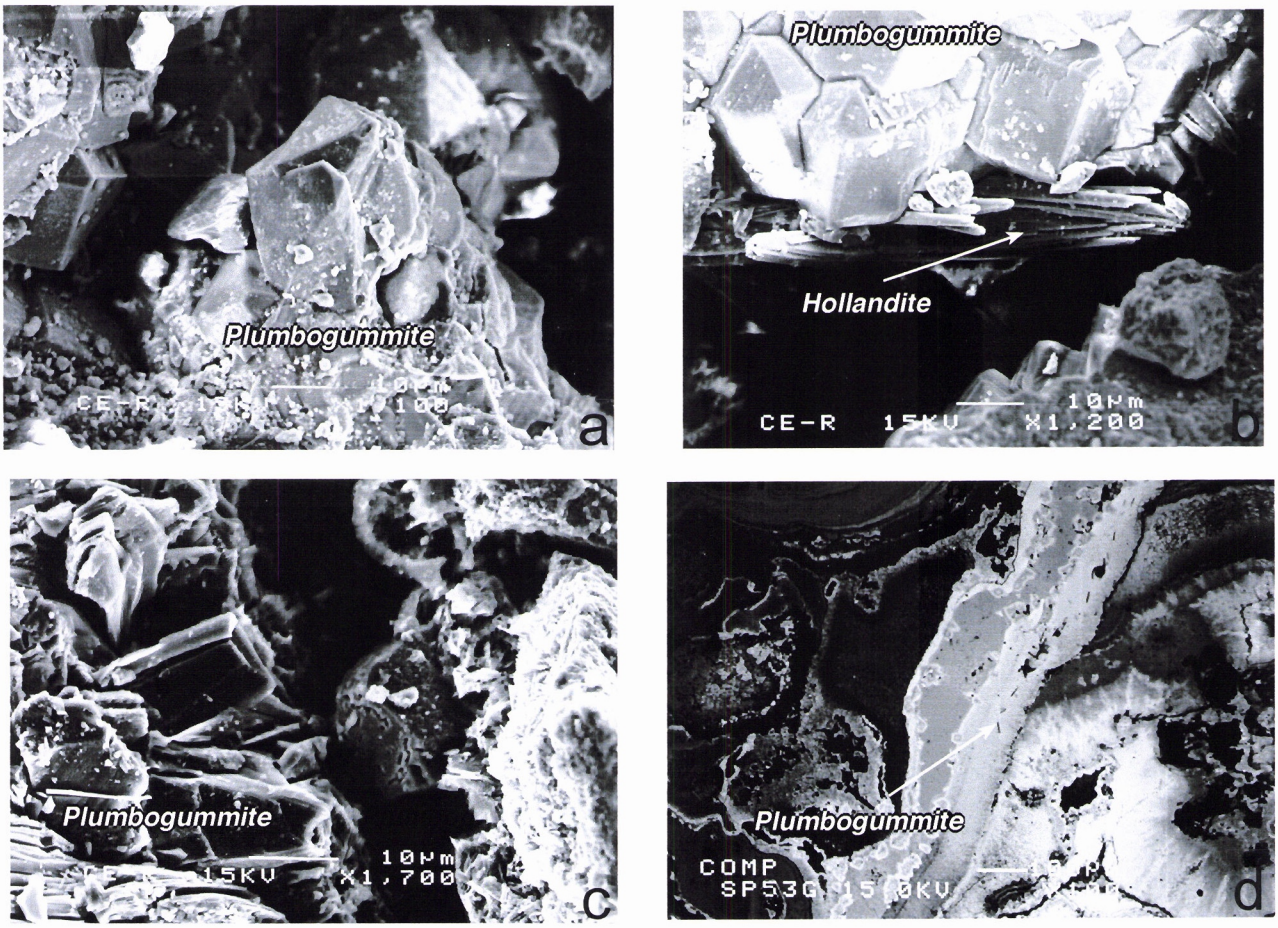

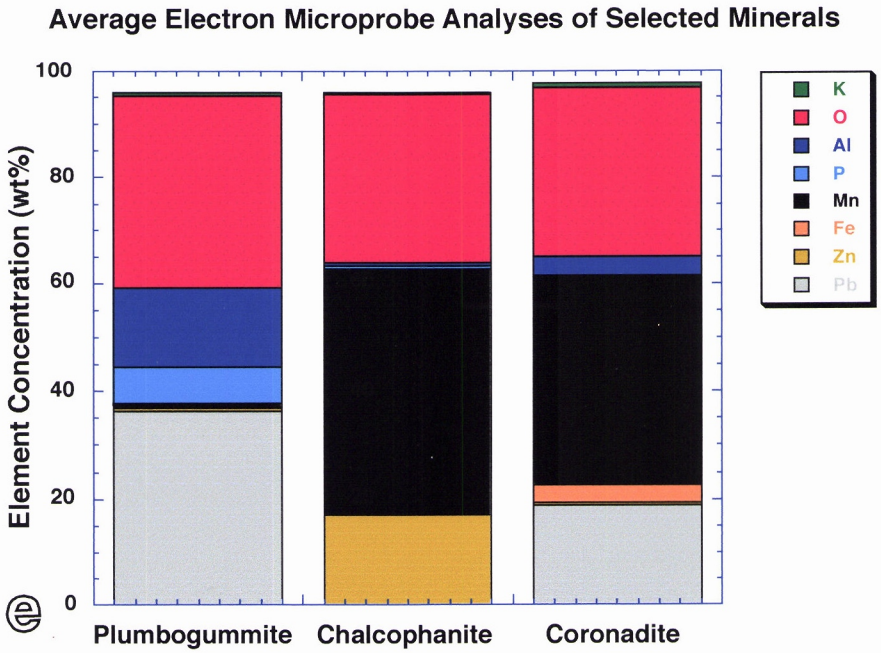

Figure 52. (a) Scanning electron photomicrograph of plumbogummite sample in Century outcrop samples. (b) Notice the intimate intergrowth textures between plumbogummite and acicular hollandite crystals suggesting the transport of Pb, P, Al, and Mn in the same weathering solution. (c) SEM photomicrograph shows cavity filling plumbogummite. (d) Backscattered SEM photomicrograph displays plumbogummite vein cross-cutting previously precipitated supergene phases. (e) The stack diagram illustrates the average composition of plumbogummite, chalcophanite, and coronadite samples from the Century Discovery Hill "False Gossan" outcrops. The high Pb and Zn contents in this samples require a local source for these elements (weathering Century orebody?) and are not likely to reflect long range transport of Pb and Zn along the Cambrian-Proterozoic unconformity.

Table 5. K-Ar results for samples from the Century "false gossans" outcrops.

Sample No.	Weight (g)	Wt% K_2O	$^{40}Ar^*$ (cc/g)	*Age (Ma)*	*± 1σ (Ma)*	% Rad.
CE-26	0.1133	4.465	4.185×10^{-6}	***8.7***	***0.7***	30.0
CE-N	0.2765	1.510	2.768×10^{-6}	***5.6***	***1.5***	10.0
CE-R	0.2303	1.355	4.887×10^{-6}	***10.7***	***2.9***	9.6
CE-1L	0.2131	3.300	9.159×10^{-6}	***11.5***	***2.6***	13.4

Seven grains from the four different hand specimen above were also analysed by the laser-heating $^{40}Ar/^{39}Ar$ method at the BGC. The results yielded well defined plateau ages ranging from 5.6 ± 0.1 to 9.0 ± 0.3 Ma (Fig. 53), consistent with the values obtained by the K-Ar method. The only sample not derived from the Discovery Hill outcrop (Fig. 53g, Termite Range outcrop) yielded a plateau age 7.7 ± 1.1 Ma within the range of ages obtained for the Discovery Hill outcrops.

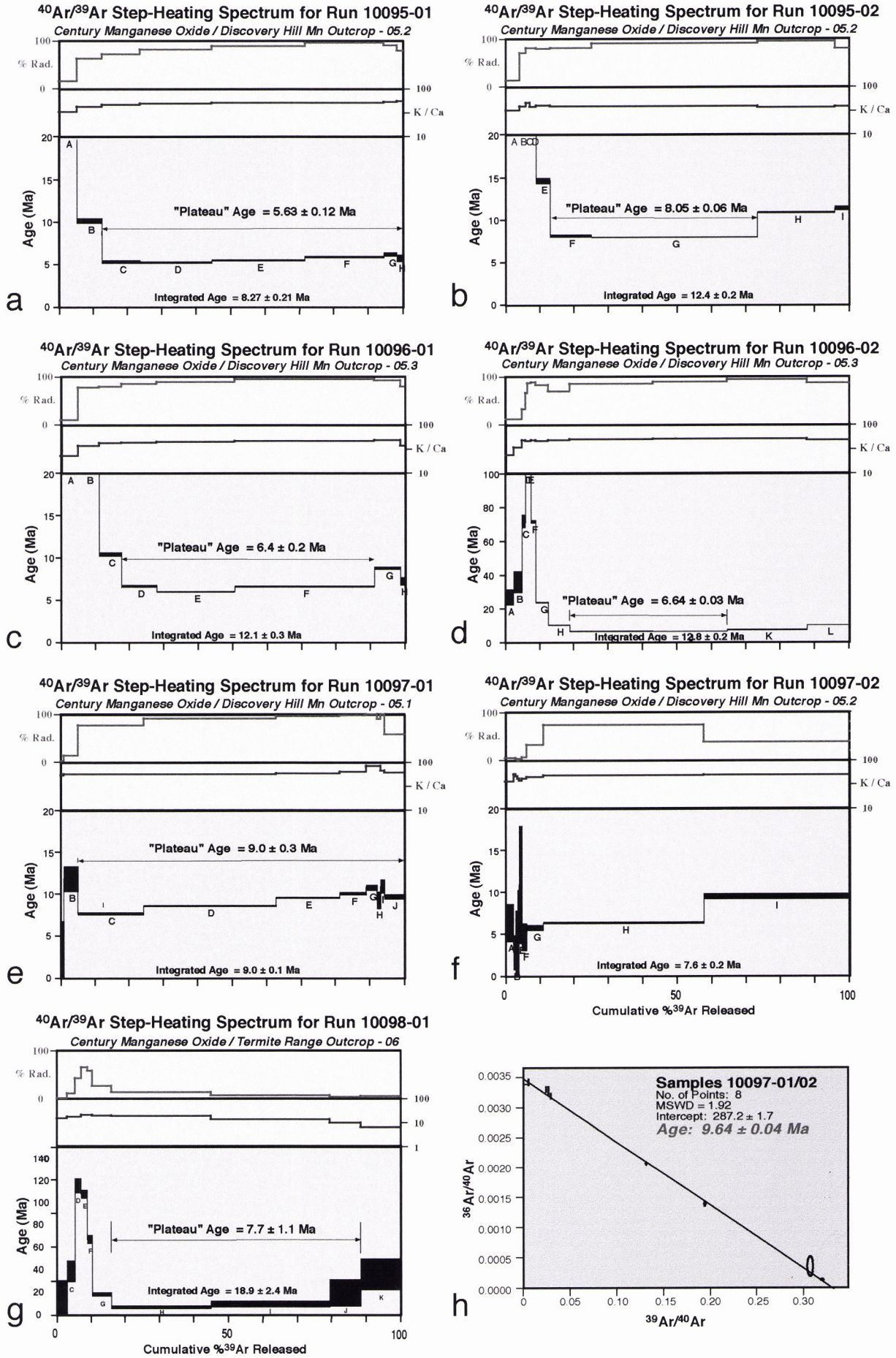

Figure 53. (a) to (g) illustrate representative step-heating spectra for Century Mn-oxides. The results obtained suggest a relatively young age (5-10 Ma) for the precipitation of Mn-oxides in this system when compared to samples from other Mount Isa Block outcrops.

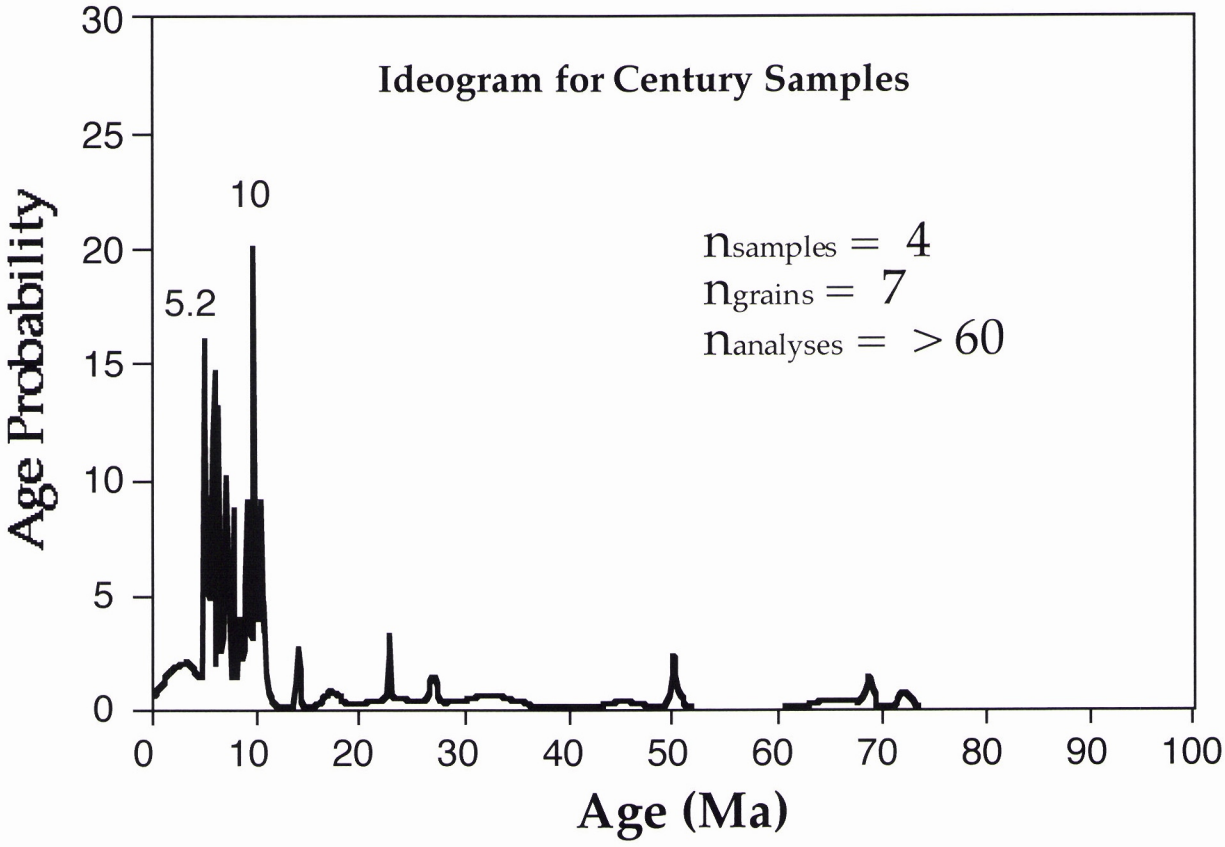

Figure 54. Ideogram illustrating the two most probable age groups (ca 5 and 10 Ma) for the Century Mn-oxide outcrops.

2.3.2 Discussion - Lawn Hill Region

The geochronology results indicate that the weathering profiles present at Century are much younger than the weathering profiles dated in the Mount Isa, Western Succession, and Eastern Succession (below) areas. The immaturity of the weathering profiles and the young ages obtained suggest that the area has undergone significant erosion throughout the Tertiary and that only recently formed weathering crusts are preserved. The mineralogy of the "false gossans" outcrops also suggests that the source of the elements contained in the Mn-oxide minerals is probably the weathering Century orebody (Pb isotope studies of these samples support this interpretation (Whitbread, 1995)). Elements such as Zn, Pb, and Mn had to leave their sources at the Century orebody and travel to the deposition site at the contact between the Proterozoic sediments and the overlying limestone. Since Mn is mobile in its reduced state, it is unlikely that the weathering crust present at the surface today formed in the oxygen-rich unsaturated part of the weathering profile. A more likely scenario is the migration of Mn, Pb, and Zn in the saturated, relatively reduced, part of the groundwater system. These elements were released from the weathering orebody and dissolved in the acidic solutions generated by the weathering sulphide orebody. As these reduced acidic solutions encountered the

geochemical barrier imposed by the nearby limestones, Mn-oxides precipitated. The precipitation of these oxides acted as catalyst for the precipitation of other elements from solution (Zn, Pb, Fe, P, etc.). This hypothetical geochemical scenario is illustrated below (Fig. 55) and the hypothesised geochemical conditions leading to the precipitation of Mn-oxides are shown by the arrows in Fig. 5.

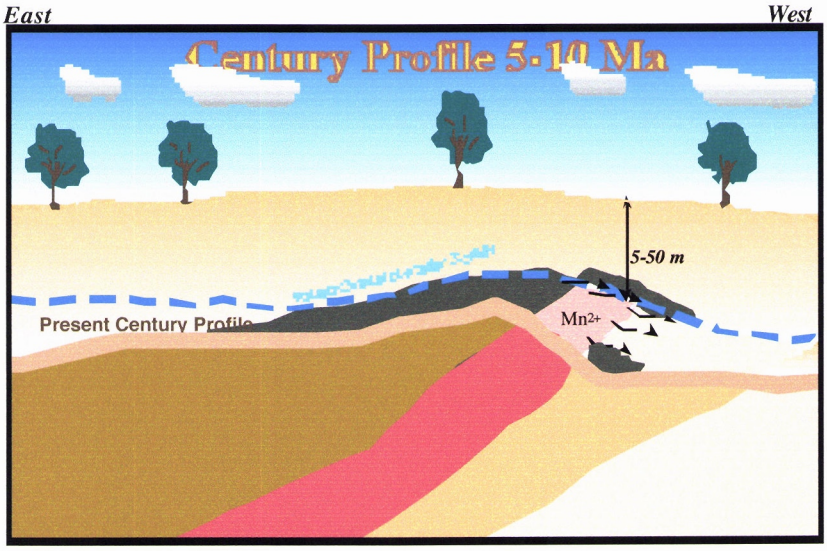

Maximum Erosion Rate: 10 mMa^{-1}

Minimum Erosion Rate: 0.5 mMa^{-1}

Figure 55. Diagrammatic illustration showing a possible evolution model for the Century weathering profiles. The Mn-oxide outcrops now found at the surface precipitated at the contact between the mineralised Proterozoic bedrock and the overlying Cambrian limestone. The alkaline barrier imposed by the presence of the limestone forced the precipitation of soluble Mn^{2+} from solution as illustrated in Figure 5.

Similarly to the Mount Isa gossan samples, the Mn-oxides associated with the Century weathering profiles are preferentially enriched in the target elements Pb and Zn when compared to coexisting Fe-oxides, clay minerals, and other coexisting supergene phases, with the exception of plumbogummite. These results further reinforce the suggestion that the unique crystal structures of the Mn-oxides found in these weathering profiles promotes the preferential enrichment of these phases in base metals.

The presence of several Mn-oxide rich "gossans" in the Lawn Hill region (Andy White, personal communication) suggests that the routine study of the crystal chemistry of these Mn-oxides in exploration targets in the area may be a simple way of quickly assessing their mineralisation potential.

2.4 Eastern Succession

The landscape in the Eastern Succession, particularly in the area between Cloncurry and Selwyn, is characterised by steeply scarped ridges and plateaus (400-500 m elevation) surrounded by deeply dissected valleys (200-350m). These ridges and plateaus are often associated with ironstones and banded iron and manganese Proterozoic metasediments. Given the nature of the parent material, some of the plateaus and ridges host deeply weathered, oxide-rich profiles. Where Mn-oxides are present, the samples are invariably suitable for weathering geochronology.

The concordant hills', mesas' and ridges' summits in the region have been considered by many authors as evidence for the presence of a now partially truncated erosion surface developed sometime in the Mesozoic. Workers such as King (1957) and Twidale (1994) have named this hypothesised surface the Gondwana surface, which they correlated to similar landscape features in Africa and eastern South America. The presence of deep, near complete weathering profiles on top of the ridges and hill tops, allows us to determine if the ages of weathering in these surfaces support the hypothesis of a widespread weathering surface covering the Gondwana paleocontinent.

2.4.1 Overhang Deposit

2.4.1.1 Site Selection Criteria: exposure of a complete weathering profile, formed on manganesiferous bedrock and situated in the remnants of a high elevation ridge surrounded by several dissected valleys, makes this site ideal for investigation.

2.4.1.2 Location: 343650E-7679000N

2.4.1.3 Elevation: ~360-400 m

2.4.1.4 Geomorphologic Setting: ridge on deeply weathered (60 m) and dissected Proterozoic bedrock.

2.4.1.5 Geomorphologic Regime: relict.

2.4.1.6 Sample in Relation to Landscape Position: the weathering profile sampled in this site forms a residual ridge, protected from erosion by the resistant nature of the host lithologies. The ridge summit is nearly concordant with the summits of nearby ridges. These ridge summits are also concordant with surrounding mesas which characterise the highest elevation features in the area.

2.4.1.7 Sample in Relation to Regolith: Mn-oxides occur as the primary weathering product of Proterozoic banded manganese-formations. At the bottom of the weathering profile (valley bottom, 280-300m elevation), weathering is incipient and pseudomorphic. Samples at this level are considered part of the saprock (Figs. 56d and 57f, g and h). Toward the middle of the profile, Mn-oxides indicate at least two periods of weathering, with dissolution of primary minerals and first generation Mn-oxides followed by the precipitation of second generation Mn-oxides in the resulting voids (Figs. 56d and 57c, d, and e). Samples from this

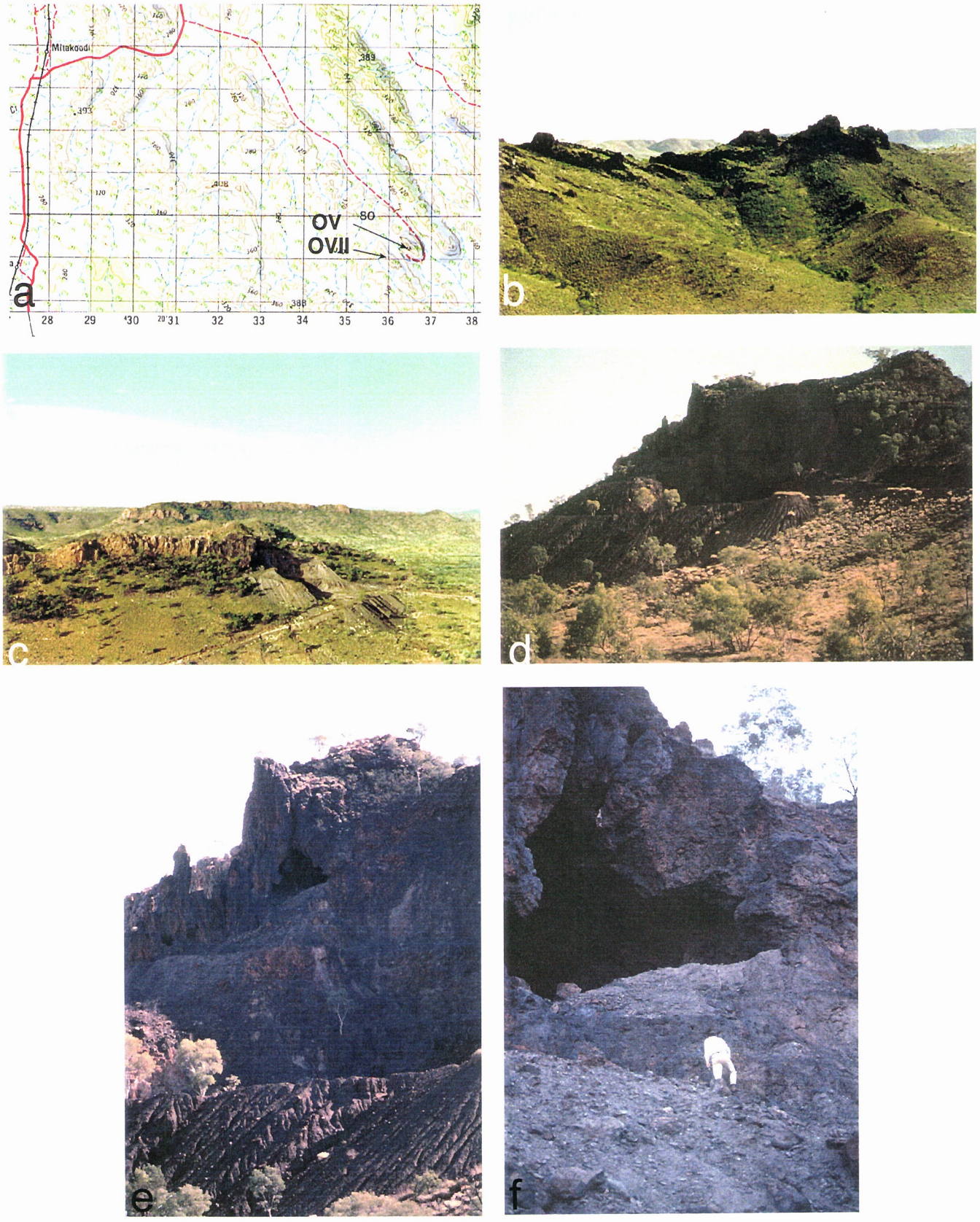

Figure 56. (a) The topographic map illustrates the geomorphological setting of the Overhang manganese deposit. (b) West-facing view from Overhang deposit illustrates the concordance of elevation between adjacent ridges and plateaus in the area. (c) East-facing view of the ridge hosting the Overhang deposit shows the surrounding dissected valleys and the concordant hill summits in the background. Geochronological results in this study support the view that the flat-lying higher elevation part of the landscape may have been exposed to weathering processes since the Mesozoic. (d) This north-facing view of the Overhang deposit shows the continuity of the weathering profile from the ridge top to the valley bottom. (e) Close-up of the area in (d) shows the near complete exposure of the weathering profile which allowed that manganese oxide samples be collected from various depths in this profile. (f) Significant mass loss during the protected weathering history of this area has led to the formation of open cavities in the competent Mn-oxide lithologies.

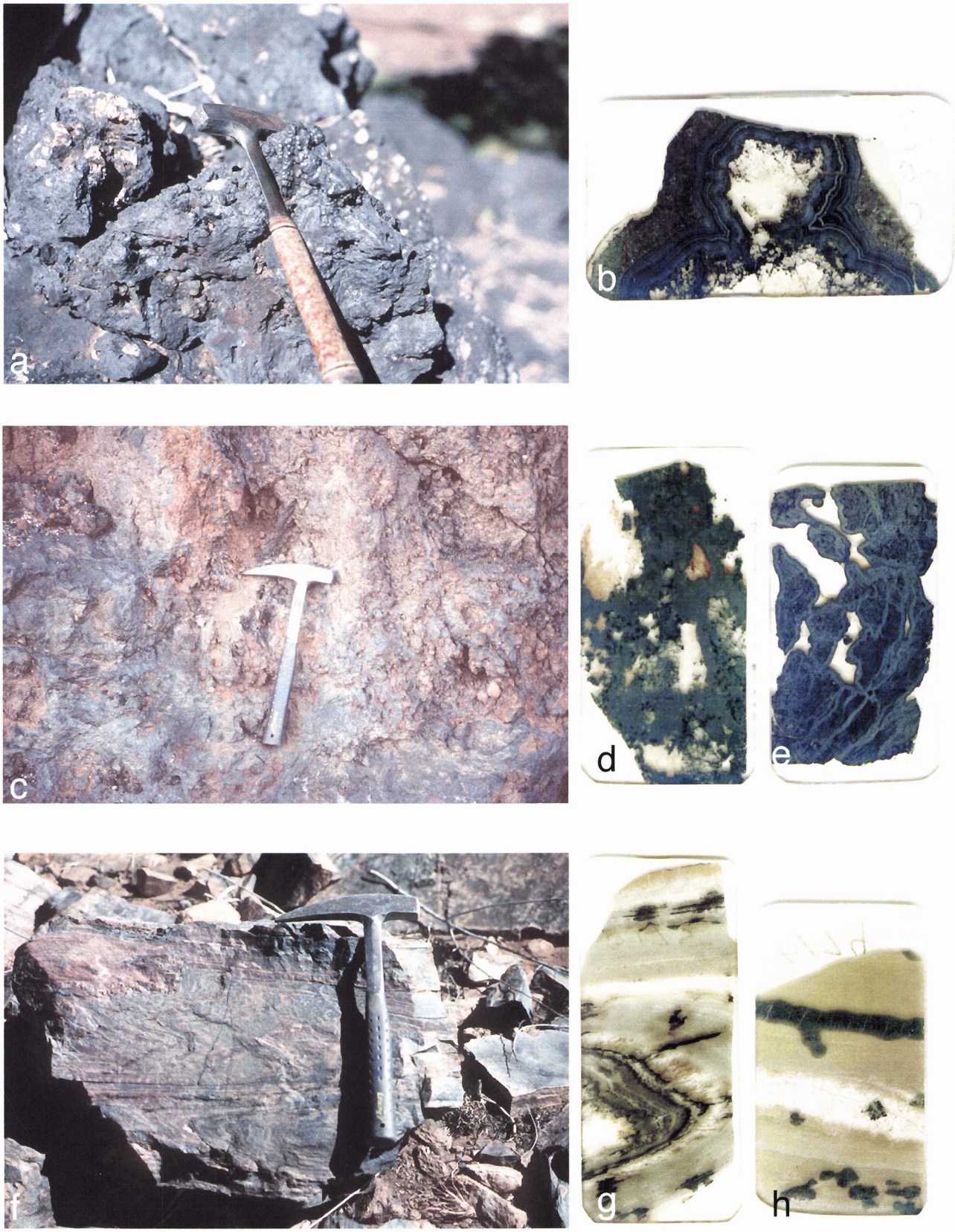

Figure 57. (a-b) These illustrations shows the botryoidal character of the uppermost Mn-oxide samples in the Mn-rich hardcap. The petrographic slide is (b) is approximately 5 cm long. (c-d) The saprolite in Mn-rich protolith is formed by the in situ weathering of underlying banded Mn-formation while maintaining some of the original textural features. (e) This petrographic slide illustrates mass loss and initiation of botryoidal texture development in the saprolite horizon. (f-h) The saprock of folded banded Mn-formation illustrates the character of the bedrock exposed at the low elevation dissected valleys adjacent to the deeply weathered ridges. Incipient weathering is visible in the left-hand upper corner of the sample. Penetration of oxidising meteoric waters along bedding planes and fractures promotes the in situ oxidation of Mn derived from Mn-silicates in the host rock. Mn-oxide precipitation in these samples could not be dated due to the intimate relationship between supergene Mn-oxides and partially preserved hypogene phyllosilicates in these samples.

level are considered part of the saprolite. At the top of the profile, Mn-oxides occur as botryoidal, void filling concretionary masses, sometimes still surrounding and overgrowing remnants of first stage Mn-oxides (Figs. 56d and 57a and b). These samples are considered as part of the hardcap or manganesiferous duricrust. Hardcap, saprolite, and saprock samples were collected.

2.4.1.8 Datable Minerals/Host Rock Relationship: in situ weathering of local minerals, with minor textural disruption and local recrystallisation of minerals, with major textural disruption.

2.4.1.9 Sources of Elements: manganese is locally derived from weathering Mn-carbonates and/or silicates present in the metamorphosed banded manganese formation. Potassium and Ba are derived from feldspars and micas in the host Proterozoic rocks.

2.4.1.10 Overview

A deeply weathered (>60 m) Proterozoic banded-manganese formation hosts the now abandoned Overhang manganese mine. The host rock to the weathering profile is a rhodochrosite-rhodonite-bearing banded-manganese formation. Relatively unweathered bedrock (Fig. 57f, g and h) outcrops at the bottom of the valley (~280-300m elevation) immediately SW of the Overhang deposit (Fig. 56d). The weathered manganese formation forms a resistant oxide-rich ridge (Fig. 56), which hosts abundant manganese ore in the form of hollandite, cryptomelane, pyrolusite and lithiophorite (Figs. 57 and 58).

2.4.1.11 Results

2.4.1.11.1 Electron Microprobe and SEM Analysis

Petrographic sections for samples from the Overhang deposit (Figs. 57 and 58) clearly show the distinct changes in textures as the primary silicate-carbonate bedrock undergoes progressively more intense weathering. Incipient stages of weathering is characterised by the penetration of oxidising solutions along fractures and bedding planes, promoting the in situ oxidation of Mn^{2+}-bearing minerals (Figs. 57g and h). Mn-oxides formed at this stage are intimately intergrown with unweathered primary minerals and are not suitable for weathering geochronology, with few exceptions. As weathering progresses, mass loss associated with the dissolution of silicates and carbonates promotes the formation of open cavities in the samples (Figs. 57d and e). At this stage, some of the supergene oxides precipitated during the initial stages of weathering are dissolved and reprecipitated as high purity bands, overgrowths and cross-cutting veins (Figs. 57d and e). These samples are characteristic of the saprolite horizon and are suitable for $^{40}Ar/^{39}Ar$ dating. As weathering proceeds even further, the dissolution of primary minerals and previously precipitated Mn-oxides leads to the formation of large botryoidal masses (Figs. 57a and b). The banded, concentrically grown Mn-oxides in these masses are very pure. These masses often enclose resistant fragments of the bedrock,

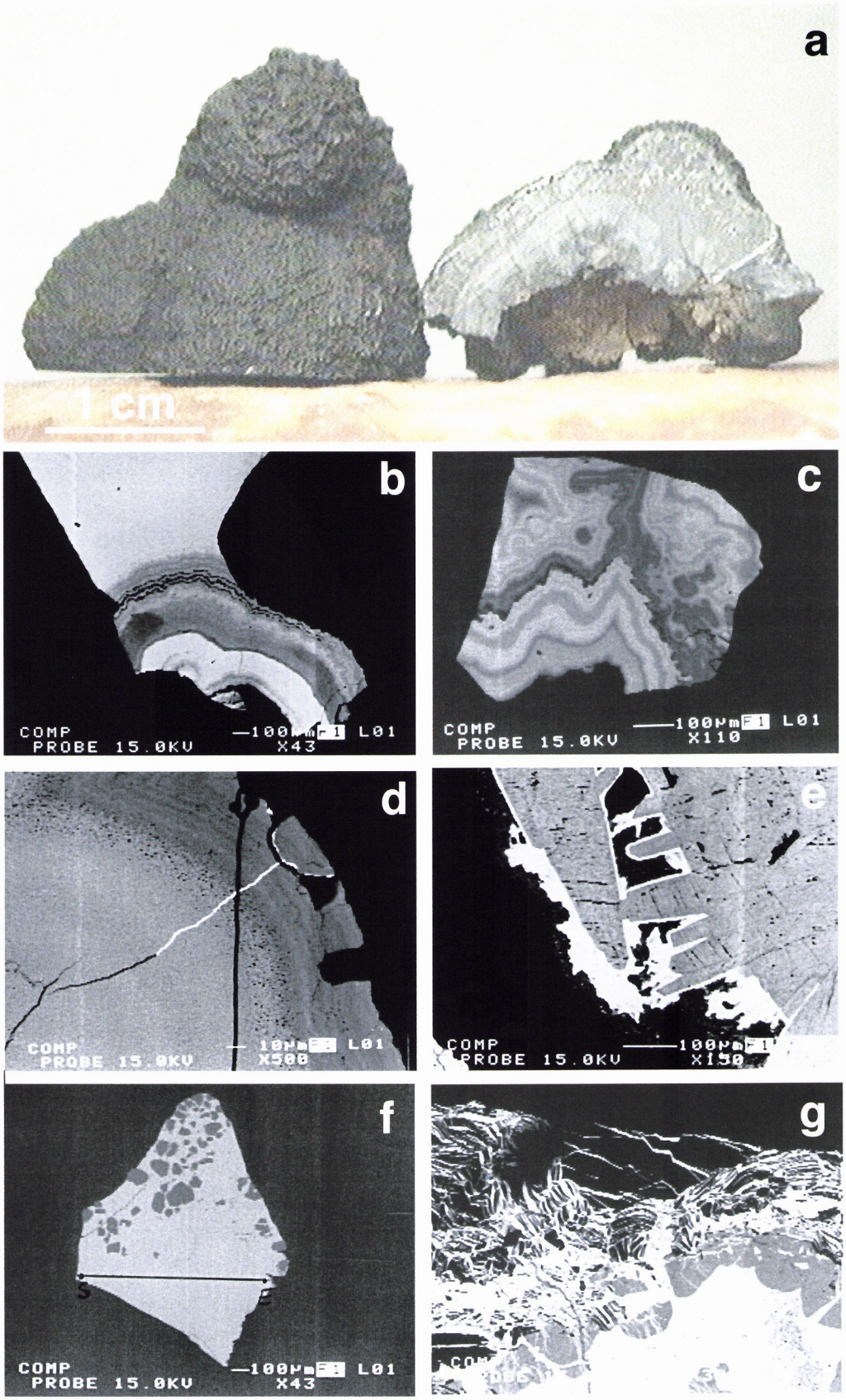

Figure 58. (a) A cross-section through botryoidal Mn-oxide sample illustrates the concentric distribution of inner hollandite bands surrounded by an outer growth of pyrolusite. (b) This massive Mn-oxide sample represents the material used in the geochronological analyses in this study. Notice the alternation between K-rich (dark bands) and Ba-rich (light bands) in the backscattered SEM photomicrographs (b-c). The high purity of these samples makes them suitable to geochronology. However, some of the Ba-rich Mn-oxides are completely devoid of K and have proven unsuitable to Ar/Ar dating. (c) This backscattered SEM photomicrograph shows the distribution of alternating light and dark bands of respectively Ba-rich and K-rich Mn-oxides. (d) Late-stage desiccation cracks in the botryoidal Mn-oxides indicates transition towards relatively arid conditions after the precipitation of these oxides. The desiccation cracks in these samples are often filled with barite. Barium is probably derived from the Mn-oxides while sulphur probably has a meteoric origin. (e) SEM photomicrograph shows barite overgrowths on pyrolusite. (f) Some manganese oxide grains may still host unweathered quartz (and other primary minerals) impurities. When these contaminated grains are dated, complex spectra climbing toward unreasonably old ages suggest the presence of the contaminants. (g) When the contaminant present in the Mn-oxide samples is composed of unweathered primary muscovite crystals, the age of metamorphism of the bedrock, and not weathering, is obtained.

particularly quartz veins (Fig. 57b). These masses characterise the hardcap in the area and are ideal for geochronology.

SEM investigation of samples from the Overhang deposit shows the presence of botryoidal oxides composed of alternating cryptomelane, hollandite, and lithiophorite bands. These samples are very often overgrown by a pyrolusite layer (Fig. 58a). SEM screening of grains selected for geochronology indicated that some samples yielded very pure Mn-oxide fragments (Figs. 58c-e), while other samples contained abundant primary quartz and muscovite contamination (Figs. 58g-h). Samples whose grains contained contamination were not dated by the $^{40}Ar/^{39}Ar$ method. Due to the limited nature of this study, very few samples from this deposit where analysed in this project. A subsequent Honours theses in the area (Fleming, 1997) yielded a wealth of information about the geochronology of weathering in the area. Most of Fleming's results have confirmed the preliminary numbers contained in this report.

SEM observation also indicates the presence of late-stage barite and opal filling desiccation cracks and overgrowing Mn-oxide crystals (Figs. 58e-f). The significance of the precipitation of late-stage sulphates and supergene quartz will be discussed below.

EMP traverses for the Mn-oxide samples from this deposit are illustrated in Fig. 59. These traverses indicate that the K content of the samples varies significantly from sample to sample. This variation in K contents indicates that some grains (K-rich) from a sample may be suitable for $^{40}Ar/^{39}Ar$ dating, while other grains (K-poor) from the same specimen may not yield significant $^{40}Ar/^{39}Ar$ results due to low K contents. The electron microprobe analyses also show that the samples in this deposit are devoid of Zn, Pb, and Co, consistent with Mn-oxide samples derived from Archean and Proterozoic banded manganese-formations elsewhere (Vasconcelos, 1994a).

2.4.1.11.2 Geochronology

Three distinct hand specimens from the area were analysed by the K-Ar method during an Honours project (Herlihy, 1995) at UQ. The results are presented in the table below:

Table 6. K-Ar results for samples from the Overhang deposit.

Sample No.	Weight (g)	Wt% K_2O	$^{40}Ar^*$ (cc/g)	Age (Ma)	$\pm 1\sigma$ (Ma)	% Rad
Con01	0.4036	0.530	1.373×10^{-6}	**80.3**	**6**	31.6
Con03	0.5050	2.130	5.296×10^{-6}	**77.0**	**1**	72.0
Con04	0.9065	0.820	2.164×10^{-6}	**81.8**	**2**	53.5

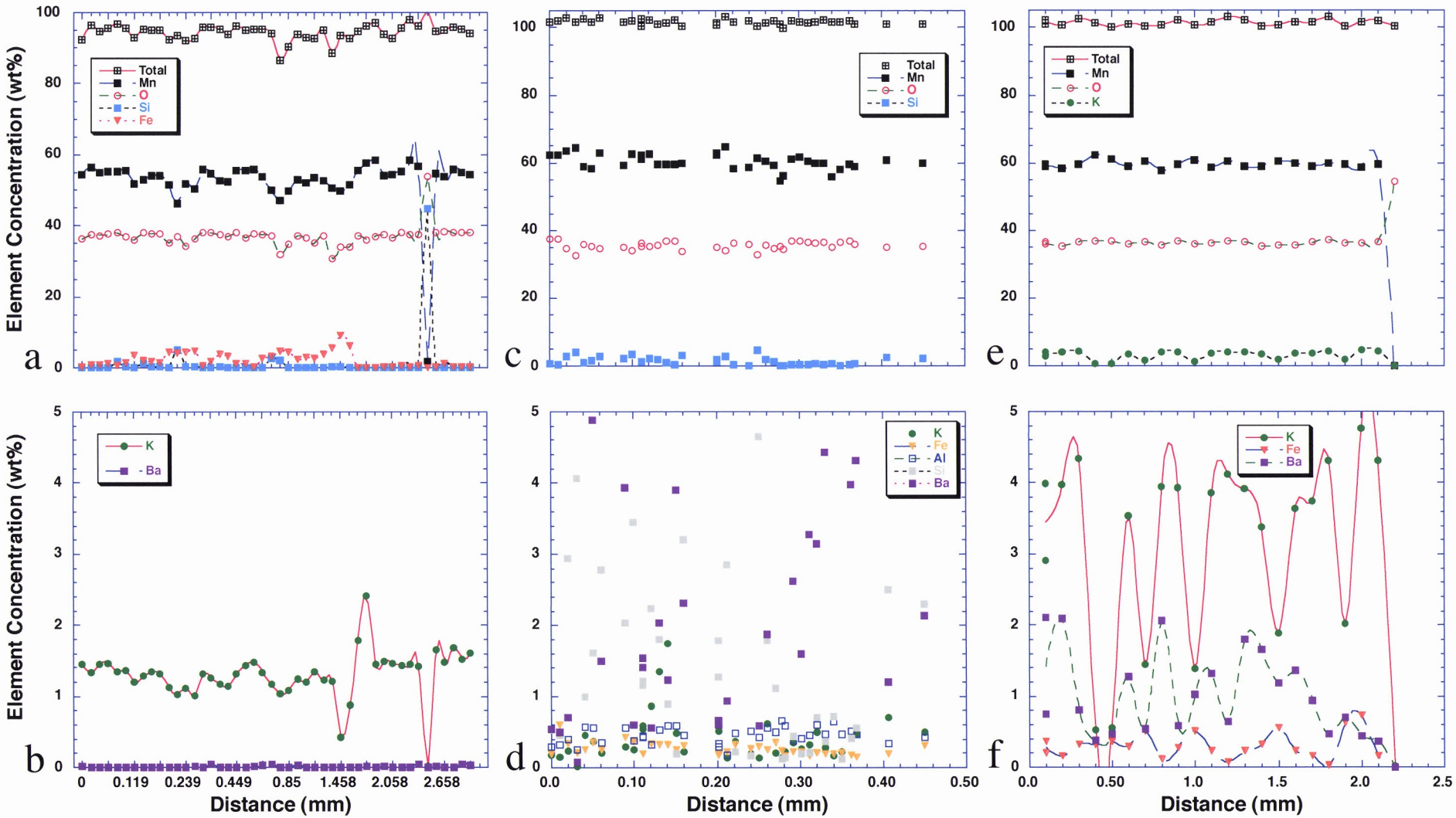

Figure 59. Major (a) and minor (b) elemental analyses of traverse in Mn-oxide grain from the Overhang deposit illustrates the relative purity and suitable K-content of this sample. Major (c) and minor (d) element distribution in EMP traverse through another manganese oxide grain shows the relatively higher Ba content of this sample and its low K content. Major (e) and minor (f) element distribution in a third grain from the Overhang deposit shows the high (ca. 4 wt%) K content in this sample, confirming its suitability for $^{40}Ar/^{39}Ar$ dating. A noticeable feature in all three samples is the lack of Co, Zn, and Pb (not plotted, but presented in appendix) indicating absence of hydrothermal mineralisation in this area.

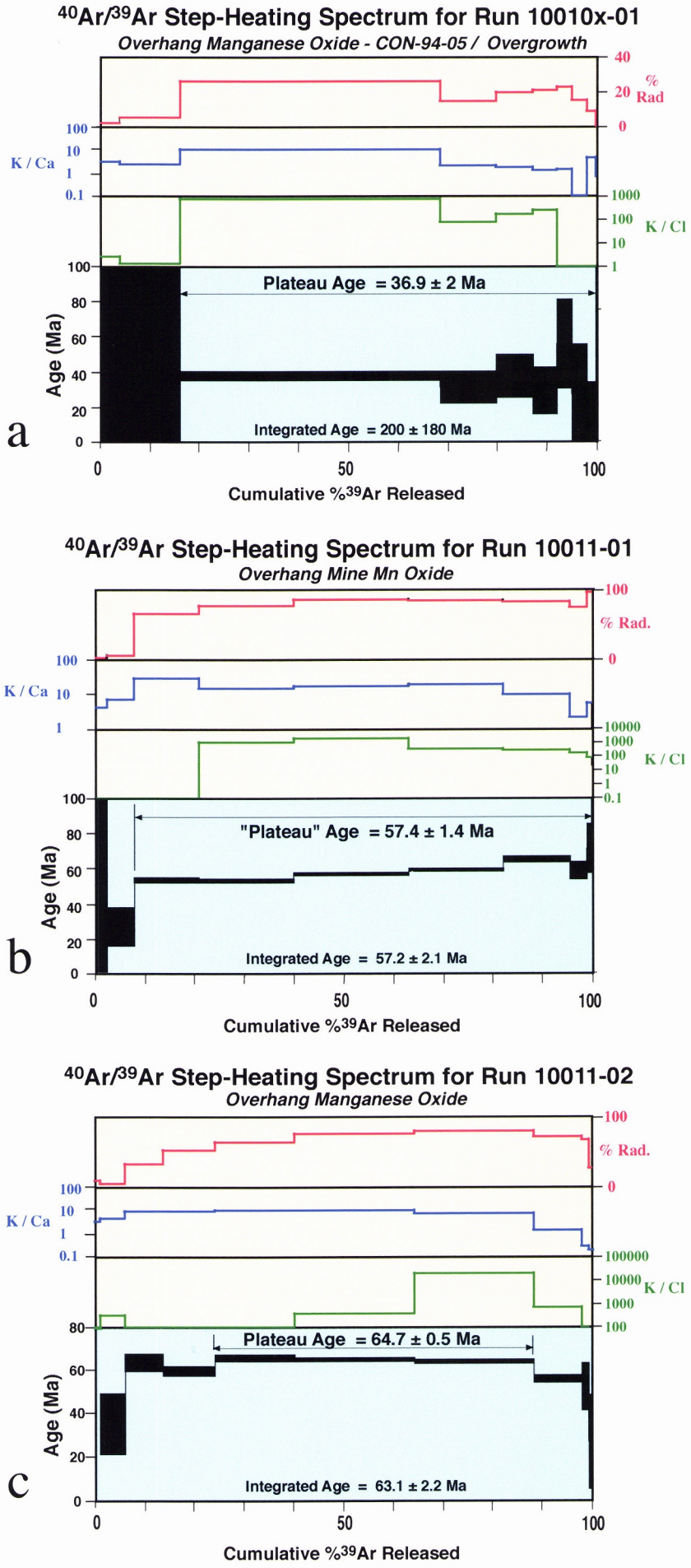

Figure 60. $^{40}Ar/^{39}Ar$ laser probe step-heating spectra of three distinct grains of Mn-oxides from the Overhang deposit illustrating ages ranging from 36.9 ± 2, 57.4 ± 1.4, and 64.7 ± 0.5 Ma. These results have been confirmed by subsequent work and indicate the presence of a very ancient weathering profile in this area.

Three distinct grains from the same samples were analysed by the $^{40}Ar/^{39}Ar$ laser step-heating method at the BGC. The results (36.9 ± 2, 57.4 ± 1.4, and 64.7 ± 0.5 Ma) (Fig. 60) confirm the presence of very old Mn-oxides in the system; however, the dates obtained by the $^{40}Ar/^{39}Ar$ method are significantly younger than those obtained by the K/Ar method. The most likely explanation for the disparaging dates obtained by the two methods is the presence of intergrown unweathered muscovite and quartz crystals in some of the samples. The bulk nature of the K-Ar method does not permit the selection of 100% pure samples; the high spatial resolution and small samples required by $^{40}Ar/^{39}Ar$ single grain method, on the other hand, permit the analysis of very pure samples.

2.4.2 Selwyn Mine

2.4.2.1 Site Selection Criteria: sample provided by CSIRO researchers.

2.4.2.2 Location: 447188E-7601545N

2.4.2.3 Elevation (estimated): ~340- 380 m

2.4.2.4 Geomorphologic Setting: 350-460m ridges surrounded by deeply weathered and dissected (~300m elevation valleys) Proterozoic bedrock.

2.4.2.5 Geomorphologic Regime: relict to erosional.

2.4.2.6 Sample in Relation to Landscape Position: undetermined.

2.4.2.7 Sample in Relation to Regolith: undetermined.

2.4.2.8 Datable Minerals/Host Rock Relationship: undetermined.

2.4.2.9 Sources of Elements: undetermined.

2.4.2.10 Overview

Mn-oxides occur as weathering products of Proterozoic banded iron-formations and are also associated with fractures and void spaces in quartzite ridges in the Selwyn region (Fig. 61) (Fleming, 1997). Mn-oxides occur on ridge tops and on valley floors (Fleming, 1997). One surface sample of barren ironstone from the Selwyn Mine (SE159) was submitted for $^{40}Ar/^{39}Ar$ geochronology by CRCLEME researchers. No information on elevation or geomorphologic setting is available for the sample, but estimate from ARIMCO's topographic maps indicate that the sample came from approximately 340-380m elevation on a ridge flank. A subsequent study conducted as part of a UQ Honours project (Fleming, 1997) partially supported by ARIMCO enabled us to determine the controls on the distribution of Mn-oxides in the local weathering profiles. Over 40 samples analysed during Fleming's (1997) thesis confirms the geochronological results obtained for the sample analysed in this study.

2.4.2.11 Results

2.4.2.11.1 Electron Microprobe and SEM Analysis

This sample supplied by the CRCLEME was not subject to petrographic, SEM, nor electron microprobe studies.

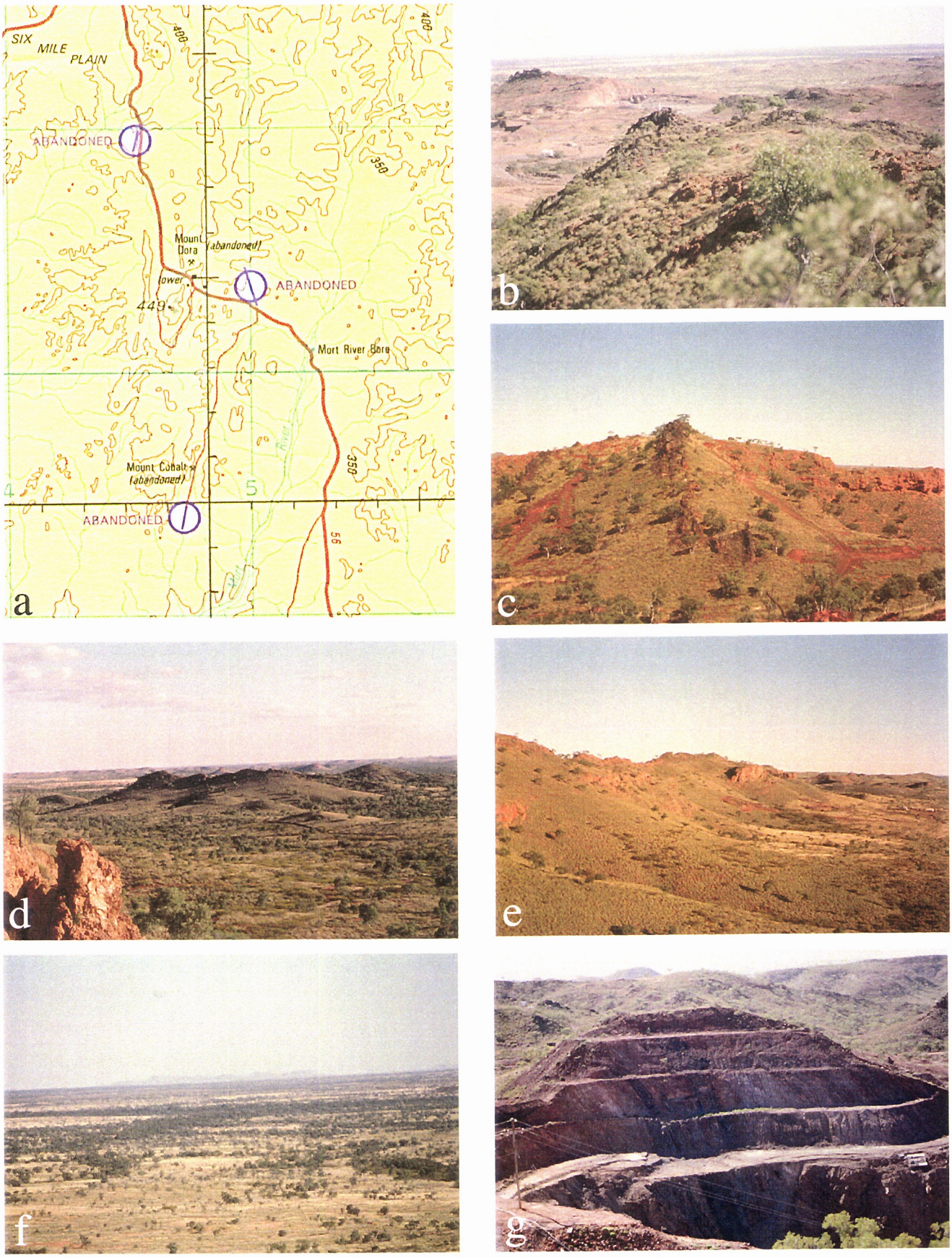

Figure 61. (a) The topographic map illustrates the geomorphological setting in the Selwyn Mines region. (b) This west-facing view from eastern ironstone ridge shows the open pit along the western ironstone. (c) A south-facing view of the eastern ironstone ridge hosting the Selwyn Mine orebodies illustrates the prominent landscape position of the ironstone and the presence of indurated/silicified hardcap draping from the ironstones towards the west. (d) This west-facing view from the easternmost ironstone ridge shows, in the foreground, the dissected valley between the two ironstone ridges; in the middle ground, the western ironstone ridge is prominent; and in the background, several mesas on granitic lithologies are prominent. (e) A south-facing view of the eastern ironstone ridge shows the indurated hardcap. (f) In this west-facing view from the eastern ironstone one sees, in the foreground, the flat plains of the Burke river embayment; in the background, the Tick Hill and Monument mesas are visible. (g) Close-up view of one of the open pits at the Selwyn shows the darker colour at the center of the pit wall. Manganese oxide samples occur throughout these pits and are suitable to $^{40}Ar/^{39}Ar$ dating.

2.4.2.11.2 Geochronology

Three Mn-oxide grains from sample SE159 were analysed by the $^{40}Ar/^{39}Ar$ method at the BGC. Two grains yielded well defined plateaus at 41.1 ± 0.3 and 43.8 ± 1.2 Ma (Figs. 62a and b). The third grain analysed did not yield a plateau age (Fig. 62c). When all the results obtained are plotted as an ideogram, three most probable peaks occur (Fig. 62e). The two peaks in the 40's range are consistent with the results obtained in the age plateaus. However, a third peak (or series of peaks) centred at 65.4 Ma is not obvious from the plateau ages. These peaks are associated with steps F and G in Fig. 62a and with steps D and F in Fig. 62c.

2.4.3 Discussion - Eastern Succession

The results for the Overhang and Selwyn deposit samples substantiate a view held by previous authors that the weathering profiles associated with hill summits in this region preserve evidence of weathering events which occurred during the Mesozoic. The long timing of exposure of these profiles to surficial conditions also implies that the profiles should host evidence of weathering processes which may have taken place since the onset of exposure in the Mesozoic. If a large enough number of samples were to be analysed from these long lived profiles, and if exposures to complete weathering profiles were available, a comprehensive history of weathering should be retrieved from these profiles. If additional information could be obtained about the chemistry of the minerals precipitated with each weathering event and if the masses of minerals precipitated during each event could be estimated, it would be possible to determine the geochemical conditions prevalent during each weathering episode and the intensity of weathering reactions through time. Although we are far from gathering enough data to achieve these goals, the information obtained in this study support the hypothesis of long lived weathering profiles (Mesozoic) in the Mount Isa block.

The results obtained for the Overhang and Selwyn deposits (Fig. 62e) during this study do not permit a comprehensive interpretation of the history of weathering in the region. However, when combined with the results obtained for other profiles in this study, and when complemented by subsequent detailed studies conducted in the region, the results obtained for the Overhang and Selwyn deposits permit the assessment of various models of landscape evolution for the area. These models will be assessed at the end of the Mount Isa Block section.

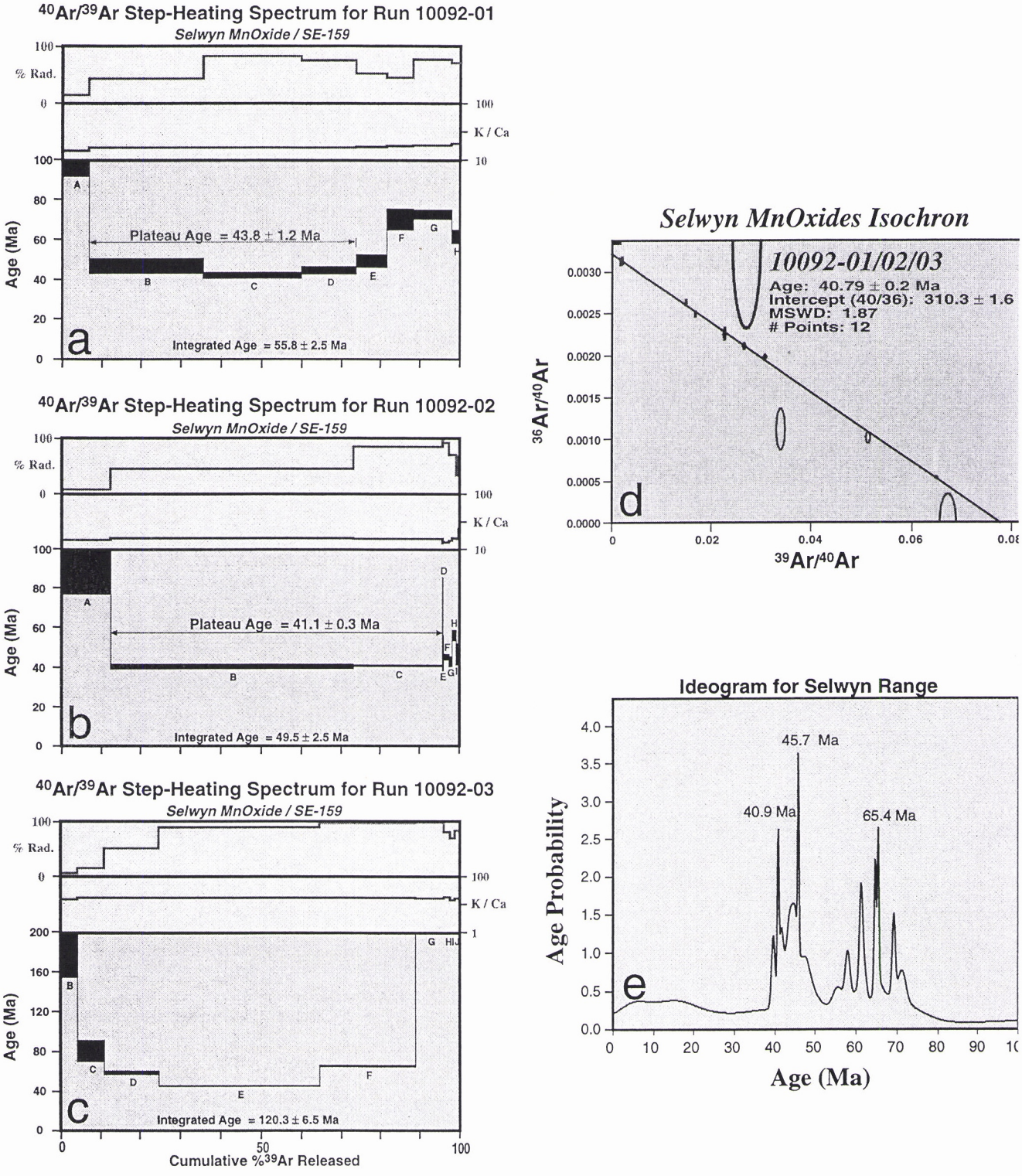

Figure 62. (a)-(c) illustrate three step-heating spectra from three distinct grains extracted from CSIRO sample SE-159. No outcrop information is available for this sample. Two of three grains yielded concordant ages within two sigma. The ages obtained are comparable to ages obtained from the Overhang deposit. The isochron (d) age for these grains agree remarkably well with the ages obtained for the Overhang deposit. An ideogram for all the Overhang and Selwyn samples is shown in Fig. 61e. Subsequent work in this area (Fleming, 1997) confirmed the most probable weathering ages shown in Fig. 61e.

2.5 Tick Hill Region

2.5.1 TV Tower Mn-Breccia

2.5.1.1 Site Selection Criteria: massive outcrops of Mn-oxide cements replacing silcretes along the Pilgrim Fault were deemed ideal to determine the minimum age of silcrete formation in the area.

2.5.1.2 Location: 392550E-7604920N

2.5.1.3 Elevation (sampled outcrops): ~300-320 m

2.5.1.4 Geomorphologic Setting: manganesiferous "breccia" on silcrete blanket in low-lying surface. Manganese occurrences are strongly correlated with a major fault in the area (Pilgrim Fault) which separates the high elevation mesas (450-470m) west of the fault from the low-lying plains of the Burke River embayment east of the fault.

2.5.1.5 Geomorphologic Regime: erosional.

2.5.1.6 Sample in Relation to Landscape Position: manganesiferous ridges occur as local topographic highs in the dissected part of the landscape. These manganese-rich ridges are hosted by silcrete horizons present in the low elevation part of the landscape.

2.5.1.7 Sample in Relation to Regolith: Mn-oxides replacing silcrete possibly superposed on mottled zone.

2.5.1.8 Datable Minerals/Host Rock Relationship: influx of elements, in solution, from outside sources located at stratigraphic positions below the precipitation site.

2.5.1.9 Sources of Elements: Mn is derived from weathering silicates in the amphibolites present west of the Pilgrim fault. Sources of manganese may be several kilometres away from precipitation site. K and Ba are derived from feldspars and micas in the underlying Proterozoic rocks. All these elements are interpreted to have been introduced to the precipitation site by meteoric solutions ascending along the Pilgrim fault.

2.5.1.10 Overview

The Tick Hill gold mine site is located adjacent to a 450-470 m elevation silcrete-capped mesa (Fig. 63). Several other silcrete-capped mesas occur in the area (Fig. 63b). In addition, similar silcretes and some ferricretes are also present on the low lying plains (300-340 m elevation) east of the Tick Hill deposit (Figs. 63-69). The silcrete-capped mesas are separated from the plain silcretes and laterites by the Pilgrim Fault, a dominant structural feature in the region (Fig. 63d).

These silicified weathering profiles occur blanketing plateaus (ranging from 400-500m elevation) surrounded by flat plains (Figs. 63-69). Brecciated Cambrian sediments (laminated siltstones, shales, fossiliferous carbonates, and quartz arenites) are strongly silicified and/or ferruginised and lie uncomformably on Proterozoic igneous rocks (Figs. 63-69). Field evidence suggests that the silicification process is associated the formation of weathering

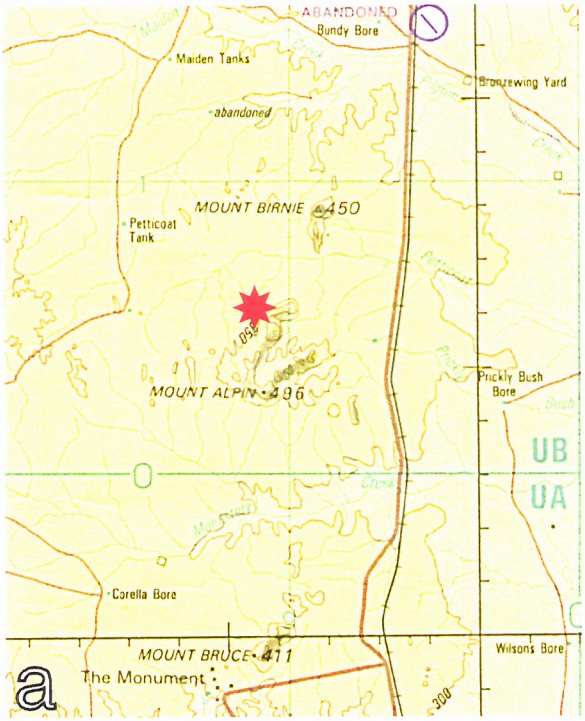

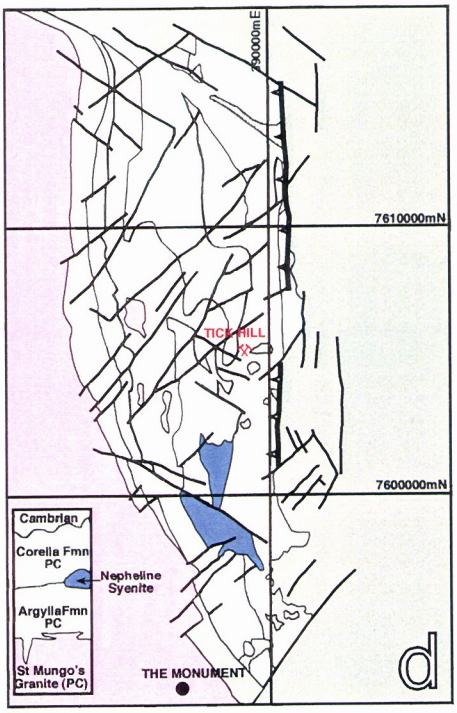

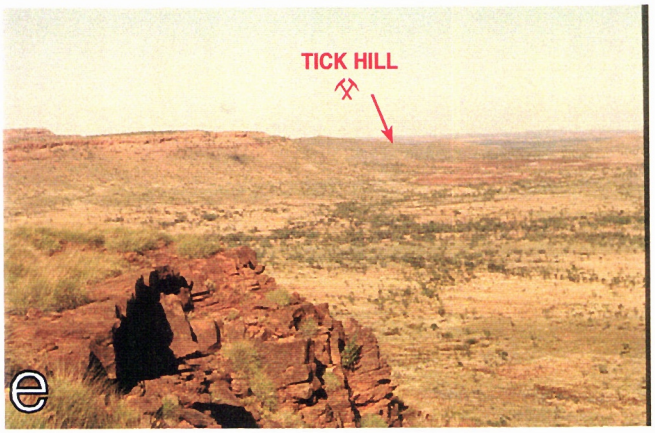

Figure 63. (a) The topographic map illustrates the geomorphologic setting in the region surrounding the Tick Hill deposit (red star). (b) A west-facing view from Burke River embayment shows the series of silcrete capped mesas which characterise the Tick Hill region. (c) Two silcrete and mottled zone capped mesas (Tick Hill and Tick Hill South Mesas) occur adjacent to the Tick Hill deposit. (d) A simplified geological map of the area surrounding the Tick Hill deposit illustrates the presence of Cambrian sediments remnants as thin inliers within the Proterozoic terrain. The timing of silcrete formation in these Cambrian sediments addressed in this project. (e) A view from Mount Birnie towards the SW shows the position of the Tick Hill pit adjacent to a prominent silcrete capped mesa. (f) A close-up view of the Tick Hill gold mine pit shows a thin layer of colluvium covering the Proterozoic bedrock in the area. The mineralised Proterozoic lithologies show signs of incipient weathering; however, some units may be friable and leached of mobile cations suggesting weathering to lower saprolite/saprolite stages. Petrographic studies of pyrite-bearing samples from the pit indicate that the pyrite is now replaced by hematite/goethite pseudomorphs and that gold has been dissolved and locally reprecipitated during pyrite weathering.

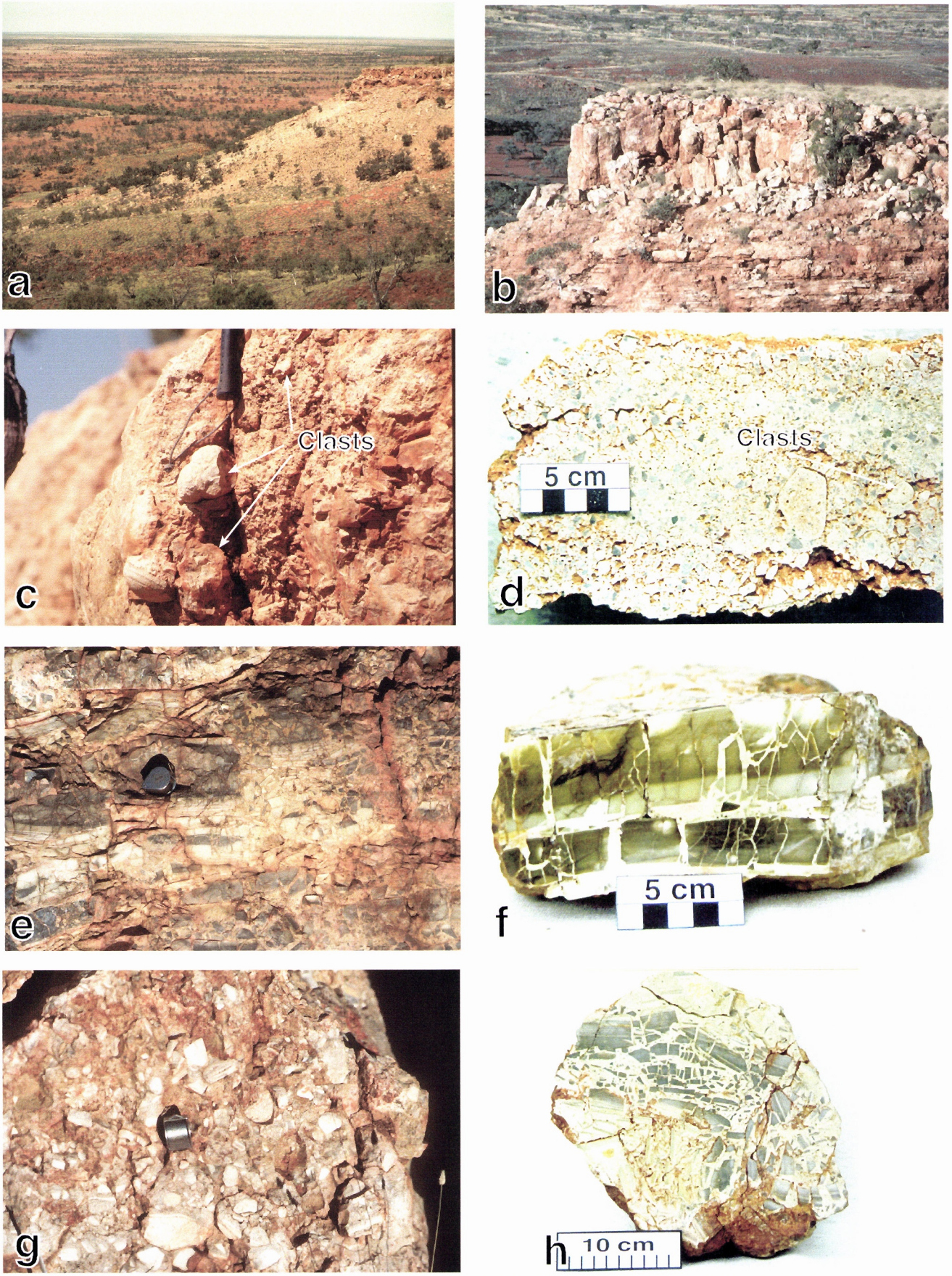

Figure 64. (a) The silcrete-capped Birnie mesa on the right-hand side of the photo is surrounded by eluvial deposits composed of silcrete fragments. Ferruginous duricrusts occur at the lower level plains between the silcrete-capped mesas and the flat landscape of the Burke River embayment. (b) The silcretes capping Birnie mesa are composed of locally silicified flat-lying sediments (bottom of picture) overlain by massive to brecciated silcretes and channel deposits. (c) Silcrete clasts occur in the channel deposits capping the mesa. (d) A cross section through one of the channel deposit silcretes shows clasts surrounded by a silicified matrix. (e) Completely silicified Cambrian sediments still show remnants of the horizontal bedding planes. (f) A cross-section through a strongly silicified Cambrian limestone/calcareous shale shows the contrasting colours of supergene silica. (g) This image illustrates the strongly brecciated nature of some of the silcretes in the Tick Hill region. (e) A cross section through a silcrete breccia illustrates the rotation and collapse of silicified limestone/calcareous shale blocks. The mechanisms involved in the development of this texture are still not resolved.

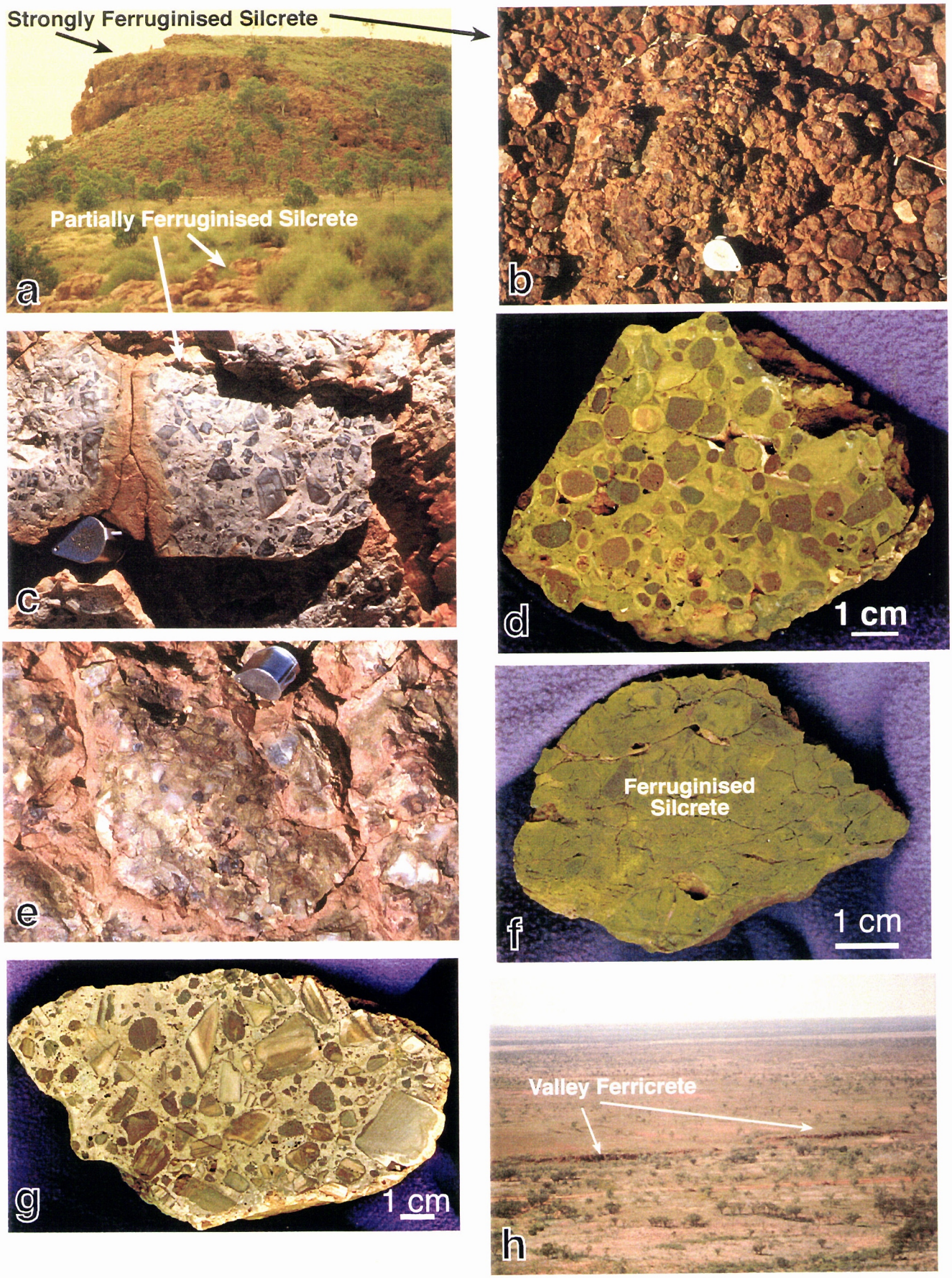

Figure 65. (a) Strongly ferruginised silcrete forms the upper 10m of the silcrete-cap overlying the Tick Hill mesa. Where the ferruginised silcrete has been removed by recent erosion a less ferruginised silcrete is exposed. (c), (e) and (g) illustrate the progressive ferruginisation of silcrete caps. (b), (d) and (f) show close-up views of strongly ferruginised silcretes. If silcretes represent evidence for supergene silica precipitation during arid conditions, the process of ferruginisation and silica replacement of silcrete by iron oxides suggests that humid conditions, which favour iron mobility, must have post-dated silcrete formation. (h) Ferricretes at the western margin of the Burke River embayment may represent strongly ferruginised silcretes. These ferricretes were not studied in detail in this project.

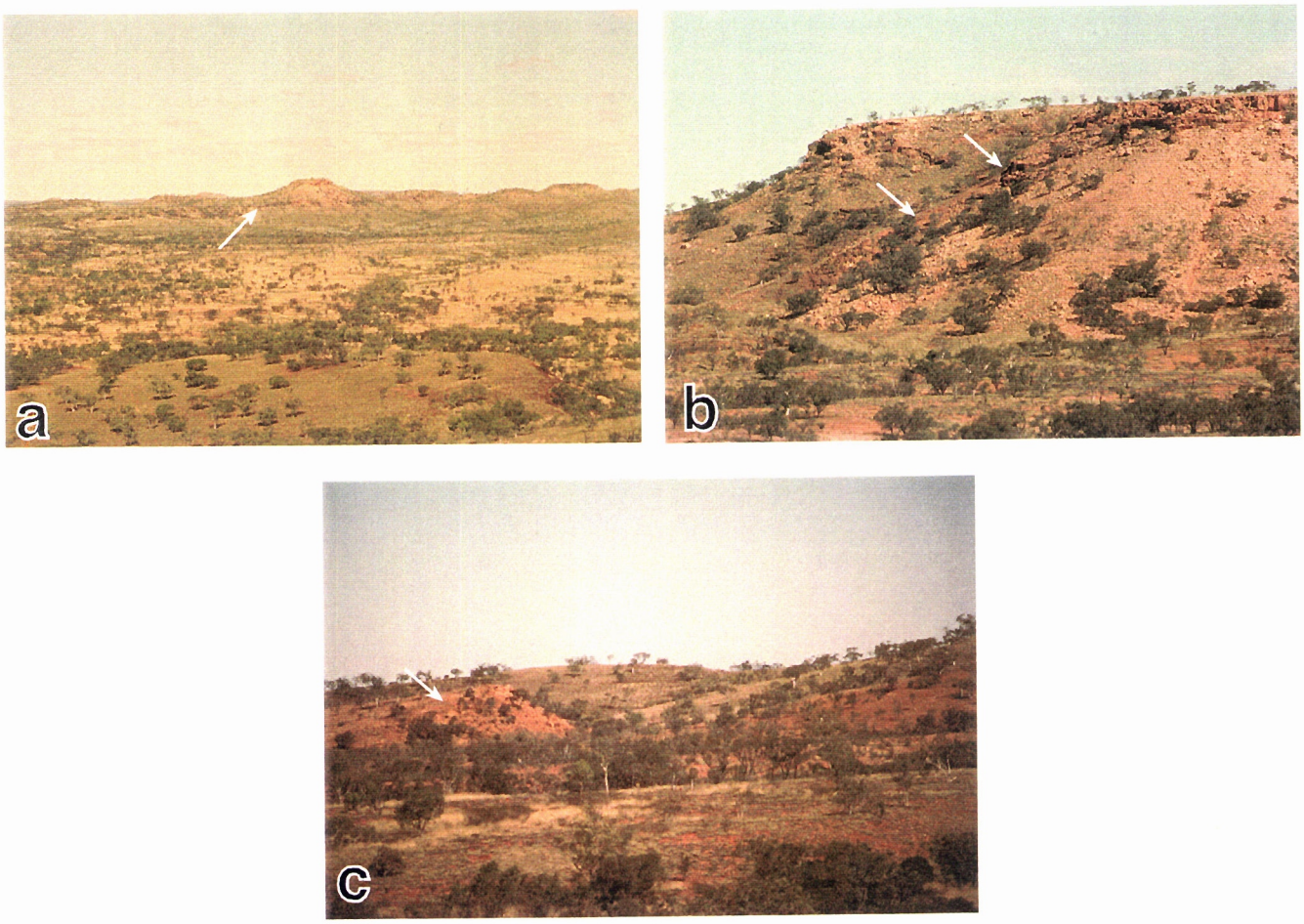

Figure 66. (a) Pediments formed by strongly ferruginised silcrete breccias drape the silcrete-capped mesas, as shown in this figure. (b) Ferruginised silcrete accounts for most of the eluvium adjacent to this mesa. (c) Possible paleo-pediment, now separated from the eluvial source by recent erosive processes, ascend toward Birnie mesa. (d) View of possible paleo-pediment shown in (c) as viewed from Birnie Mesa. These apparent paleo-pediments are common in the western margins of the Burke River embayment and they may suggest large-scale erosion of the silcrete mesas (possibly due to increasing relief due to tectonic reactivation of regional faults) some time in the remote past. (e) The transported silcretes associated with these possible paleo-pediments are strongly ferruginised and display a chocolate-brown colour easily distinguishable in the field.

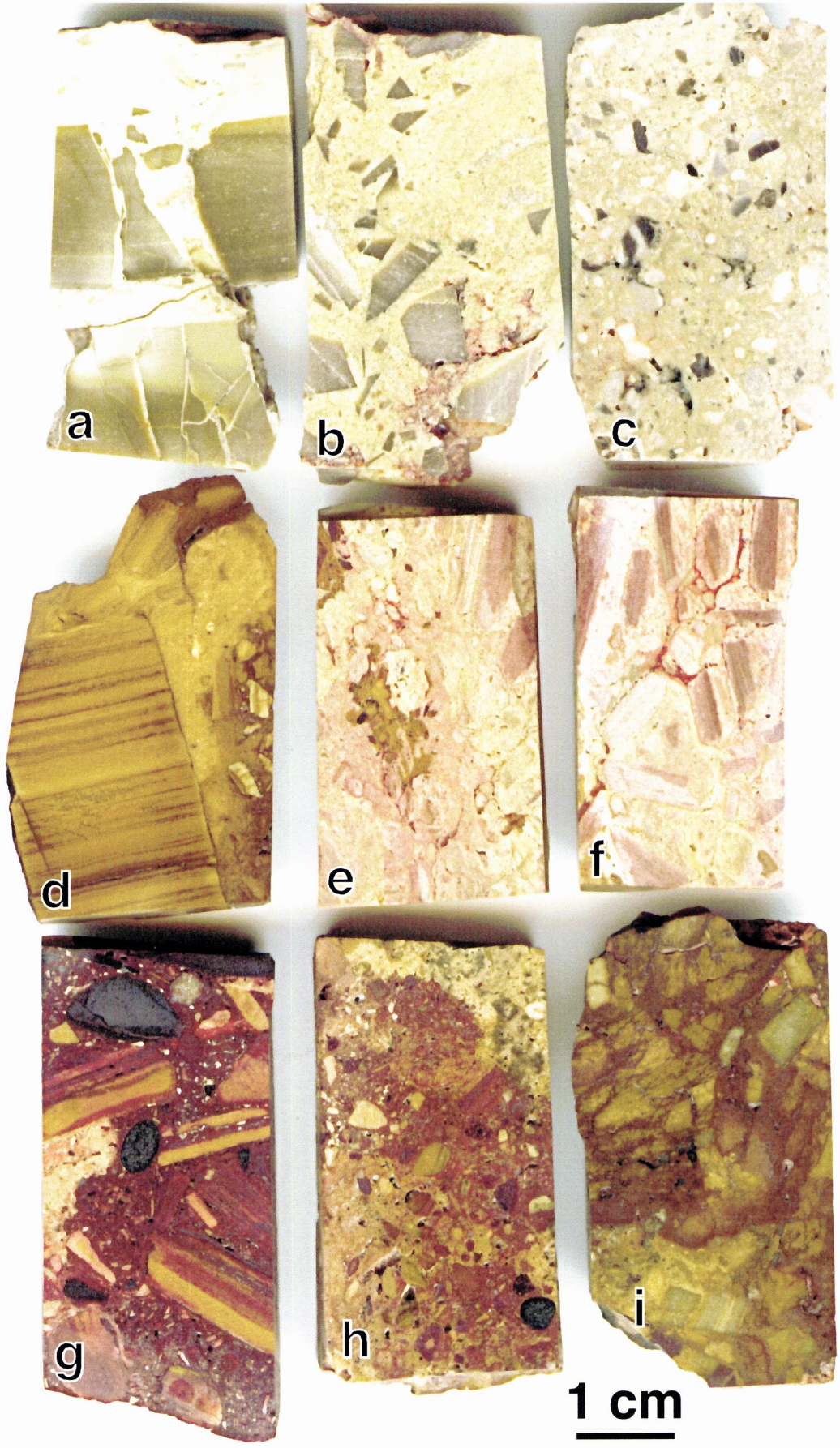

Figure 67. (a) to (i) illustrate the evolution of textures acquired by the Cambrian calcareous sediments during the development of silcretes and ferruginised silcretes in the Tick Hill region.

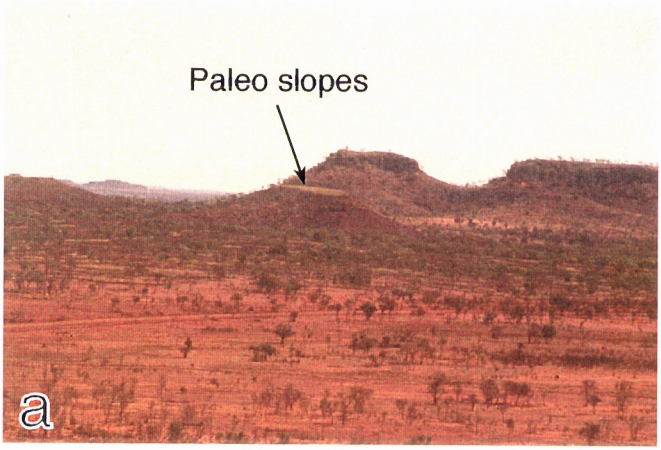

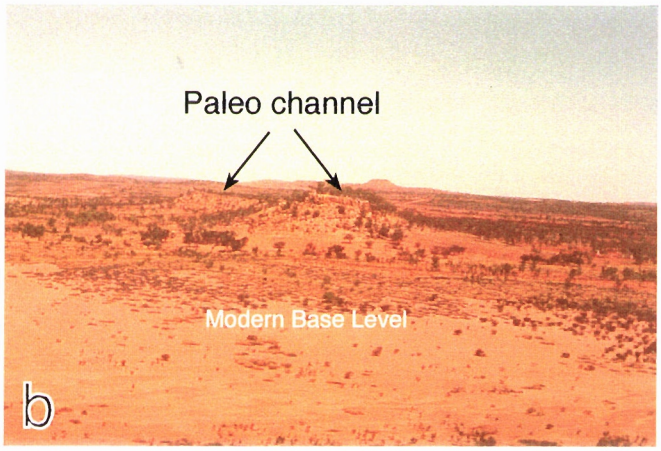

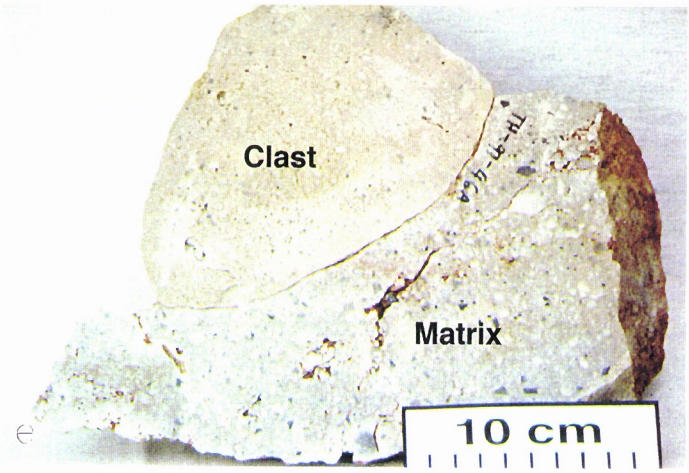

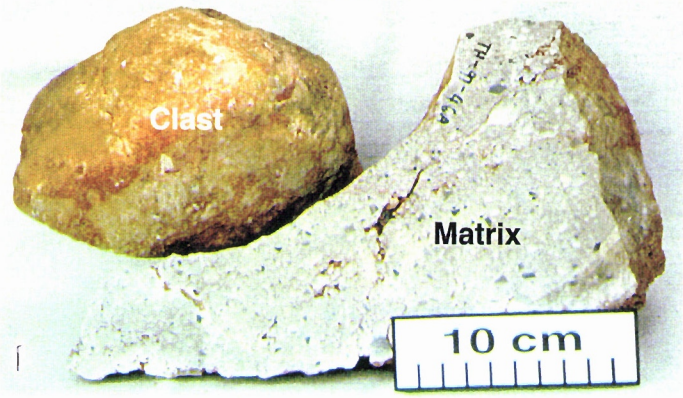

Figure 68. (a) Possible paleo-pediments, now separated from their sources, present in the western margin of the Burke river embayment next to the Monument town, south of Tick Hill. (b) Suspended, strongly silicified, paleochannel deposits, now exposed as prominent meandering ridges 20-40 m higher than the adjacent plains (modern base level). (c) The sediments in these paleo channels are composed of silcrete fragments and fine grained matrix. These sediments have been strongly silicified, which accounts for their resistance to erosion and the resulting relief inversion implied by their occurrence. (e) and (f) The silicified clasts have been eroded, transported, deposit at a river channel and then re-silicified. This relationship implies at least two periods of strong silicification in the region. Alternatively, this relationship could imply a protracted period of silicification, when climatic conditions were also propitious for partial erosion, transportation, redeposition, and resilicification of silcrete fragments.

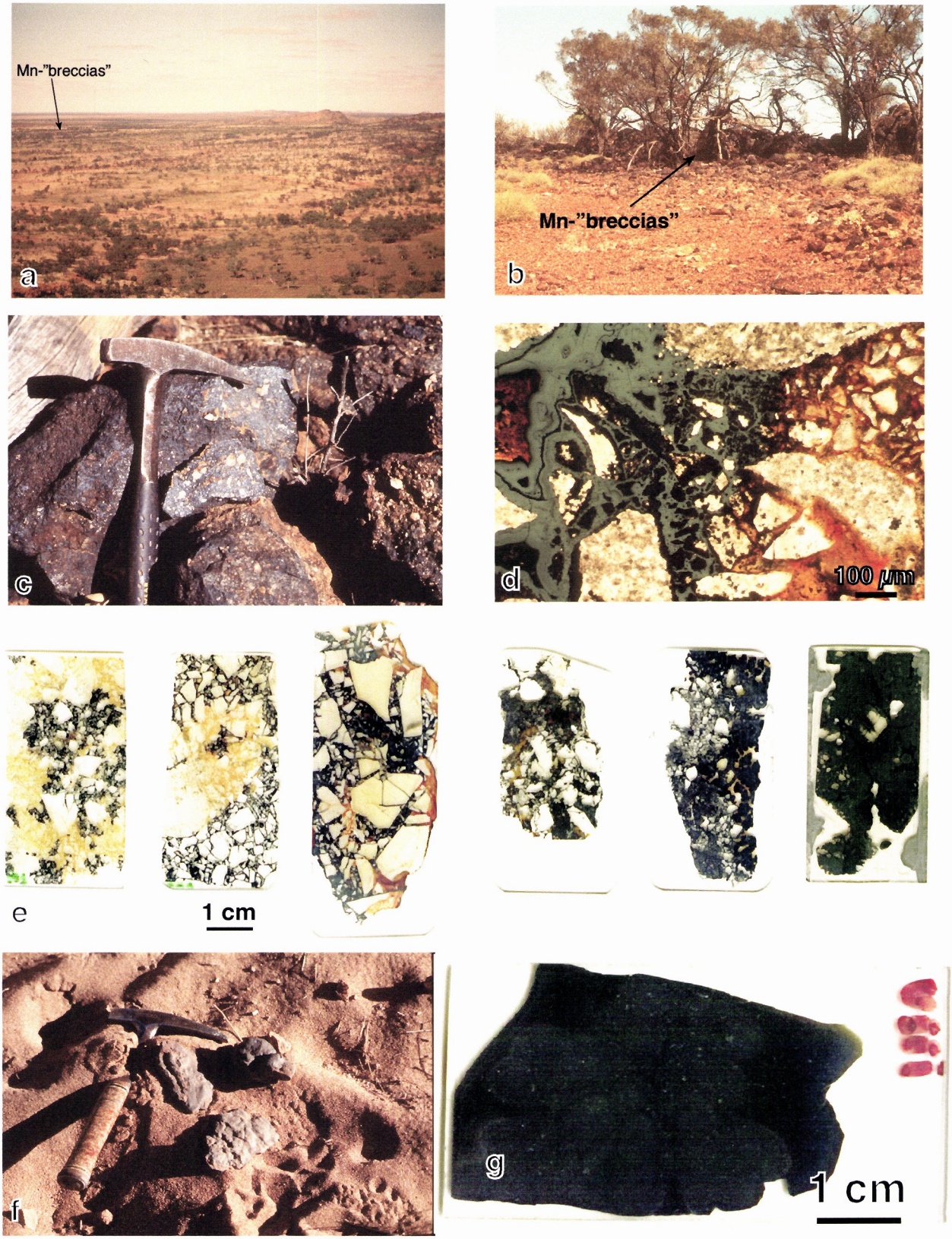

Figure 69. (a) Mn-rich "breccias" east of the silcrete-cap mesas at Tick Hill (western margin of Burke River embayment) are composed of fractured and tectonised silcrete blocks partially replaced by Mn-oxides along the Pilgrim Fault. (b) and (c) illustrate outcrops of tectonised silcretes partially replaced by manganese oxides along the Pilgrim fault. (d) Combined reflected and transmitted-light photomicrograph illustrates the partial replacement of silica cements in silcrete breccias by iron (orange-red) and manganese (grey-black) oxides. (e) This series of petrographic slides illustrate the progression of silcrete replacement by Mn-oxide cements. These cements are K-rich, very pure, and suitable for $^{40}Ar/^{39}Ar$ geochronology. The Mn-oxide ages obtained from Ar/Ar dating of these cements impose a minimum age on silcrete formation. (f) In addition to the Mn-oxide replaced silcrete breccias, the Tick Hill region is also rich in botryoidal Mn-oxide occurrences associated with the banks of intermittent creeks which drain the silcrete-capped mesas. (g) Petrographic studies of these botryoidal manganese oxides indicate that they are composed of thin films of Mn-oxide cements precipitated along the grains of alluvial sediments, cementing these sediments together. This genetic model, if correct, indicates the periodic discharge of reducing groundwaters saturated in dissolved Mn and other cations. When reaching the near-surface environment, these waters are oxidised and precipitate their dissolved Mn content (and other cations in solution) as Mn oxides.

profiles. Silicified Cambrian sediments also occur sporadically below a thin soil layer in the low relief areas surrounding the plateaus.

Mn-oxides occur only in the low relief areas (Fig. 69). Two types of manganese oxide occurrences have been identified in the region: massive Mn-oxide cements replacing silcretes along regional faults (Mn-"breccias") (Fig. 69a-e); and finely disseminated Mn-oxide cements partially replacing detrital sediments in gullies associated with intermittent streams (Fig. 69f,g). Only the first type of Mn-oxide occurrence has proven suitable to geochronology and will be discussed in further detail here.

These Mn-oxide "breccias" are confined to fault zones where Mn-oxide replaces silica cements. In strongly Mn-metasomatised samples, sometimes Cambrian sediment clasts are also replaced (Fig. 69). Reflected-light optical microscopy, scanning electron microscopy, and electron microprobe analyses indicate that, in the samples studied, cryptomelane replaces cryptocrystalline silica cements (Fig. 69). The replacement textures are characterised by a dissolution front, where the silica cement becomes porous due to silica loss, an iron metasomatism intermediate zone (generally less than 1-3 mm wide, and a manganese-rich zone ((Fig. 69d). The Mn-oxide may occur as films surrounding silica and iron oxide grains (initial stages of replacement) and evolves to massive, botryoidal Mn-oxide crusts in the advanced states of replacement (Fig. 69d and e). Electron microprobe analyses for the Mn-oxide cements are shown in Figs. 70-77. All samples analysed in this study were collected from one locality along the Pilgrim fault (TV Tower outcrop) (Fig. 69a-e).

2.5.1.11 Results

2.5.1.11.1 Electron Microprobe and SEM Analysis

Petrographic studies and SEM/EMP analyses of Mn-oxide samples are shown in Figs. 69 to 77. These images and analyses clearly indicate that the Mn-oxides present in the Pilgrim Fault "breccias" are very rich in K (up 5.5wt%) making them ideal for $^{40}Ar/^{39}Ar$ dating. In some samples, the Mn-oxides are very pure and display botryoidal growth (e.g., Fig. 75), indicating precipitation in open cavities in the sample.

A major difference between the Mn-oxides found along the Pilgrim Fault and Mn-oxides from other sites in this study is the relatively high Ca and Na contents of the former (Figs. 70, 74-77).

2.5.1.11.2 Geochronology

In the Tick Hill area, silcretes blanket 400-500 m high plateaus and also occur below a thin soil layer in the low relief 300m high areas surrounding the plateaus. Silicification is related to the formation and evolution of the weathering profiles and is typical of silcretes found in

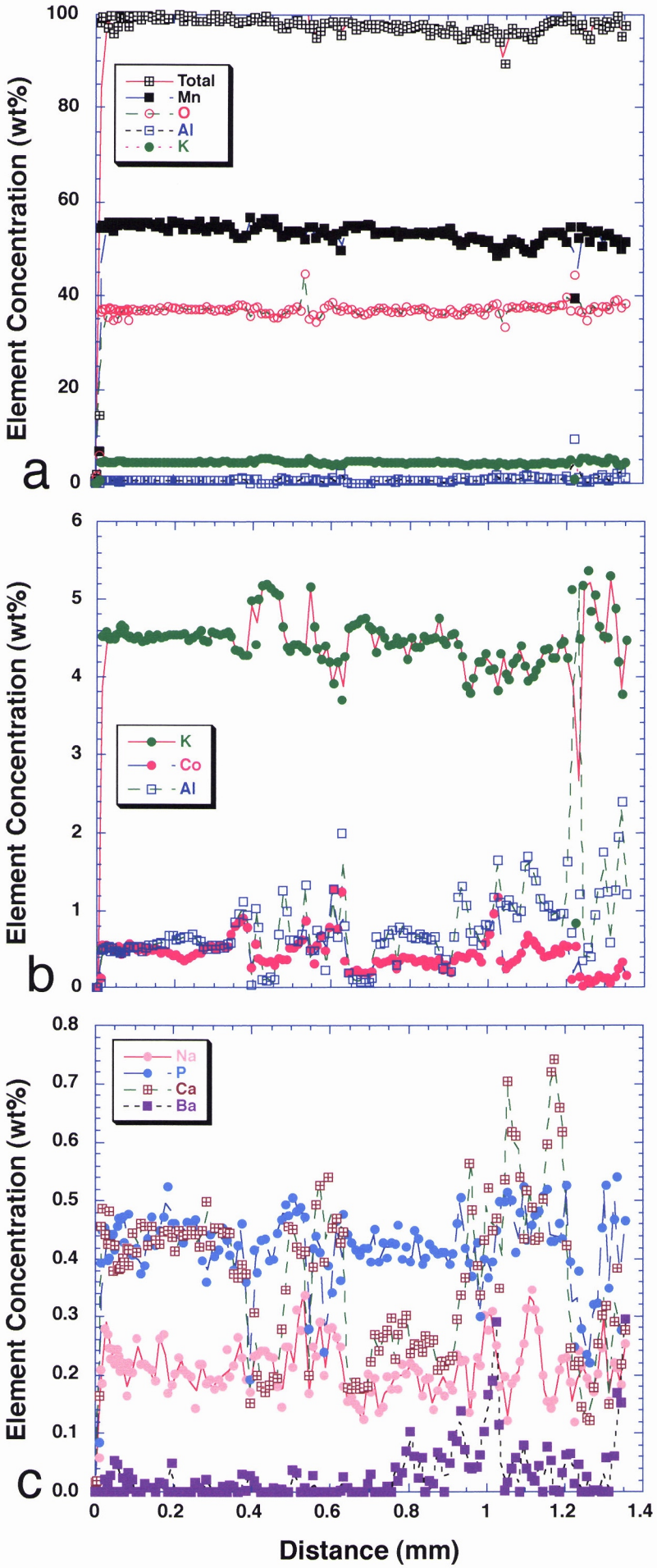

Figure 70. Major (a) and minor (b-c) elements determined by an EMP traverse through a Mn-oxide cement sample. Notice the very high K contents in this sample. Notice also the high Na and Ca contents of this Mn-oxide, which clearly contrasts with most of the Mn-oxide compositions shown so far in this study.

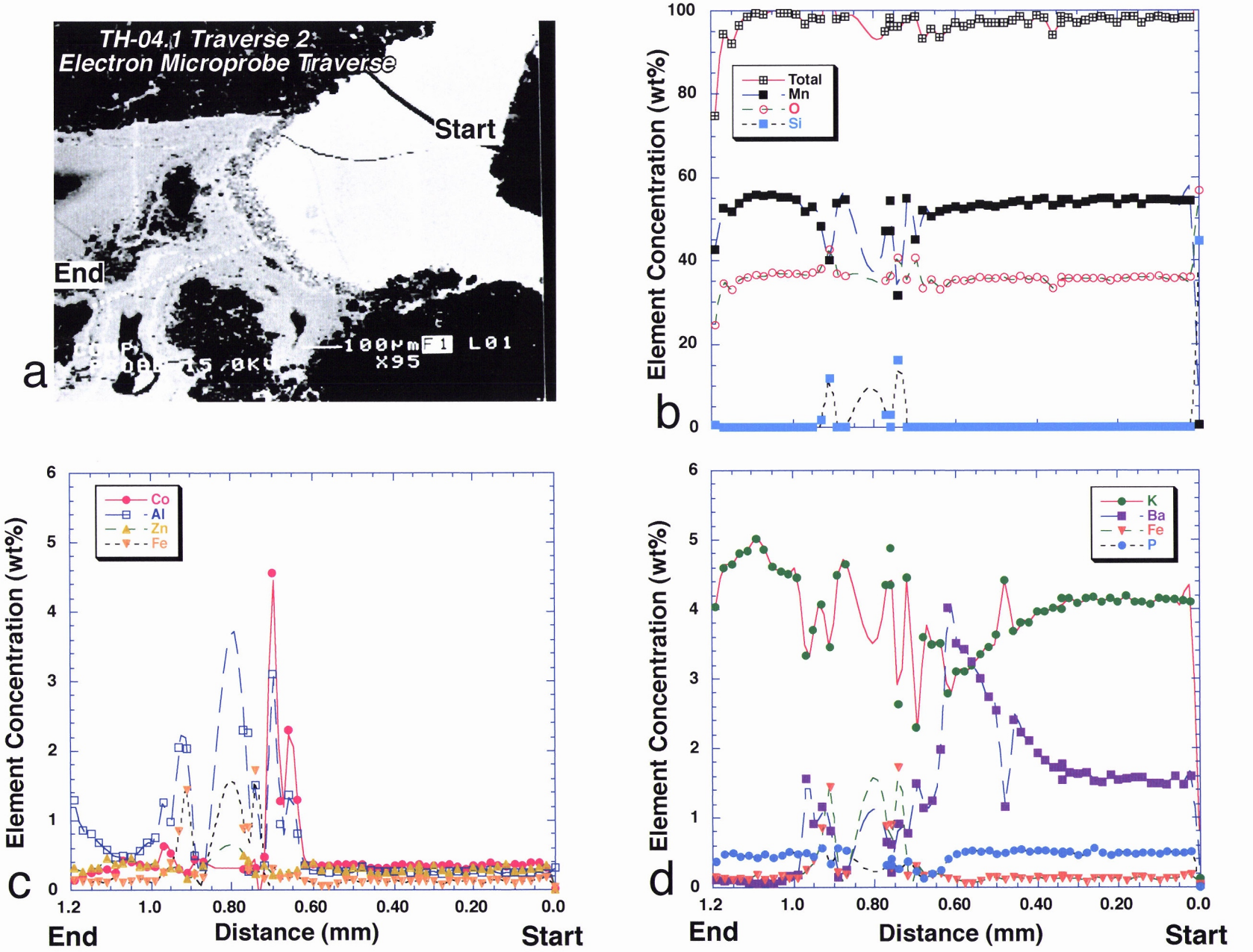

Figure 71. (a) Backscattered SEM photomicrograph illustrating a Mn-oxide cement replacement front and the traverse where EMP analyses were performed. Major (b) and minor (c-d) element distribution along the traverse shown in (a) illustrates the antipathetic relationship between K and Ba in this sample.

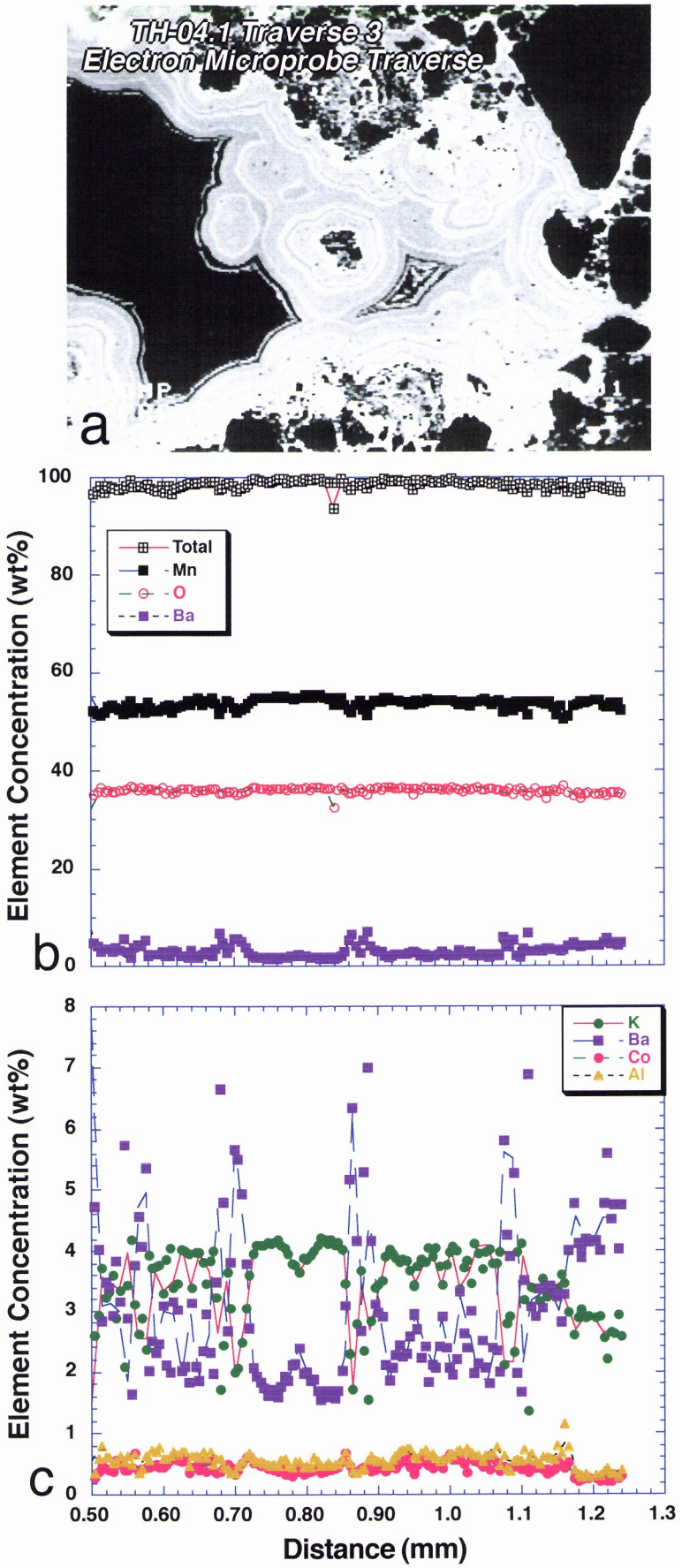

Figure 72. (a) This backscattered SEM photomicrograph illustrates a botryoidal Mn-oxide replacing silcrete cements. Major (b) and minor (c) element distribution along the EMP traverse show once again the high K contents and the antipathetic relationship between K and Ba in the sample.

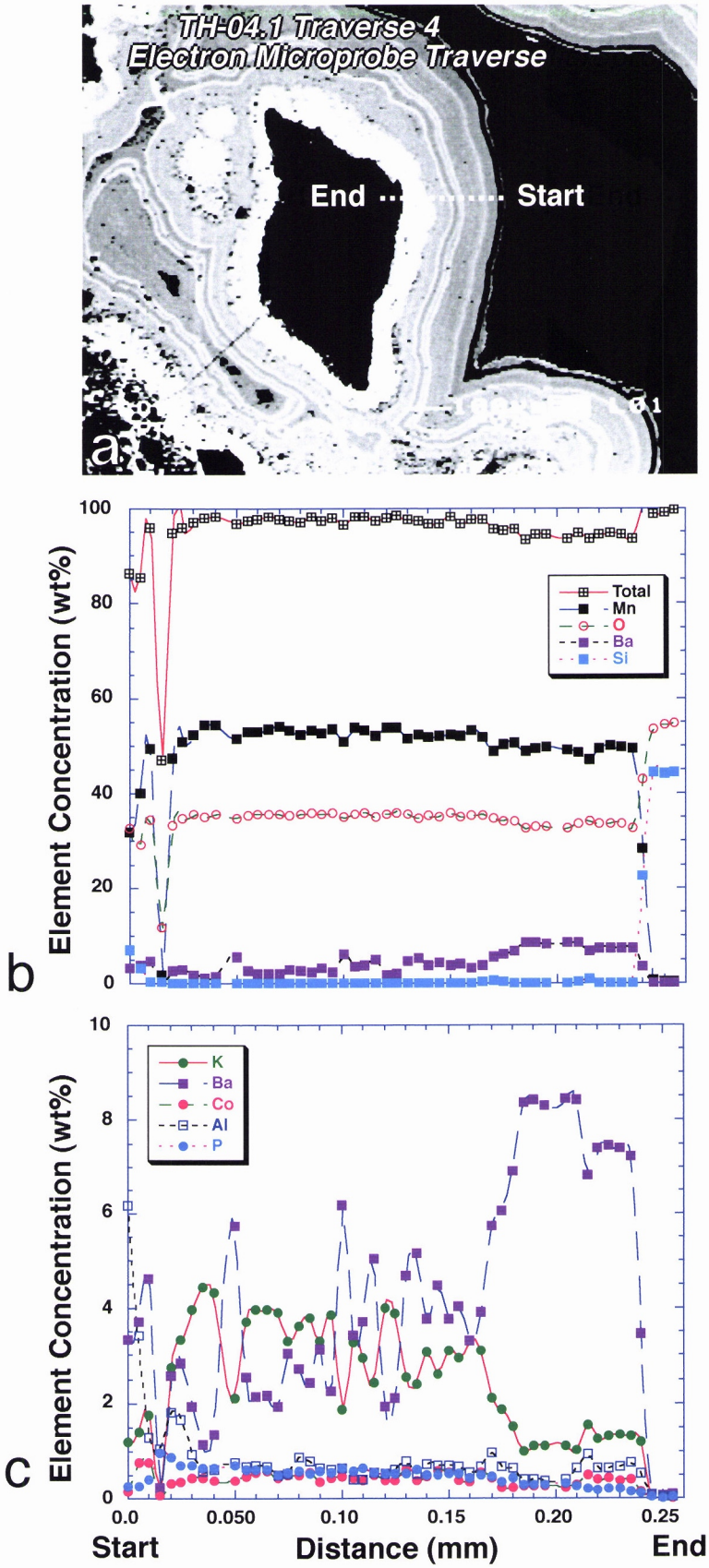

Figure 73. (a) Backscattered SEM photomicrograph illustrates a botryoidal Mn-oxide replacing silcrete cements and the traverse where EMP analyses were performed. Major (b) and minor (c) element distribution along the EMP traverse also show high K contents and an antipathetic relationship between K and Ba in

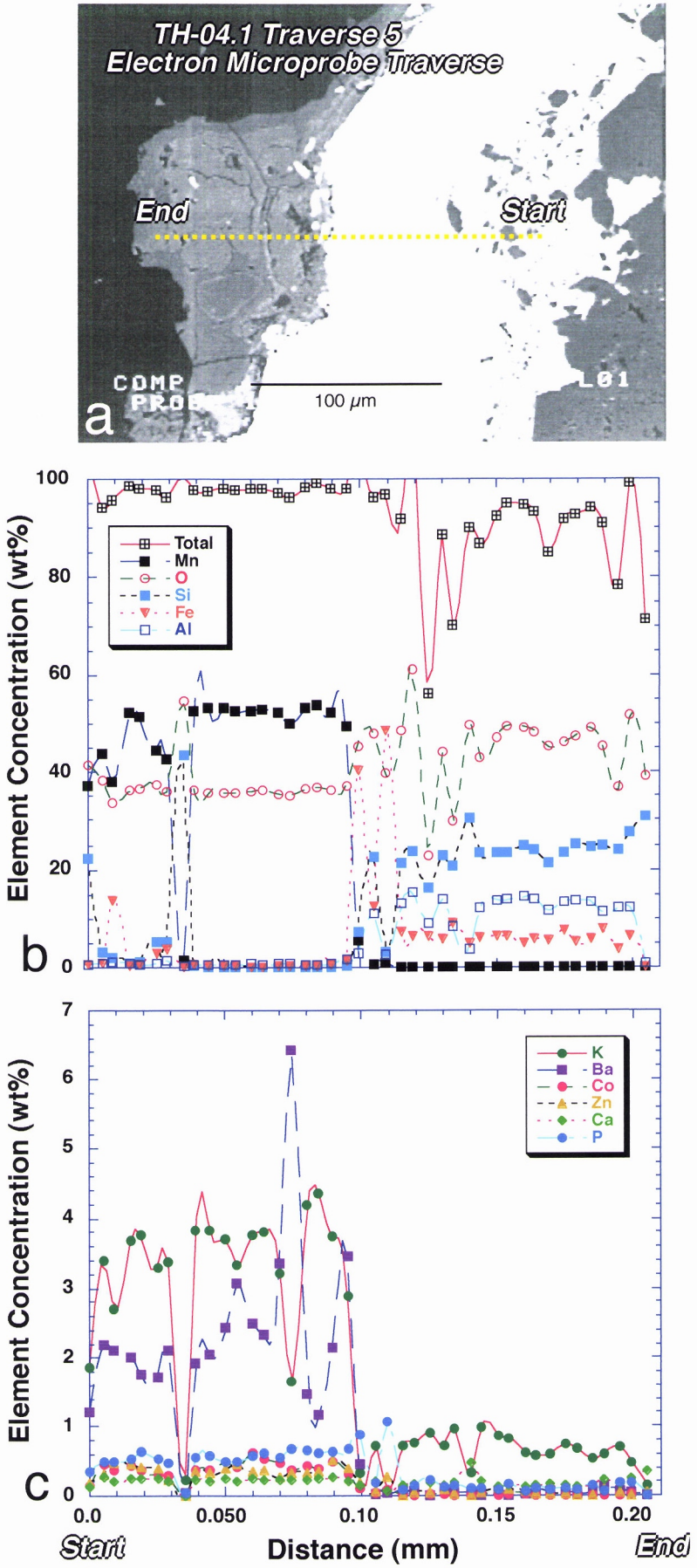

Figure 74. (a) Backscattered SEM photomicrograph illustrates botryoidal Mn-oxide and a K-Fe-Al silicate overgrowth replacing silcrete cements and the traverse where EMP analyses were performed. Major (b) and minor (c) element distribution along the EMP traverse show the presence of quartz, cryptomelane, and an unidentified K-Fe-Al silicate (supergene celadonite?).

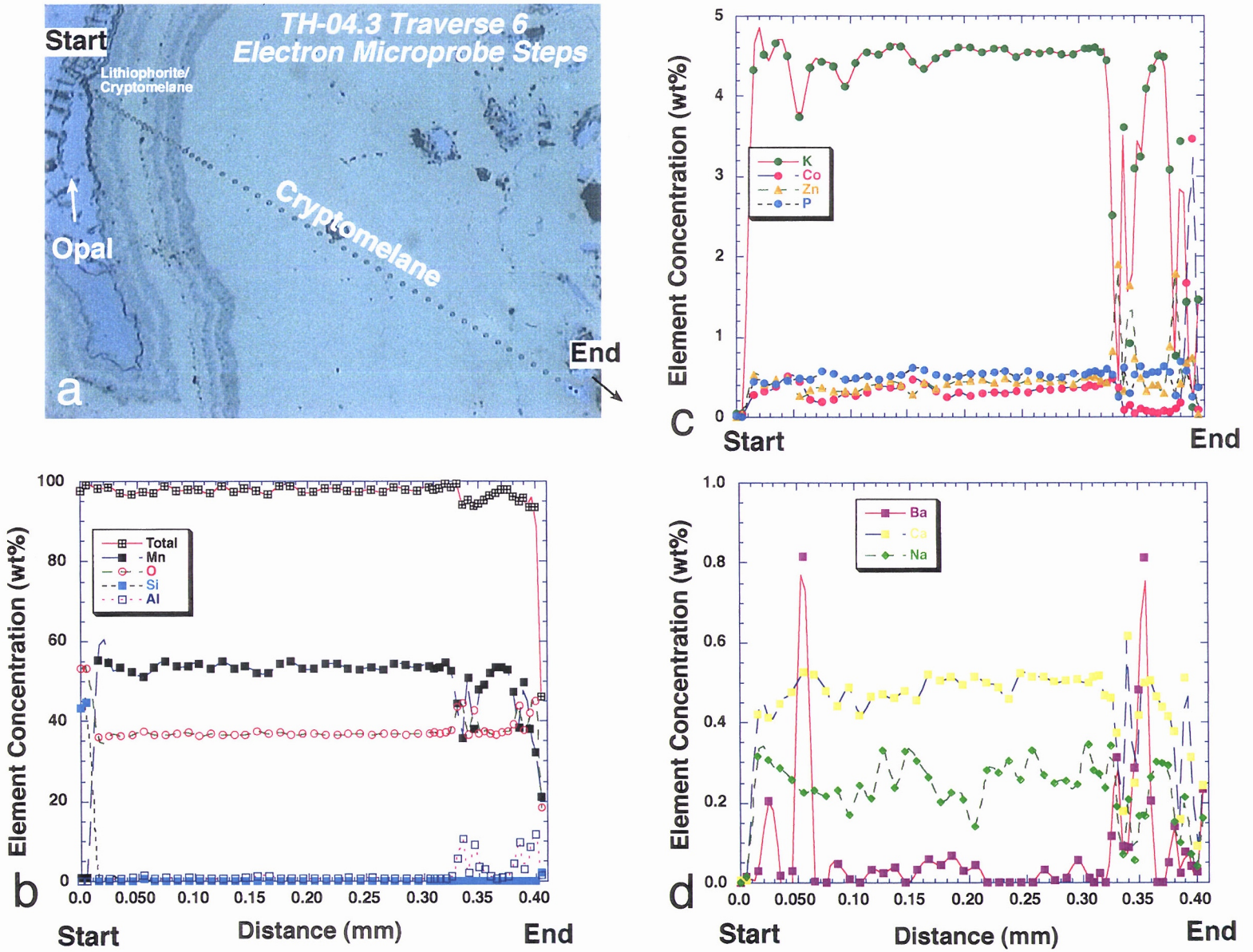

Figure 75. (a) A reflected-light photomicrograph illustrate Mn-oxide cement replacement front and the traverse where EMP analyses were performed. Major (b) and minor (c-d) element distribution along the traverse shown in (a) illustrate the high Ca and Na contents of the Pilgrim Fault breccias Mn-oxides. In addition to Mn-oxides, this sample also shows the presence of late-stage opal. Opal layers partially covering iron and manganese oxides are common in supergene samples from the Mount Isa region and they may suggest a regional transition toward aridity after Mn-oxide precipitation.

TH-04.1 Traverse 7 - Electron Microprobe Analyses

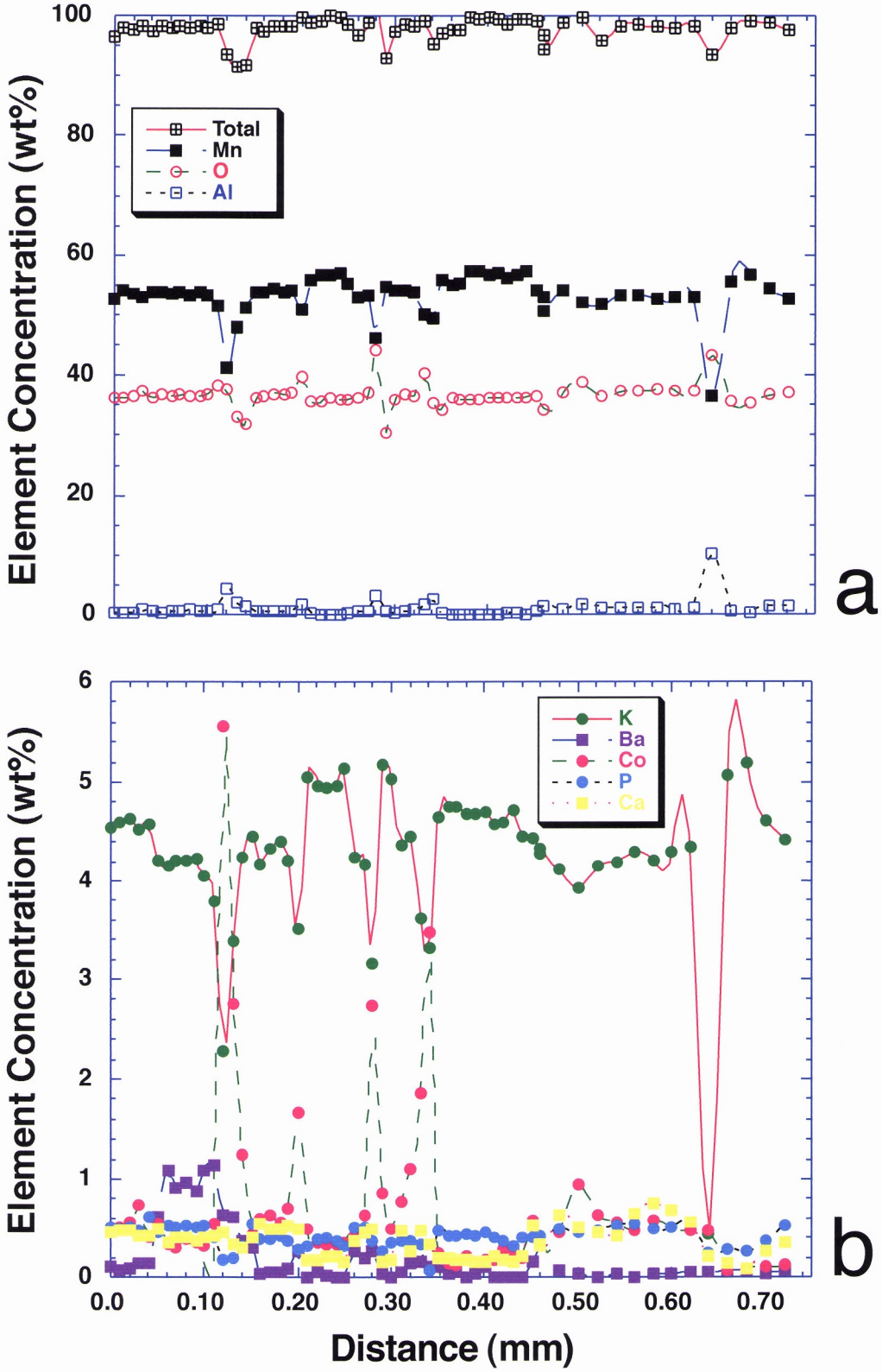

Figure 76. Major (a) and minor (b) elements determined by an EMP traverse through another Pilgrim Fault Mn-oxide cement sample show very high K and Co contents and the relatively high Ca-content of this Mn-oxide.

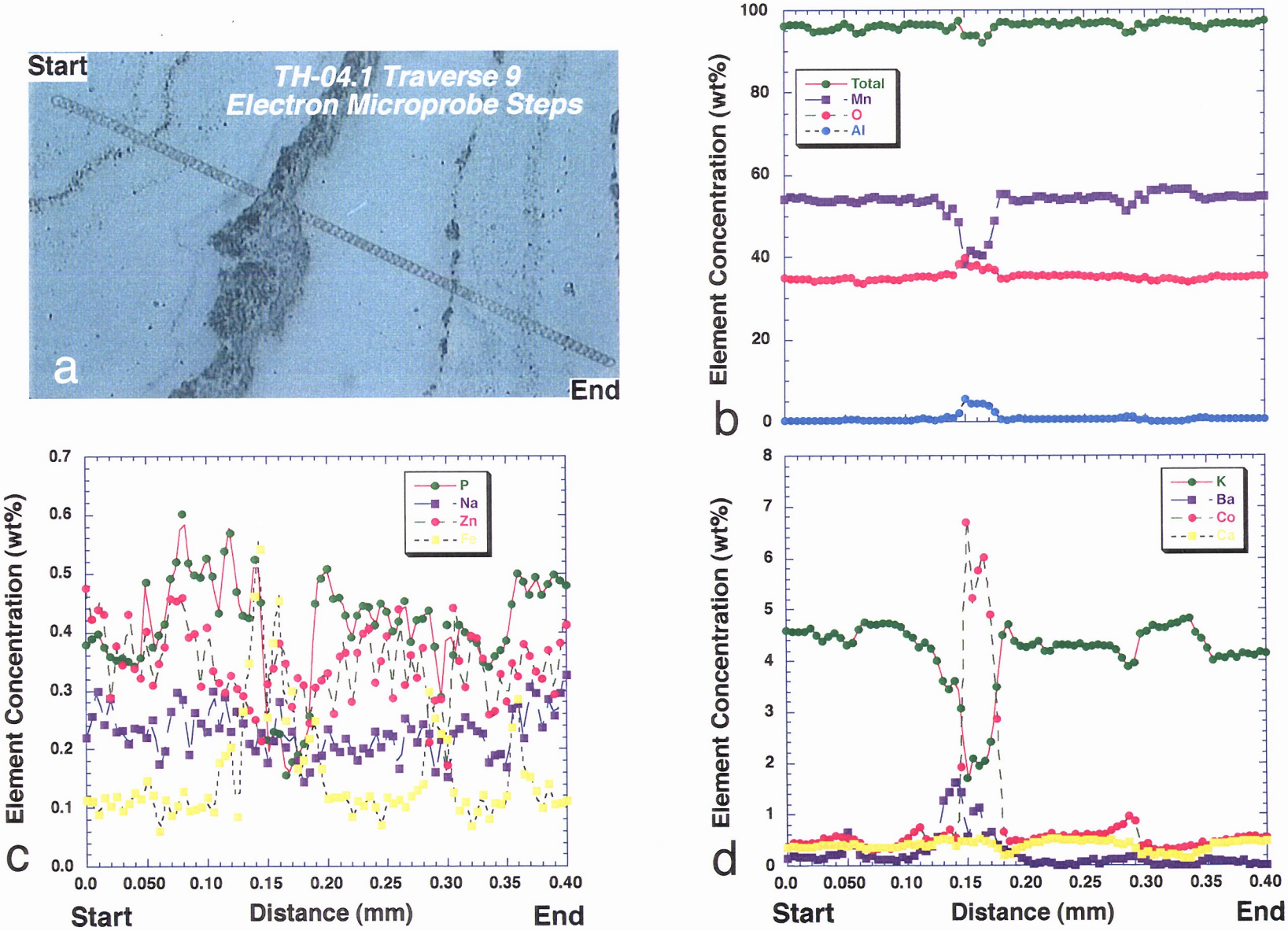

Figure 77. (a) This reflected-light photomicrograph illustrates a detailed EMP traverse through Mn-oxide cement growth bands. The major element traverse (b) illustrates a drop in the Mn content and analyses' totals and an increase in O and Al along the dark central band shown in (a). The minor element analyses shown in (b) show an increase in Co and a decrease in K content along the same band. This relationship suggests that the dark central band contains lithiophorite as opposed to cryptomelane in the rest of the sample. Also noticeable in this sample is the high Ca (c) and Na (d) contents of the Pilgrim Fault Mn-oxides.

Queensland and elsewhere in Australia. K-Mn oxides replacing silcretes are only found along fault zones in low relief areas. Field distribution of cryptomelane-replaced silcretes and textural observations from optical and electron microscopy indicate that the influx of manganese post-dates silcrete formation.

Laser-heating $^{40}Ar/^{39}Ar$ dating of K-Mn oxide epigenetically replacing silica cement in the Tick Hill silcretes imposes minimum ages on silcrete formation (Figs. 78-79). Step-heating analyses of seven cryptomelane (K-Mn oxide) grains from one sample collected from a Mn-oxide-rich outcrop (TV Tower site) yield the following plateau dates: 16.5 ± 0.1 Ma, 16.4 ± 0.1 Ma, 18.9 ± 0.5 Ma, 18.1 ± 0.5 Ma, 17.2 ± 0.1 Ma, 16.3 ± 0.3 Ma, and 18.4 ± 0.1 Ma. Close clustering of the step-heating results suggests that the $^{40}Ar/^{39}Ar$ dates correspond to the age of precipitation of cryptomelane in these silcretes.

A more comprehensive study of the geochronology of manganese oxide replacement of silcrete samples was undertaken by Lilley (1997). This study indicates that older manganese oxides are present along the Pilgrim Fault next to Mount Birnie and in outcrops further North. $^{40}Ar/^{39}Ar$ dating of these oxides pushes the minimum ages for silcrete formation to ca. 38 Ma (Lilley, 1997).

2.5.2 Discussion - Tick Hill Region

The electron microprobe analyses of the Mn-cements indicates that the solutions responsible for the genesis of the Mn-oxide "breccias" were rich in alkali (K, Na), alkali-earth (Ca, Ba) and transition metals. The Ca- and Na-rich nature of the Mn-oxides along the Pilgrim fault indicates a very different mechanism of precipitation from Mn-oxides found elsewhere in the Mt. Isa Block.

One may postulate that the Mn-oxides cements in the Mn-"breccias" were derived from weathering of Cambrian sediments, now completely eroded, which may have overlain the silcrete zones. These overlying lithologies would have to be rich in Mn, K, Ca, Na, Co, Ba, Al, and Si. Yet, this material would have to have undergone a significant leaching of silica to account for the underlying silcrete. It is unlikely that Na, Ca, and Ba would remain in a weathered rock from which the silica had been so strongly leached. In addition, if an overlying source existed, Mn-oxide distribution would not necessarily be restricted to the fault zones.

Another possible source for the elements present in the Mn-oxide "breccias" are solute-rich groundwaters ascending along the Pilgrim Fault. The occurrence of Mn-oxides restricted along the fault and the composition of the Mn-oxide cements favour this second hypothesis.

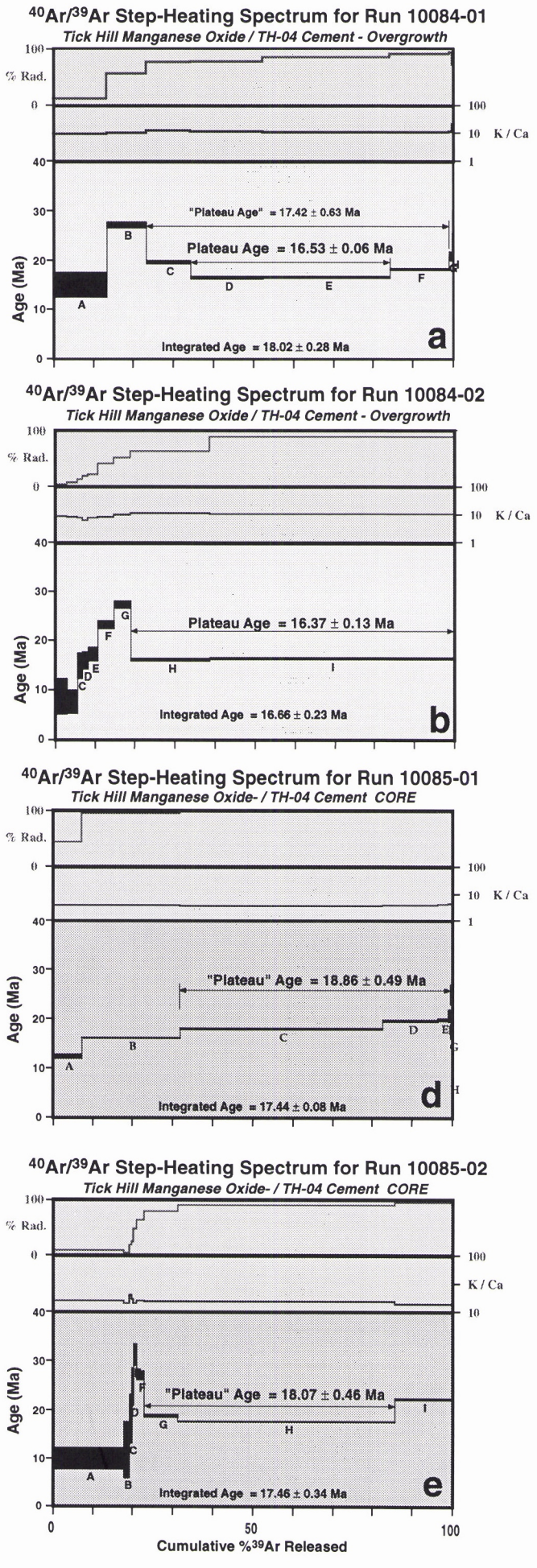

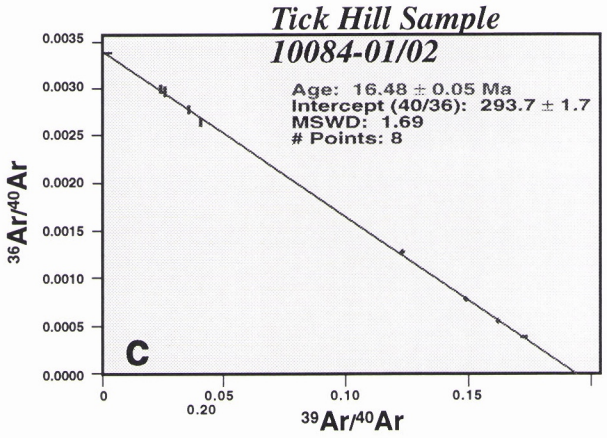

Figure 78. (a-b) $^{40}Ar/^{39}Ar$ step-heating analyses of two grains from overgrowth bands in hand-specimen TH-04. The plateaus obtained are reasonable and concordant. The isochron (c) age for the sample is 16.48 ± 0.05 Ma. (d-e) $^{40}Ar/^{39}Ar$ step-heating analyses of two grains from the inner growth bands in hand-specimen TH-04. The ages obtained are 18.86 ± 0.49 and 18.07 ± 0.46, which are indistinguishable at the 2-sigma level. The isochron age (f) for this sample is 17.96 ± 0.5 Ma. The results are internally consistent. The geochronology results again show a consistent relationship between the paragenetically older inner bands and the younger overgrowths, suggesting that the ages obtained may be interpreted as true Mn-oxide precipitation ages.

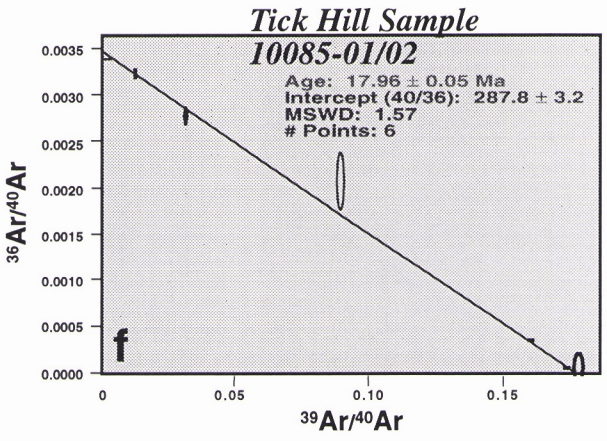

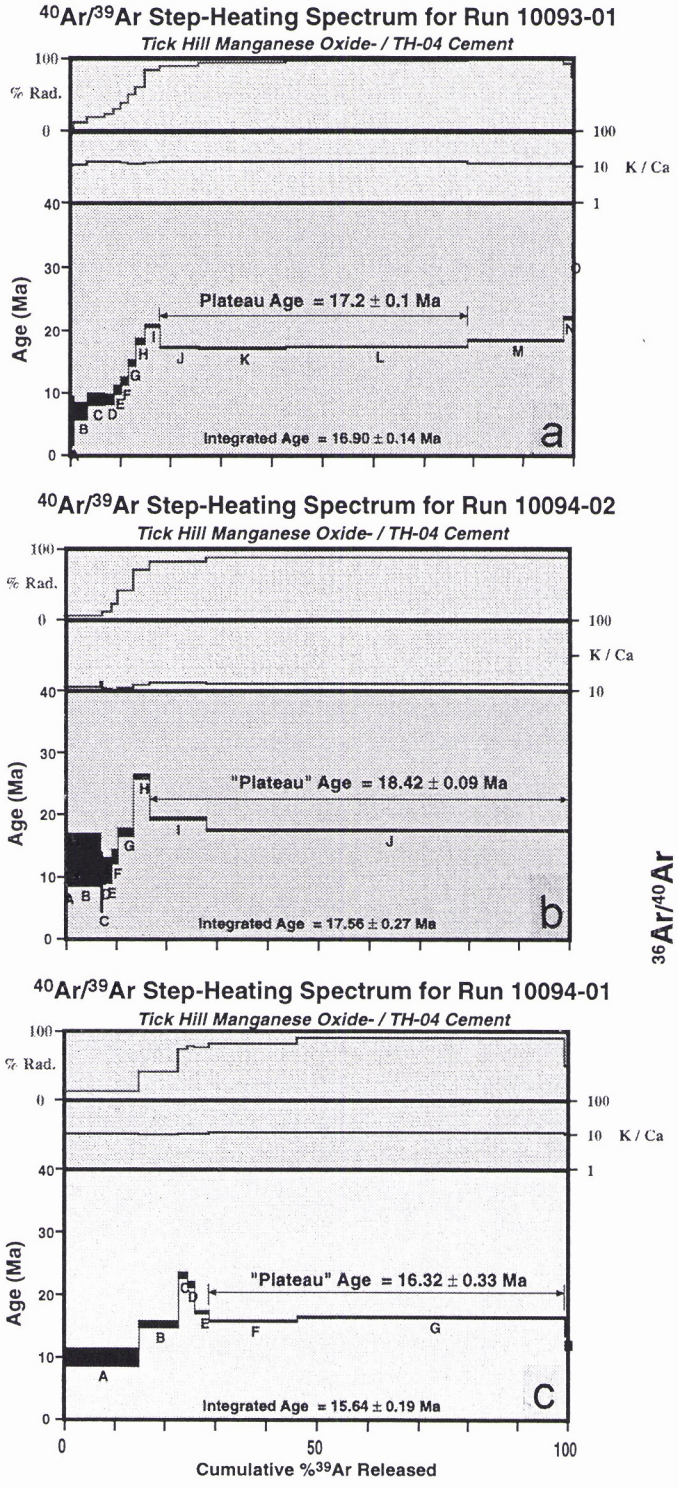

Figure 79. $^{40}Ar/^{39}Ar$ step-heating analyses (a-c) of three additional grains from sample TH-04 yield ages concordant with the ages illustrated in Figure 77. The isochron age for these grains is 16.71 ± 0.06 Ma and the ideogram age for all the Tick Hill samples analysed is 16.3 Ma. These ages represent a minimum constraint silcrete formation in the area. Further work in the region (Lilley, 1997) pushes the minimum age for the silcretes to ca. 38 Ma.

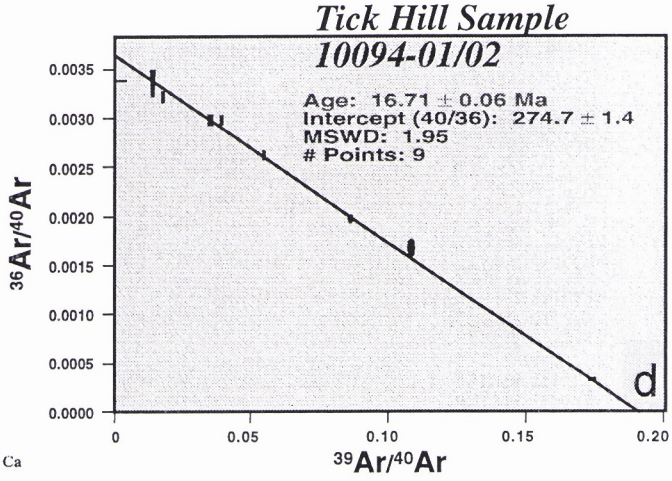

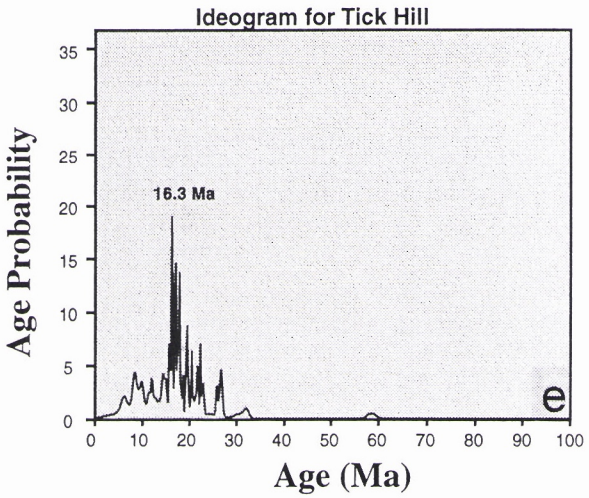

Upward migration of groundwaters may have been driven by an increase in hydraulic head caused by raised fluid pressure at recharge areas, reflecting an increase in precipitation. Alternatively, increase in hydraulic head may reflect increase in the elevation potential at recharge areas caused by local changes in relief during tectonically driven reactivation of basement faults. $^{40}Ar/^{39}Ar$ dating of cryptomelane cements in the Tick Hill area (this study) imposes a minimum age for silcrete formation (ca. 19 Ma). Subsequent studies by Lilley (1997) pushes this minimum age to ca. 38 Ma. Given the little information available about the paleoclimatic and tectonic history of the Mount Isa block during the Cenozoic, either mechanism of groundwater ascension is plausible.

An important result of the postulated models for Mn-oxide precipitation along the Pilgrim fault is that the chemistry of the cements precipitated along the fault reflects the composition of bedrocks and possible mineralisation sites present West of the Pilgrim Fault. The K-, Ba-, and Co-rich, and Pb- and Zn-poor composition of the Mn-oxide breccia cements is consistent with the composition of Mn-oxides associated with Cu-Au and Au mineralisation elsewhere (Vasconcelos, 1992; Vasconcelos, unpublished data).

The singular nature of the Mn-oxide occurrences in the Tick Hill area and their possible mechanisms of precipitation preclude using the $^{40}Ar/^{39}Ar$ results for the Tick Hill samples as indicators of paleoclimatic conditions at this early stage.

2.6 Cannington Area

South of the Selwyn Ranges the landscape becomes relatively subdued (Fig. 80). Small mesas and plateaus, sitting at 5-40m above the surrounding landscape, are covered by deeply weathered Mesozoic sediments (Fig. 80). The surrounding plains in the area are also deeply weathered (Fig. 80). Several prospects occur in the area. Manganese oxides commonly occur in the vicinity of these prospects. Samples from three of these prospects (Pegmont, Tringadee, and Cowie Prospects) where provided by CRCLEME researchers.

2.6.1 Tringadee Prospect

2.6.1.1 Site Selection Criteria: CSIRO request.

2.6.1.2 Location: 486108E-7589140N

2.6.1.3 Elevation (sampled outcrops): ~250 m

2.6.1.4 Geomorphologic Setting: deeply weathered plains surrounded by 5-20 m high Mesozoic sediment mesas (also deeply weathered).

2.6.1.5 Geomorphologic Regime: erosional.

2.6.1.6 Sample in Relation to Landscape Position: sample collected from approximately 20m below present land surface.

2.6.1.7 Sample in Relation to Regolith: Mn-oxides occur in saprolite formed on black shale.

2.6.1.8 Datable Minerals/Host Rock Relationship: Manganese and iron oxide concentrations in weathered black shale.

2.6.1.9 Sources of Elements: undetermined.

2.6.1.10 Overview

Author not familiar with the sample location.

2.6.1.11 Results

2.6.1.11.1 Electron Microprobe and SEM Analysis

An electron microprobe traverse across a cryptomelane vein is shown in Fig. 81. The traverse indicates the presence of unweathered or partially weathered silicates in the host rock. The Mn-oxide vein cross-cutting the parent material displays distinct compositional banding, visible both optically (Fig. 80a) and from the electron microprobe analyses (Figs. 81b-c). Growth bands in the vein contain varying K/Ba ratios, as illustrated by the EM results. The Mn-oxides in this sample are also interesting because of their relatively high Co contents (average ~ 0.3 wt%). High Co values are not found in other samples from the Cannington area (Cowie and Pegmont Prospects).

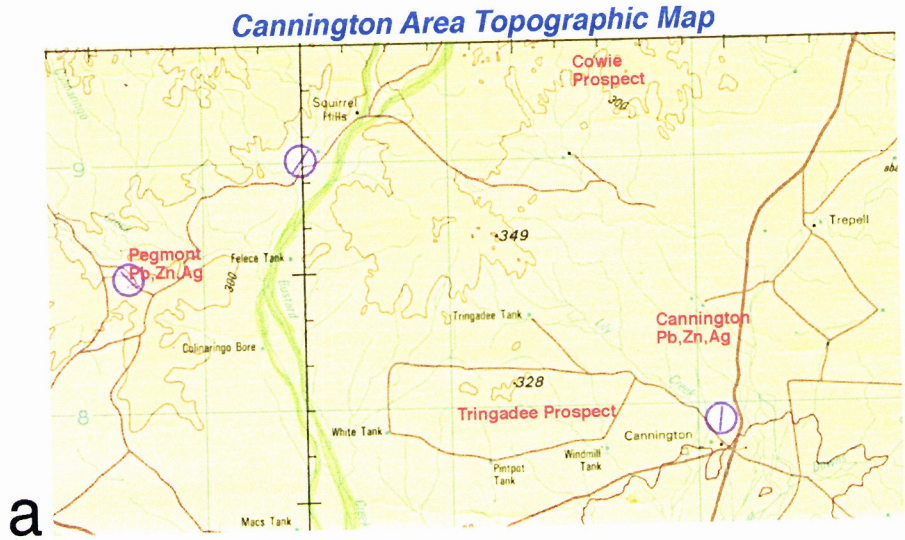

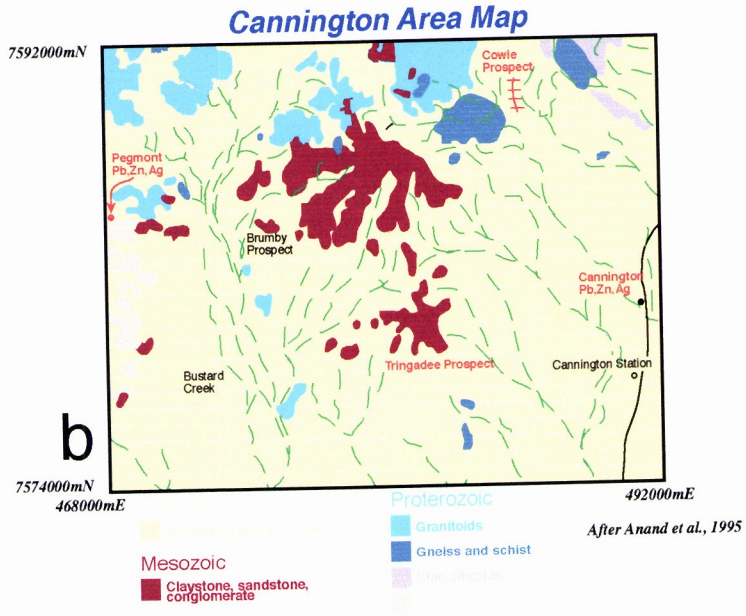

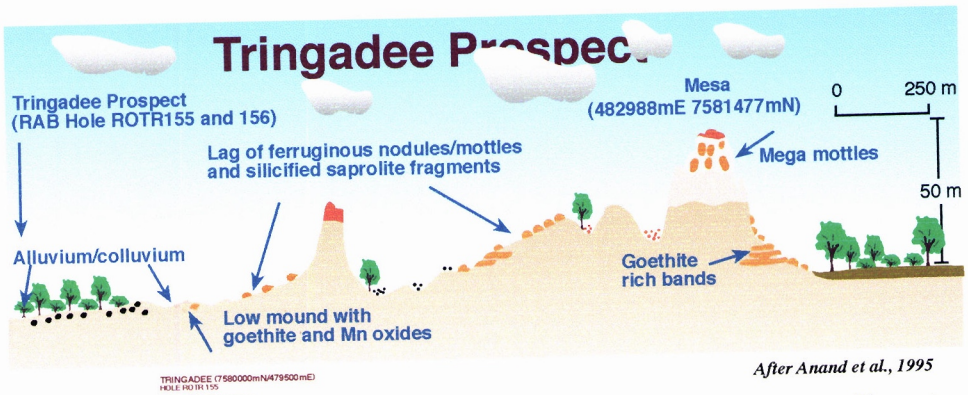

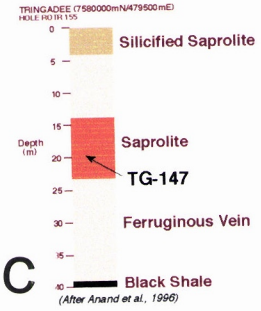

Figure 80. (a) The topographic map illustrates the relative subdued landscape in the Cannington area. (b) A simplified geological map of the Cannington area shows the locations of the Tringadee, Pegmont, and Cowie prospects. (c) The schematic diagram illustrates the landscape in the vicinity of the Tringadee prospect. The location of the sample analysed in this study is also shown in relation to the host weathering profile.

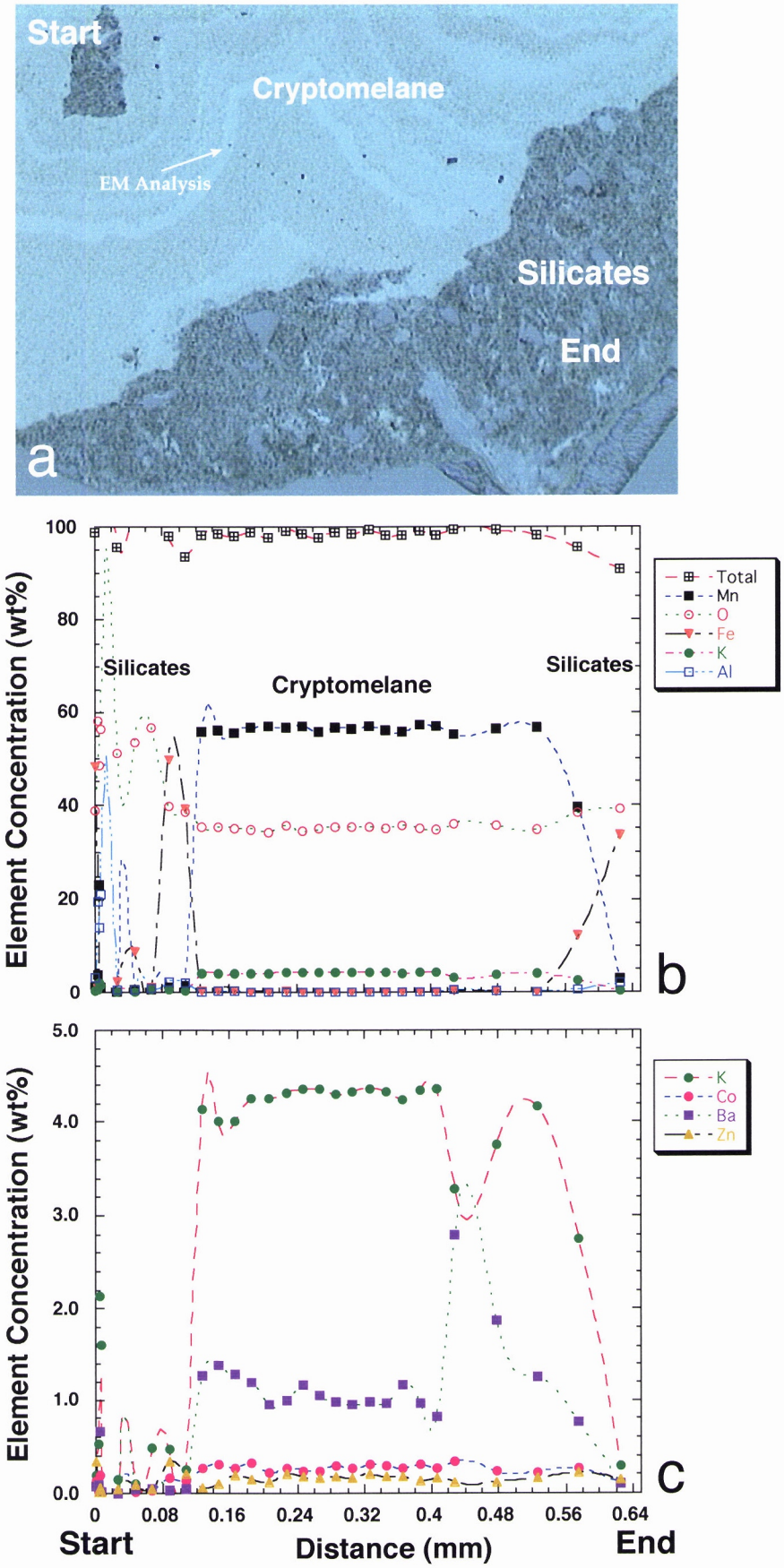

Figure 81. (a) This reflected-light photomicrograph illustrates a Mn-oxide vein cross-cutting the weathered host shale and the traverse where EMP analyses were performed. Major (b) and minor (c) element distribution along the traverse shown in (a) is also illustrated. Notice the varying Al, Si, and K contents in the silicate area, indicating the possible presence of hypogene muscovite. The cryptomelane vein has relatively homogeneous Mn and O contents, and K and Ba show antipathetic variation. The high K content of the vein material makes this sample ideal for dating, provided no

2.6.1.11.2 Geochronology

The presence of unweathered silicates may prevent successful dating of the sample. However, several grains were crushed in a agate mortar, ultrasonically cleaned in distilled water, and hand-picked under the binocular microscope. Only samples displaying homogeneous lustre on all surfaces (typical of pure Mn-oxides) were selected for irradiation and $^{40}Ar/^{39}Ar$ analysis. The high K contents of the vein material (4.18 ± 0.28 wt%) suggests that if pure cryptomelane is obtained, the sample should be suitable for $^{40}Ar/^{39}Ar$ dating.

Six grains from a surface Mn-oxide sample from the Tringadee Prospect (Sample TG147) were dated by the $^{40}Ar/^{39}Ar$ method at the BGC. The samples yielded relatively well defined plateau ages ranging from 12.6 ± 0.1 to 13.1 ± 0.2 Ma (Fig. 82).

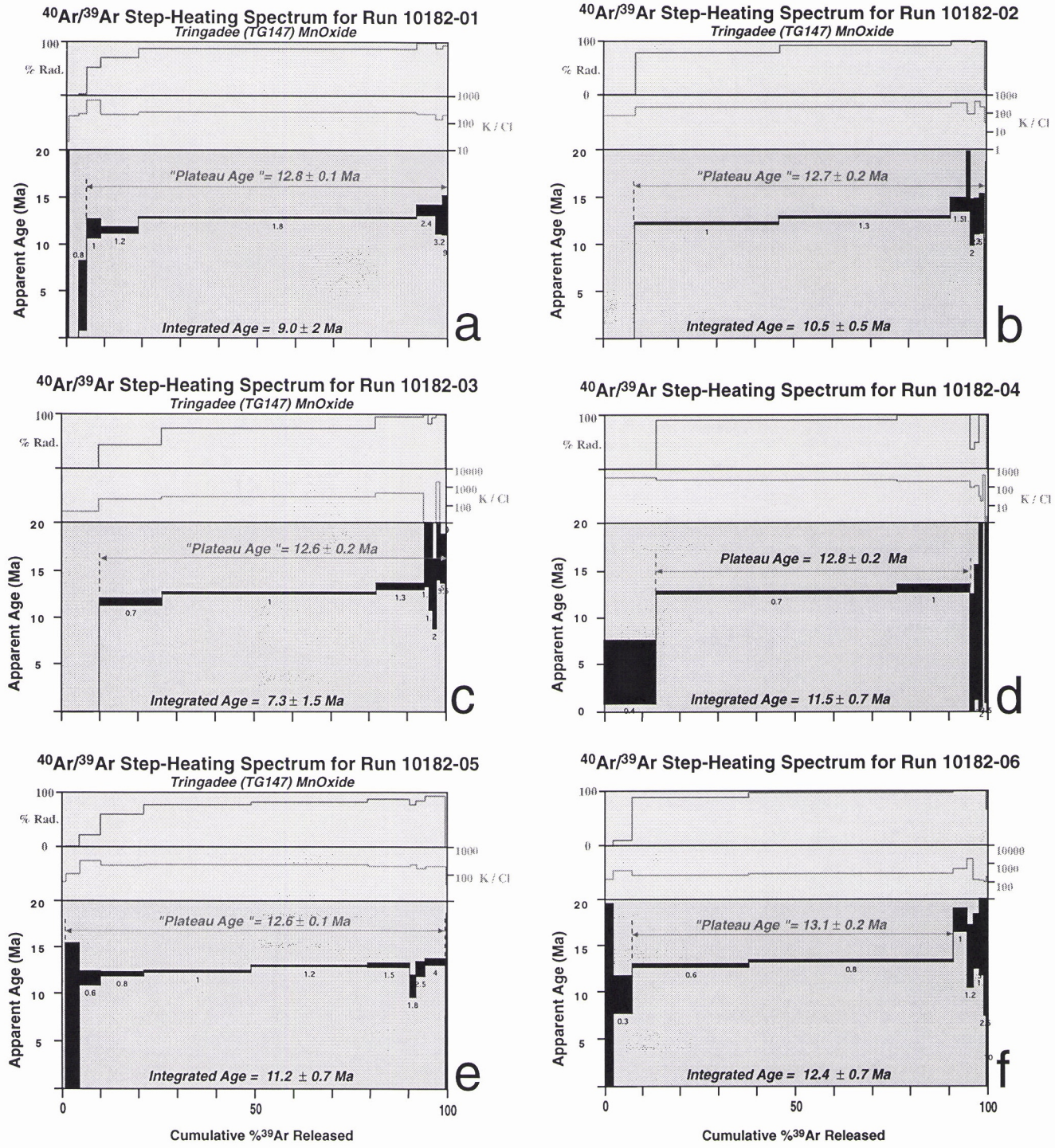

Figure 82. $^{40}Ar/^{39}Ar$ step-heating analyses of six grains from sample TG147 (a-f). Although not every grain produce plateaus, all the plateaus and plateau-like spectra yielded essentially the same age (ca. 13 Ma). This age is also determined by the ideogram plotted for this sample (g).

2.6.2 Pegmont Prospect

2.6.2.1 Site Selection Criteria: CSIRO request.

2.6.2.2 Location: 467660E-7683300N

2.6.2.3 Elevation (sampled outcrops): ~300 m

2.6.2.4 Geomorphologic Setting: undetermined.

2.6.2.5 Geomorphologic Regime: undetermined.

2.6.2.6 Sample in Relation to Landscape Position: undetermined.

2.6.2.7 Sample in Relation to Regolith: undetermined.

2.6.2.8 Datable Minerals/Host Rock Relationship: undetermined.

2.6.2.9 Sources of Elements: undetermined.

2.6.2.10 Overview

Author not familiar with the sample location.

2.6.2.11 Results

2.6.2.11.1 Electron Microprobe and SEM Analysis

Samples from the Pegmont prospect show relatively high Zn contents (maximum value of 1.8 wt%) (Fig. 83). The main Mn-oxide present in this sample is coronadite. In this sample, Pb and Zn are clearly associated with Mn-oxides, not Fe-oxides (Fig. 83). Two distinct Fe-oxide phases are present: martite, formed after *in situ* weathering of hypogene magnetite, and late-stage botryoidal goethite, which forms cross-cutting veins and overgrowths on Mn-oxides (Fig. 83a). Cross-cutting relationships indicate that late-stage influx of iron promotes the dissolution and flushing of elements such as Zn and Pb.

The high Pb content in this sample suggests that the source of base metals is nearby, since large amounts of Pb do not move significantly away from source zones in weathering solutions. Even during iron influx, Pb is only locally remobilised, since it reprecipitates close to the source in late-stage, cross-cutting coronadite veins (Fig. 83a). Barium, in the form of barite veins (detected from back-scattered analysis) is another late-stage fracture/desiccation crack-filling material.

2.6.2.11.2 Geochronology

Two grains from a Mn-oxide sample recovered at 2 m depth (Sample 11-0445) were dated by the $^{40}Ar/^{39}Ar$ method at the BGC. The samples yielded well defined plateau ages ranging from 13.0 ± 0.1 to 13.8 ± 0.1 Ma (Fig. 84).

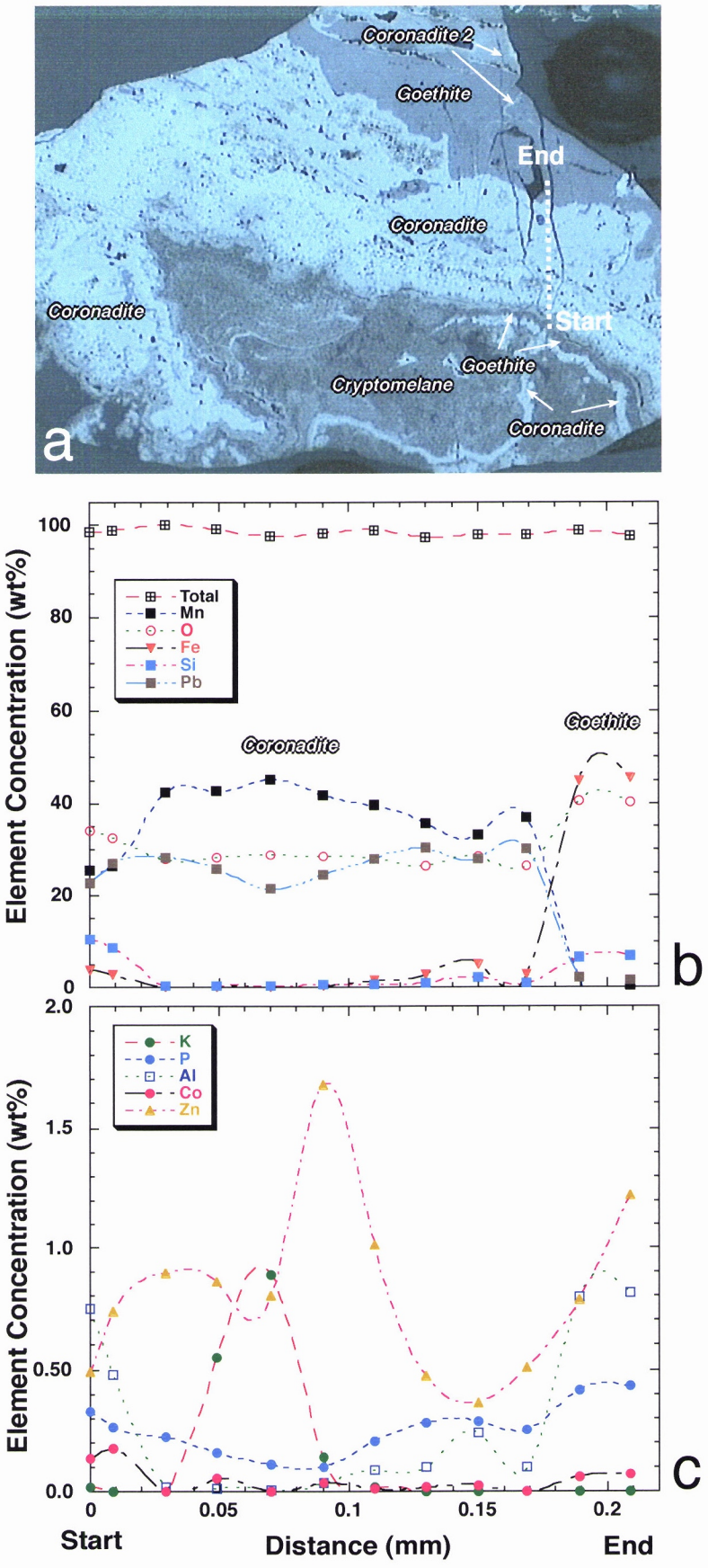

Figure 83. (a) Reflected-light photomicrograph illustrating Mn-oxides from the Pegmont prospect. The location of the EMP traverse is also shown. Major (b) and minor (c) element distribution along the traverse shown in (a). Notice the preferential association of Pb with Mn. Relatively high Zn values occur in association with both Mn and Fe oxides.

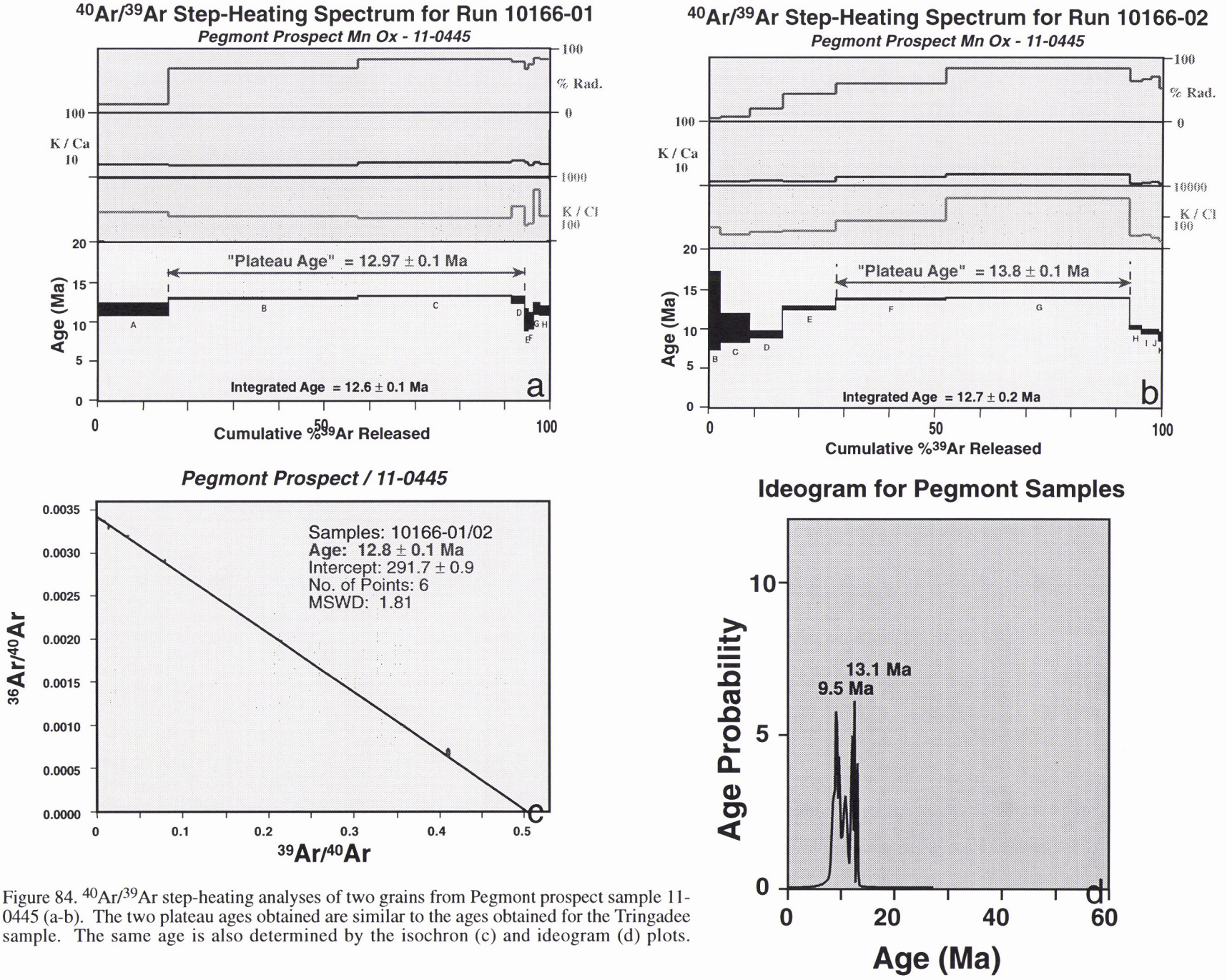

Figure 84. $^{40}Ar/^{39}Ar$ step-heating analyses of two grains from Pegmont prospect sample 11-0445 (a-b). The two plateau ages obtained are similar to the ages obtained for the Tringadee sample. The same age is also determined by the isochron (c) and ideogram (d) plots.

2.6.3 Cowie Prospect

2.6.3.1 Site Selection Criteria: CSIRO request.

2.6.3.2 Location: 486108E-7589140N

2.6.3.3 Elevation (sampled outcrops): ~250 m

2.6.3.4 Geomorphologic Setting: Undetermined.

2.6.3.5 Geomorphologic Regime: Undetermined.

2.6.3.6 Sample in Relation to Landscape Position: Undetermined.

2.6.3.7 Sample in Relation to Regolith: Undetermined.

2.6.3.8 Datable Minerals/Host Rock Relationship: Undetermined.

2.6.3.9 Sources of Elements: Undetermined.

2.6.3.10 Overview

Author not familiar with the sample location.

2.6.3.11 Results

2.6.3.11.1 Electron Microprobe and SEM Analysis

Figures 84a and 84b show photomicrographs illustrating electron microprobe results for Cowie Prospect samples. These samples contain supergene Mn-oxides in intimate association with martite. At least two distinct types of Mn-oxides are present: botryoidal and pore-space filling cryptomelane and bands and clusters of chalcophanite (Figs. 85-b). Although the electron microprobe traverse does not intersect any of the pure chalcophanite bands/clusters (the Zn content should reach 16-18 wt% in these areas), the results clearly indicate the presence of Zn and the direct correlation between Zn and Mn contents. This correlation suggests that Zn is hosted by the Mn-oxides and is not associated with Fe-oxides. Although Zn is a relatively mobile phase in weathering environments, the presence of chalcophanite suggests relatively close proximity to the zinc source.

2.6.3.11.2 Geochronology

Three grains from a surface Mn-oxide sample from the Cowie Prospect (Sample 11-0446) were dated by the $^{40}Ar/^{39}Ar$ method at the BGC. The samples yielded relatively well defined plateau ages ranging from 11.7 ± 0.3 to 12.7 ± 0.1 Ma (Fig. 86).

2.6.4 Discussion - Cannington Area

The Pegmont, Cowie, and Tringadee prospects are located in the same geomorphologic province and the samples analysed in this study are possibly derived from similar weathering profiles. The remarkable concordance in the ages obtained for the samples from the three prospects suggests a common history for the weathering profiles hosting these mineral occurrences. The ideogram for the results obtained for all the samples from the Cannington area (Fig. 86) suggests that the results are closely clustered. The Middle Miocene ages

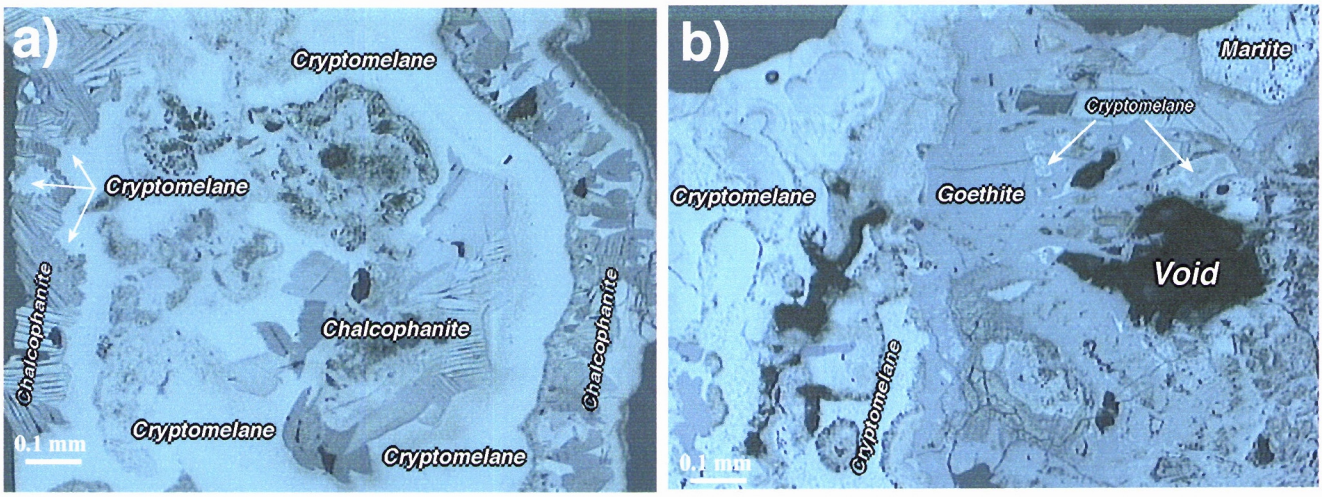

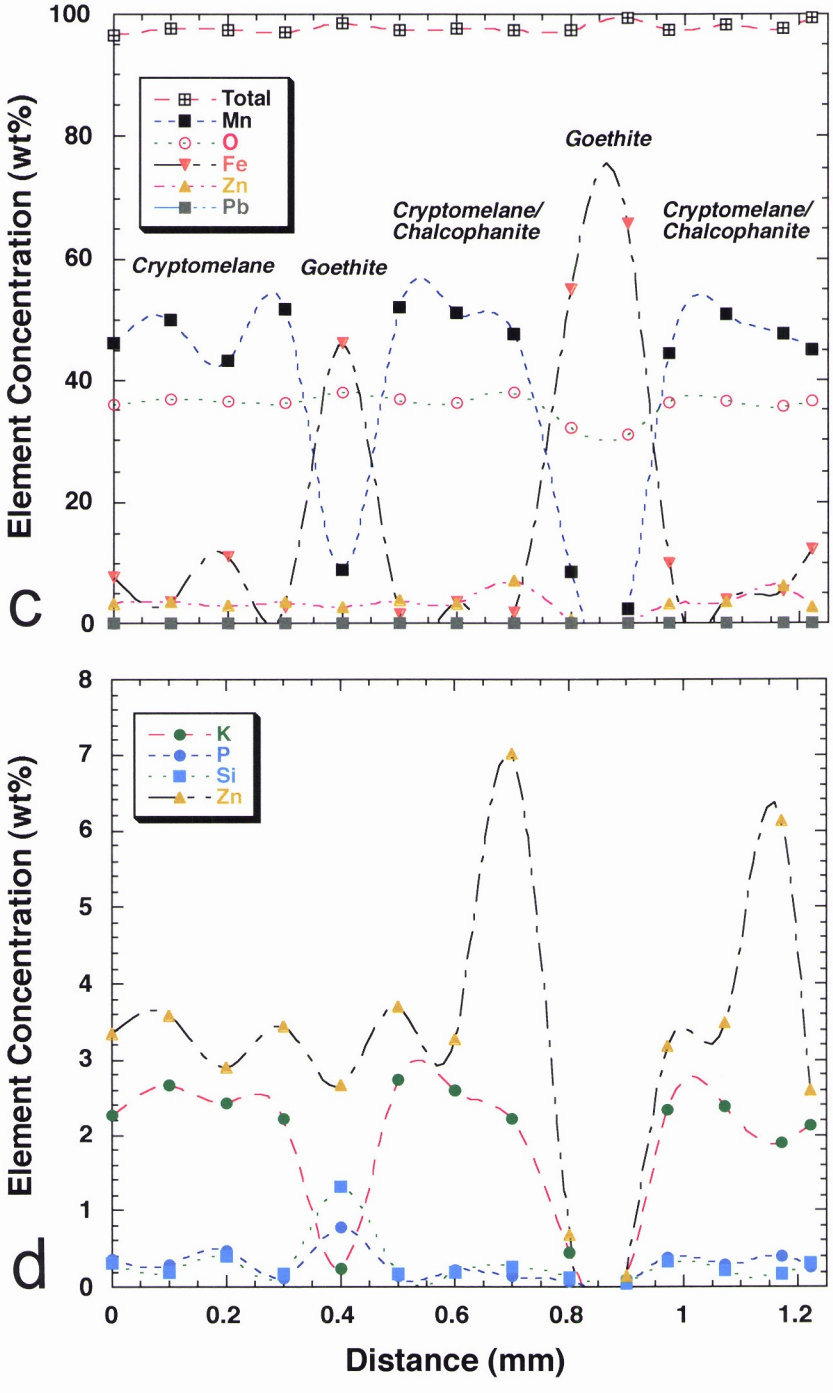

Figure 85. (a) This reflected-light photomicrograph illustrates Mn-oxides from the Cowie prospect. The location of an EMP traverse is also shown. Major (c) and minor (d) element analyses along the traverse shown in (a) indicate that the botryoidal Mn-oxides are composed of alternating bands of chalcophanite and cryptomelane. Some late stage cryptomelane appears to replace chalcophanite (arrows). Figure 85 (b) illustrates the complex relationship between primary magnetite, now weathered to martite, which undergoes hydration to goethite. Goethite also seems to replace some early manganese oxides. Well preserved botryoidal cryptomelane and chalcophanite are present on the left side of the photomicrograph.

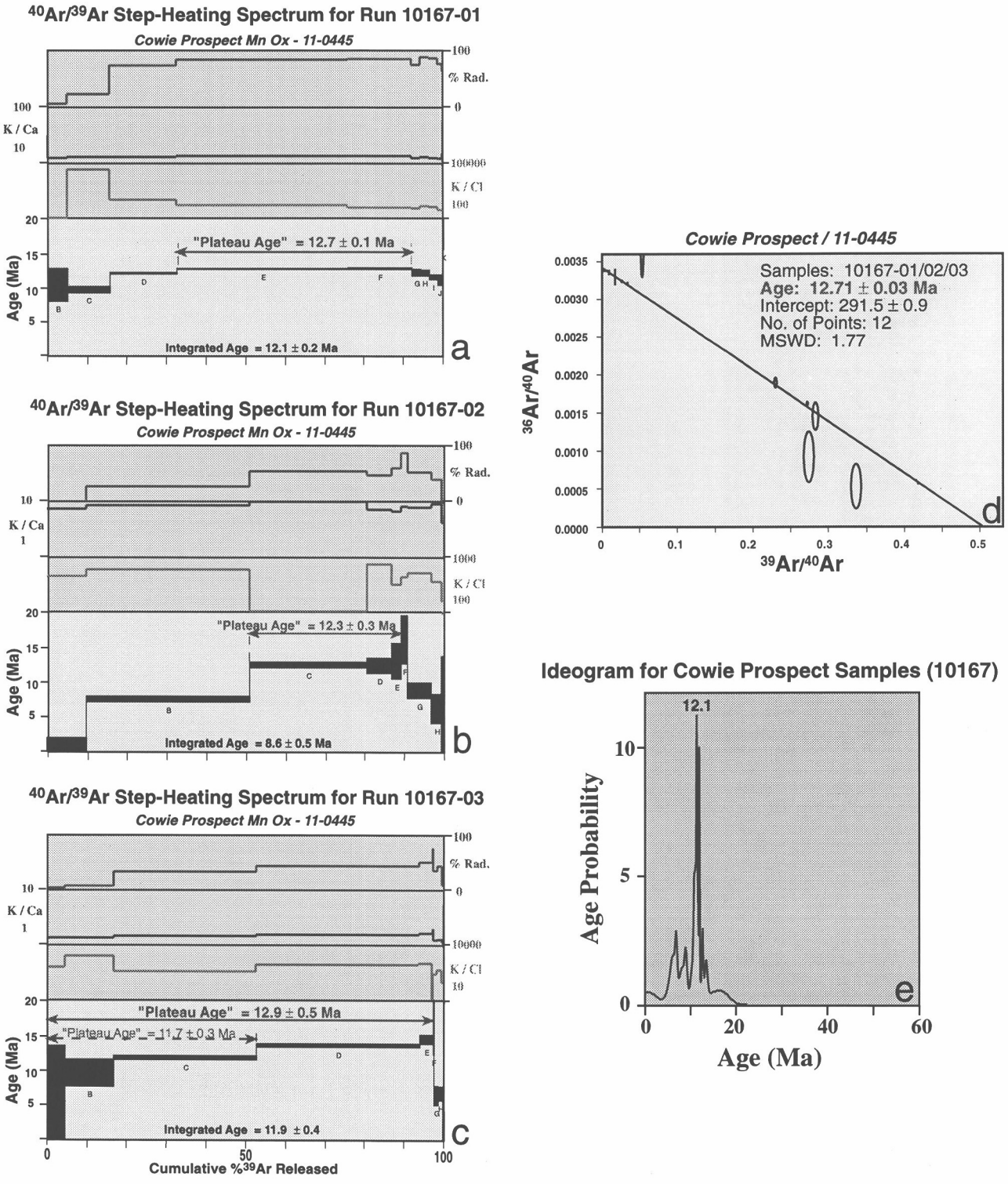

Figure 86. $^{40}Ar/^{39}Ar$ step-heating analyses of three grains from Cowie prospect sample 11-0446 (a-c) shows that none of the grains yielded well defined plateau ages. However, the plateau-like spectra obtained suggest apparent ages consistent with the results obtained for the Tringadee and Pegmont prospects. The isochron (d) and ideogram (e) plots for the grains in this sample also yielded well defined results which are consistent with the results obtained for the Tringadee and Pegmont prospects.

obtained for weathering processes in this location is significantly younger than the ages obtained for other weathering profiles in the Mount Isa area, with the exception of Century deposit.

The presence of Mesozoic sediments capping plateaus in this area indicates that the area has not been subject to significant denudation throughout the Tertiary. The late Tertiary weathering ages obtained cannot be interpreted as reexposured, by denudation of ancient weathering profiles, of relatively unweathered lithologies during the late Cenozoic. These weathering ages must, therefore, reflect a complex history of weathering, with superposition of weathering processes and the pervasive resetting of the system by a very strong weathering pulse in the Middle Miocene.

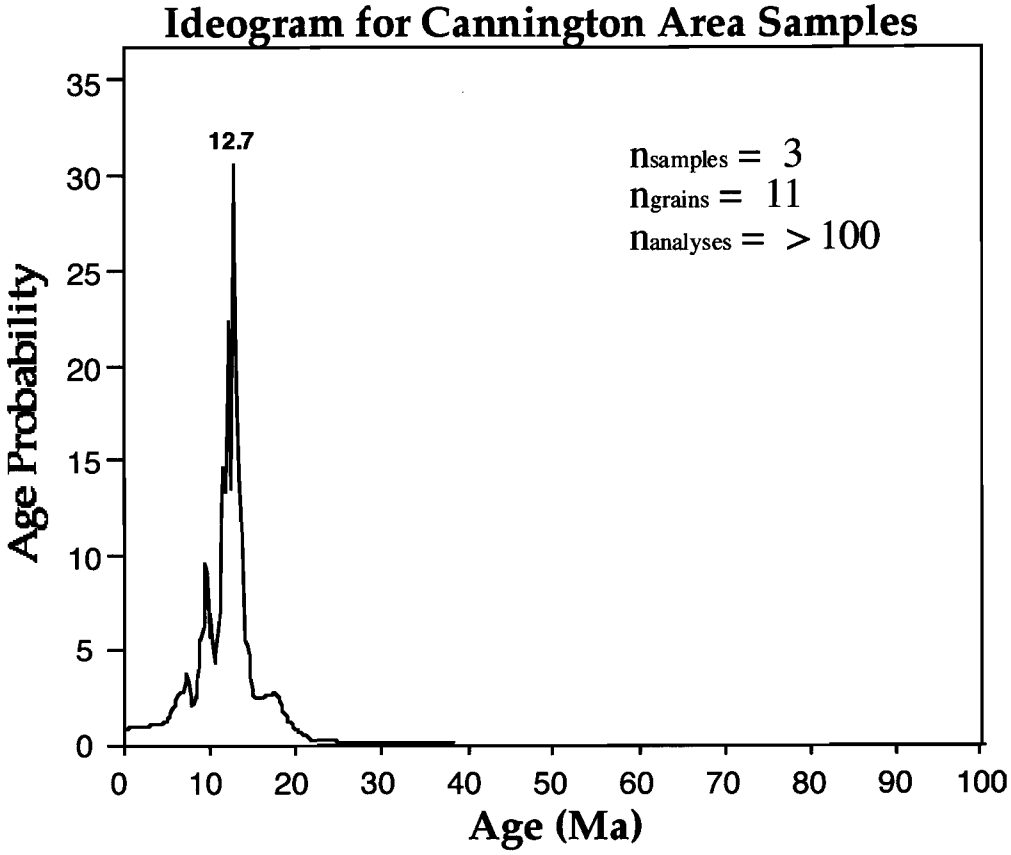

Figure 87. Ideogram for all the samples analysed from Tringadee, Cowie, and Pegmont indicate that the middle Miocene was a time of significant migration of ore elements through the groundwater system in the region.

2.7 Interpretation of Mount Isa Region Geochronology Results

This project is the most comprehensive weathering geochronology study ever undertaken in a single region. More than 103 $^{40}Ar/^{39}Ar$ laser step-heating and 11 K-Ar analyses provide a substantial geochronology database which permits answering some surficial geochemistry and

landscape evolution questions for the region. In addition to the results presented here, subsequent work by the author and UQ students (Fleming, 1997; Lilley, 1997, Vasconcelos, unpublished results) further support the conclusions drawn below. The total $^{40}Ar/^{39}Ar$ laser step-heating database supporting the conclusions below exceeds 200 step-heating analyses.

The geochronology results indicate that the evolution of the weathering profiles in the Mount Isa Block spans the entire Tertiary, possibly extending into the Cretaceous. The $^{40}Ar/^{39}Ar$ results obtained for the jarosite samples also indicate that weathering-related mineral precipitation continued into the Quaternary.

2.7.1 Continuous Versus Episodic Weathering

A current controversy in the geological community is whether weathering processes are continuous through time or whether weathering profiles record an episodic history of evolution. The continuous weathering model implies that weathering profiles undergo chemical reactions at a continuous rate through time. In the continuous weathering model, rates of reaction are independent of climate.

The episodic weathering model implies that chemical reactions in weathering profiles are mostly driven by water-rock interaction. During times when abundant water is available, weathering reactions are favoured and the mass of newly formed minerals is significant. During arid conditions, when water becomes deficient and a limiting factor in weathering reactions, the mass of authigenic minerals is small to insignificant. Since weathering profiles host the products of weathering reactions integrated through time, the mass of minerals formed in humid conditions is larger than the mass of minerals precipitated under arid conditions. The episodic weathering model does not imply that weathering reactions cease during arid conditions; it implies only that the mass of minerals precipitated during arid conditions is insignificant.

A possible way to address the continuous versus episodic weathering model controversy is to analyse a statistically significant number of samples from several weathering profiles in the same region. If the weathering processes are continuous through time, the distribution of ages should not cluster at any specific time interval. The biggest difficulty in addressing this question in the past has been the small dataset obtained for any region studied by the Mn-oxide geochronology methodology. Given the comprehensive history of weathering obtained for the Mount Isa Block in this study and subsequent studies by the author and students at UQ, it is possible to plot a statistically significant frequency distribution for weathering ages in Mount Isa.

The results for all the samples analysed for the Mount Isa Block (except for the Tick Hill samples, since it is unclear whether these samples reflect climatic or tectonic factors) are plotted in Fig. 88. The ideogram obtained suggests an episodic distribution of ages through time, with three main peaks centred at the Cretaceous-Tertiary boundary (65-70 Ma), a second peak centred at 35 Ma (Late Eocene-Oligocene boundary) and a third peak spanning the early to middle Miocene (20-13 Ma). The large dataset and the large number of samples analysed in each profile seems to support the episodic weathering model. Episodicity in the distribution of weathering ages occur in each profile dated and is also reflected in the comprehensive database generated for the region.

Proponents of the continuous weathering model may argue that the episodic distribution of ages simply reflect the fact that only manganese oxides were dated, and that the low frequency intervals in the plot represent times of precipitation of other minerals (i.e., iron and aluminium oxides/hydroxides, clay minerals, etc.). This argument implies that fundamentally distinct mechanisms control the precipitation of manganese oxides as opposed to the precipitation of other minerals in the weathering environment. Until geochronological techniques suitable to date each mineral present in a weathering profile are developed, the different opinions will persist.

In the absence of any geochemical evidence suggesting that fundamentally distinct mechanisms control the precipitation of Mn-oxides versus Fe-Al oxides/hydroxides and clay minerals, it is reasonable to conclude, based on the geochronology results presented in this study, that the Mount Isa Block history preserved in the Mn-oxide precipitation record indicates alternating wet, weathering-prone conditions, and dry, erosion-prone conditions throughout the Cenozoic.

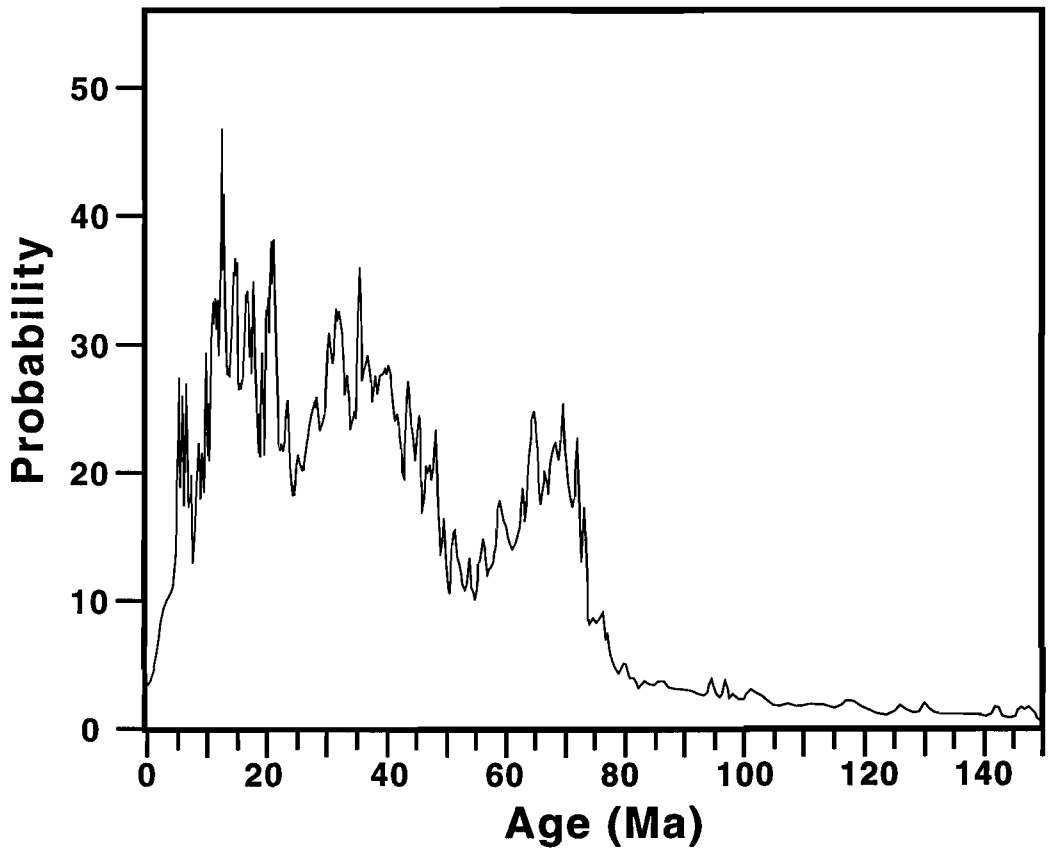

Figure 88. Ideogram of all the Mn-oxide analyses for the Mount Isa samples (> 200 grains analysed by the step-heating method, > 3000 individual analyses). The three major age clusters (65-70Ma, 30-40Ma and 10-20 Ma) suggest an episodic evolution for the weathering profiles in the region.

2.7.2 Weathering and Paleoclimates

The geochronological results obtained in this study may also aid in the interpretation of the climatic history in the region. However, the precipitation, dissolution, and reprecipitation of Mn-oxides in weathering environments do not reveal, explicitly, the climatic conditions at the time of mineral precipitation. **Climatic conditions** are **inferred** from the lines of evidence explained below.

From a purely geochemical viewpoint, most weathering reactions result from rock-water interaction. The fractionation of elements in different horizons in weathering profiles clearly depends on water as a transport medium. As water is an important reactant in most weathering systems, a simplistic application of the Law of Mass Action suggests that humid environments are more conducive to the formation of weathering profiles. In this study, textural and paragenetic relationships indicate that the Mn-oxide samples analysed from the Mount Isa Block result from the precipitation from aqueous solutions. Therefore, I conclude that manganese oxide precipitation ages record times of humid paleoclimates.

The textural relationships documented in this study also show the occurrence of multiple generations of Mn-oxides precipitated in the same profile. Multiple generations often occur in a single hand-specimen, indicating multiple periods of precipitation-dissolution-reprecipitation of manganese oxides. The Eh-pH diagram in Fig. 5 shows that acid-reducing conditions are required for the dissolution of Mn-oxides. The single most important factor creating acid-reducing conditions in weathering environments is the biota. Plant exudates and decay products of organic matter supply the dissolved organic acids necessary to create acid-reducing conditions in near surface environments. Consequently, Mn-oxide generations formed by the dissolution and reprecipitation of early oxide generations are interpreted as evidence for abundant vegetation at the time of mineral dissolution-reprecipitation. Vegetation abundance is also controlled by moisture availability, reinforcing the interpretation that Mn-oxide ages represent wet paleoconditions.

Both warm-humid and cold-humid environments could create the conditions necessary for the dissolution-reprecipitation of manganese oxides in weathering profiles. However, chemical kinetics shows that reaction rates increase with temperature. The magnitude of that increase is poorly determined. From theoretical arguments, it is known that reaction rates double with every 10 °C increase in average ambient temperature. More recently, Brady and Carrol (1994) have shown, from experimental studies, that weathering rates of silicates may increase by a factor of 2 to 5 for an increase in temperature from 15 to 25 °C. When averaged over millions of years, these factors would have significant implications to the relative masses of weathered regolith generated under warm-humid versus cold-humid conditions.

In addition to the chemical processes discussed above, the influence of plants and burrowing organisms on the physical desegregation and digestion of minerals is well established (Gilkes, 1996). Biomass primary productivity (plants, ants, termites, etc) is much larger in tropical humid environments than in cold-humid environments (Ricklefs, 1976), suggesting that warm-humid environments would favour chemical and physical weathering by organisms. Lastly, the influence of microorganisms on the dissolution and reprecipitation of minerals in the weathering environment is also significant (Brady, 1984). The abundance of microorganisms is favoured by higher ambient temperatures and humidity, further enforcing the view that warm-humid conditions favour weathering reactions (Brady, 1984).

The evidence above, although mostly circumstantial, suggest a direct correlation between warm-humid climates and increased rates of weathering. The Mn-oxide precipitation ages obtained in this study are, therefore, interpreted as evidence of warm-humid paleoclimates in the Mount Isa Block. I made an attempt to substantiate these conclusions with independent paleoclimatic evidence (fossil and pollen record, O-isotope curve for oceanic carbonates, etc.).

Unfortunately, these records are either incomplete or missing for areas adjacent to the Mount Isa Block or the existing record is too poorly dated to offer any independent constraints on the geochronology results presented in this study. A possible exception is the Riversleigh fossil site, in the Lawn Hill area. If the interpretation regarding paleoclimates favoured by researchers who have study that site is correct, their results substantiate the conclusions presented here that the early to middle Miocene was a time of warm-humid climates in the Mount Isa Block.

2.7.3 Weathering and Landscape Evolution

A remarkable feature of this study is the concordance in the ages obtained for samples derived from similar geomorphic provinces/regimes, even if these samples were derived from chemically distinct and spatially distant profiles. The ages obtained from the Mount Isa Mines gossans (14.5-21 Ma range, with 20.9 Ma most intense age peak) and the gossans exposed at the Lake Moondarra locality (17-24 Ma range (this study), 14-24 (subsequent studies), with 19.5 or 20.7 Ma most intense age peaks) indicate that the Mn-oxide minerals exposed at the dissected part of the landscape were precipitated during the early to middle Miocene. The results obtained for the Kennedy Gap area are also very consistent. Mn-oxides from the Mesa 1 and the Gunpowder Creek Road site yield ages ranging from 30-40 Ma. The samples derived from the Cowie, Pegmont, and Tringadee prospects display an absolute concordance of results for the weathering ages (12-13 Ma) for the Cannington Region. Finally, samples from plateau and ridge summits in the Overhang and Selwyn deposits also yield consistent ages (age clusters at ca. 65 Ma, 40 Ma, and 20Ma).

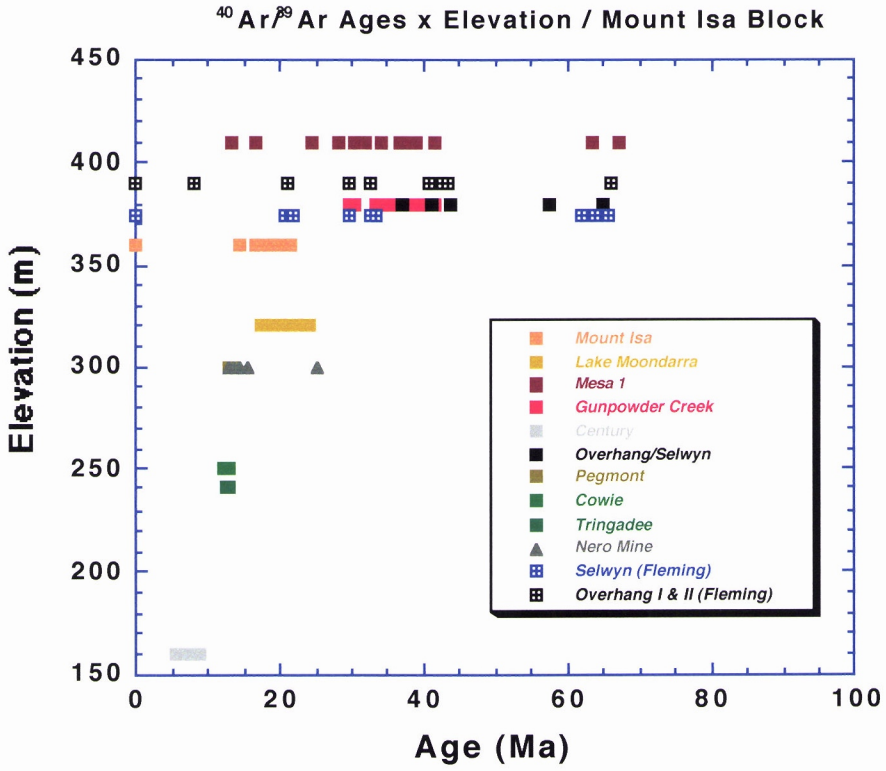

Figure 89. Diagram illustrating the distribution of weathering ages with the elevation of the weathering profiles from which the samples were collected. The diagram illustrates clearly that the high elevation profiles located on hill tops and mesas host evidence of a protracted weathering history which spans most of the Cenozoic. Samples collected at lower elevation weathering profiles suggest that the supergene minerals preserved in these truncated weathering profiles were precipitated during Miocene weathering processes.

Figure 89 illustrates the distribution of ages with elevations for samples analysed in this study and samples analysed subsequently (Fleming, 1997). The plot clearly illustrates the correlation between age and elevation. The high elevation sites, hosting the most complete and complex weathering profiles present (Overhang, Selwyn, and Kennedy Gap), also host the most comprehensive distribution of ages. The high elevation sites yield clusters of ages which extend from the Late Cretaceous to the Miocene, with some "zero ages" also present. The lower elevation sites, located on the more dissected parts of the landscape and hosting less complex weathering profiles (Mt Isa, Lake Moondarra, Cannington area), show ages clustering in the Miocene. The site located in the most dissected, lowest elevation location (Century) yielded the youngest Mn-oxide ages in this study. Even younger ages (e.g., jarosite Pliocene and Quaternary ages) are detected at the bottom of weathering profiles, at elevations below the current surface level.

Three hypothetical models for the weathering and landscape evolution of the Mount Isa Block are illustrated in Fig. 90. These models are not exhaustive and do not reflect all landscape evolution possibilities. The three models assume no differential tectonic movement within the area illustrated, which is an oversimplification.

Model 1 - Constant Weathering-Constant Erosion

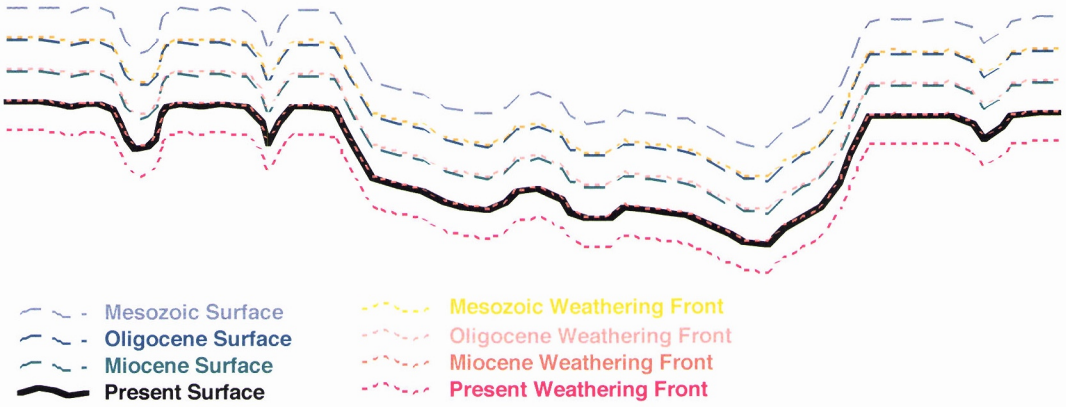

Model 2 - Differential Weathering and Erosion - Davisian Model

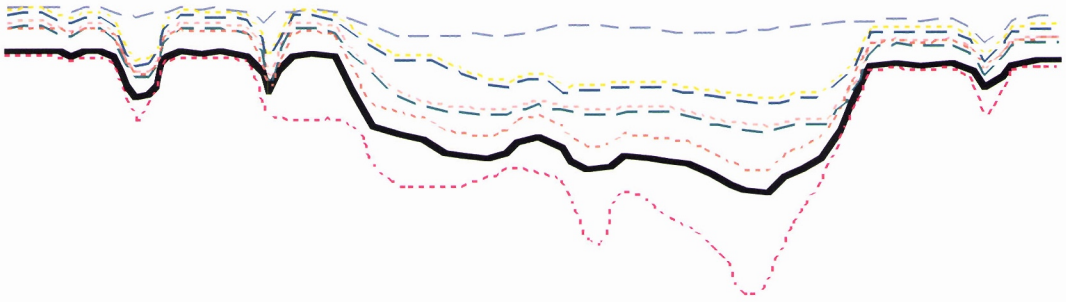

Model 3- Differential Weathering and Erosion - Scarp Retreat Model

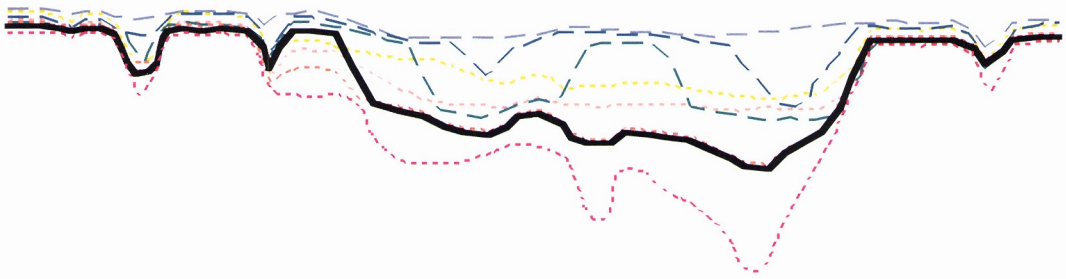

Figure 90. Diagrammatic illustration of three possible landscape evolution models proposed for the Mount Isa region. See text for discussion regarding these models.

The first model (Fig. 90a) is the "constant relief-constant weathering model". It assumes that the relief present in the landscape today is similar to the relief present in the landscape at the end of the Mesozoic. It also assumes that the weathering front follows a pattern similar to the evolution of surface relief. In this model, a surface is exposed, weathered and eroded through

time without much change in local relief. Since the minimum rate of erosion ever measured for stable cratons ranges from 1-3 $m.Ma^{-1}$, the geochronological studies presented here would suggest that between 70-210 m of denudation would have occurred since the Cretaceous. The key factor in this model is the absence of differential weathering or erosion. All rocks, independent of composition or landscape position, weather and erode equally fast.

The second (Fig. 90b) and third (Fig. 90c) models assume that a more subdued landscape existed in the Mesozoic. Evidence for this subdued Mesozoic landscape is the presence, today, of Mesozoic sediments capping mesas and plateaus. Since these Mesozoic sediments are marine and fluviatile sediments, they must have been deposited in the low lying areas of the landscape. Their present topographic positions imply differential erosion, possibly with relief inversion. Since these sediments often cap resistant lithologies, now topographic highs, it is likely that these sediments may have had a much larger aerial distribution on a more subdued paleosurface. These sediments were preferentially removed from areas where they capped more erodable and weathereable lithologies.

In the second hypothetical model (Fig. 90b), the subdued Mesozoic landscape was subject to differential weathering and erosion through time. Surface evolution followed a Davisian cycle (Fig. 118), and landscaped evolved by surface ablation. All lithologies were eroded, and no ancient weathering profiles are preserved, although some more erodable lithologies were ablated faster than more resistant units. In this model, relief changed through time and the relief today is more accentuated than that in the Mesozoic.

In the third hypothetical model (Fig. 90c), a subdued Mesozoic landscape was subject to weathering and erosion following essentially a scarp retreat process (Fig. 118). In this model, the differential weathering and erosion of lithologies of distinct compositions has led to the relief identified in the region today.

The only model capable of accounting for the geological features present in the Mount Isa region and the geochronological results obtained in this study is the third model. The presence of Mesozoic sediments capping some mesas and plateaus suggests that denudation was not homogeneous and did not follow a Davisian denudation model, invalidating models 1 and 2. The presence of ancient weathering ages in current outcrops in the Mount Isa region invalidates models 1 and 2, since the landscape evolution processes implicit in these models would prevent the preservation of old weathering profiles.

Given the considerations above, it is possible to conclude that model 3 is the most realistic given the results of this investigation. However, the distribution of ages obtained in this study do not resolve one specific question related to landscape evolution in the region: "Are the

Miocene ages obtained from the more subdued parts of the landscape the preserved roots of ancient and more complete weathering profiles which have been partially dissected since the Miocene? Or are these ages the result of denudation of all regolith cover in these parts of the landscape before the Miocene, with renewed Miocene and post-Miocene weathering accounting for the regolith cover present in these areas today?" This question, which may have important implications to geochemical exploration in the region, can only be answered by weathering geochronology if closed space sampling and dating is applied to determine rates and mechanisms of scarp retreat. Until such study is carried out, this question will remain unanswered.

2.7.4 Weathering and Exploration Geochemistry

The geochronology results imply that the Mount Isa region has seen some periods of wet conditions, when dissolution, redistribution, and reprecipitation of elements within weathering profiles was facilitated by the abundance of meteoric water. From the results in this study, it appears that the late Cretaceous-early Palaeocene, the early to middle Oligocene, and the early to middle Miocene were the periods most conducive to the dissolution and reprecipitation of elements in the weathering profiles.

From a geochemical exploration viewpoint, the significance of the geochronology results rests on the possibility of combining mineral chemistry with geochronology to predict mechanisms, pathways, and rates of element migration in the past. This, in turn, may aid in explaining patters of geochemical anomalies encountered at the surface today. Some important features are presented below:

2.7.4.1 Mount Isa City and Vicinity

- The Mn-oxides overlying the Mount Isa deposit are rich in Pb, Zn, and Ba. In addition to cryptomelane (KMn_8O_{16}), the minerals coronadite ($PbMn_8O_{16}$), chalcophanite ($ZnMn_3O_7.3H_2O$), hollandite ($BaMn_8O_{16}$) and barite are present, suggesting large-scale migration of Pb, Zn, and Ba in solution between 14-21 Ma.

- Similarly to the Century orebody, the presence of coronadite and chalcophanite in the weathering profiles overlying the Mount Isa orebody indicate that these minerals are generally located close to the source of Pb and Zn and may be useful indicators of mineralisation if properly identified in the field.

- The presence of supergene enrichment blanket overlying the Mount Isa Pb-Zn and Cu deposits may suggest that the weathering profile preserved in the area today is associated with the roots of a much deeper and complex weathering system, now partially eroded.

2.7.4.2 Western Succession

• The Mn-oxides studied in the Buckley River area are not directly related to any known mineralisation. However, the composition of these oxides indicates an affinity toward Cu mineralisation given the high Co, Ba, and K, and low Pb and Zn contents of these oxides.

• The relatively old weathering ages obtained for this area would promote efficient leaching, transport, and redeposition of metals in the supergene environment, creating supergene orebodies and depleting surficial deposits of tracer elements.

2.7.4.3 Century Deposit

• The Mn-oxides derived from the Century profiles host coronadite, chalcophanite and barite. In addition, plumbogummite ($PbAl_3(PO_4)_2OH_5.H_2O$) is present. The large concentrations of Pb and Zn in these occurrences suggest that these elements were derived from a nearby source, and did not precipitate at the Cambrian-Proterozoic unconformity by long-range transport in the groundwater system. The most likely source for the elements present in the Mn-oxide outcrops (Mn, Zn, Pb, Ba and K) is the weathering Century orebody.

• Since solubility and oxidation-reduction constraints would prevent large-scale migration of Pb, Zn, and Mn in solution by oxidising surface waters, the precipitation of the Mn-rich "false gossans" at Century most likely occurred in a shallow subsurface environment. Lead, Zn, and Mn derived from a weathering Century orebody migrated in solution and were immobilised at the chemical barrier imposed by the basal Cambrian limestone, as illustrated in the Century section. Erosion of 5-50 m of overburden in the past 5 Ma is implied by this model.

2.7.4.4 Eastern Succession

2.7.4.4.1 Overhang Deposit

• The Overhang deposit is the direct effect of the weathering (and the preservation of the weathering assemblages) of Precambrian banded manganese-formations, consisting a classic example of a deposit generated primarily by supergene enrichment processes. Its location implies that the higher elevations plateaus and hill tops, which host the deepest and most complex weathered assemblages, are the most likely localities to host supergene ore systems.

• The preservation of manganese oxides dating as far back as the Late Cretaceous in the Overhang weathering profiles indicate that these minerals, once precipitated in the oxidising environment, are relatively resistant to further dissolution and leaching. This characteristic of manganese oxides makes them useful indicators of nearby mineralisation in areas such as Mount Isa. In areas where the climate has been much more humid for a much longer time (e.g., Amazon), these minerals are often partially or totally leached from surface outcrops.

2.7.4.4.2 Selwyn Deposit

• The preservation of ancient weathering ages in the ridges and hilltops associated with the Selwyn deposit clearly indicate the presence of a long lived supergene system in the area. This long lived system would account for the effective leaching of Cu, Au and Ag from surficial environments, creating difficulties in mineral exploration.

• The ancient weathering ages obtained for this deposit also account for the efficient leaching, transport, and redeposition of Cu in the supergene environment, creating supergene Cu orebodies such as those present in the Selwyn Ranges.

• The Mn-oxides at Selwyn are enriched in Cu (EDS analyses only), Co, K and Ba and display moderate Zn (~0.5 wt%) and negligible Pb contents; these features are indicative of Mn-oxides associated with Cu and Cu-Au deposits (Vasconcelos, 1992).

2.7.4.5 Tick Hill Area

• Mn-oxides found along the Pilgrim Fault in the Tick Hill area replace silcretes. Given the extreme cation-depleted nature of the silcretes (devoid of most cations except for Si and Ti), it is unlikely that the cation-rich Mn-oxides (rich in Mn, K, Ca, Ba, Na, Co, etc.) were precipitated from descending groundwaters. The most likely mechanism for the precipitation of these oxides is the ascension of mineralised groundwaters along the Pilgrim Fault.

• The Mn-oxides at Tick Hill are enriched in Co, Ba, and K and display moderate Zn (~0.5 wt%) and negligible Pb contents; these features differentiate these oxides from those associated with Pb-Zn deposits.

• The geochemical anomalies associated with these manganese "breccias" may reflect leaching of elements from distal sources (100's to 1000's of meters) and may not necessarily be associated with immediately underlying mineralisation.

• The ages of Mn-oxides replacing silcretes poses numerical constraints on the minimum age of silcrete formation in the area. The silcretes in Tick Hill are at least 38 Ma old, indicating that these silcretes are not associated with postulated transition toward arid conditions in the Neogene. If these silcretes indicate arid conditions, these conditions occurred in the Paleocene or Mesozoic.

• Brecciation of silcretes along fault zones and the ascension of groundwaters along these faults are possibly driven by differential uplift of faulted blocks in the area.

2.7.4.6 Cannington Area

• The Mn-oxides from Pegmont and Cowie are, similarly to Mn-oxides in the Century and Mount Isa deposits, significantly enriched in Pb and Zn, respectively (coronadite and chalcophanite are present), indicating association with nearby Pb and Zn occurrences.

• Mn-oxides from the Tringadee prospect are devoid of Pb, show only moderate Zn contents (~0.5 wt%), and are enriched in Co, Ba, and K, consistent with an association with Cu-Au or Au mineralisation.

3 Charters Towers Region

Weathering profiles in the Charters Towers region indicate an extremely complex evolution, with several alternating periods of weathering- and erosion-prone conditions. The weathering profiles are deep (Fig. 91b-d) (exceeding 100-150 in places) and ferruginous duricrusts, when present, are often composed of transported lateritic crusts and previously weathered, kaolinite-rich, sediments. Despite the complexity of the weathering profiles, previous dating of supergene minerals associated with some of these weathering profiles identified only Pliocene ages (Bird *et al.*, 1990). In this study, one well developed weathering profile overlying the Scott Lode deposit was sampled in detail.

3.1 Pajingo Area

The gold deposits in the Pajingo area are associated with deeply weathered volcanic rocks partially overlain by Tertiary sediments. These sediments consist of clay minerals and fragments of ferruginous duricrusts which have been truncated, transport, and redeposited. These Tertiary sediments have been reweathered after deposition.

3.1.1 Scott Lode Pit

3.1.1.1 Site Selection Criteria: deep weathering profile overlying significant gold deposit in the region.

3.1.1.2 Location: 20°32'S Latitude and 147°27' Longitude

3.1.1.3 Elevation (sampled outcrops): ~ 400-450 m

3.1.1.4 Geomorphologic Setting: deeply weathered Devonian volcanic rocks overlain by lateritic sediments.

3.1.1.5 Geomorphologic Regime: erosional.

3.1.1.6 Sample in Relation to Landscape Position: Mn-oxide veins and replacement zones in weathered volcanic rocks. No outcropping Mn-oxide occurrences were identified in the region, but the deep mining pit permitted access to samples at several levels within the weathering profile.

3.1.1.7 Sample in Relation to Regolith: samples were obtained from the upper saprolite, middle saprolite, and lower saprolite horizons.

3.1.1.8 Datable Minerals/Host Rock Relationship: influx of elements, in solution, from outside sources located at stratigraphically positions equivalent to or higher than the deposition site.

3.1.1.9 Sources of Elements: Mn is probably derived from weathering carbonates, Zn is derived from weathering sulphides, K is derived from feldspars and micas, while Ba maybe derived from feldspars, micas, of sulphates in the system.

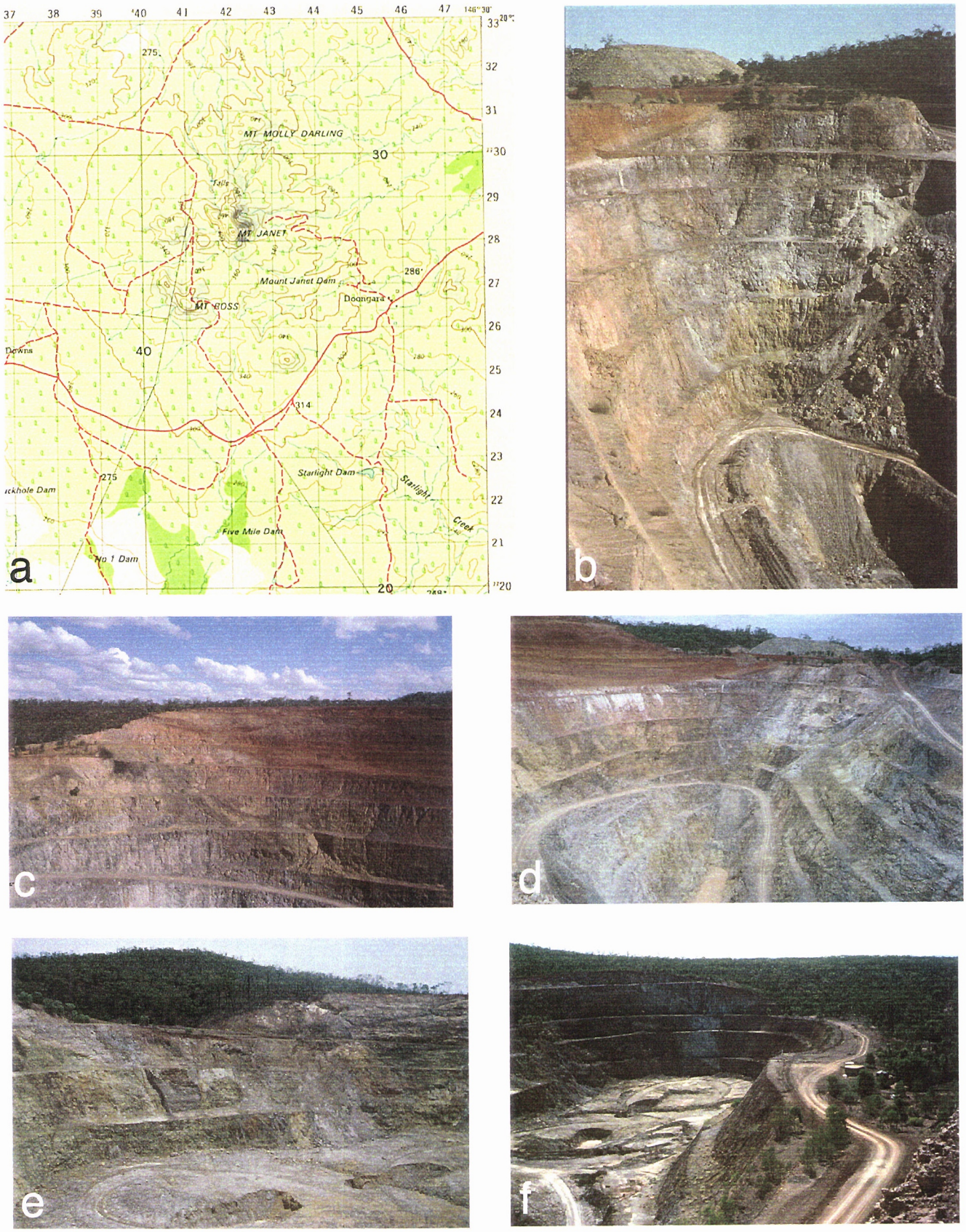

Figure 91. (a) The topographic map illustrates the relief in the area proximal to the Scott Lode pit. (b) West facing view of the Scott Lode pit shows the depth and complexity of the weathering profile in the area. (c) This panoramic view of the southern pit wall illustrates the unconformity between Cenozoic sediments and the underlying weathered volcanic units host to mineralisation. (d) A panoramic view of the western pit wall also shows the unconformity between Cenozoic sediments and the underlying weathered volcanic rocks. (e) View of the northeastern pit wall shows that altered volcanic rocks outcrop in this area and no sedimentary cover is present on this side of the pit. (f) This ENE pit wall view illustrates the location of the mine access road on the right.

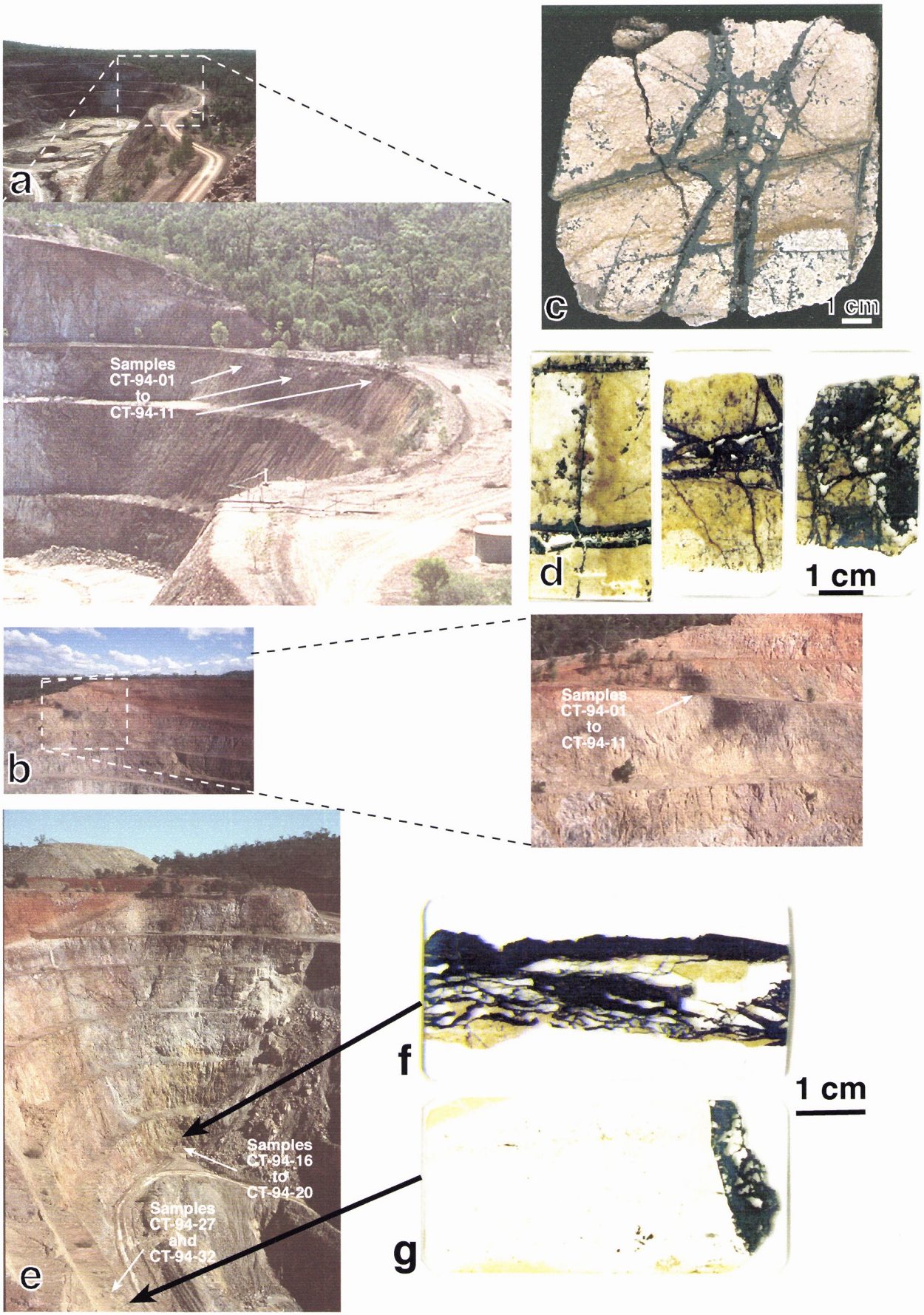

Figure 92. (a) Panoramic and close-up view of the eastern pit wall illustrating the occurrence of abundant manganese oxides at the mine access road level. The location of samples analysed in this study are shown by the arrows. Mn-oxides occur as veins and cavity fills in the saprolitised volcanic rocks (c-d). The Mn-oxides appear to fill desiccation cracks in the strongly weathered volcanic rocks. This mode of occurrence suggests that the volcanic rocks were deeply weathered to mostly smectite clays. Transition toward more arid conditions promoted the dehydration and shrinking of the smectite clays, forming desiccation cracks which were posteriorly filled by the influx of Mn-rich solutions during renewed humid conditions. These manganese oxides can be physically extracted and dated by the Ar/Ar method. In (b), the same Mn-oxide outcrops as shown in (a) are illustrated from another angle. The western wall of the pit (e) host Mn-oxides at intermediate and lower levels of the weathering profile. Access to these occurrences permitted dating of the propagation of the weathering front in the pit.

3.1.1.10 Overview

The deep weathering profiles exposed at the Scott Lode gold deposit were sampled in detail at the start of this project (Figs. 91 and 92). Despite the occurrence of Mn-oxides and K-bearing sulphates (alunite and jarosite) throughout the extent of the profile, only selected benches were accessible for sampling due to safety reasons. In addition, no mineral suitable to $^{40}Ar/^{39}Ar$ geochronology was present in the ferruginous channel deposits overlying the mineralised volcanic rocks. Therefore, only weathering of the underlying volcanic bedrock was investigated in this study. Mn-oxide samples were collected at the bench along the mine access road (Figs. 92a-d). Mn-oxide samples were also collected at approximately 20 m and 60 m below the mine access road level (Figs. 92e-g). Thirty-eight grains from 13 distinct Mn-oxide samples were analysed by the $^{40}Ar/^{39}Ar$ laser-heating method at the UQ-Ar Lab. Four grains from 2 distinct jarosite hand specimens collected at ~ 20 m below the mine access road level were also analysed.

Field and hand-specimen investigation of samples from the Scott Lode pit shows two distinct types of Mn-oxide occurrences: deep in the profile, Mn-oxides occur as massive to botryoidal coatings and fracture filling material deposited on quartz veins and on ferruginous zones (Figs. 92e-g); at shallower depths, Mn-oxides occur as botryoidal growths on the walls of desiccation cracks or as dendritic masses penetrating through pore spaces in smectite and/or kaolinite-rich weathered andesites (Figs. 92a-d). The presence of Mn-oxides in these desiccation cracks suggests that the andesites had been previously weathered to a clay-rich saprolite under relatively humid conditions. Transition toward arid conditions promoted the dehydration of the saprolite zones and the development of desiccation cracks. Return of humid conditions promoted the penetration of solutions rich in dissolved manganese along these cracks leading to the precipitating Mn-oxides on the fracture walls. Mn-oxide ages in these samples provide only a minimum age of weathering for the system.

3.1.1.11 Results

3.1.1.11.1 Electron Microprobe and SEM Analysis

Electron microprobe traverses perpendicular to Mn-oxide growth bands (Figs. 93-99) clearly show the variable composition of the botryoidal Mn-oxides. This variation in composition is symmetrical across the fracture filling Mn-oxides (Figs. 93 and 94), suggesting open space growth and consistent with the precipitation mechanisms suggested above.

Petrographic and electron microprobe investigation of the manganese oxide samples associated with the Scott Lode deposit reveals a consistent pattern, where early precipitated Mn-oxides are Ba-K hollandite-group solid-solutions, while late stage Mn-oxides consist of Co-rich lithiophorite (Figs. 94, 95). In some cases, lithiophorite also occurs preferentially filling dehydration cracks in previously precipitated Mn-oxides (Fig. 98).

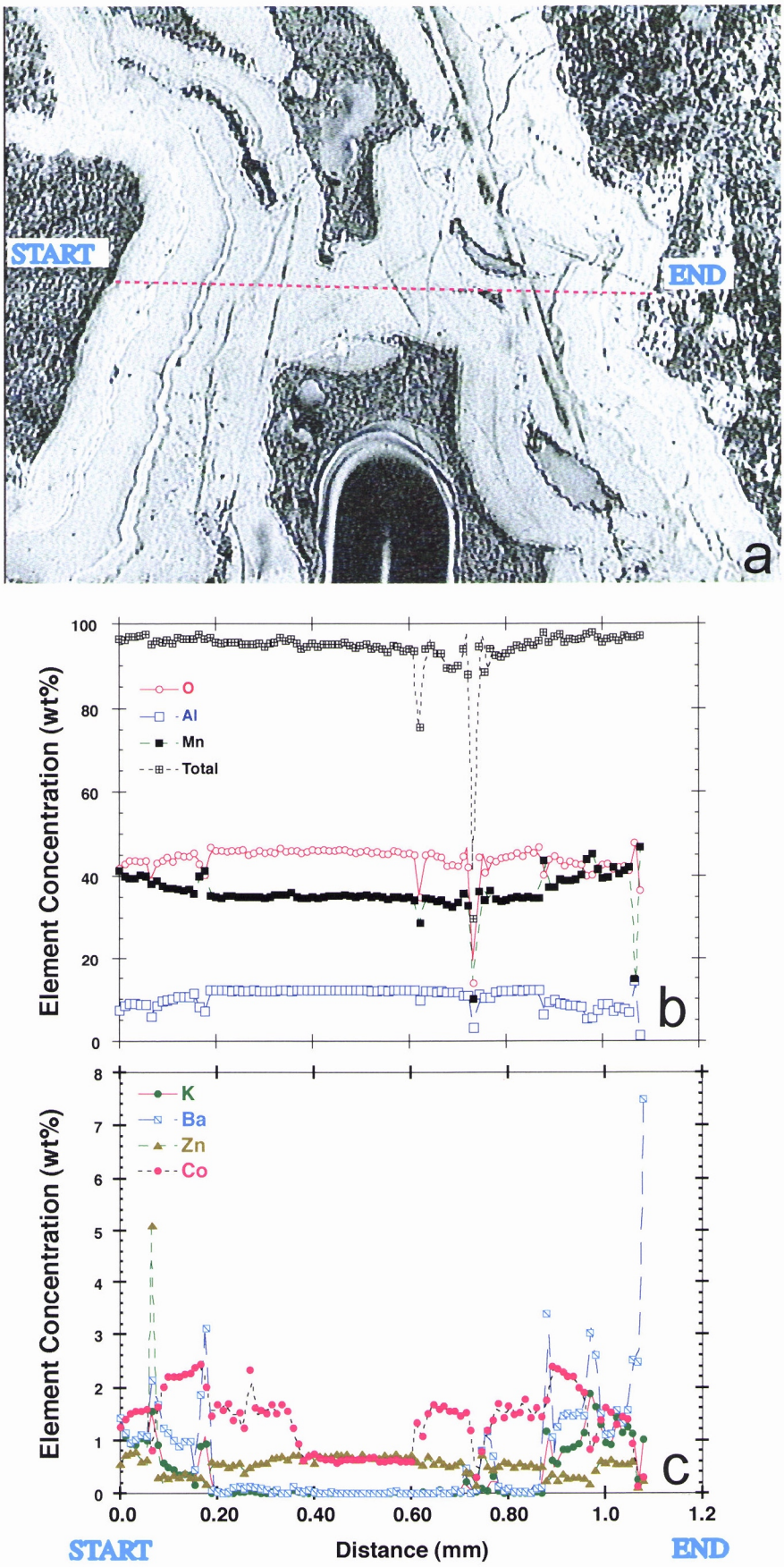

Figure 93. (a) This backscattered SEM photomicrograph illustrates a Mn-oxide vein precipitated in a desiccation crack in the weathered volcanic host rock. An EMP traverse was analysed across this vein. Major (b) and minor (c) element distribution along the traverse shown in (a) indicate that the vein is symmetric about the wall, confirming the precipitation of Mn-oxides by open cavity precipitation. Notice the high Co contents of this Mn-oxide occurrence and the symmetric distribution of Co in relation to the vein walls.

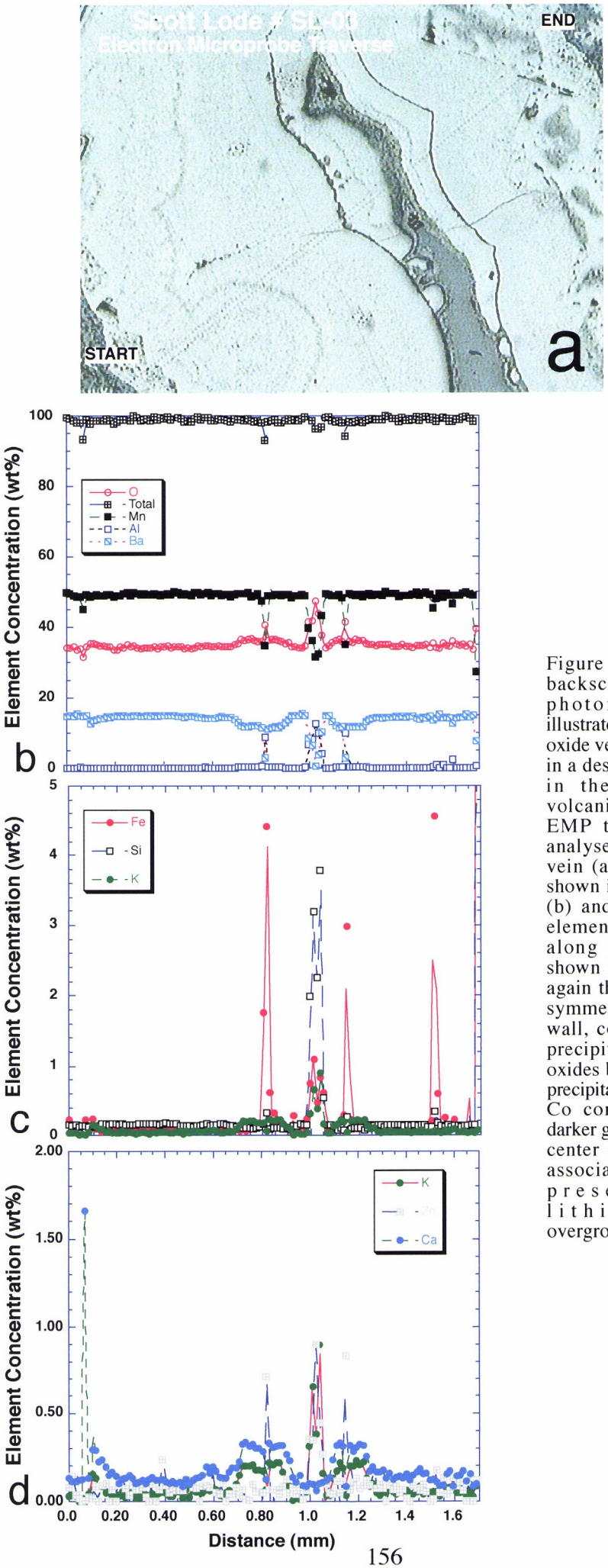

Figure 94. (a) This backscattered SEM photomicrograph illustrates another Mn-oxide vein precipitated in a desiccation crack in the weathered volcanic hosts. An EMP traverse was analysed across this vein (analyses spots shown in (a)). Major (b) and minor (c-d) element distribution along the traverse shown in (a) indicate again that the vein is symmetric about the wall, confirming the precipitation of Mn-oxides by open cavity precipitation. The high Co contents in the darker grey band in the center of the vein is associated with the presence of lithiophorite overgrowths.

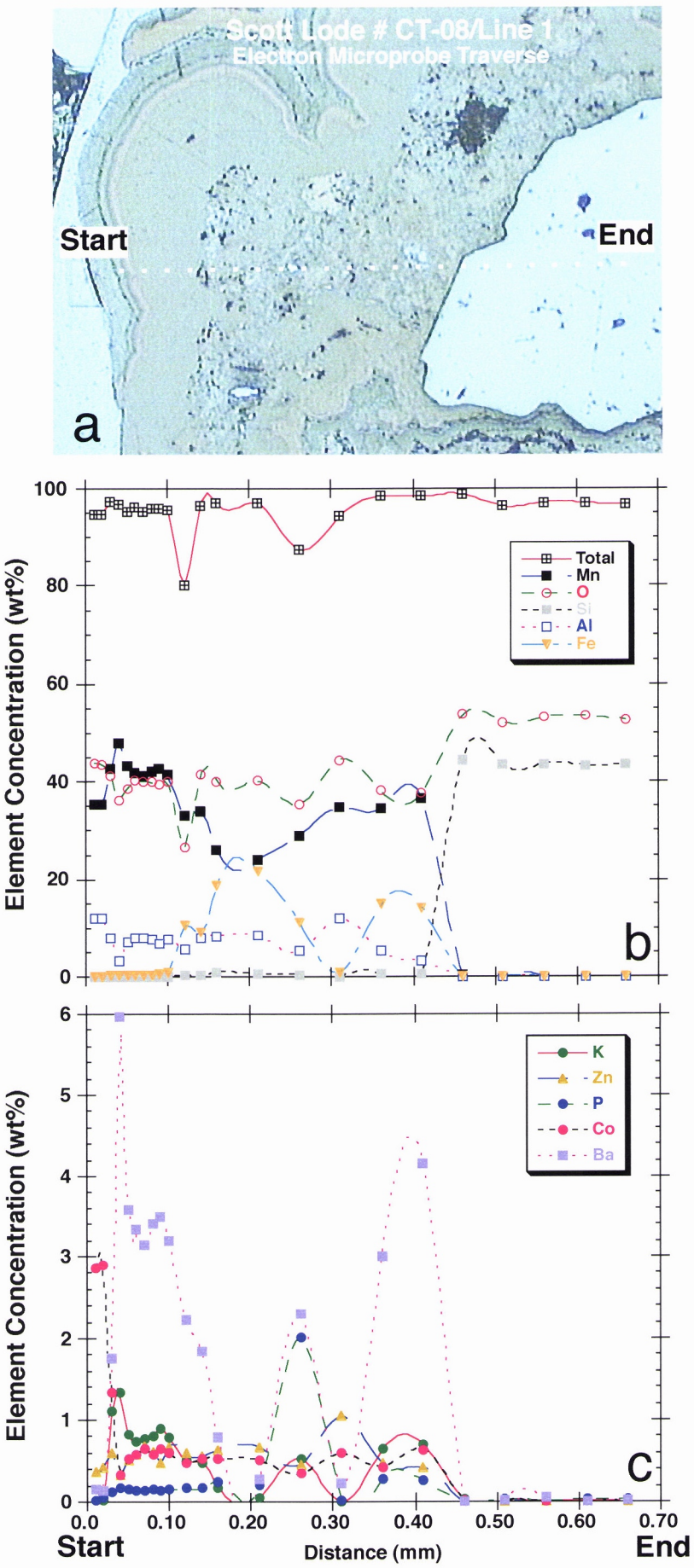

Figure 95. (a) A reflected-light photomicrograph illustrates a detailed EMP traverse through the Mn-oxide growth bands. The light colour grain to the right is quartz. The Co- and Al-rich (see analyses in (c)) darker band at the start of the traverse is composed of lithiophorite. The light brown (colour due to carbon coating of the sample) relative K-rich band adjacent to lithiophorite is suitable to Ar/Ar geochronology. Only the high spatial resolution possible with the laser method allows such fine bands to be dated successfully.

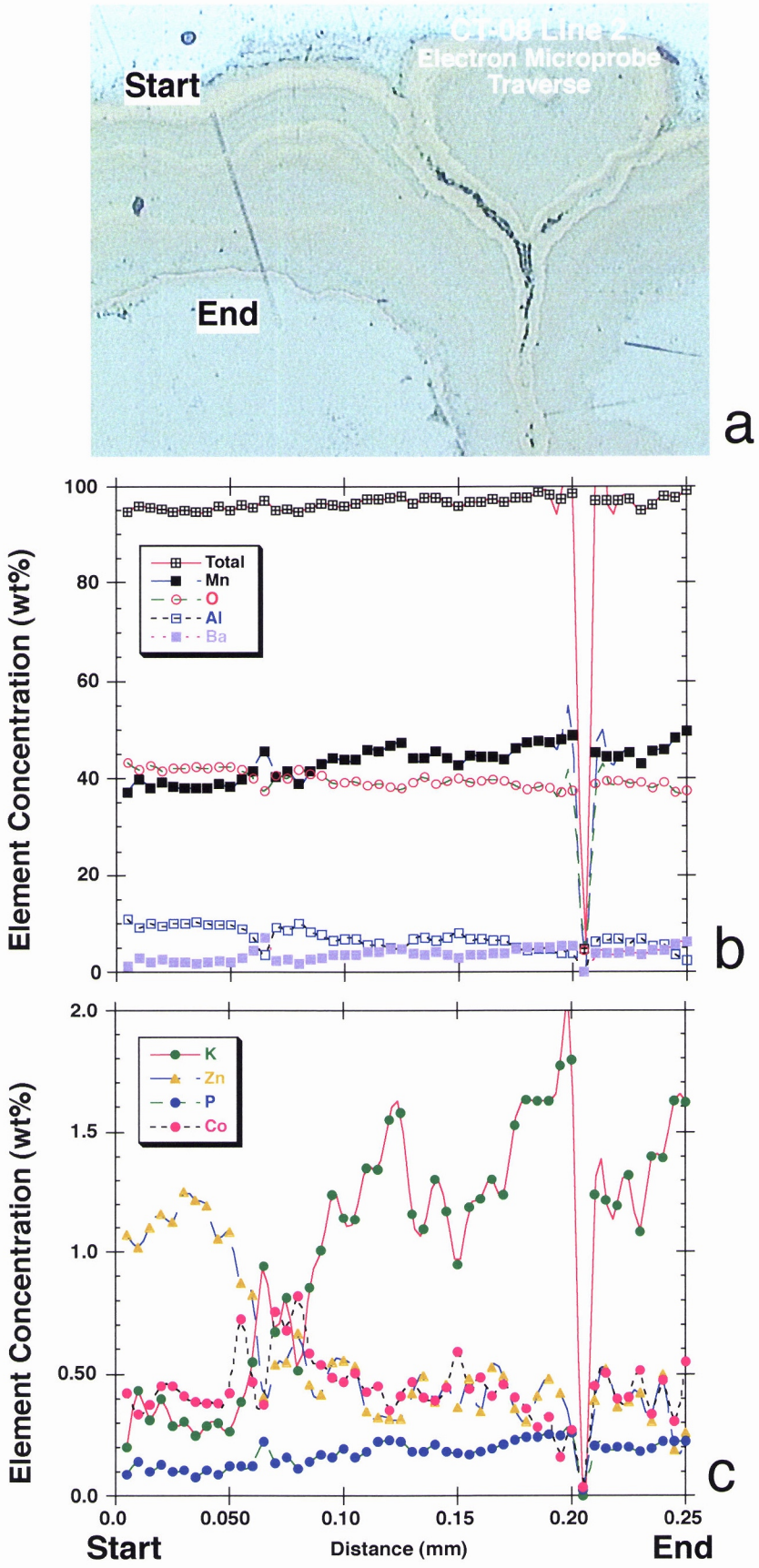

Figure 96. (a) This reflected-light photomicrograph illustrates a detailed EMP traverse through the Mn-oxide growth bands. Notice the variation in colour of the Mn-oxide bands as the Ba to K ratios vary across the bands. The drop in totals (b) is due to a cavity in the sample. In addition to relatively high K, some of the Mn-oxide bands in this sample also show relatively high Zn and Co (c).

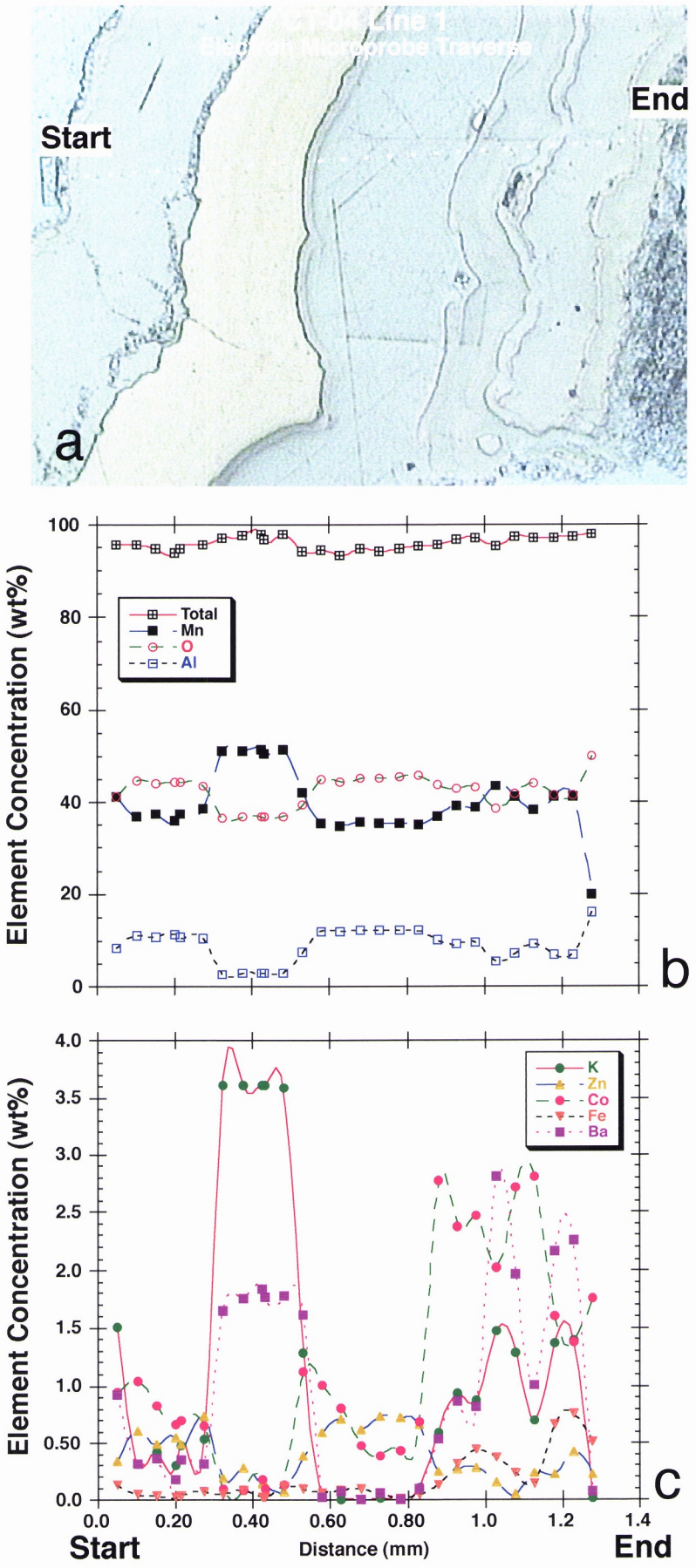

Figure 97. (a) This reflected-light photomicrograph illustrates an EMP traverse through Mn-oxide growth bands. Only the light colour band which shows high K and Ba contents is composed of hollandite. This band is 0.25 mm wide and can only be dated due to the high spatial resolution of the laser-heating method. The darker Mn-oxide bands in this sample are composed of lithiophorite (notice the high Al-contents shown in (b)).

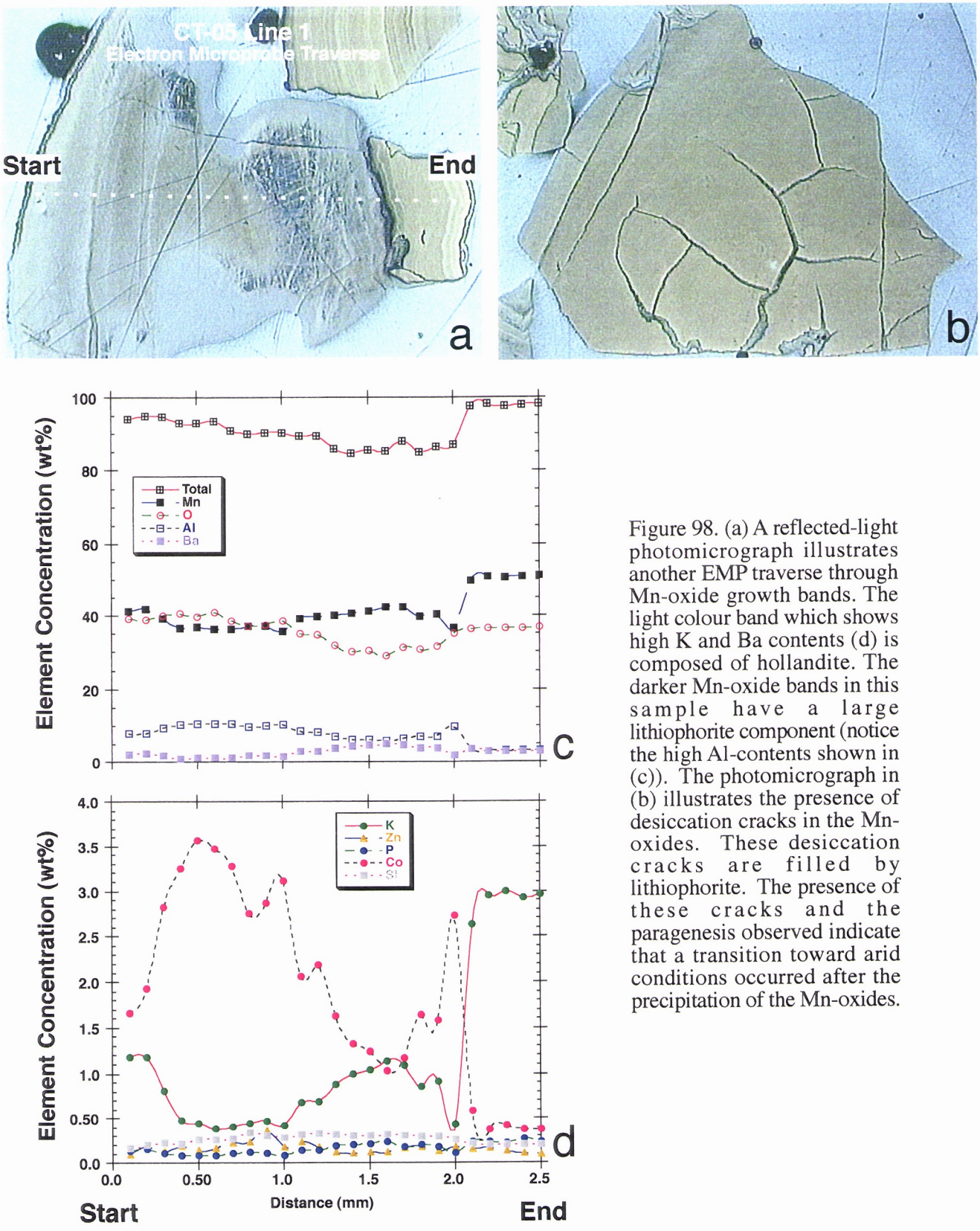

Figure 98. (a) A reflected-light photomicrograph illustrates another EMP traverse through Mn-oxide growth bands. The light colour band which shows high K and Ba contents (d) is composed of hollandite. The darker Mn-oxide bands in this sample have a large lithiophorite component (notice the high Al-contents shown in (c)). The photomicrograph in (b) illustrates the presence of desiccation cracks in the Mn-oxides. These desiccation cracks are filled by lithiophorite. The presence of these cracks and the paragenesis observed indicate that a transition toward arid conditions occurred after the precipitation of the Mn-oxides.

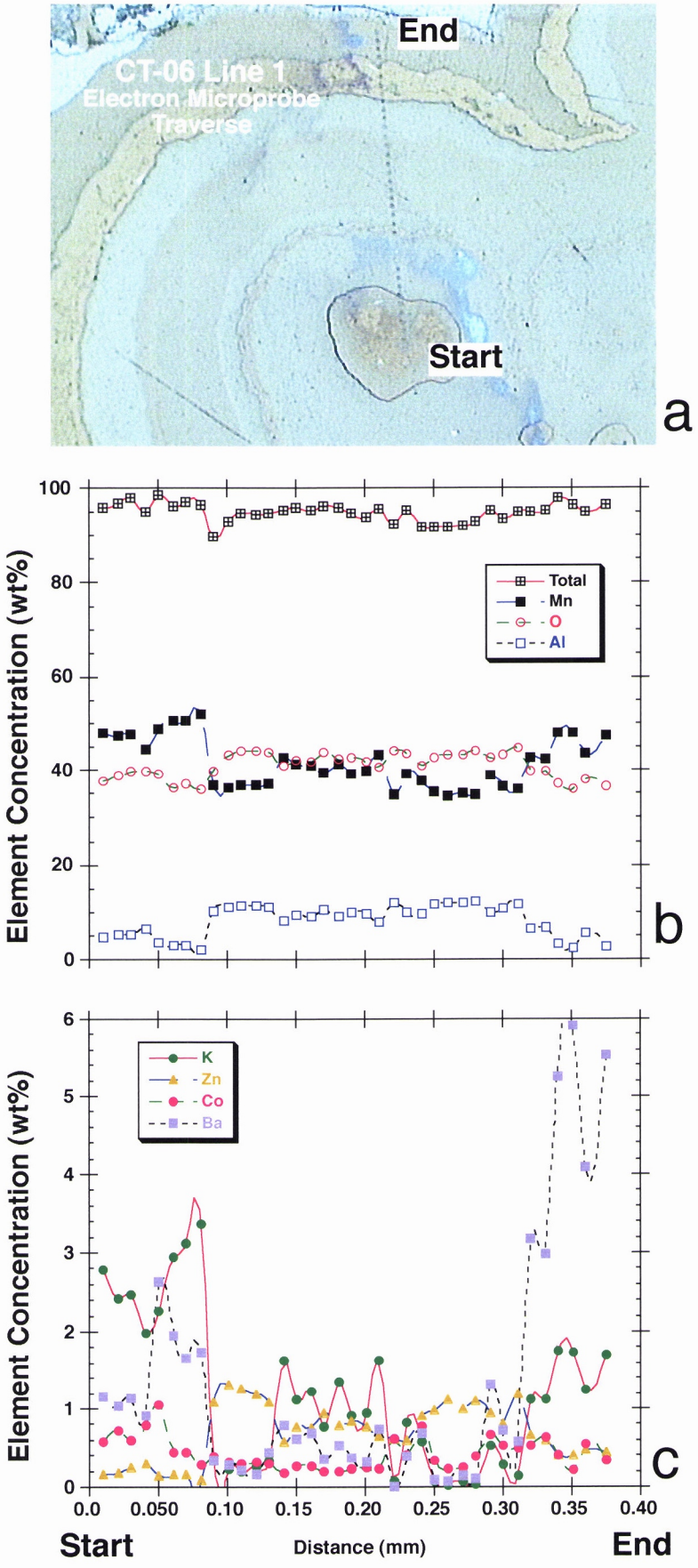

Figure 99. (a) Reflected-light photomicrograph illustrating an EMP traverse through Mn-oxide cement growth bands show the variation in colour of the Mn-oxide bands, varying Al and Mn contents (b), varying Ba and K contents (c), and a high Zn content of the lithiophorite-rich

A remarkable and consistent feature of the Mn-oxide samples from the Scott Lode pit is the relatively high Co-contents of all the samples analysed (Figs. 93-99). High Co may simply reflect the volcanic affinity in the environment or it may be associated with the alteration halo of the epithermal gold system. The electron microprobe results also show a highly variable K content in the Mn-oxide samples, suggesting that some grains may yield more consistent $^{40}Ar/^{39}Ar$ results than other grains from the same hand-specimen.

3.1.1.11.2 Geochronology

The 13 Mn-oxide samples analysed (in excess of 500 individual analyses) yielded remarkably reproducible results (Figs. 100-115). Plateau ages ranged from 3.9 ± 0.1 Ma at the bottom of the pit (Figs. 92e-g) to 16.2 ± 0.2 Ma at the uppermost part of the weathering profile at the western edge of the pit (Figs. 92a-d). The jarosite samples analysed also produced remarkably reproducible results; however, only one jarosite grain yielded a plateau age (4.5 ± 0.1 Ma) (Fig. 112). The other three grains displayed a plateau-like series of steps a low temperatures, but the dates became unreasonably old at the high temperature steps (Fig. 111). The climbing spectra obtained suggests that the jarosite grains are intermixed with unweathered/partially weathered hypogene silicates. SEM investigations confirmed the presence of contaminants.

One Mn-oxide sample from the Scott Lode was also dated by the K-Ar bulk method at UQ. The result obtained by this method (39.5 ± 2 Ma) is drastically different from the ages obtained for the same sample by the $^{40}Ar/^{39}Ar$ method. The only reasonable explanation for the discrepancy is the presence of contaminants in the bulk K-Ar sample, which further justifies using the K-Ar method only as a screening technique in weathering studies.

All the results obtained for the Scott Lode samples are plotted on the ideogram below (Fig. 115). This frequency diagram indicates that the samples collected from the Scott Lode pit indicate a protracted weathering history spanning the middle and late Miocene and the Pliocene. No plateau or pseudo plateau ages younger than 2.7 Ma were dated in this study. However, it is likely that these ages occur in the profile study. Further, more detailed sampling is necessary to address this issue.

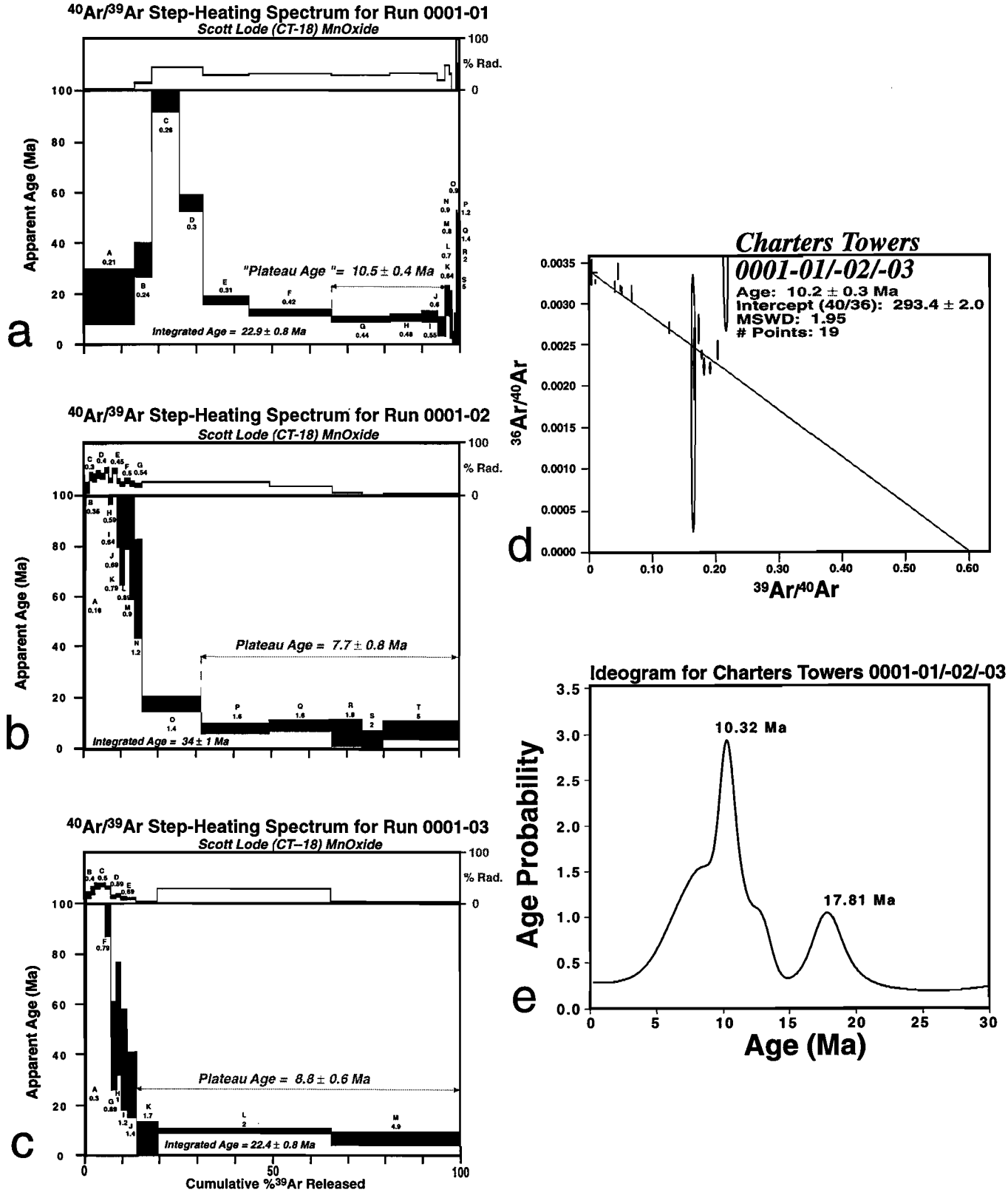

Figure 100. Step-heating spectra for three grains from sample CT-18 yield three plateau-like spectra with ages of 7.7 ± 0.8, 8.8 ± 0.6 and 10.5 ± 0.4 Ma. All three spectra show some Ar recoil at the low temperature steps indicating that the Mn-oxides in these samples is extremely fine grained. The isochron age (d) for this sample (10.2 ± 0.3 Ma) and the ideogram age (10.32 Ma) agree reasonably well with the step-heating ages obtained.

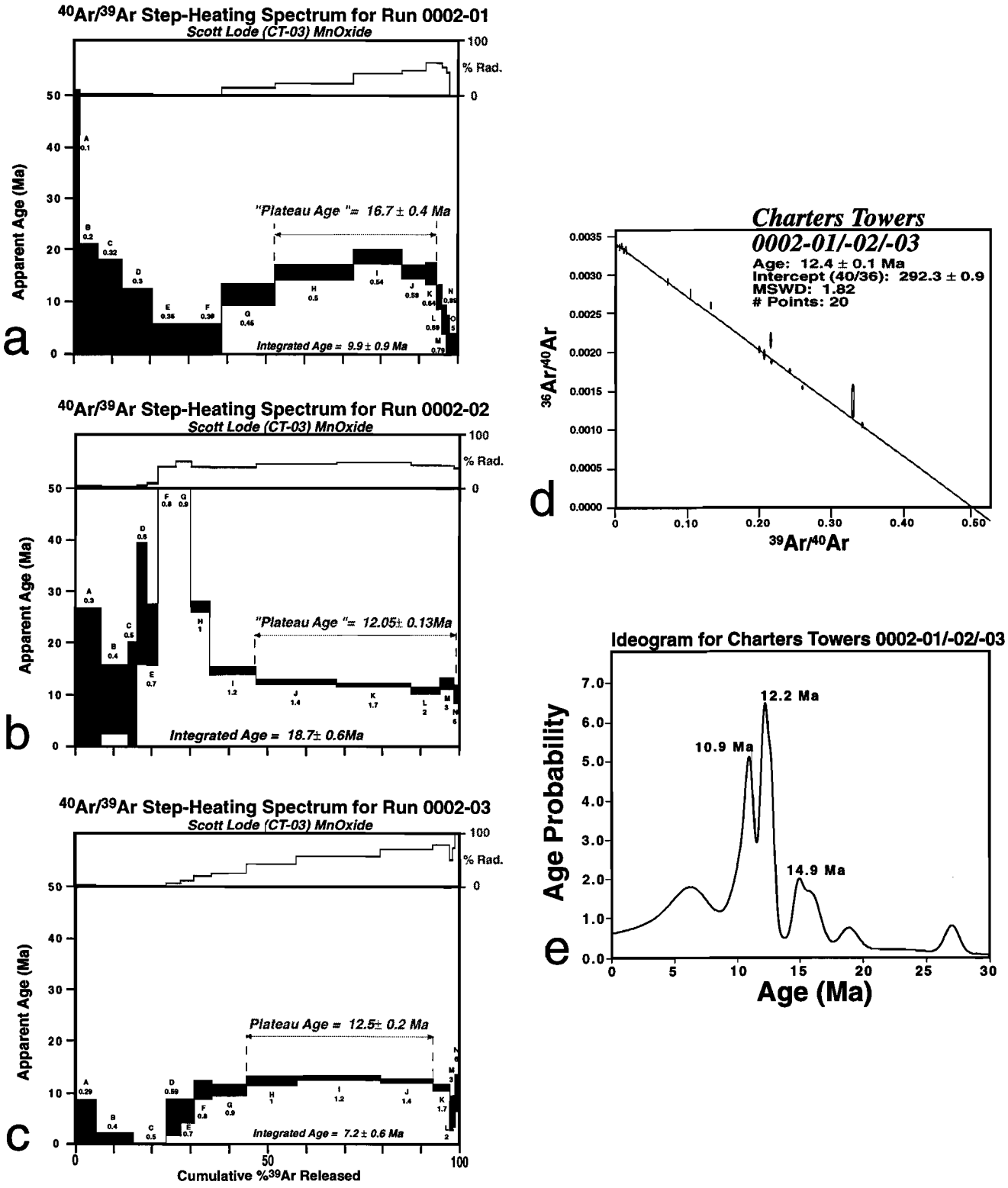

Figure 101. Step-heating spectra for three grains from sample CT-03 (mine access road level) yield one well defined plateau age of 12.5 ± 0.2 Ma and two plateau-like spectra with ages of 16.7 ± 0.4 and 12.05 ± 0.13 Ma. These three spectra also show some ^{39}Ar recoil at the low temperature steps. The isochron age (d) for this sample (12.4 ± 0.1 Ma) and the ideogram age (12.2 Ma) agree reasonably well with the step-heating ages obtained.

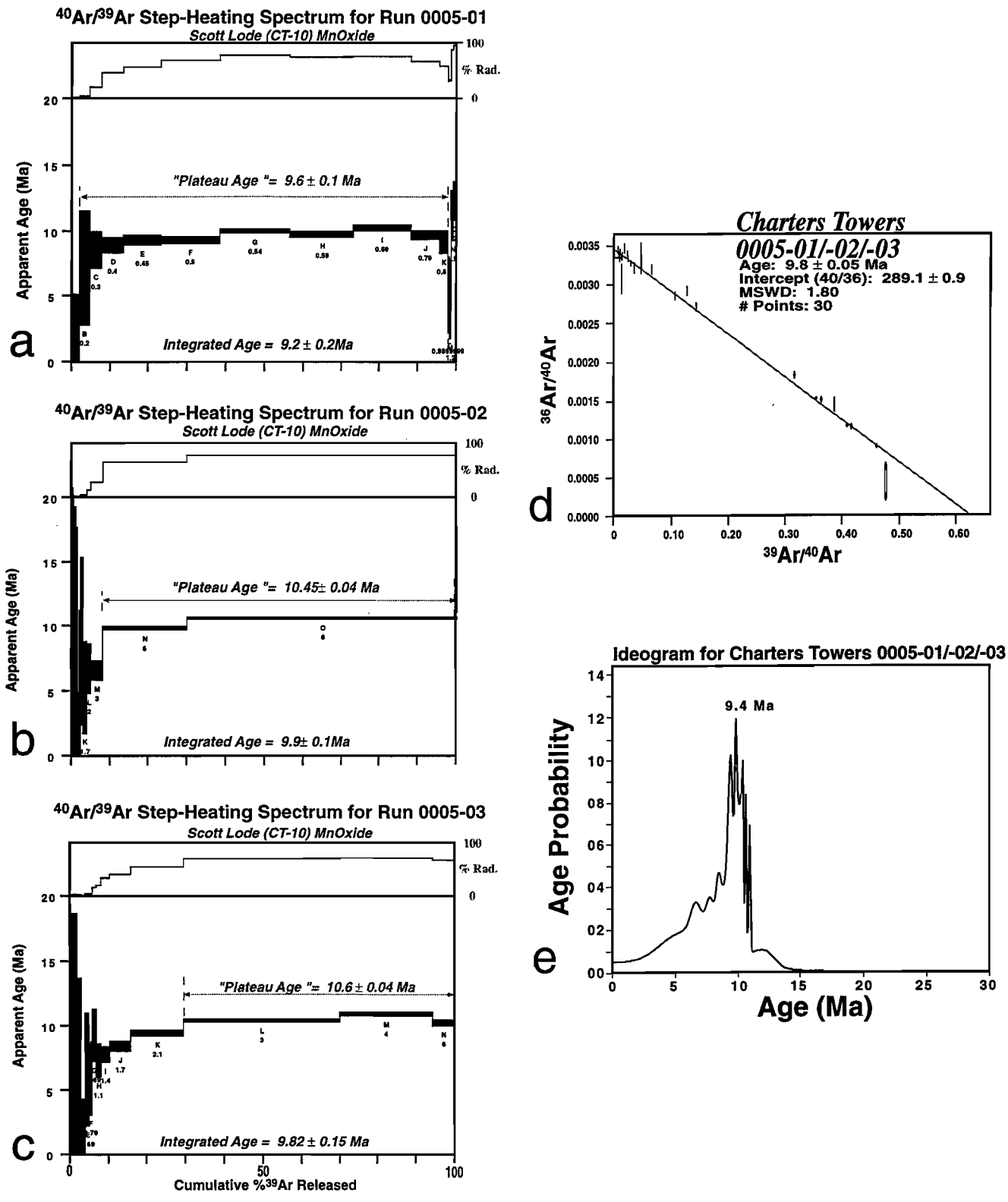

Figure 102. Step-heating spectra for three grains from sample CT-10 (mine access road level) yield three very well defined plateau or plateau-like ages of 9.6 ± 0.1, 10.45 ± 0.04, and 10.6 ± 0.04 Ma, identifying a major pulse of weathering at approximately 10 Ma. Equivalent ages are also identified by the isochron and ideogram methods.

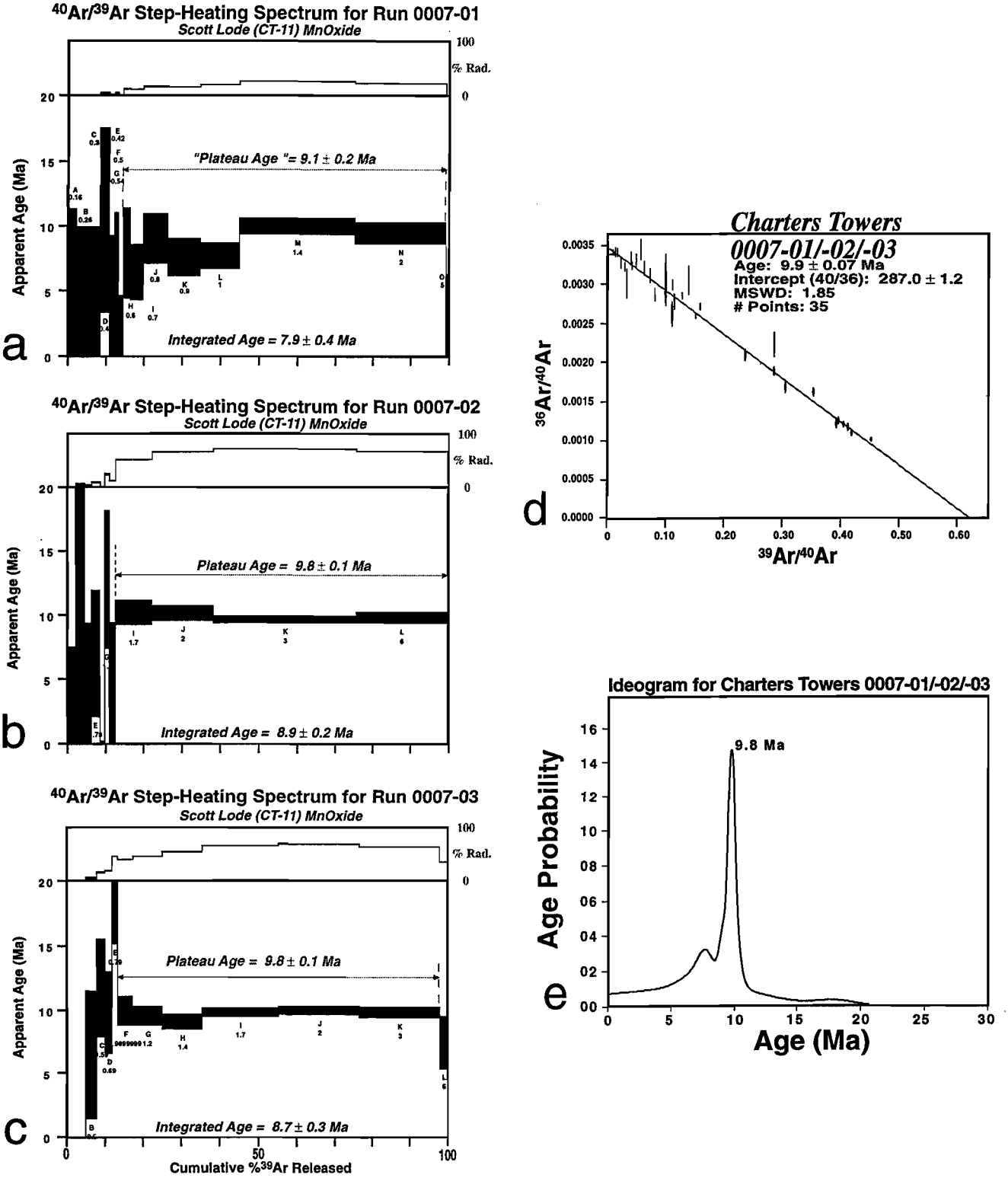

Figure 103. Step-heating spectra for three grains from sample CT-11 (mine access road level) yield three very well defined plateau or plateau-like ages of 9.1 ± 0.2, 9.8 ± 0.1, and 9.8 ± 0.1 Ma, confirming the results obtained for the previous samples. The same ages are also identified by the isochron and ideogram methods.

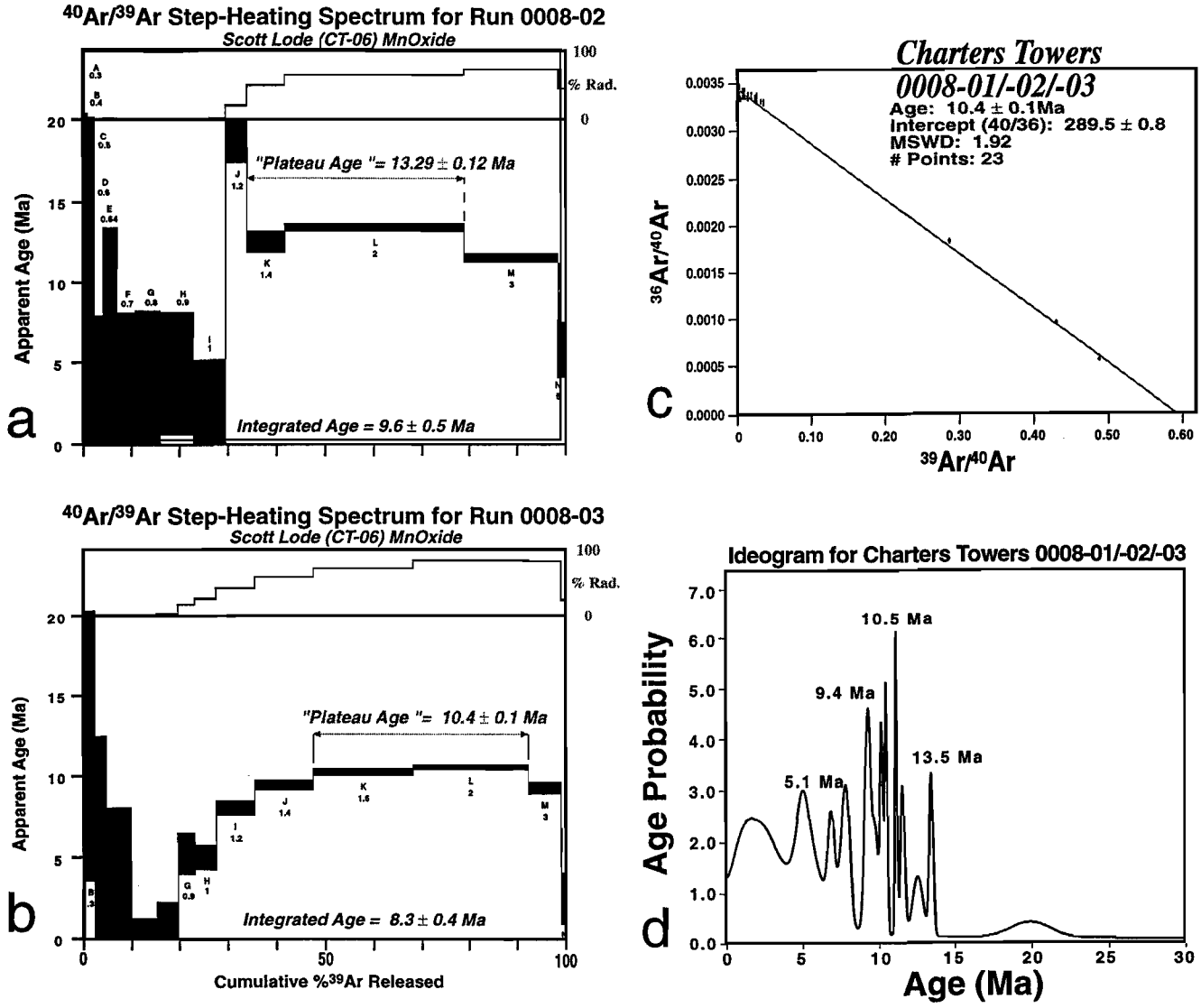

Figure 104. Step-heating spectra for two grains from sample CT-06 (mine access road level) yield two poorly defined plateau-like spectra with ages of 13.29 ± 0.12 and 10.4 ± 0.1 Ma. The isochron age for this sample is well defined at 10.4 ± 0.1 Ma, while the ideogram ages show a large scatter. However, the most probable peak in the ideogram is also 10.5 Ma, suggesting a reasonable agreement between these results and those of the previous samples for the mine access road sampling site.

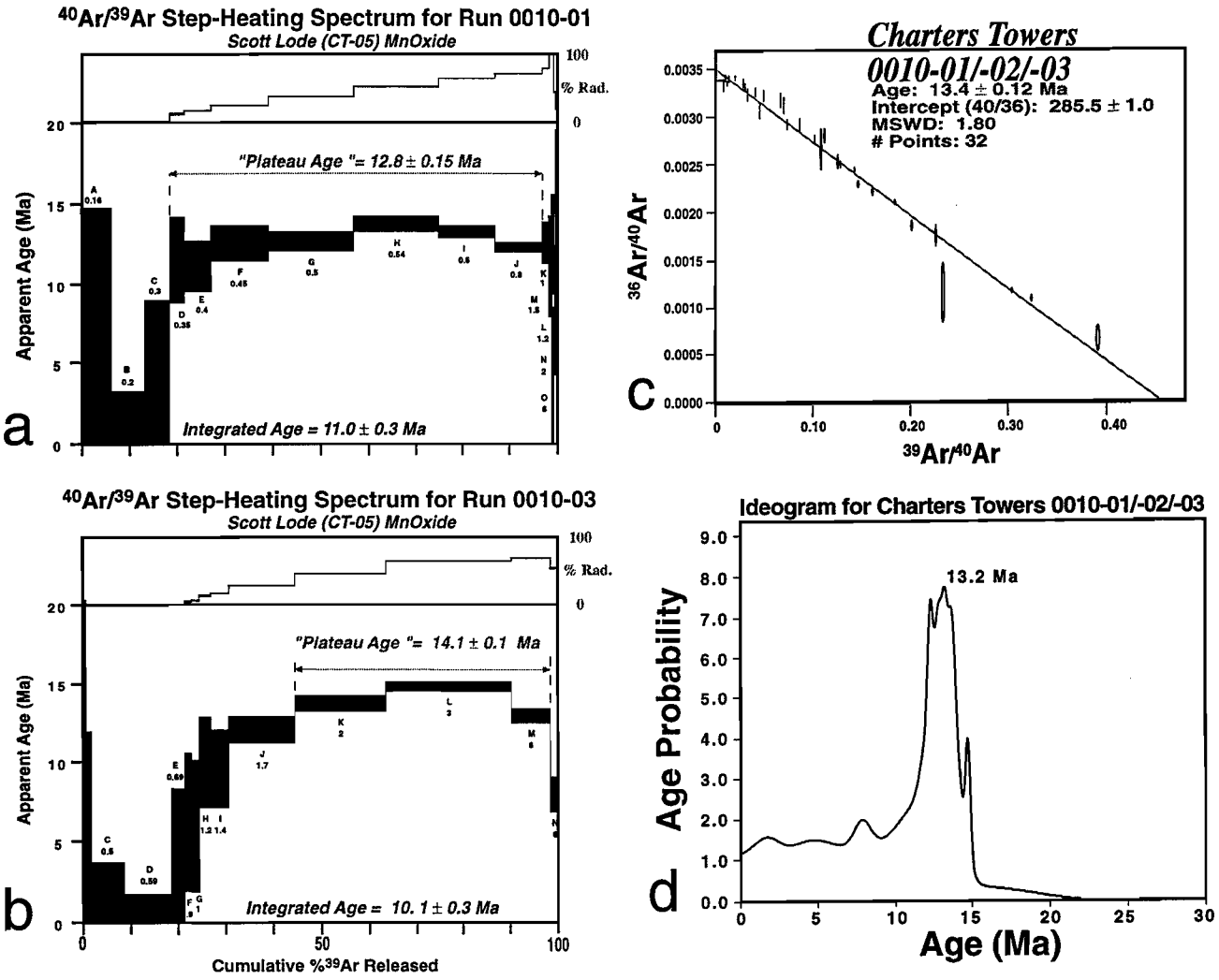

Figure 105. Step-heating spectra for two grains from sample CT-05 (mine access road level) yield one well defined plateau-like age of 12.8 ± 0.15 Ma and one not so well defined plateau-like age of 14.1 ± 0.1 Ma. The isochron (13.4 ± 0.12 Ma) and ideogram (13.2 Ma) ages for this sample suggest that this Mn-oxide sample is slightly older than the other grains analysed from the mine access road site.

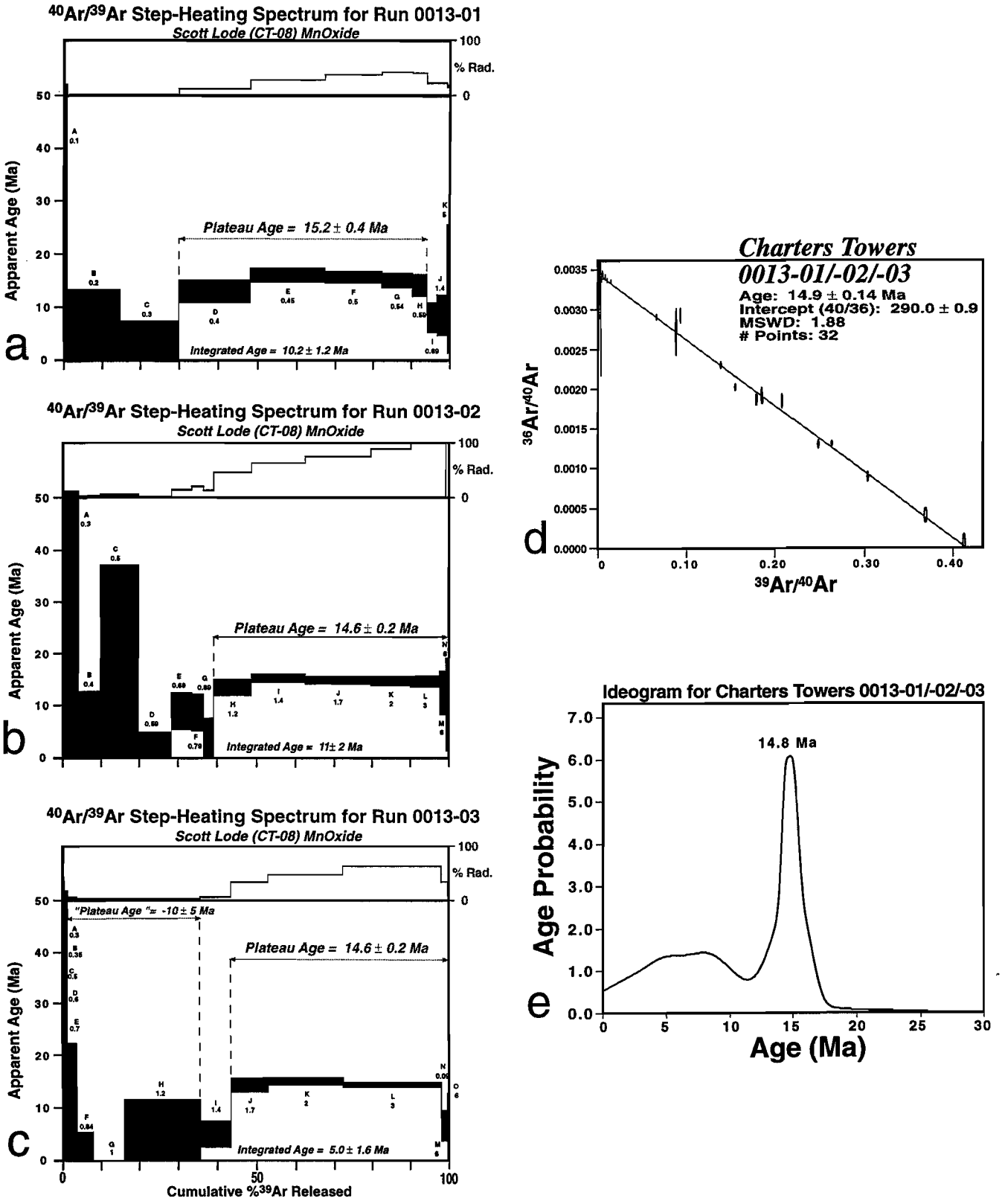

Figure 106. Step-heating spectra for three grains from sample CT-08 (mine access road level) yield three well defined plateau ages of 15.2 ± 0.4, 14.6 ± 0.2, and 14.2 ± 0.2 Ma, confirming the older ages obtained for mine access road samples in the previous figure. The same ages are also identified by the isochron (14.9 ± 0.14 Ma) and ideogram (14.8 Ma) methods.

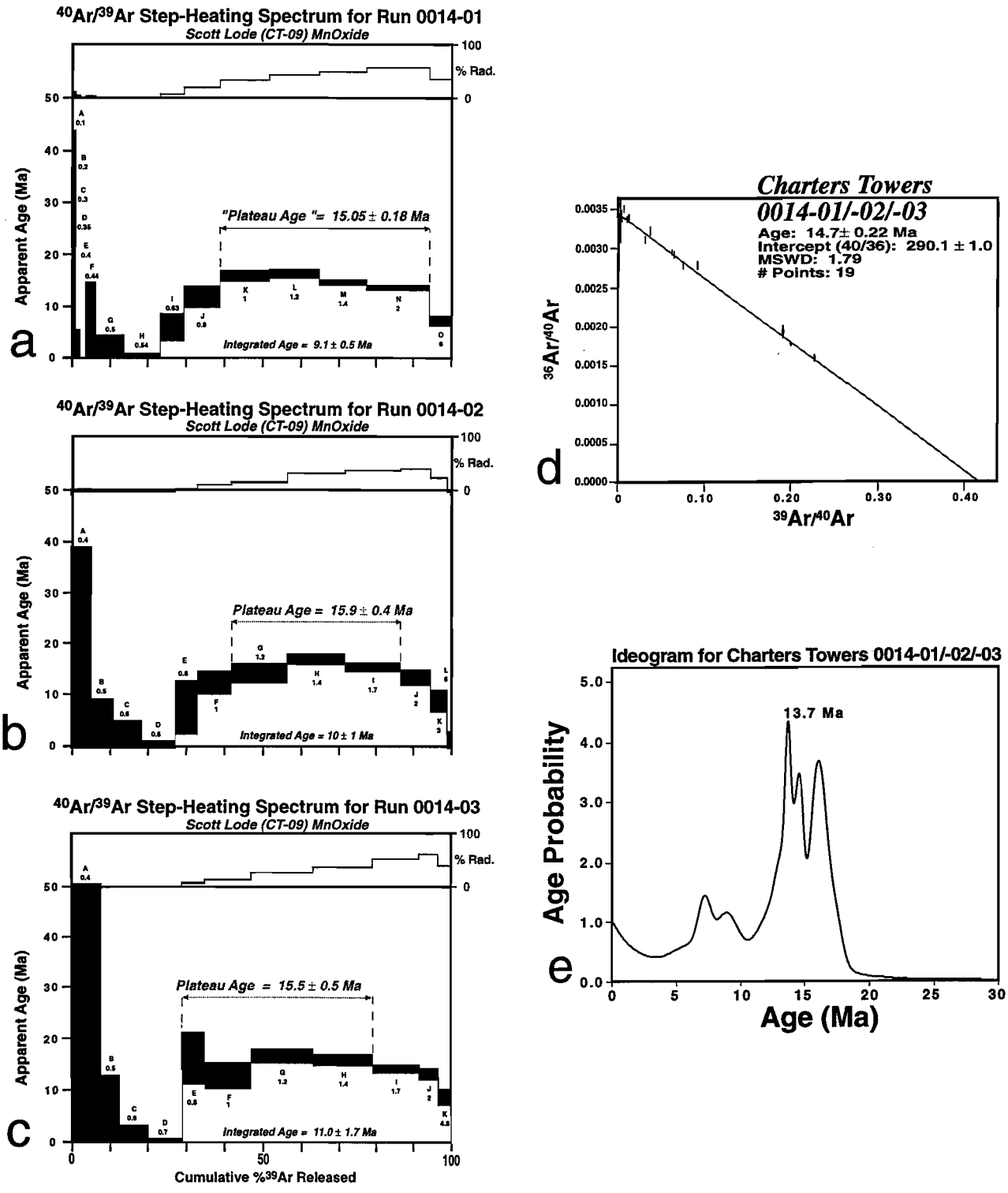

Figure 107. Step-heating spectra for three grains from sample CT-09 (mine access road level) yield three relatively well defined plateau ages of 15.05 ± 0.18, 15.9 ± 0.4, and 15.5 ± 0.5 Ma, once again confirming the older ages obtained for mine access road samples. The same ages are also identified by the isochron (14.7 ± 0.22 Ma) method. The ideogram plot shows a broad peak ranging from 13.7 to 15.5 Ma.

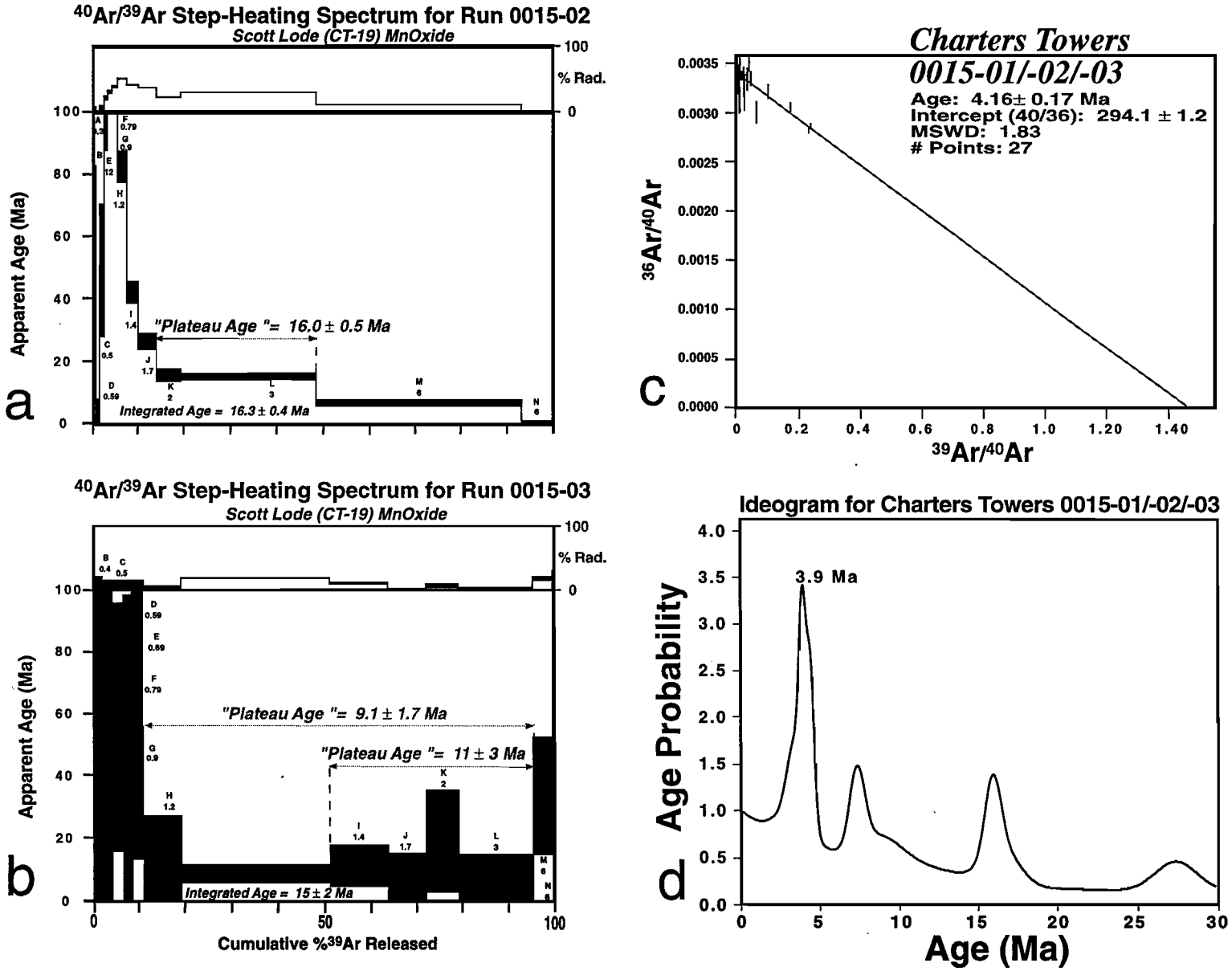

Figure 108. This sample yielded two poorly defined spectra.

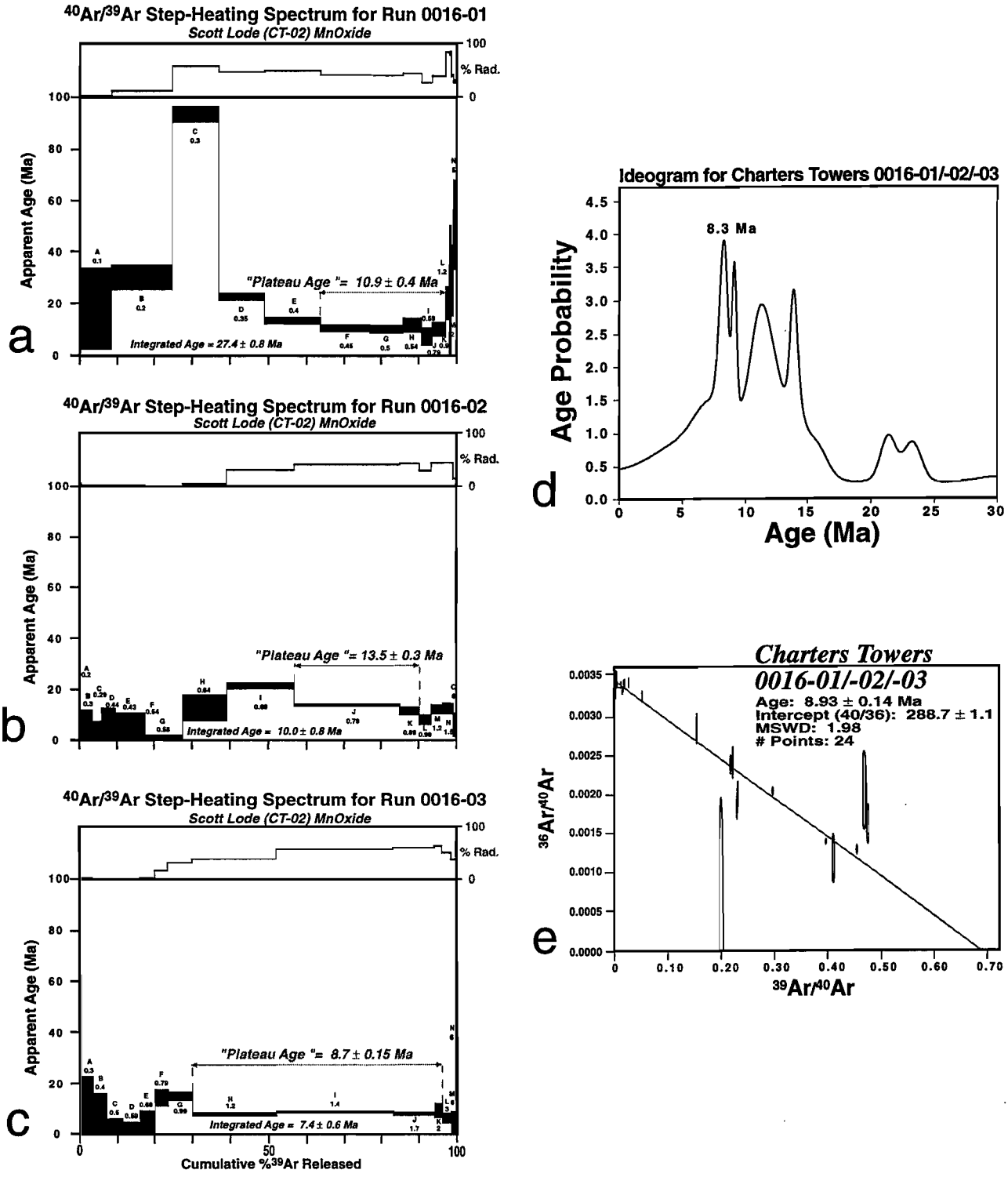

Figure 109. This sample yielded one well defined spectrum with a plateau age of 8.7 ± 0.15 Ma and two poorly defined spectra with plateau-like ages of 10.9 ± 0.4 and 13.5 ± 0.3 Ma. The isochron (8.93 ± 0.14 Ma) and the ideogram (8.3 Ma) ages are strongly controlled be the results obtained for the well behaved spectrum.

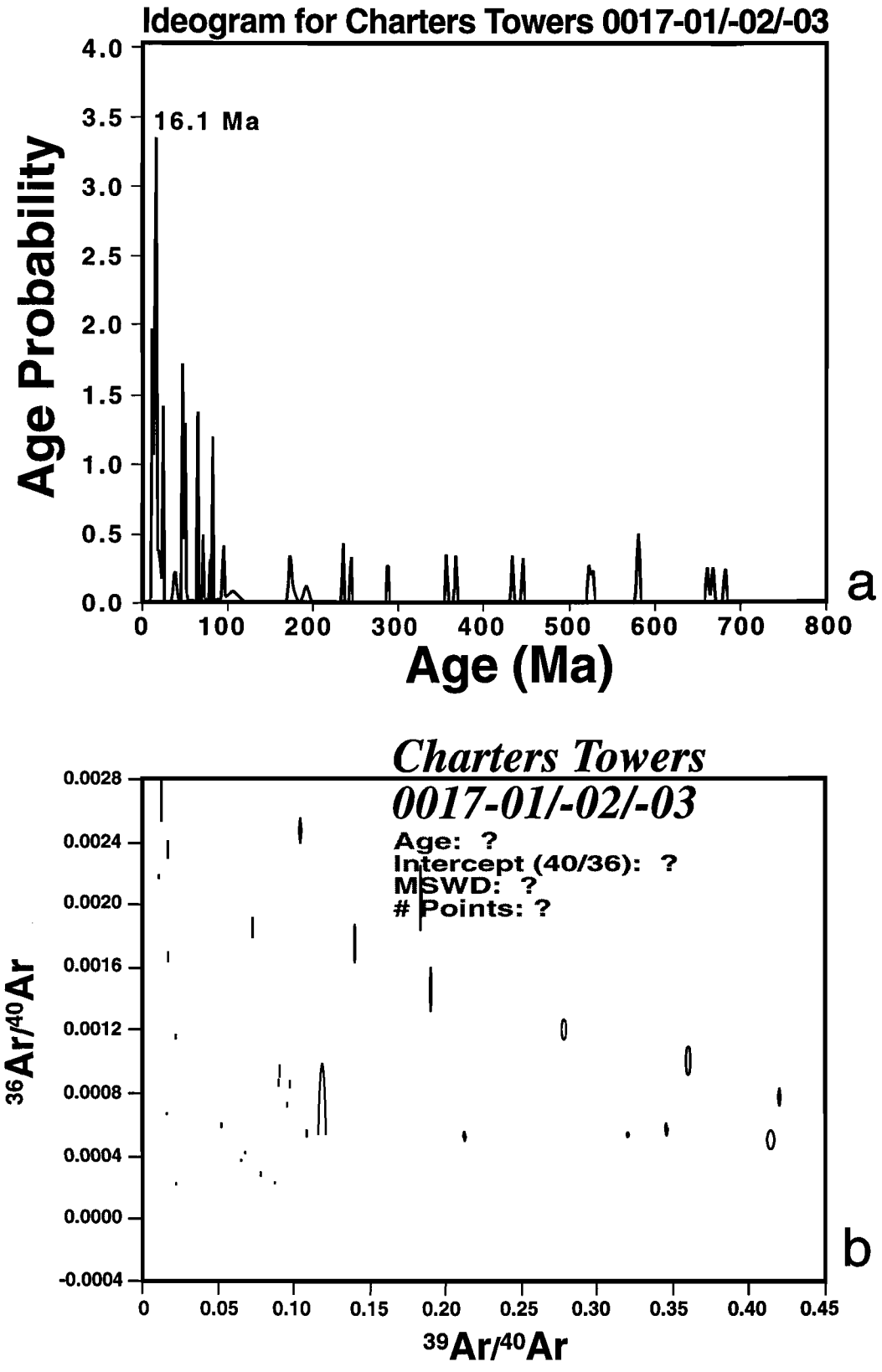

Figure 110. None of the grains analysed for this sample yielded meaningful spectra. The isochron for the results did not converge due to the large scatter of the results (b). The ideogram for the grains suggests a best age of 16.1 Ma, but due to the poor quality of the spectra obtained, this result is of dubious significance.

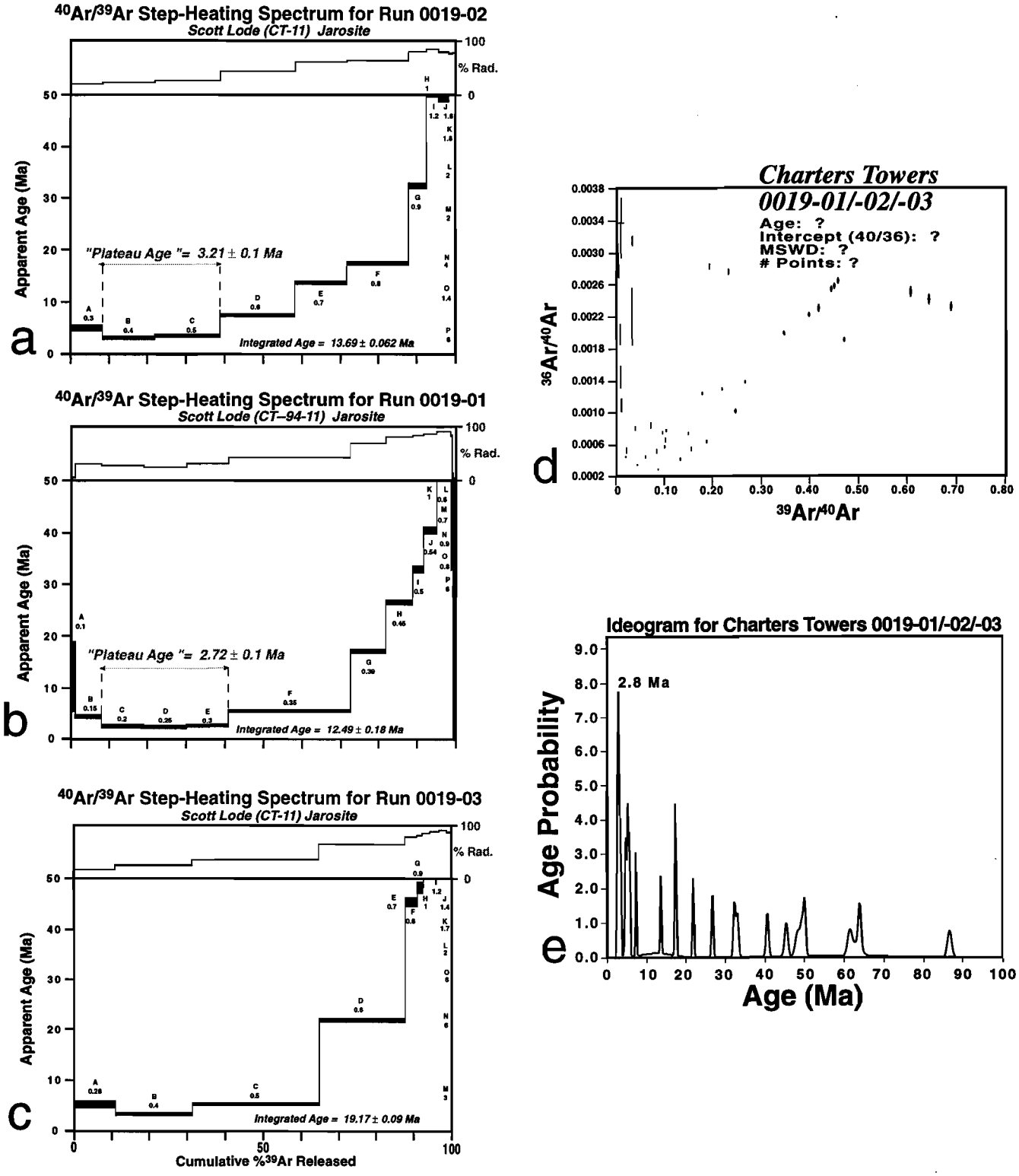

Figure 111. Three step-heating spectra for three distinct jarosite grains from intermediate levels in the weathering profile yielded similar results, with a young age plateau at low temperatures which climb to unreasonable older ages at the high temperature steps. The pattern obtained for the three grains indicates a young age for the jarosite (2-3 Ma) but also indicates that the samples are partially contaminated by unweathered primary silicates. SEM studies of these samples indicate that the jarosite grains partially replace primary feldspars. Remnants of unweathered feldspars account for the climbing spectra at higher temperatures. The isochron plot for this sample did not converge due to the mixed nature of the material.

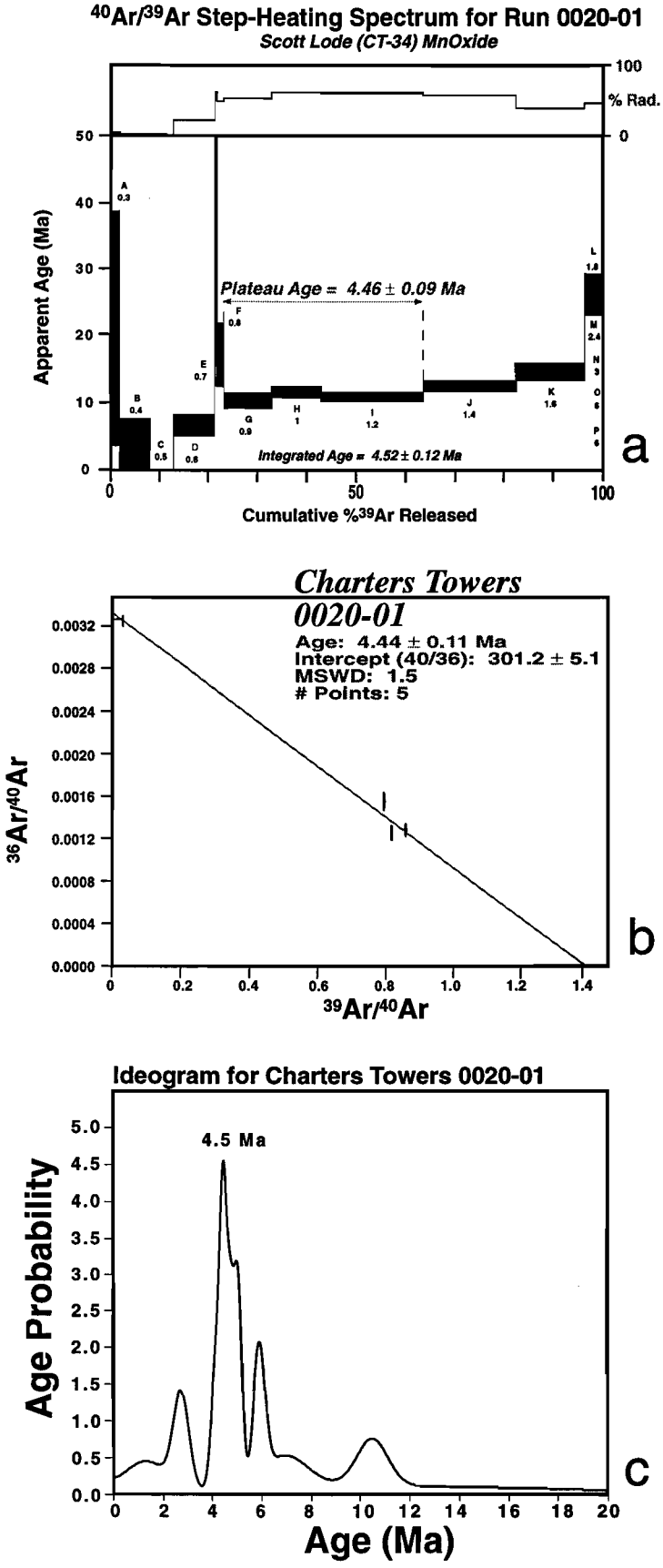

Figure 112. This jarosite sample yielded a better defined step-heating spectra than the previous samples, yielding consistent plateau (4.46 ± 0.09 Ma), isochron (4.44 ± 0.11 Ma) and ideogram (4.5 Ma) ages.

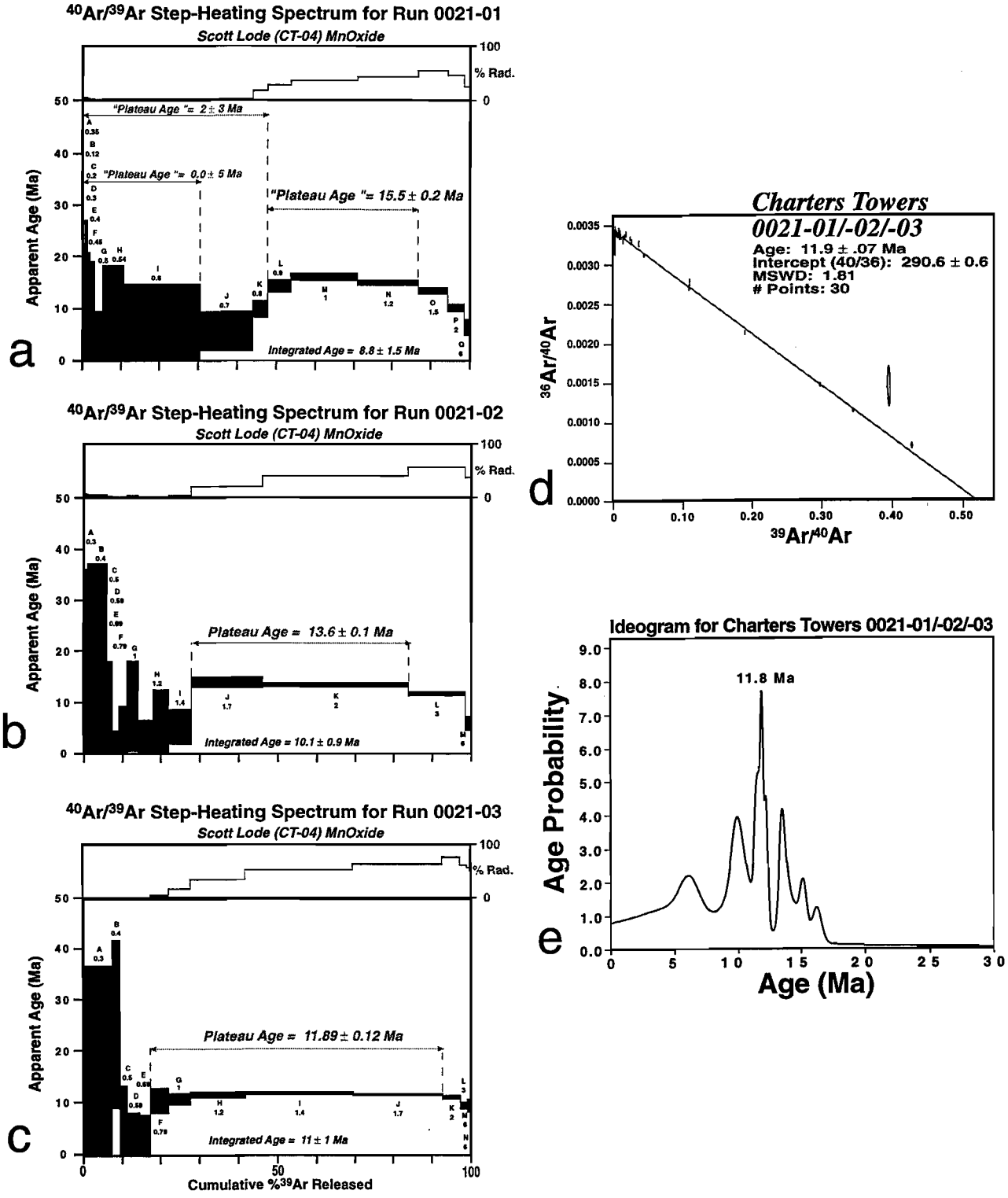

Figure 113. Step-heating spectra for three grains of Mn-oxide from sample CT-04 (mine access road level) yield relatively well defined plateau to plateau-like ages ranging from 15.5 ± 0.2, 13.6 ± 0.1, and 11.89 ± 0.12 Ma. The isochron (11.9 ± 0.07 Ma) and the ideogram (11.8 Ma) ages are strongly controlled by the well defined plateau in (c). The ages obtained for this sample are consistent with the ages obtained for other Mn-oxide samples from the mine access road sampling site.

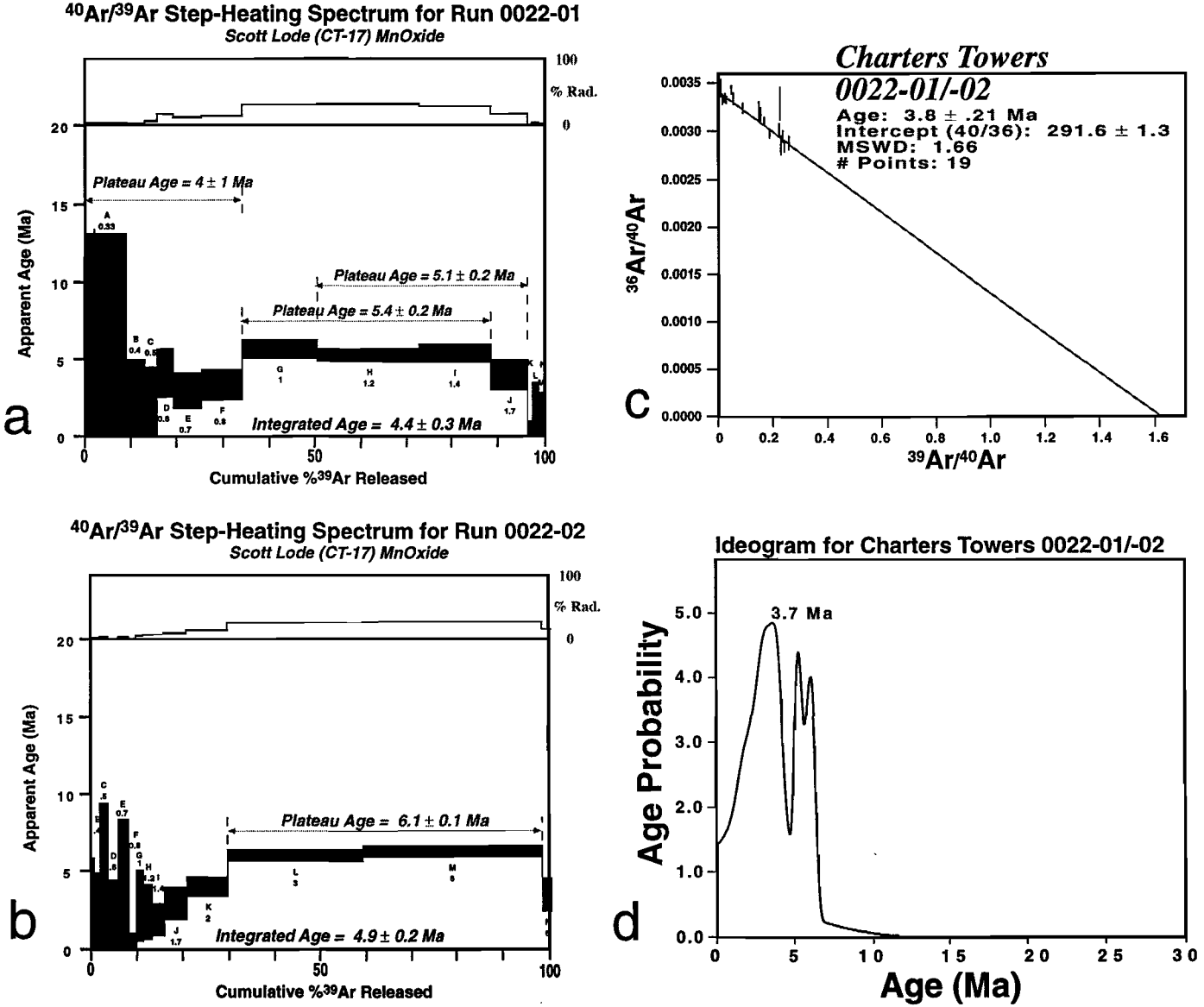

Fig. 114. Two well defined plateau (5.4 ± 0.2 Ma and 6.1 ± 0.1 Ma), isochron (3.8 ± 0.21 Ma) and ideogram (3.7 Ma) ages for the samples from the bottom levels of the Scott Lode pit (see Fig. 91 for sample locations) yield younger ages for the Mn-oxides found at greater depths in the profile.

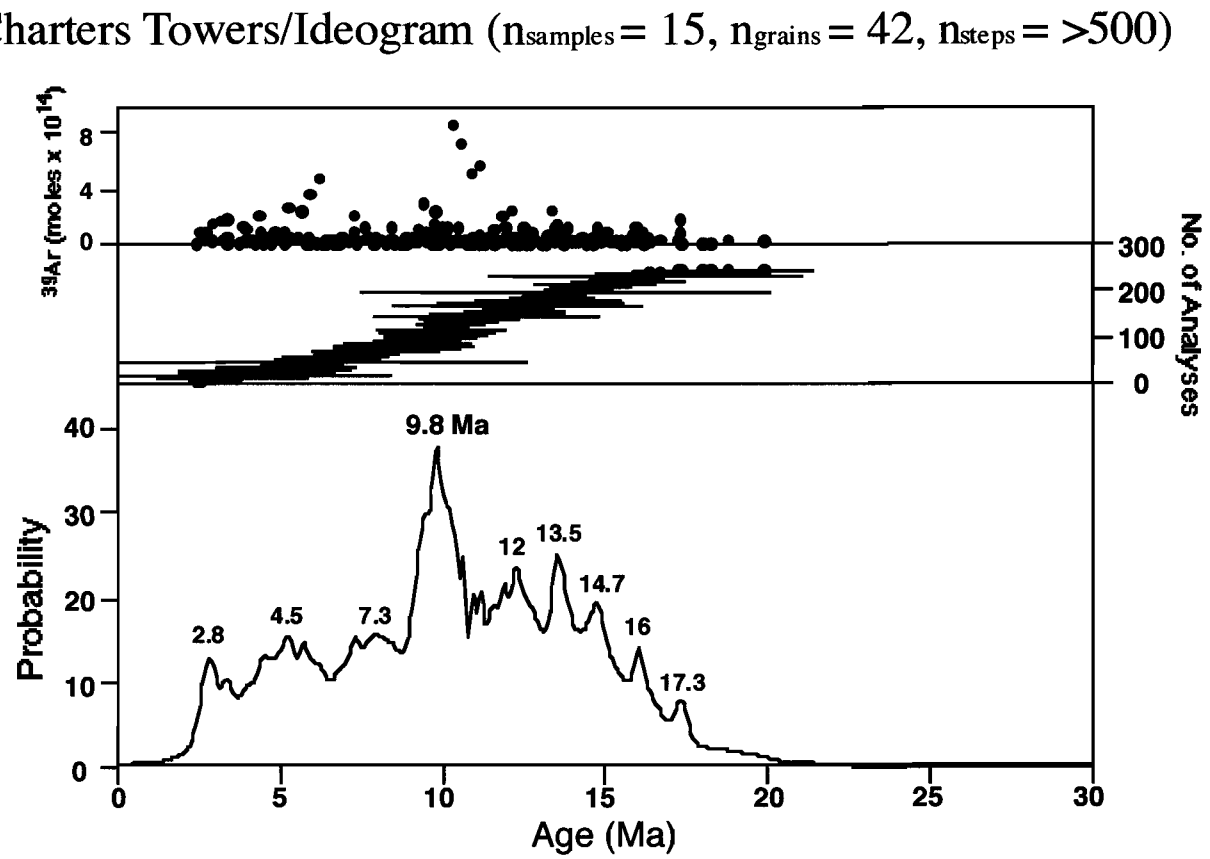

Figure 115. Ideogram indicating the most probable weathering ages for the Scott Lode samples analysed. The ages obtained in this study suggested a protracted history of weathering spanning all the middle and late Miocene and the Pliocene. The Mn-oxide ages obtained for the Scott Lode deposit are consistently younger than the Mount Isa Block samples analysed in this study. These younger ages are interpret to indicate persistence into the Neogene of more humid, weathering prone conditions along Queensland's eastern margin.

3.2 Interpretation of Charters Towers Geochronology Results

Weathering profiles overlying the Mount Leyshon and Kidston ore deposits, in the Charters Towers region, were dated by K-Ar analysis of alunite (Bird *et al.*, 1990). The results for Kidston (1.85 ± 0.04, 1.61 ± 0.04, 1.52 ± 0.03, 3.91 ± 0.07, 4.1 ± 0.2 Ma) and Mount Leyshon (3.1 ± 0.2 and 4.1 ± 0.1 Ma) identify only Plio-Pleistocene ages, a surprising result given the long history of weathering in the region (Bird *et al.*, 1990). The $^{40}Ar/^{39}Ar$ results for the jarosite samples analysed in this study (plateau age of 4.5 ± 0.1 Ma and plateau-like steps at 3.2 ± 0.1 and 2.7 ± 0.1 Ma) are consistent with the young ages determined by the K-Ar results above.

However, Mn-oxide $^{40}Ar/^{39}Ar$ ages indicate that weathering in the system is much more ancient than suggested by the jarosite or alunite ages. The Mn-oxide samples dated in this study fill cavities and desiccation cracks in kaolinitised volcanic rocks, indicating that the host sequence

was already strongly weathered at the onset of Mn-oxide precipitation, at approximately 17 Ma. An important result obtained from the Mn-oxide ages is the occurrence of older ages (10-17 Ma) at the shallower horizons and younger precipitation ages at the bottom of the profile (4-6 Ma), consistent with a downward propagation of the weathering front.

Electron microprobe analysis of MnOx samples from the Scott Lode profiles indicate that Mn-oxides in the system are Co-rich (up to 2.5 wt% Co), Ba-rich (up to 15 wt% Ba), moderately Zn-rich (0.5 wt% Zn), and devoid of Pb, consistent with Mn-oxide compositions associated with Au deposits.

4 Conclusions

The results of this investigation agree remarkably well with the Cenozoic geology of Queensland proposed by Day *et al.* (1983). These authors recognised 3 broad cycles of geologic activity in Queensland in the Cainozoic, each consisting of an initial upwarp phase accompanied by erosion and deposition, followed by a shorter stable phase during which deep weathering dominated. They have suggested that during the Late Cretaceous, while the Tasman and Coral Seas opened and initiated an active phase in eastern Queensland, the Inland and south Carpentaria Plains regions experienced deep weathering and relative tectonic quiescence. During the Late Eocene-Early Oligocene (45-30 Ma) much of the state experienced similar conditions, and the Isa Highlands were deeply weathered to form siliceous and ferruginous duricrusts. They believe that warping of duricrusted surfaces in the Inland region commenced in the Late Oligocene-Early Miocene (30-17 Ma) when the Highlands were uplifted and some of the weathering profiles were partly eroded. The Mid Miocene (ca. 15 Ma) was again a period of weathering in the Inland Region.

The history proposed by Day *et al.* (1983) based on geological considerations is substantiated by the geochronology results presented in this study. However, the causal mechanism proposed by those authors and those proposed in this study need further, independent confirmation. Particularly the correlation between warm-humid conditions and the development of deep weathering profiles needs confirmation by independent methods (well dated fossil sites, O-isotope temperature curves, etc.). The history of weathering, paleoclimatic evolution, and landscape processes proposed in this study need complementation by more comprehensive dating of well studied sites in Queensland. It is my objective to generate the necessary database to provide confirmation or disproval of some of the conclusions presented here.

Paulo Vasconcelos
Brisbane, March 31, 1998.

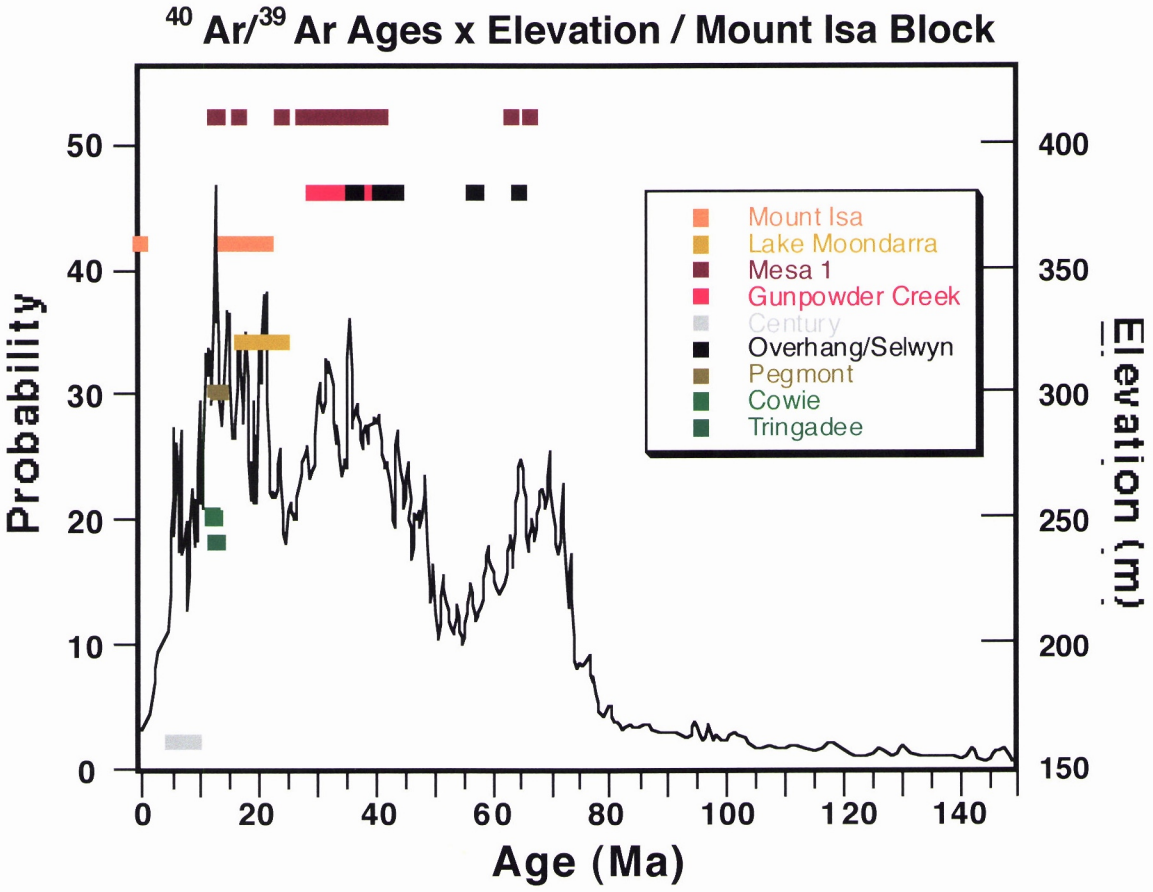

Figure 116. Summary diagram combining the distribution of ages with elevation and the combined ideogram for all the Mount Isa $^{40}Ar/^{39}Ar$ analyses carried out in this and a subsequent project. The figure illustrates clearly that the high elevation profiles have been exposed to the most prolonged and complex weathering history. The weathering profiles found in the lower elevation, more dissected part of the landscape, are generally truncated and more immature. These low elevation weathering profiles are also younger, according to the results obtained in this study.

References:

Alpers C. N. and Brimhall G. H. (1988) Middle Miocene climatic change in the Atacama Desert, northern Chile: Evidence from supergene mineralization at La Escondida. *Geol. Soc. Am. Bull.* 100, 1640-1656.

Alpers C. N., Nordstrom D. K. and Ball J. W. (1989) Solubility of jarosite solid solutions precipitated from acid mine waters, Iron Mountain, California, USA. *Sci. Géol. Bull.* 42, 281-298.

Anand R., Phang C., Wilford J., Wildman J., Shu L., Robertson I., and Munday T. (1996) Regolith-landscape Characteristics, Evolution and Regional Synthesis of the Mt. Isa Region. CRC LEME-AMIRA Project 417 Progress Report, 142p.

Anand R., Fraser S., Jones M., Shu L., Munday T., Shu L., Phang C., Robertson I., Scott K., Vasconcelos, P., Wildman J., and Wilford J. (1997) Geochrmical Exploration in Regolith-Dominated Terrain, North Queensland. CRC LEME-AMIRA P417 Final Report, 130p.

Anderson J. A. (1981) Characteristics of leached capping and techniques of appraisal. In *Advances in geology of the porphyry copper deposits, southwestern North America.* (ed. S.R.Titley), pp. 245-287, Univ. Arizona Press.

Andrews S (1998) The Regional Setting of Base Metal Mineralisation in the Mid Proterozoic Upper MAcNamara Group, Lawn Hill Region. PhD Thesis, University of Queensland, Brisbane.

Bird M. I. and Chivas A. R. (1989) Stable-isotope geochronology of the Australian regolith. *Geoch. et Cosmoch. Acta* 53, 3239-3256.

Bird M. I., Chivas A. R. and McDougall I. (1990) An isotopic study of surficial alunite in Australia: 2. Potassium-argon geochronology. *Chem. Geol.* 80, 133-145.

Bladh K. W. (1982) The Formation of goethite, jarosite, and alunite during the weathering of sulfide-bearing felsic rocks. *Econ. Geol.* 77, 176-184.

Blanchard R. (1968) Interpretation of leached outcrops. *Nevada Bur. Mines Bull.* 66, 196 p.

Brady N. (1984) The Nature and Properties of Soils. Macmillan, New York, 750 p.

Brady P. and Carrol S. (1994) Direct effects of CO_2 and temperature on silicate weathering: Possible implications for climate control. *Geochim. Cosmochim. Acta*, 58, 1853-1856.

Bricker O. (1965) Some stability relations in the system $Mn\text{-}O_2\text{-}H_2O$ at 25 °C and one atmosphere total pressure. *Am. Mineral.* 50, 1296-1354.

Brophy G. P., Scott E. S. and Snellgrove R. A. (1962) Sulfate studies II. Solid solution between alunite and jarosite. *Am. Mineral.* 47, 112-126.

Brophy G. P. and Sheridan M. F. (1965) Sulfate studies IV: The jarosite-natrojarosite-hydronium jarosite solid solution series. *Am. Mineral.* 50, 1595-1607.

Burns R. G. and Burns V. M. (1979) Manganese oxides. In *Marine minerals* (ed. P. H. Ribbe), pp. 1-46, Mineral. Soc. Am.

Byström A. and Byström A. M. (1950) The crystal structure of hollandite, the related manganese oxide minerals, and a-MnO_2. *Acta Cryst.* 3, 146-154.

Chivas A. R., Andrew A. S. , Lyons W. B. , Bird M. I. and Donnelly T. H. (1991) Isotopic constraints on the origin of salts in Australian playas. I. Sulphur. *Palaeogeogr., Palaeoclimatol., Palaeoecol.* 84, 309-332.

Crerar D. A., Cormick R. K. and Barnes H. L. (1972) Organic controls on the sedimentary geochemistry of manganese. Acta Mineral.-Petrogr., Szeged. 20, 217-226.

Crerar D. A., Cormick R. K. and Barnes H. L. (1980) Geochemistry of manganese: an overview. In *Geology and Geochemistry of Manganese* (eds. I. M. Varentsov and G. Grasselly), Vol. 1, pp. 293-334, E. Schweizerbart'sche Verlagsbuchhandlung.

Dammer D., Chivas A. and McDougall I. (1996) Isotopic Dating of Supergene Manganese Oxides from the Groote Eylandt Deposit, Northern Territory, Australia. Econ. Geol. 91, 386-401.

Day R. W., Whitaker W. G., Murray C. G., Wilson I. H. and Grimes K. G. (1983) *Queensland Geology.* Geological Survey of Queensland Publication 383. Brisbane, Geological Survey of Queensland, 194 p.

Deino A. L. and Potts R. (1990) Single -crystal $^{40}Ar/^{39}Ar$ dating of the Olorgesailie Formation, southern Kenya Rift. *J. Geophys. Res.* 95, 8453.

Deino A. L., Tauxe L., Monaghan M. and Drake R. (1990) $^{40}Ar/^{39}Ar$ age calibration of the litho- and paleomagnetic stratigraphies of the Ngorora Formation, Kenya. *J. Geol.* 98, 567-587.

Deino A. (1997) Mass Spect V.4.85 Software Program Documentation, 124p.

Fleming E. (1997) Weathering in the Selwyn Ranges, Northwest Queensland: Regolith and Geochronology. Honours Thesis, University of Queensland, Brisbane.

Gilkes R.J (1996) Biology and the Regolith: an Overview. In Eggleton R.(ed.) The State of the Regolith, Geological Society of Australia Inc. Special Publication No. 20, 110-125.

Hem J. D. (1963) Chemical equilibria and rates of manganese oxidation. *U. S. Geol. Surv. Water Supply Paper 1667-A.*.

Hem J.D. (1989) Study and Interpretation of the Chemical Characteristics of Natural Water. USGS Water-Supply Paper 2254, 263p.

Herlihy T.E. (1994) The Temporal and Spatial Distribution of Elements and Supergene Minerals in the Urquhart Shles, Mt. Isa, Northwest Queensland. Honours Thesis, University of Queensland, Brisbane.

Keith W. J., Calk L. and Ashley R. P. (1979) Crystals of coexisting alunite and jarosite, Goldfield, Nevada. *US Geol. Surv. Prof. Paper.* 1124-C: C1-C5.

King L. (1957) : Basic palaeogeography of Gondwanaland during the late Palaeozoic and Mesozoic eras. Proceedings of the Geological Society of London. 1549; Pages 73-81.

Lilley G.J. (1997) Regolith Distribution and Genesis, Tick Hill Region, Northwest Queensland. Honours Thesis, University of Queensland, Brisbane.

Michel F. A. and van Everdingen R. O. (1987) Formation of a jarosite deposit on cretaceous shales in the Fort Nornam area, Northwest Territories. *Can. Mineral.* 25, 221-226.

Nordstrom, D. K. (1982) Aqueous pyrite oxidation and the consequent formation of secondary iron minerals. In *Acid Sulfate Weathering* (eds. J. A. Kittrick, D. S. Fanning, and L. R. Hossner), Soil Sci. Soc. of Amer. Spec. Pub., 10, p. 37-55.

Ricklefs R.E. (1976) The Economy of Nature. Chiron Press, New York, 455p.

Scott K. M. (1987) Solid solution in, and classification of, gossan-derived members of the alunite-jarosite family, northwest Queensland, Australia. *Am. Mineral.* 72, 178-187.

Scott K. M. (1990) Origin of alunite- and jarosite-group minerals in the Mt. Leyshon epithermal gold deposit, northeast Queensland, Australia. *Am. Mineral.* 75, 1176-1181.

Stone A.T. (1987) Reductive dissolution of manganese (III/IV) oxides by substituded phenols. *Environ. Sci. Technol.* 21, 979-988.

Stone A.T. and Morgan J.J. (1984) Reduction and dissolution of manganese (III) and manganese (IV) oxides by organics: 1. Reaction with hydroquinone. *Environ. Sci. Technol.* 18, 450-456.

Stone A.T. and Morgan J.J. (1984) Reduction and dissolution of manganese (III) and manganese (IV) oxides by organics: 2. Survey of the reactivity of organics. *Environ. Sci. Technol.* 18, 617-624.

Taylor G.F. and Scott K.M. (1982) Evaluation of gossans in relation to lead-zinc mineralisation in the Mount Isa Inlier, Queensland. *BMR J. Aust. Geol. Geoph.*, 7, 159-180.

Twidale C. R. (1956) Chronology of denudation in northwest Queensland. *Geol. Soc. America Bull.* 67, 867-882.

Twidale C. R. (1994) Gondwanan (Late Jurassic and Cretaceous) palaeosurfaces of the Australian Craton. Palaeogeography, Palaeoclimatology, Palaeoecology. 112; 1-2, Pages 157-186.

van Breeman N. (1988) Redox processes of iron and sulphur involved in the formation of acid sulfate soils. In *Iron in soils and clay minerals* (eds. J. W. Stucki, B. A. Goodman, and U. Schwertmann), p. 825-841, NATO.

Vasconcelos P. M. (1992) Timing and rates of evolution of hydrochemical systems in semiarid and humid environments by application of ^{40}K-^{40}Ar and laser-heating $^{40}Ar/^{39}Ar$ dating of K-bearing weathering product minerals. Ph. D., University of California, Berkeley.

Vasconcelos P.M., Becker T.A., Renne P.R. and Brimhall G.H (1992) Age and duration of weathering by ^{40}K-^{40}Ar and $^{40}Ar/^{39}Ar$ analysis of K-Mn Oxides. *Science* 258, 451-455.

Vasconcelos P. M.,Wenk, H. -R., and Echer, C. (1994) In situ study of the thermal behavior of cryptomelane by high voltage and analytical electron microscopy. *Am. Mineral.*, 79, 80-90.

Vasconcelos P. M., Brimhall G. H, Becker T. A., and Renne P. R. (1994) $^{40}Ar/^{39}Ar$ analysis of supergene jarosite and alunite: Implications to the paleo weathering history of western US and West Africa. *Geochim. Cosmochim. Acta*, 58, 401-420.

Vasconcelos P.M., Becker T. A., Renne P.R. and Brimhall G.H (1994) Direct dating of weathering phenomena by K-Ar and $^{40}Ar/^{39}Ar$ analysis of supergene K-Mn oxides. *Geochim. Cosmochim. Acta.*, 58, 1635-1665.

Vasconcelos P.M., Renne P.R., Becker T.A., and Wenk, H.-R., (1995) Mechanisms and kinetics of atmospheric, radiogenic, and nucleogenic argon release from cryptomelane during $^{40}Ar/^{39}Ar$ analysis. *Geochim. Cosmochim. Acta*, 59, 2057-207.

Vasconcelos P.M. (1996) K-Ar and $^{40}Ar/^{39}Ar$ Geochronology of Weathering Reactions. 17th In K. Camuti (ed.) International Geochemical Exploration Symposium, Extended Abstract, p. 45-46.

Whitbread M. (1995) The effects of Weathering on the Geochrmical Migration of Zn and Pb Derived from the Century Deposit. Honours Thesis, University of Queensland, Brisbane.